Experimental Investigation in Autothermal Chemical Looping Gasification

Experimentelle Untersuchung der Autothermen Chemical Looping Vergasung
Zur Erlangung des akademischen Grades Doktor-Ingenieur (Dr.-Ing.)
Genehmigte Dissertation von Falko Sokrates Marx aus Kassel
Tag der Einreichung: 2024-01-19, Tag der Prüfung: 2024-05-15

1. Gutachten: Prof. Dr.-Ing. Bernd Epple
2. Gutachten: Prof. Dr.-Ing. Christian Hasse
Darmstadt, Technische Universität Darmstadt

TECHNISCHE UNIVERSITÄT DARMSTADT

Mechanical Engineering Department

Institut for Energy Systems & Energy Technology

Experimental Investigation in Autothermal Chemical Looping Gasification
Experimentelle Untersuchung der Autothermen Chemical Looping Vergasung

Accepted doctoral thesis by Falko Sokrates Marx

Date of submission: 2024-01-19
Date of thesis defense: 2024-05-15

Darmstadt, Technische Universität Darmstadt

Zusammenfassung

In Anbetracht des derzeitigen Klimawandels sind Anstrengungen zur Verringerung der Emission von Treibhausgasen in die Atmosphäre erforderlich. Die nachhaltige Nutzung von Biomasse als Kohlenstoff- und Energieträger eröffnet die Möglichkeit von kohlenstoffneutralen oder sogar kohlenstoffnegativen Technologien. Eine Technologie, bei der Biomasse zur Erzeugung eines stickstofffreien, hochkalorischen Synthesegases genutzt werden kann, für das keine energieintensive Luftzerlegunsanlage erforderlich ist, ist die Chemical Looping Vergasung (CLG), die in letzter Zeit verstärktes Forschungsinteresse erfahren hat. Es wurde nachgewiesen, dass CLG in extern beheizten Reaktoren im Labormaßstab kontinuierlich funktioniert. Für eine kommerzielle, wirtschaftlich rentable Anwendung des Verfahrens ist jedoch ein autothermer Betrieb erforderlich, der noch nicht nachgewiesen wurde. Darüber hinaus gibt es kein Prozesssteuerungskonzept, das sich auf großtechnische Reaktoren anwenden lässt.

In dieser Arbeit wird die CLG-Technologie auf den $1\,\mathrm{MW_{th}}$-Maßstab hochskaliert und unter autothermen Bedingungen untersucht. Mit Hilfe von Gleichgewichtsprozesssimulationen wird ein geeignetes Prozesssteuerungskonzept für den autothermen Betrieb auf der Grundlage eines substöchiometrischen Betriebs entwickelt. Auf der Grundlage von Wärme- und Massenbilanzen für eine bestehende Pilotanlage wurden Modifikationen entworfen und umgesetzt, um die Pilotanlage für CLG umzurüsten.

In dieser Arbeit werden Experimente beschrieben, die mit Industrieholzpellets, Kiefernforstrückständen und Weizenstroh-Pellets als Biomasse-Einsatzstoff und Ilmenit als Sauerstoffträger durchgeführt wurden. In der nicht optimierten Pilotanlage wurde ein Kaltgaswirkungsgrad von etwa $50\,\%$ erreicht, was darauf hinweist, dass in einer kommerziellen Anlage höhere Werte erreicht werden können, wenn die Wärmeverluste minimiert werden. Die Kohlenstoffumwandlung lag bei über $90\,\%$, und es wird erwartet, dass dieser Wert auf fast $100\,\%$ ansteigt, wenn die Temperatur, die Verweilzeit und die Zykloneffizienz in einer kommerziellen Anlage erhöht werden. Das Synthesegas hat eine sehr hohe Qualität mit geringen Methankonzentrationen im Bereich von 7 vol.-% bis 10 vol.-% und einem gravimetrischen Teergehalt unter $1\,\mathrm{g/Nm^3}$, gemessen mittels Teerprotokoll. Eine neue Methode zur Bestimmung der Feststoffzirkulation in einem dualen Wirbelschichtsystem unter Verwendung von Feststoffproben aus Kopplungselementen zur Berechnung des Feststoffflusses wurde entwickelt und während der Experimente getestet. Die Feststoffzirkulation wurde mit $1.2\,\mathrm{kg\,s^{-1}\,MW^{-1}}$ bis $4.3\,\mathrm{kg\,s^{-1}\,MW^{-1}}$ mit einer Messunsicherheit von weniger als $20\,\%$ bestimmt.

Abstract

In light of the current climate change efforts to reduce the emission of greenhous gases (GHGs) to the atmosphere are required. The sustainable utilization of biomass as carbon carrier and energy carrier opens up the possibility of carbon neutral or even carbon negative technologies. One technology where biomass can be utilized for the generation of a nitrogen free, high calorific syngas where no energy intensive air separation unit (ASU) is required is the chemical looping gasification (CLG) which has lately seen increased research interest. CLG has been demonstrated to work continuously within externally heated lab-scale reactors. In order to be economically viable commercial application of the process requires autothermal operation, which has not yet been demonstrated. Moreover, no process control concept applicable to large-scale reactors exists.

In this work, the CLG technology is upscaled to the $1\,\mathrm{MW_{th}}$ range and investigated under autothermal conditions. Equilibrium process simulations are used to develop a suitable process control concept for autothermal operation based on sub-stoichiometric air reactor (AR) operation. Based on heat and mass balance for an existing pilot plant modifications were designed and implemented retrofitting the pilot plant for CLG.

Experiments carried out with industrial wood pellets (IWP), pine forest residue (PFR), and wheat straw pellets (WSP) as biomass feedstocks and ilmenite as oxygen carrier (OC) bed material are described in this work. A cold gas efficiency of around $50\,\%$ was achieved in the non-optimized pilot plant, indicating that higher values can be reached in a commercial unit when minimizing heat losses. The carbon conversion was above $90\,\%$, and this value is expected to increase to almost $100\,\%$ when raising the temperature, residence time, and cyclone efficiency in a commercial unit. The syngas has a very high quality with low methane concentrations in the range of 7 vol.-% to 10 vol.-% and gravimetric tar content below $1\,\mathrm{g/Nm^3}$ measured via tar protocol. A new method for the determination of the solid circulation in a dual fluidized bed system utilizing solid samples from coupling elements to calculate the solids flux has been devised and was tested during the experiments showing a solid circulation of $1.2\,\mathrm{kg\,s^{-1}\,MW^{-1}}$ to $4.3\,\mathrm{kg\,s^{-1}\,MW^{-1}}$ with measurement uncertainty smaller than $20\,\%$.

Acknowledgements

First and foremost I would like to thank the European Union for providing the generous funding of the experimental investigation through the Horizon 2020-Research and Innovation Framework Programme under the grant agreement No. 817841 (Chemical Looping gAsification foR sustainAble production of biofuels — CLARA).

I gratefully acknowledge the freedom in technical matters and support of my decisions from my supervisor Prof. Dr.-Ing. Bernd Epple. Without his ability to acquire resources this dissertation would not have been possible.

I am grateful to Prof. Dr.-Ing. Christian Hasse for agreeing to be the second examiner[1].

I would like to extend my sincere thanks to Dr.-Ing. Jochen Ströhle for his support and reviewing during drafting of the research papers. His standard and attention to detail were the highest bar set during the preparation and review process and made everything go smoothly.

I would like to express my deepest appreciation to my colleague Paul Dieringer, who worked with me on the research project CLARA. He splendidly handled almost all of the administrative work by himself, leaving me free to work on the detail engineering, preparation, and commissioning of the pilot plant without much distraction. He was my first sounding board for any ideas during design and technology selection and during the drafting of the research papers. His practical suggestions and constructive criticism increased the quality of the pilot plant and my research papers.

I would like to thank all partners from the CLARA-consortium for any contribution towards the experiments. From information input over direct support during HAZOP analysis to the preparation and provisioning of the feedstocks, without their support the experiments would not have been possible.

Special thanks go to my colleagues who were operating the pilot plant during my and Paul's absence, slaving away in night-shifts, on weekends, and holidays so that we could catch some much needed sleep. Your willingness to support Paul's and my experiments allowed us to obtain a huge amount of data. I sincerely appreciate your struggle with this new process and the effort emptying barrels for me. I hope to have made up for the dirt, grime and sweat you had to wash off by the emptying of barrels we did together afterwards.

Thanks also go to the workshop colleagues. Your rebuilding of the pilot plant to enable the new process to run smoothly was great. Your many weldseams, installed and insulated wires and pipes, and the equipment serviced made the pilot plant run smoothly during experiments.

I would like to recognize the assistance that I received from all students who processed the samples taken during pilot plant operation in the laboratory. Your valuable contributions have been very useful in creating a holistic picture of the investigated process.

I would also like to acknowledge the assistance of my brother Bernhard in proofreading my third thesis now. Your many catches of punctuation, spelling, and grammar errors were a huge improvement on readability.

[1] In German the term *Korreferent* is used, for which there is no good English translation.

Contents

Publications

Journal Articles

1. Dieringer, P., Marx, F., Alobaid, F., Ströhle, J. & Epple, B. Process Control Strategies in Chemical Looping Gasification—A Novel Process for the Production of Biofuels Allowing for Net Negative CO2 Emissions. *Applied Sciences* **10,** 26. ISSN: 2076-3417. doi:10.3390/app10124271. https://www.mdpi.com/2076-3417/10/12/4271 (2020) (June 22, 2020).
2. Marx, F., Dieringer, P., Ströhle, J. & Epple, B. Design of a 1 MWth Pilot Plant for Chemical Looping Gasification of Biogenic Residues. *Energies* **14,** 2581. ISSN: 1996-1073. doi:10.3390/en14092581. https://www.mdpi.com/1996-1073/14/9/2581 (2021) (Apr. 30, 2021).
3. Marx, F., Dieringer, P., Ströhle, J. & Epple, B. Solid Flux Measurement in Dual Fluidized Bed Processes Based on Solid Samples. *Fuel* **341,** 127589. ISSN: 00162361. doi:10.1016/j.fuel.2023.127589. https://linkinghub.elsevier.com/retrieve/pii/S0016236123002028 (2023) (June 2023).
4. Dieringer, P., Marx, F., Michel, B., Ströhle, J. & Epple, B. Design and Control Concept of a 1 MWth Chemical Looping Gasifier Allowing for Efficient Autothermal Syngas Production. *International Journal of Greenhouse Gas Control* **127,** 103929. ISSN: 17505836. doi:10.1016/j.ijggc.2023.103929. https://linkinghub.elsevier.com/retrieve/pii/S1750583623000993 (2023) (July 2023).
5. Dieringer, P., Marx, F., Ströhle, J. & Epple, B. System Hydrodynamics of a 1 MWth Dual Circulating Fluidized Bed Chemical Looping Gasifier. *Energies.* ISSN: 1996-1073. doi:10.3390/en16155630. https://www.mdpi.com/1996-1073/16/15/5630 (2023).
6. Marx, F., Dieringer, P., Ströhle, J. & Epple, B. Process Efficiency and Syngas Quality from Autothermal Operation of a 1 MWth Chemical Looping Gasifier with Biogenic Residues. *Applications in Energy and Combustion Science* **16,** 100217. ISSN: 2666352X. doi:10.1016/j.jaecs.2023.100217. https://linkinghub.elsevier.com/retrieve/pii/S2666352X23001061 (2023) (Dec. 2023).
7. Dieringer, P., Marx, F., Lebendig, F., Müller, M., Di Guiliano, A., Galucci, K., Ströhle, J. & Epple, B. Fate of Ilmenite as Oxygen Carrier during 1 MWth Chemical Looping Gasification of Biogenic Residues. *Applications in Energy and Combustion Science,* 100227. ISSN: 2666352X. doi:10.1016/j.jaecs.2023.100227. https://linkinghub.elsevier.com/retrieve/pii/S2666352X23001164 (2023) (Nov. 2023).

Conference Contributions

1. Marx, F. *The CLARA Project: Chemical Looping Gasification for the Production of Biofuels* 8th High Temperature Solid Looping Cycles Network MeetingGeleen. Jan. 20, 2020.

2. Dieringer, P. *Chemical Looping Gasification – A Novel Process for the Sustainable Production of Biofuels*. 6th Central European Biomass Conference (CEBC)Graz. Jan. 2020. doi:10.26083/TUPRINTS-00024417. https://tuprints.ulb.tu-darmstadt.de/id/eprint/24417 (2023).
3. Marx, F., Dieringer, P., Ströhle, J. & Epple, B. *Solid Flux Measurement in Chemical Looping Gasification Based on Solid Samples* in. Fluidized Bed Conversion (Gothenburg, May 2022).
4. Dieringer, P. *Design and Control Concept of a 1 MWth Chemical Looping Gasifier Allowing for Efficient Autothermal Syngas Production* 6th International Conference on Chemical LoopingZaragoza. Sept. 2022. doi:10.26083/TUPRINTS-00024418. https://tuprints.ulb.tu-darmstadt.de/id/eprint/24418 (2023).
5. Marx, F. *Autothermal Operation of a 1MWth Chemical Looping Gasifier for Biogenic Residues* 9th High Temperature Solid Looping Cycles Network MeetingPiazenza. Mar. 14, 2023.
6. Marx, F. *Autotherme Chemical-Looping-Vergasung Biogener Reststoffe* Statuskonferenz BioenergieLeipzig. Sept. 21, 2023.

Thesis

1. Marx, F. *Analysis of Heat Release Rate in Multi-Regime Combustion Processes Based on Numerical and Experimental Data of Laminar and Turbulent Flames* MA thesis (Technische Universität Darmstadt, Darmstadt, Mar. 2019).
2. Marx, F. *Modeling the Vapour-Liquid Equilibrium Sulfur Dioxide — Nitrogen with Equations of State* BA thesis (Technische Universität Darmstadt, Darmstadt, Sept. 2016).

Authors' Contribution

The present cumulative dissertation consists of five (I-V) research papers. The six researchers (1-6) listed below have contributed to these research papers:

1. **Falko Marx (F.M.)**
   Institute for Energy Systems and Technology, Otto-Berndt-Str. 2, 64287 Darmstadt, Germany
2. **Paul Dieringer (P.D.)**
   Institute for Energy Systems and Technology, Otto-Berndt-Str. 2, 64287 Darmstadt, Germany
3. **Benjamin Michel (B.M.)**
   Institute for Energy Systems and Technology, Otto-Berndt-Str. 2, 64287 Darmstadt, Germany
4. **Falah Alobaid (F.A.)**
   Institute for Energy Systems and Technology, Otto-Berndt-Str. 2, 64287 Darmstadt, Germany
5. **Jochen Ströhle (J.S.)**
   Institute for Energy Systems and Technology, Otto-Berndt-Str. 2, 64287 Darmstadt, Germany
6. **Bernd Epple (B.E.)**
   Institute for Energy Systems and Technology, Otto-Berndt-Str. 2, 64287 Darmstadt, Germany

For each of these papers, the authors' contributions are defined within the paper itself. These original authors' contributions are listed below. Contributions by the author of this dissertation (F.M.) are marked in bold font. For term explanation, please refer to the CRediT taxonomy. Three of the five research papers (research paper I., II., and IV.) are also part of a second cumulative dissertation by Paul Dieringer.

I. **Research Paper** Process Control Strategies in Chemical Looping Gasification – A Novel Process for the Production of Biofuels Allowing for Net Negative CO2 Emissions
Paul Dieringer, Falko Marx, Falah Alobaid, Jochen Ströhle and Bernd Epple
Author Contributions: conceptualization, J.S. and P.D.; methodology, P.D.; writing - original draft preparation, P.D.; writing - review and editing, **F.M.**, J.S. and F.A.; visualization, P.D.; supervision, B.E.

II. **Research Paper** Design of a $1\,\mathrm{MW_{th}}$ Pilot Plant for Chemical Looping Gasification of Biogenic Residues
Falko Marx, Paul Dieringer, Jochen Ströhle and Bernd Epple
Author Contributions: conceptualization, **F.M.**, J.S. and P.D.; simulation, P.D. and **F.M.**; writing - original draft preparation, **F.M.**; writing-review and editing, P.D., J.S. and **F.M.**; visualization, **F.M.** and P.D.; supervision, B.E.

III. **Research Paper** Solid flux measurement in dual fluidized bed processes based on solid samples
Falko Marx, Paul Dieringer, Jochen Ströhle and Bernd Epple
Author Contributions: **F.M.**: conceptualization, methodology, investigation, software, writing - original draft, writing - review & editing, visualization. P.D.: investigation, software, writing - review & editing. J.S.: writing - review & editing, project administration, funding acquisition. B.E: supervision, funding acquisition

IV. **Research Paper** Design and Control Concept of a $1\,\mathrm{MW_{th}}$ Chemical Looping Gasifier Allowing for Efficient Autothermal Syngas Production
Paul Dieringer, Falko Marx, Benjamin Michel, Jochen Ströhle, Bernd Epple
Author Contributions: P.D.: conceptualization, methodology, investigation, data curation, writing - original draft, visualization. **F.M.**: writing - review & editing, methodology, investigation, data curation. B.M.: investigation. J.S.: writing - review & editing, supervision, project administration, funding acquisition. B.E.: resources, funding acquisition.

V. **Research Paper** Process Efficiency and Syngas Quality from Autothermal Operation of a $1\,\mathrm{MW_{th}}$ Chemical Looping Gasifier with Biogenic Residues
Falko Marx, Paul Dieringer, Jochen Ströhle and Bernd Epple
Author Contributions: **F.M.**: conceptualization, investigation, data curation, software, writing - original draft, writing - review and editing, visualization; P.D.: investigation, data curation, software, writing - review and editing; J.S.: writing - review and editing, project administration, funding acquisition; B.E.: supervision, funding acquisition

Erklärungen laut Promotionsordnung

§ 8 Abs. 1 lit. c PromO

Ich versichere hiermit, dass die elektronische Version meiner Dissertation mit der schriftlichen Version übereinstimmt.

§ 8 Abs. 1 lit. d PromO

Ich versichere hiermit, dass zu einem vorherigen Zeitpunkt noch keine Promotion versucht wurde. In diesem Fall sind nähere Angaben über Zeitpunkt, Hochschule, Dissertationsthema und Ergebnis dieses Versuchs mitzuteilen.

§ 9 Abs. 1 PromO

Ich versichere hiermit, dass die vorliegende Dissertation selbstständig und nur unter Verwendung der angegebenen Quellen verfasst wurde.

§ 9 Abs. 2 PromO

Die Arbeit hat bisher noch nicht zu Prüfungszwecken gedient.

Darmstadt, 2024-01-19

F. Marx

List of Figures

List of Tables

Abbreviations

AR	air reactor
ASU	air separation unit
CAPEX	capital expenditures
CCS	carbon capture and storage
CCU	carbon capture and utilization
CCUS	carbon capture and utilization/storage
CFB	circulating fluidized bed
CFD	computational fluid dynamics
CGE	cold gas efficiency
CLC	chemical looping combustion
CLG	chemical looping gasification
CLOU	chemical looping with oxygen uncoupling
d.b.	dry base
DFBG	dual fluidized bed gasification
FR	fuel reactor
FT	Fischer-Tropsh
GC	gas chromatography
GHG	greenhouse gas
HAZOP	hazard and operability study
HTW^{TM}	High Temperature Winkler
IEA	International Energy Agency
IPCC	Intergovernmental Panel on Climate Change
IWP	industrial wood pellets
KPI	key performance indicator
MSW	municipal solid waste
NPP	net primary production
OC	oxygen carrier
OPEX	operational expenditures

OSR	oil seed rape
PA	proximate analysis
PFR	pine forest residue
PSD	particle size distribution
PV	photovoltaic
RDF	refuse derived fuel
SNG	synthetic natural gas
SRC	short rotation crop
SRF	solid recovered fuel
TGA	thermo-gravimetric analysis
TRL	technology readiness level
UA	ultimate analysis
WSP	wheat straw pellets

Symbols

E	energy	J
LHV	lower heating value	$\mathrm{MJ\,kg^{-1}}$, $\mathrm{MJ\,mol^{-1}}$
M	molar mass, atomic mass	$\mathrm{g\,mol^{-1}}$
R_{OC}	oxygen transport capacity	
X_C	carbon conversion	
X_{SG}	syngas content	
X_S	oxidation degree	
Y_{SG}	syngas yield	$\mathrm{Nm^3/kg}$
ϕ	oxygen carrier to fuel equivalence ratio	
$\dot{m}$	mass flow	$\mathrm{kg\,s^{-1}}$
$\dot{n}$	molar flow	$\mathrm{mol\,s^{-1}}$
η_{CG}	cold gas efficiency	
λ	air to fuel equivalance ratio	
m_{tar}	tar load	$\mathrm{g\,m^{-3}}$
w	mass fraction in solid phase	
x	mole fraction	

Subscripts

AR	air reactor
FR	fuel reactor
FS	feedstock

OC	oxygen carrier
out	stream leaving reactor
ox	oxidized
red	reduced
ter	terestrial

1 Introduction

In view of human activity being the main contributor to the current climate change, most governments signed the Paris Agreement [1], which emphasizes the need for a drastic reduction of fossil carbon emissions to the atmosphere. It articulates the immediate requirement to radically reduce the amount of emissions of greenhous gases (GHGs) to the atmosphere which have increased dramatically with human industrial activity since 1750 [2]. Although the necessity to reduce the amount of GHGs released to the atmosphere has been internationally recognized with the Kyoto Protocol [3] since 1997, emissions are still increasing [2, 4, 5]. However, the rate of increase has slowed in the last decade [2, 5]. The main contributing factors of this slowdown are the reduction of emissions in industrialized nations and the slowdown of economic growth in China [2]. Nonetheless, the Intergovernmental Panel on Climate Change (IPCC) assessed the current reduction rate and policy to be insufficient to limit global warming to $1.5\,^{\circ}\mathrm{C}$ [5, pp.57], indicating the need of increasing GHG emission reduction efforts.

Reduction of GHG emissions can be done through decreasing the amount of energy consumed or the deployment of technologies which reduce the amount of GHG emissions per unit of energy produced. Although the path of reducing consumption has been advocated since shortly after the Second World War (e.g. [6]), humanity has increased its activities and average living standards ever since [7, 8]. Therefore, it is very unlikely that consumption will fall in a world with a growing population and increasing wealth. Since reducing energy consumption means significantly reducing production, it is clear that technological solutions must be part of any transition to a sustainable future. In fact, currently modelled pathways to a sustainable $1.5\,^{\circ}\mathrm{C}$ future all involve reducing atmospheric GHG concentrations [5] by either technological or forestry means.

There is a technological aspect to reducing energy consumption in the form of increased efficiency at all stages from energy production to final consumption. However, reduction only by increasing efficiency will likely not reach the goal and might even free up capital for further industrial activity and corresponding higher GHG emissions, leading to a rebound effect[1]. In many cases the option of increased efficiency is also economically interesting as increased efficiency, usually at the cost of higher capital expenditures (CAPEX), reduces the operational expenditures (OPEX). Other pathways offering the possibility of a reduction of GHG emissions are the deployment of carbon capture and utilization/storage (CCUS) technologies and the switch to non fossil energy resources. A combination of high efficiency coupled with the deployment of CCUS technology and the switch to renewable energy sources is a possible route to limit GHG emissions and thus the global

[1] Interestingly enough the rebound effect, also called Jevons paradox, was first observed and described by William Stanley Jevons on an energy related topic: He observed the increase of coal usage in England after James Watt introduced his more efficient steam engine [9]. While this may not be true for industrialized societies, it is still relevant for developing countries.

temperature increase. For the production of heat and electricity the deployment of carbon capture and storage (CCS) technologies is an option to continue the exploitation and combustion of fossil carbon reservoirs. This route reduces emission at centralized sites of carbon emissions and all end use cases can thus profit from reduced climate impact, becoming carbon neutral without any adaption. Fixing the carbon into value added products via carbon capture and utilization (CCU) offers the same short term advantages as CCS. Nonetheless, most products end up being used for a limited amount of time or are consumed during usage and can therefore not be considered as permanently fixing sinks for the embedded carbon. Instead, the carbon used in the products is later released into the atmosphere through various pathways.

For all applications where electrification is possible, the switch to renewable energy sources can be made utilizing electrical energy from wind turbines or photovoltaic (PV), instantly reducing the related GHG emissions. However, there are hard-to-electrify applications, such as maritime transport and aviation where different options have to be considered. Moreover, GHG emissions in the transport sector increased in the last years even for regions where overall emissions dropped, e.g. in the European Union [10]. Furthermore, the chemical industry still needs a constant and reliable source of carbon for the production of base chemicals and subsequent products. Here, the switch to non-fossil sources is only possible by using biogenic or recycled carbon instead of fossil carbon. The utilization of CO_2 [11] and energy or the utilization of waste streams (e.g. refuse derived fuel (RDF), solid recovered fuel (SRF), municipal solid waste (MSW) with some biogenic fraction) [12–14] are often described as the pathways to close the carbon cycle. Nonetheless, these material streams need to be supplemented with an additional, renewable carbon source to account for inevitable losses, of which biomass is the only form containing a major fraction of carbon [15] in non-oxidized form. Hence, biomass is the only remaining make-up source of carbon for the chemical industry.

Nonetheless, it is stated in the Paris Agreement [1] that no measure to reduce GHG emissions should impact the food supply. As such, only biogenic residues coming from agriculture (e.g. straw) or foresting are an option for the provision of carbon and for the bunkering of solid feedstocks for energy demands. Technologies or process chains utilizing these biomasses as energy or carbon source are inherently carbon neutral, releasing the same amount of carbon to the atmosphere that has been fixed by photosynthesis during plant growth. If these biomass technologies are combined with CCS, the overall process or technology becomes carbon negative removing carbon from the atmosphere as required for all sustainable scenarios described by the IPCC [5]. In theory, direct air capture is an alternative for removing CO_2 from the atmosphere, but practical application requires energy input, whereas biomass processes provide energy. Moreover, the IPCC assesses that carbon dioxide recovery from biomass processes will be necessary to compensate for residual carbon emissions in a net negative future to limit global warming below $1.5\,^{\circ}\mathrm{C}$ [16, p. 85]. Nonetheless, critical voices say that biomass based CCS technologies will not necessarily perform as adequately as required [17]. Therefore, a key parameter in limiting global warming is the development of biomass-based processes with inherent CO_2 capture at pilot and demonstration scale. Gasification is a promising option for converting biomass into easily storable energy and carbon carriers that can be integrated with carbon capture. A very efficient gasification

process is chemical looping gasification (CLG), which provides a nitrogen-free syngas for further processing into liquid fuels or base chemicals. Here, autothermal operation, i.e. without external reactor heating, is required to develop the process for commercial application.

The technical development of CLG towards pilot scale is described in this cumulative dissertation which is structured as follows. At first, in Section 1.1 biomass energy potential is assessed and how much of it is available for usage in biomass processes. This is compared to the current and projected utilization. Afterwards, an overview of possible processes for the valorization of the available bioenergy is provided in Section 1.2 with an emphasis on thermo-chemical conversion and gasification technologies in particular. Section 1.3 discusses the state of development of the CLG technology from which the research questions in Section 1.4 are derived. Chapter 2 contains the synthesis of the research papers included in this cumulative dissertation highlighting the progress towards autothermal CLG process operation. Section 2.4 and Section 2.5 contain a conclusion of the main results from the CLG experiments and and an outlook on further investigations respectively. The research papers are included in Chapter 3.

1.1 Biomass Energy Potential and Utilization

Biomass is a natural storage of energy and comes in the form of plant based biomass (primary biomass) and animals and their excrements (secondary biomass). For energetic purposes primary biomass is of higher interest as it makes up the majority of biomass. Nonetheless, manure, and other secondary biomasses, can be utilized through various technologies.

1.1.1 Global Biomass Potential

The global potential of biomass as an energy resource is vast. A very rough estimate of the theoretically available biomass energy can be calculated from the annual carbon fixation by photosynthesis, called net primary production (NPP). The NPP is estimated to be in the range[2] of $40\,\mathrm{Pg\,C\,yr^{-1}}$ to $66\,\mathrm{Pg\,C\,yr^{-1}}$ for terrestrial surfaces by various models including water availability with a mean of $54.9\,\mathrm{Pg\,C\,yr^{-1}}$ [18]. More current reviews and simulation come to a conclusion of $(56.4 \pm 9.0)\,\mathrm{Pg\,C\,yr^{-1}}$ [19] and $54.57\,\mathrm{Pg\,C\,yr^{-1}}$ [20] respectively. As approx. half of the biomass is carbon [21], and with an average lower heating value (LHV) of $18\,\mathrm{MJ\,kg^{-1}}$ the estimate results in:

$$E_{ter} = NPP \cdot 2 \cdot LHV = 56.4\,\mathrm{Pg\,C\,yr^{-1}} \cdot 2 \cdot 18\,\mathrm{MJ\,kg^{-1}} = 2030.4\,\mathrm{EJ\,yr^{-1}}$$

Additionally, biomass is produced in the ocean with an NPP estimated to be $48.5\,\mathrm{Pg\,C\,yr^{-1}}$ [22] giving a total yearly energy of $E = 3776\,\mathrm{EJ\,yr^{-1}}$ fixed by biomass which is a bit lower than the $4500\,\mathrm{EJ\,yr^{-1}}$ stated by Sims [23].

[2] The unit $\mathrm{Pg\,C\,yr^{-1}}$ (Peta gram carbon per year) is commonly used to asses biomass production.

Table 1.1: Listing of literature estimating energy potential from biomass sources

Potential 2050 in $\mathrm{EJ\,yr^{-1}}$	Remarks	sources	Year
126 to 216	considers water constraints	[26]	2011
367 to 1548	optimistic assumptions on available biomass and technology	[27]	2007
	optimistic assumptions on technology availability, irrigation and agricultural yield in developing countries		
160 to 270	conservative assumptions on agricultural yield	[28]	2010
approx. 250	conservative assumptions on agricultural yield	[29]	2013
200 to 600	herbaceous energy crops competing with food crops	[30]	2014
149 to 245	considers impact of environmental policy and socio economic transformation	[31]	2019
200 to 500	considers water, food demand and biodiversity protection	[32]	2010
58 to 180	data based on remote sensing of vegetation, considers accessibility	[25]	2012
300	critical review of assumptions in current estimates	[33]	2014
64 to 312	considers impact of dietary habits and yield improvements	[34]	2023

However, human focus is on terrestrial biomass, more specifically the above ground NPP, and there is disagreement on how much energy can be supplied by biogenic sources sustainably. In their 2009 literature review Ladanai & Vinterbäck [24] come to the conclusion that the biomass potential in 2050 is larger than the projected world primary energy consumption (approx. $1000\,\mathrm{EJ}$) so long as political support is sufficient and infrastructure investment is ramped up. However, they mention that much difference in assumptions about yield increase in agriculture and population increase and the corresponding availability of arable land for energy production can be found in the reviewed literature. An overview of different studies is given in Table 1.1 and shows the range estimated for future biomass energy supplies. It should be noted that the high estimates assume average yields which are comparable to today's top values. Moreover, even the lower range studies assume the conversion of land areas the size of Europe or larger [25] to supply the estimated energy.

Given the estimate that approx. $23\,\%$ to $25\,\%$ of terrestrial NPP is already appropriated by humans in various forms [35, 36], increases in biomass energy usage will have a noticeable impact on ecosystems. The actual harvested biomass accounts for approx. $300\,\mathrm{EJ\,yr^{-1}}$ from which about $100\,\mathrm{EJ\,yr^{-1}}$ are directly lost as unused residues or roots left under ground [35]. The addition of another $250\,\mathrm{EJ\,yr^{-1}}$ in bioenergy harvest, which is in the range of most bioenergy potential studies, would increase the utilization of NPP by humans to $44\,\%$ [36]. The lowest impact would be achieved by the utilization of the available residues which are in the range of $58\,\mathrm{EJ\,yr^{-1}}$ to $100\,\mathrm{EJ\,yr^{-1}}$ [25, 35] and are accessible and produced anyway.

1.1.2 Biomass Utilization

The actual utilization of biomass for energy purposes including projections for demand in 2050 can be seen in Figure 1.1. Considering the $100\,\mathrm{EJ\,yr^{-1}}$ projected by the International Energy Agency (IEA) [37] are lower

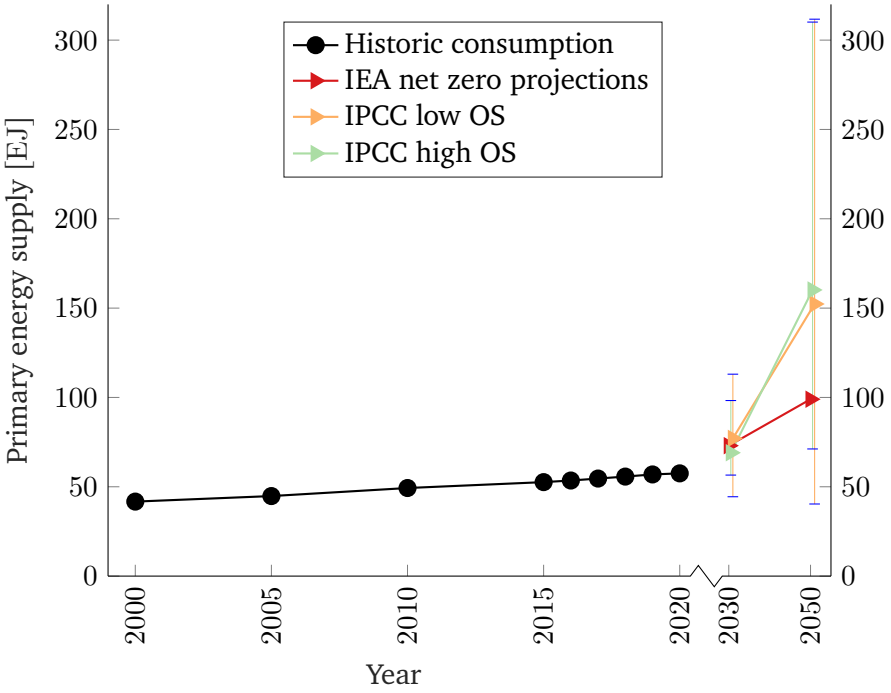

Figure 1.1: Primary energy from biomasses [40] and projections from IEA (net zero) [37] and IPCC review [38] of $1.5\,^{\circ}\mathrm{C}$ scenarios with high and low overshoot.

than most of the results from studies listed in Table 1.1 enough biomass seems to be available to satisfy demands in the future. However, the IPCC notes that a lot of studies on future energy demand/supply limit biomass to a maximum of $100\,\mathrm{EJ\,yr^{-1}}$ [16, p. 309]. In fact, an analysis of over 80 scenario pathways modelled to lead to a $1.5\,^{\circ}\mathrm{C}$ temperature increase showed up to $312\,\mathrm{EJ\,yr^{-1}}$ (median approx. $160\,\mathrm{EJ\,yr^{-1}}$) of bioenergy demand in 2050 [38]. This is at the upper limit of most availability studies making more conservative assumptions and might not be available sustainably. As Reid *et al.* [39] note, bioenergy plantations compete with food production for land and might therefore not be socio-economically feasible and biomass might also not benefit from learning curves as much as PV or wind which have much lower land requirements. Hence, bioenergy from residues might be the only option for sustainable bioenergy.

Consolidating the information on projected available bioenergy and energy demand leads to the conclusion that technology efficiency is key to maximize the valorization of this scarce resource. Therefore, the future role for biomass is likely to provide make-up carbon to chemical industries for the production of base chemicals and to account for losses in the carbon cycle instead of being burned for heat and power generation. As such, traditional biomass usage (heating and cooking with open fire or simple stoves) plays no role in future energy scenarios (eg. [37]). Instead, modern biomass usage (biofuels, biorefineries, biogas through anaerobic digestion, efficient wood pellet heating, etc.) feature in those scenarios. Nonetheless, the likelihood of total abandonment of traditional bioenergy usage until 2030 as in the net zero roadmap by the IEA [37] seems

very slim as about 2×10^9 people use traditional biomass for cooking today [37] and would have to switch to other means in only 7 years.

For efficient valorization, conversion processes have to be optimized for the combination of feedstock and application, which creates a research need for conversion processes – like gasification – for the utilization of biogenic carbon for synthesis of base chemicals or liquid energy carriers. Moreover, many technologies are at a low technology readiness level (TRL) and require advancement to be able to deploy the developed, market-ready processes to commercial operation.

1.2 Biomass Utilization Technologies

In order to optimize the utilization of the available biomass, the biogenic source material, the conversion process, and the intended end-use has to be selected in such a way that losses are minimized. Therefore, only modern bioenergy applications are described in the following. Additionally, the distribution of source material towards application has to be considered. For some applications, only certain biogenic sources are viable and even compete with high carbon footprint materials (e.g. wood competing with concrete for construction), other applications have multiple possible sources (e.g. wood, municipal waste, and sewage sludge for thermal energy). Therefore, only leftover residue woods which are not required or usable for construction should be considered for thermal conversion [39]. However, it is likely that market prices will play a role in the distribution and selection of biogenic sources for processes and end-use [39].

The processes for the conversion of biogenic sources into thermal energy or different valuable products (e.g. syngas, ethanol, bio-diesel) can be classified into three main categories based on their properties.

- Physico-chemical conversion utilizes mechanical force or pressure to extract part of the plant biomass as an high calorific oil.
- Bio-chemical conversion utilizes micro-organisms to convert part of the feedstock to high calorific gaseous or liquid form.
- Thermo-chemical conversion utilizes elevated temperatures to convert part of the feedstock to high or medium calorific liquids, gases, and solids.

Figure 1.2 shows the categories and the included processes with the applicable biomass feedstocks and the resulting converted products. Some biomasses can be efficiently used as solid fuels without prior processing which is also indicated in Figure 1.2. The remaining categories are the agricultural and industrial/domestic waste and residue and the residues from foresting which can be utilized without impacting other areas. Nonetheless, some energy crops might be used when switching from traditional bioenergy to modern bioenergy.

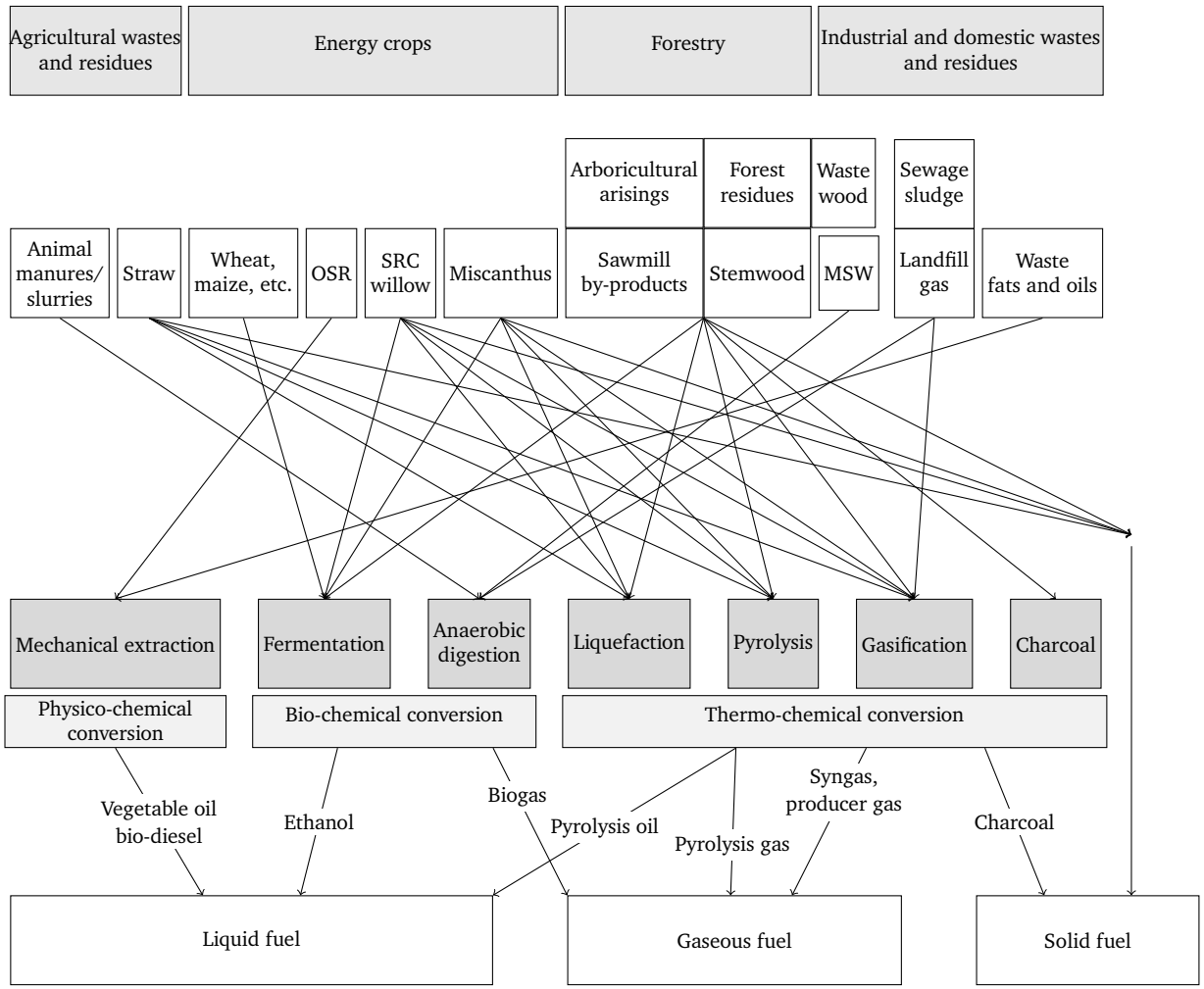

Figure 1.2: Schematic of biomasses and utilization routes adapted from [41]. OSR: oil seed rape, SRC: short rotation crop, MSW: municipal solid waste.

1.2.1 Physico-Chemical Conversion

Physico-chemical conversion for the production of bio-fuels or as a biogenic source of carbon for the chemical industries consists mainly of mechanical extraction of plant seed oil often paired with an esterification step to produce bio-diesel (fatty acid methyl ester) [42]. The residue of the seed, the oil meal cake, contains about 5 wt.-% of oil [43] and is often used as animal feed [41, 43]. In Europe the main biogenic source utilized with this route is oil seed rape (OSR) [44].

While the extracted product contains the major part of the plant energy, there is still some amount of plant energy contained in the meal, the straw and glycerine as byproduct from esterification [45]. However, the energy contained in the straw and meal can be utilized with a different conversion technology and glycerine is already a valuable reactant in the chemical industry. As OSR and other oil plants are specifically grown for

energy production, they compete with food production for land use and might therefore be in conflict with the demand of the Paris Agreement to not impact food supply [1].

1.2.2 Bio-Chemical Conversion

The two commercially successful processes utilizing micro organisms are anerobic digestion and fermentation. While the valuable product of anerobic digestion is gaseous, fermentation yields a liquid product. As both are already at a commercial level, the TRL has to be considered at level 9. Both processes can be used with biogenic wastes with up to $90\,$wt.-% moisture [46] and are therefore a good option to treat wet residues. However, they cannot completely convert materials with high content of lignin [41] and are therefore not a good option for the conversion of woody biomass.

Anaerobic Digestion

Anaerobic digestion utilizes bacteria to convert lignin free biomass in an oxgen free atmosphere into a gas consisting mainly of CH_4 and CO_2 with small amounts of CO and H_2S [46]. However only $20\,\%$ to $40\,\%$ of the energy content is available in the gas phase [46] with the rest remaining in the slurry which can be either used as fertilizer [41] or be utilized through thermochemical conversion routes.

Fermentation

Fermentation is the conversion of sugars to liquid ethanol utilizing yeast. Sugars can come from various biogenic sources (sugar cane, sugar beet) including starch (potato, wheat, maize) which can be converted to sugar. It is possible to produce sugars from cellulose by hydrolysis [21] and reports on special yeast for fermentation of celluloses exist (e.g. [47, 48]), however, this is not yet commercialized. The resulting ethanol water mixture requires an energy intensive distillation step to separate the ethanol from the water. The solid residues can be used as cattle feed or through various thermochemical routes [41].

1.2.3 Thermo-Chemical Conversion

Thermo-chemical conversion processes produce a mixture of gaseous, liquid and solid products. The distribution of the biomass mass into these fractions is influenced by the process parameters temperature, pressure, residence time and oxygen input.

Thermo-chemical conversion processes can be classified by the oxygen to fuel equivalence ratio λ under which they are operated. Figure 1.3 shows the approximate operation regions of the thermochemical conversion processes in terms of λ and temperature. Combustion processes feature $\lambda > 1$ with heat being the single product intended as all feedstock is fully converted in ideal operation. Gasification processes operate usually at the lower side of the range of $0 < \lambda < 1$ and aim to maximize either the conversion of feedstock material into the gas phase or the feedstock energy inside the gas phase as the product gas is used in subsequent application.

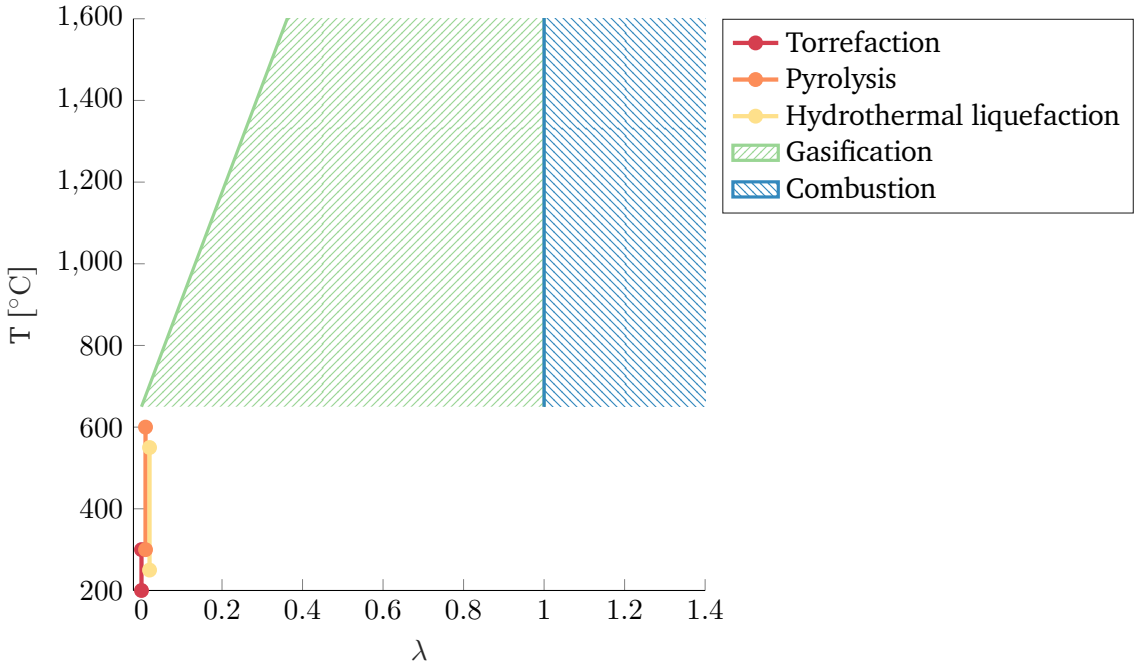

Figure 1.3: Map of thermal conversion technologies in terms of temperature and oxygen to fuel ratio.

Pyrolysis, torrefaction and hydrothermal liquefaction operate at $\lambda = 0$ with the goal of converting the feedstock into liquid products (pyrolysis, liquefaction) and/or (densified) solid fuels (pyrolysis and torrefaction). For pyrolysis, hydrothermal liquefaction and torrefaction, the required process heat has to be supplied externally while for gasification and combustion it is provided through the (partial) oxidation of the feedstock. As all thermochemical processes work at elevated temperatures well above the boiling point of water, the feedstock must contain relatively low amounts of moisture for economic process operation. The exception here is hydrothermal liquefaction which operates with high moisture content and under pressure.

Torrefaction

Torrefaction is the externally heated thermal treatment of solid biomass under oxygen free conditions ($\lambda = 0$) at temperatures between approx. $200\,^{\circ}\mathrm{C}$ to $300\,^{\circ}\mathrm{C}$ [49] braking down biomass structure. Residence times are $15\,\mathrm{min}$ to $90\,\mathrm{min}$ at atmospheric pressure with the aim of enhancing the feedstock quality for combustion as well as storage and transportation capability. During the process approx. $10\,\%$ of energy and $30\,\%$ of the feedstock mass are lost as gases [50] (mainly acetic acid, methanol, CO, CO_2 [49, p. 96]) giving a dry, solid fuel with increased energy density.

Hydrothermal Liquefaction

Hydrothermal liquefaction is the depolymerization of wet biomass under elevated pressure ($5\,\mathrm{MPa}$ to $20\,\mathrm{MPa}$) and temperature ($250\,^{\circ}\mathrm{C}$ to $550\,^{\circ}\mathrm{C}$) [41]. The product is a liquid bio-crude with a higher heating value of

$30\,\mathrm{MJ\,kg^{-1}}$ to $37\,\mathrm{MJ\,kg^{-1}}$ [49, p. 332] which can be distilled and used like mineral oil. Side products are a CO_2 rich gas phase, an aqueous phase containing some organics, and, depending on the process, char [49, p. 332]. As feedstocks can be wet and are processed in the form of slurries, hydrothermal liquefaction has the advantage of not requiring a complete drying of the feedstock.

Pyrolysis

Pyrolysis is a thermal process for the decomposition of biomass (or waste) into a solid and a liquid fraction. It is operated in the absence of oxygen ($\lambda = 0$) and in the temperature range of $300\,^{\circ}\mathrm{C}$ to $600\,^{\circ}\mathrm{C}$ with externally supplied heat. The distribution of products to the three phases solid, liquid, and gas can be influenced with temperature, heating rate, pressure and residence time [41, 51] to optimize the yield of the intended product. While higher temperatures [52] and higher heating rates with low residence times [41] favour the production of liquids, lower heating rates and low temperature lead to increased char and gas production [41].

Gasification

Gasification is the conversion of solid feedstock into gaseous products with the oxidation of a small part of the feedstock to supply the required energy. It is normally operated at temperatures above $650\,^{\circ}\mathrm{C}$ with atmospheric or elevated pressure and either with an air or steam-oxygen atmosphere with $0 < \lambda < 1$. The product is a combustible gas consisting of mainly H_2, CO, CH_4, CO_2, H_2O, and in the case of air-blown gasification also N_2. The produced gas is subsequently used for combustion or chemical synthesis. Depending on the gasification process and the operation temperature, up to $95\,\%$ of the feedstock energy are transferred to the gas phase. There exist three main gasifier types:

- **Fixed bed gasifiers** show low heating rates and long feedstock residence times. The feedstock is introduced at the top of the reactor and slowly moves downwards by gravity as feedstock in the lower part of the reactor is converted into the syngas. Initial drying happens at the top of the reactor followed by pyrolysis and gasification and the ash being removed from the bottom of the reactor. The reactor temperature can exceed the ash softening temperature of the feedstock in case equipment to remove larger agglomerates is present [15]. The gas flow can be either in the opposite direction as the solid stream (counter-flow) or in the same direction (co-flow). While the counter-flow configuration is easy to implement, it produces more heavy hydrocarbons and tars as the pyrolysis products do not pass the higher temperature zones [15]. Feedstock particle size for the fixed bed gasifier is between $6\,\mathrm{mm}$ to $50\,\mathrm{mm}$ [15]. Herbaceous biomasses like miscanthus or straw require densification to bricketts to be able to gasify them in a fixed bed reactor [15].

  Fixed bed gasifiers have been commercially operated for many years converting coal to syngas for the production of Fischer-Tropsh (FT)-products and base chemicals [15]. Especially the Sasol-Lurgi dry bottom process, a steam-oxygen process where the ash is removed in a dry state at the bottom, is very

successfully deployed with over 80 units world wide [15]. Part of the success comes from the fact that it was the first pressurized gasifier available [15]. The British-Gas-Lurgi process is an extension of the Lurgi-Process where the ash is removed as molten slag with the aim of creating higher amounts of CO and H_2 with less steam input and accepting different (e.g. MSW) and finer feedstocks [15]. The Lurgi process has been developed and tested to pressures of up to $90\,\mathrm{bar}$ [15].

- **Fluidized bed gasifiers** exhibit good mixing of solids and gas, high heating and mass transfer rates and medium feedstock residence time. The feedstock is either introduced on the top or inside the dense region of the fluidized bed with drying and pyrolysis happening very fast inside the fluidized bed. The gasification agent is introduced at the bottom of the reactor and also acts as the fluidization medium. Feedstock ash is removed from the bottom and contains a fraction of unconverted carbon due to the well mixed properties of the bed [15]. To avoid agglomeration and the following defluidization of the bed, fluidized bed gasifiers have operating temperatures below the ash softening point. Bed materials include feedstock ash [53], sand, and natural minerals like olivine and ilmenite [54–56]. The feedstock particles size is $1\,\mathrm{mm}$ to $10\,\mathrm{mm}$ [15] to avoid them falling to the bottom of the fluidized bed or being entrained before conversion. Highly reactive feedstocks like biomass [15] are considered optimal for fluidized bed gasifiers.

  The fluidized bed gasifier developed by Fritz Winkler was the first fluidized bed process and can accept a very wide range of feedstocks and more than 70 reactors have been build and operated world wide [15]. Several enhancements like High Temperature Winkler (HTW^{TM}) gasification have been developed where pressure has been raised to $30\,\mathrm{bar}$ and a cyclone has been added for higher char conversion [15] and are still the focus of ongoing research [53]. More recent developments change the operation regime of the fluidized bed from the bubbling bed used in the Winkler process to a circulating fluidized bed (CFB) like the Lurgi CFB gasifier or the transport gasifier by Kellogg Brown & Root (KBR) [15]. Most of these developments also aim to change either a part of the feedstock or the full feedstock from coal to biomass or waste [15].

  The last twenty years have seen the emergence of gasification processes utilizing two interconnected CFBs called dual fluidized bed gasification (DFBG) [56–58] and chemical looping gasification (CLG) [59, 60]. DFBG operates with two fluidized bed reactors. In the gasification reactor the feedstock is gasified in the absence of molecular oxygen, using steam as the gasification agent. The necessary heat for gasification is then supplied by a bed material (e.g. sand) which circulates between the reactors and is heated in the combustion reactor. Unconverted residual feedstock char is carried with the bed material from the gasification reactor to the combustion reactor. There, it is incinerated, providing the energy to heat the bed material. The CLG process operates similarly, using a metal oxide called oxygen carrier (OC) to transfer heat to the gasification reactor (called fuel reactor (FR)) where the oxygen carrier (OC) is reduced, supplying lattice oxygen to the gasification reactor. The bed material is subsequently reheated via the exothermic re-oxidation of OC inside the air reactor (AR) providing the required energy.

However, this type of gasifier has not been deployed to a scale larger than $20\,\mathrm{MW}$ [58] and is not yet commercially successful on the same level as other technologies, as it primarily supplies heat and power [57].

- **Entrained flow gasifiers** have the highest heating rates and short feedstock residence time. Feedstock and gasification medium are introduced at the same reactor end and the gasification agent transports the feedstock particles pneumatically through the reactor. Operation temperature is in the range of $1250\,^{\circ}\mathrm{C}$ to $1600\,^{\circ}\mathrm{C}$ and always above the ash melting point and the ash is therefore removed as slag. Almost all carbon is converted into the gas because of the full conversion of feedstock to either liquid slag or syngas species. Because of the pneumatic transport and the short residence time, feedstock particles must be small ($<100\,\mu\mathrm{m}$ [15]) which requires milling. The required milling, which is not yet economically feasible for biomass [15, 49], and the aggressive nature of molten biomass ash [15, 49] make biomass a very difficult feedstock for this gasifier type.

  Commercially successful entrained flow gasifiers have been build by Shell, Siemens, GE Energy and others [15]. They typically operate at elevated pressure with coal as feedstock [15]. A recent design is the OMB process from the Institute of Clean Coal Technology (ICCT) at the East China University of Science and Technology [15]. The endeavour to commercialise an entrained flow gasifier for biomass feedstocks, undertaken by Choren, proved to be unsuccessful in the end and resulted in the company going bankrupt [61].

Combustion

Combustion takes place under oxygen surplus atmosphere ($\lambda > 1$) to ensure the full release of the feedstock energy as thermal energy. Combustion temperature is between $650\,^{\circ}\mathrm{C}$ to $1600\,^{\circ}\mathrm{C}$ with heat being the intended product. Nonetheless, ash and flue gas are side products and need to be considered, as flue gas is commonly released to the atmosphere and ash has to be deposited or utilized somewhere. Due to energy loss, it is not optimal to convert biomass energy to electricity via combustion and then use the electricity for process heat. Therefore, biomass is better utilized directly for the generation of process heat and valuable chemical products. Nevertheless, combustion can be a valuable backup for power-generation when PV and wind cannot supply the required power. Biomasses with a moisture content below $50\,\mathrm{wt.\text{-}\%}$ dry base (d.b.) can be combusted directly while higher moisture content needs pre-drying [46]. Modern combustion for residential heating also utilizes part of the enthalpy of vaporization of the steam content inside the flue gas by cooling flue gases below the dewpoint temperature.

The combustion process can be integrated with a CO_2-separation step by supplying oxygen instead of air as the oxidizing agent to the process. This is called oxy-combustion when the molecular oxygen is provided by an air separation unit (ASU). Alternatively, the oxygen can be supplied via the chemical looping process in the form of lattice oxygen of a metal oxide (called oxygen carrier (OC)) which is regenerated in a separate reactor

by oxidation with air. This chemical looping combustion (CLC) process has the advantage of supplying the oxygen with a much lower energy penalty compared to the ASU. The resulting flue gas consists mainly of steam and CO_2, which can be utilised or sequestered.

1.2.4 Comparison

Comparing the different conversion technologies shows that thermo-chemical processes exhibit relatively high feedstock conversion and are suited for a wide range of feedstocks. Physico- and bio-chemical processes have lower feedstock conversion and have a smaller selection of possible feedstocks. Thermo-chemical processes are faster and can destroy and convert all biopolymers including lignin when compared to bio-chemical processes [41]. Currently, successful processes for producing liquid energy carriers utilize either bio-chemical or physico-chemical methods, converting feedstocks of sugar and starch to alcohol or extracting oils and fats respectively [62]. A downside to this is that transport fuels must be produced using lignocellulosic or waste biomasses as feedstock in compliance with the regulations of the European Union [63]. Thermo-chemical processes are better suited for this type of feedstock. However, to sustain high temperatures at an economical level, the plant size must be larger to obtain low relative heat losses. As biomass might not be available in the required quantity near the site of a thermo-chemical conversion facility higher transportation costs might offset the higher efficiency of the thermochemical process.

Of the thermo-chemical processes, gasification shows the most advantages for the provisioning of make-up carbon to the chemical industry as the product can be readily integrated into existing synthesis routes and/or be converted to methanol or FT products, a common base chemical and possible refinery inputs respectively. Moreover, it facilitates the conversion of waste materials into liquid energy carriers which can be handled more conveniently. Here, major interests are the gasification with steam or with steam/oxygen as gasification agents, as they lead to a N_2 free syngas. The oxygen used in gasification must be extremely pure to avoid mixing with inerts and diluting the syngas. Gaseous oxygen with a concentration of $99.9\,\text{vol.-\%}$, produced by a highly efficient cryogenic ASU, requires at least $1.2\,\mathrm{MJ\,kg^{-1}}$ of electric energy [64]. Considering an oxygen equivalence ratio of $\lambda = 0.25$, this energy demand is equivalent to a minimum of $2\,\%$ of the thermal input, which may have a significant impact on the economic feasibility. The absence of the inert N_2 allows for much smaller equipment bringing down CAPEX.

Particularly fluidized bed gasification processes are studied because of their suitability for biomass and the easy feedstock preparation. Especially the two-reactor setup of DFBG has seen increased research interest and endeavours to valorize the produced syngas in other ways than heat and power [54, 58] lately. DFBG separates the oxidation/combustion and the gasification reactions into two distinct reactors, eliminating the need for an energy-intensive ASU. The DFBG process can be enhanced by the replacement of the bed material with an OC, providing oxygen to the gasification via the chemical looping process without an ASU. CLG has seen high research activity in the past few years with multiple reviews discussing topics like OC development

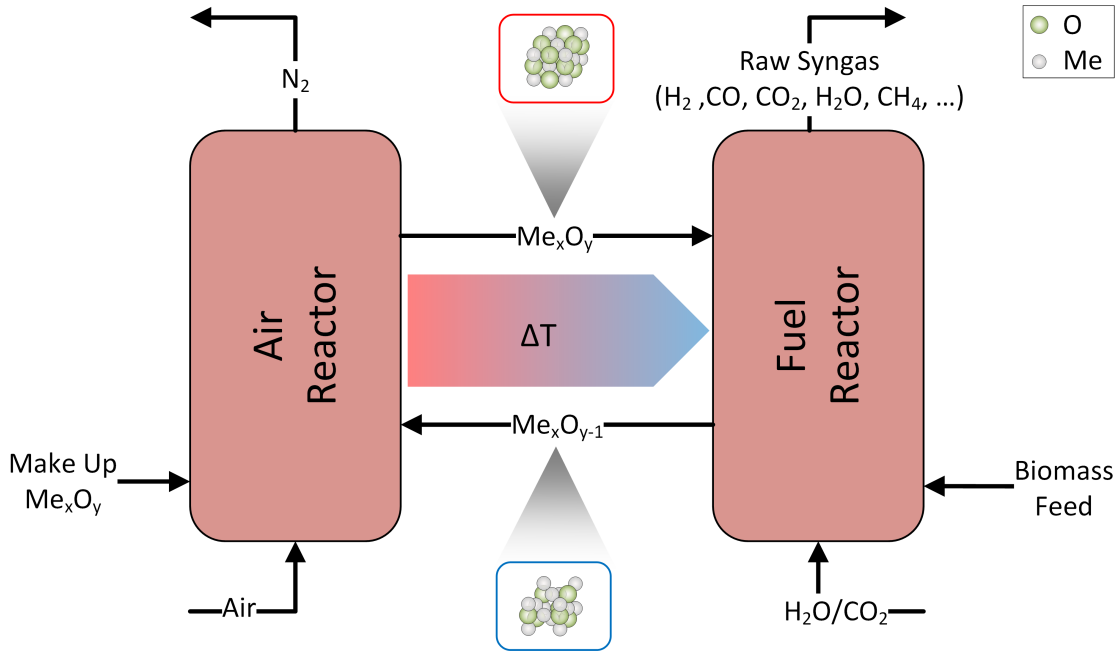

Figure 1.4: Schematic of the CLG process showing the cyclic reduction and oxidation of an OC material which is oxidized in the air reactor (AR) and reduced in the fuel reactor (FR).

[65–67], biomass in CLG [68–74], agglomeration in chemical looping [75], pollution removal [76], scale-up of biomass chemical looping [77], and pressurized chemical looping [78].

1.3 Chemical Looping Gasification

Chemical looping gasification (CLG) is a gasification process that utilizes a metal-oxide to supply lattice oxygen to the gasification process (see Figure 1.4). Inside the fuel reactor (FR) the gasification of the feedstock occurs with steam being the gasification agent and fluidization medium. During that process the metal-oxide also called oxygen carrier (OC) is reduced and thus supplies oxygen for partial feedstock oxidation inside the FR. The OC is then transported towards the air reactor (AR) where it is regenerated with air. This exothermic oxidation process generates the heat which is transported with the solid OC material from the AR into the FR and supplies the required heat for the endothermic gasification of feedstock carbon. Therefore, CLG can be considered to be an enhancement of the DFBG process which supplies only heat via an inert bed material. For DFBG this heat is generated by the combustion of residual feedstock carbon inside the AR, which is transported with the OC bed material. For the DFBG process there is operation experience in semi-commercial scale of $8\,\mathrm{MW}$ to $32\,\mathrm{MW}$ [56, 58, 79] laying a good foundation for the CLG process to build upon. The specific enhancements of CLG are:

- Concentration of carbon inside the gasifier (FR) off gas stream.
- Reduction of tar production inside the gasifier (FR).

- Elevation of gasification reactor (FR) temperature.

The concentration of the carbon into the output stream of one reactor is beneficial in case carbon credits can be sold [80] and wide-scale deployment of biomass CCS is required to limit global warming [5]. However, the reduction of tars—known to be high in biomass gasification [81]—is of utmost importance to practical application as they have an impact on the direct utilization or the required syngas cleaning. The elevation of gasifier temperature is caused by exothermic oxidation reactions inside the FR, facilitated by the OC which partially offset the endothermic gasification reactions. The temperature increase helps with tar reduction [82], higher feedstock carbon conversion inside the FR, and reduction of CH_4 content [15] but might not be possible for all feedstocks as the temperature must remain below the feedstock ash softening point in fluidized bed reactors.

So far CLG has been demonstrated to work in continuous lab scale units from $1.5\,\mathrm{kW_{th}}$ to $50\,\mathrm{kW_{th}}$ utilizing various biogenic residues as feedstock with natural minerals e.g. ilmenite [83, 84] and waste materials like steel converter slag [85, 86] as OC material. However, autothermal operation of the process has not been achieved and is a crucial step in upscaling the CLG process. Moreover, basic phenomena important for CLG are still being investigated and can also give valuable insight for the scale-up to autothermal operation.

1.3.1 Research in Chemical Looping Gasification

The research topics relevant for CLG span a wide range of topics but can be roughly sorted into the following categories:

- Feedstock
- Reaction kinetics
- Reactor design
- Gas quality
- Oxygen carrier (OC)
- Process control

with most of the published work dealing with more than one of these topics.

Feedstock Fluidized bed processes are operated well below the ash softening point to avoid agglomeration and thus defluidization. However, in practice exact ash softening points of seasonally varying biomass sourced from multiple locations vary depending on the composition [75]. Moreover, the temperature where defluidization occurs depends on the specific atmosphere and is much lower in steam or H_2 than in air or CO_2 [87, 88]. Especially herbaceous biomasses have very low ash deformation temperatures as measured by hot stage microscopy with values as low as $840\,^{\circ}\mathrm{C}$ for triticale straw [89]. Bed defluidization has been reported for even lower temperatures of $740\,^{\circ}\mathrm{C}$ for wheat straw in an olivine bed [90]. For woody biomass ash melting [89] and defluidization [90, 91] occur generally at higher temperatures, even above $1000\,^{\circ}\mathrm{C}$. However, higher

fluidization velocities increase the temperature—and correspondingly the melt-fraction of feedstock ash—at which defluidization occurs [75, 87, 92]. This is likely the reason why almost no defluidization is reported for continuous CLG operation. To mitigate defluidization at low temperatures, routes like feedstock blending [89] and pre-treatment options like leaching, additives [91, 93] and torrefaction [91] have been tested resulting in higher defluidization temperatures. Miao *et al.* [75] report in their recent review on agglomeration in biomass chemical looping, that feedstock related additives can only reduce agglomeration but not avoid it and mention emission related side effects of additives. Nonetheless, pre-treatment including washing/leaching and additivation of biomass feedstock can reduce agglomeration tendency in biomass ash-OC interaction and can therefore be considered for commercial application. Monitoring of pressure and temperature variance of the bed can be used to investigate the agglomeration behaviour of biomass-OC pairings in lab scale setups [91, 94–97] screening for good pairing candidates but also to provide early warnings of agglomeration during operation caused by changing feedstock ash properties [75].

Reaction Kinetics For the screening of OC materials and the determination of their reaction rates thermogravimetric analysis (TGA) offers a cheap setup to investigate the mass changes at various temperatures under controlled atmospheres. Additionally, feedstock reactions and even combined OC feedstock reactions under controlled atmosphere can be investigated. Wang *et al.* [98] discuss the limitations of TGA experiments compared to the fluidized bed experiments such as the slower heating rate, limited gas-solid contact, and heat and mass transfer limitations. Nonetheless, reaction kinetics can also be obtained from small scale fluidized bed reactors (e.g. [99]) and form an important basis for process modelling and computational fluid dynamics (CFD) simulations required for process optimization, equipment sizing, and reactor design. However, as the focus of this dissertation is experimental scale-up, further discussion of reaction kinetics is omitted.

Reactor Design The most widely adapted reactor configuration is the dual fluidized bed reactor as it features a uniform bed temperature, fast feedstock heating, and facilitates an easy transfer of the solid OC material between the reactors. Here, knowledge of actual solid circulation flows is important for equipment sizing. Another possible configuration is the combination of a fluidized bed as AR with a moving bed as FR [100, 101]. Nonetheless, different reactor designs have been proposed like packed bed reactors and rotating reactors, which cannot be used for solid feedstocks. However, in this dissertation only results from (dual) fluidized bed configurations are considered, as they can convert solid biomass feedstocks.

Gas Quality The composition of the produced gas is a topic of major interest as it determines potential applications and the required gas treatment, such as de-dusting, tar removal, water gas shift, and sour gas removal. Moreover, the total amount of combustible gases is directly proportional to the cold gas efficiency (CGE) (see Equation 1.2). Hence, gas compositions are usually reported by all authors focusing on CLG development and specific studies on volatile conversion for OC are conducted [102, 103]. Goel *et al.* [74] compare the yields of syngas species produced from different OC-feedstock pairings reported in literature

between batch reactor and continuous process. They show, that high yields in batch processes do not necessarily transfer to high yields in a continuous unit.

FR temperature has the most important influence on gas quality, where a higher temperature leads to lower tar production [82] and higher syngas production. However, the temperature must stay below the limits where agglomeration occurs inside the bed in order to keep the process stable. Additionally, the steam to biomass feedstock ratio, the amount of oxygen supply, the feedstock residence time, and the OC bed material circulation have an influence on the composition of permanent gases, tars, and the overall amount of the syngas. Generally, the tar content reported for continuous CLG operation is higher (e.g. [83, 85, 104–106]) than the maximal allowable contamination for most processes according to Milne *et al.* [81]. Produced CH_4 might be unwanted depending on the application. For synthetic natural gas (SNG) it is the intended product, while for methanol or FT-products it behaves like an inert and must be converted to syngas before entering the synthesis reactor (e.g. in a steam methane reformer[3]).

The important parameters for this dissertation regarding gas quality are the composition of gas species (volume fractions x_i), the syngas fraction X_{SG} (Equation 1.1), describing the fraction of the intended product in the permanent gases, the CGE η_{CG} (Equation 1.2), the H_2/CO ratio, defining the composition of the intended product, and the tar load m_{tar} showing the amount of problematic compounds.

$$X_{SG} = \frac{x_{\mathrm{CO}} + x_{\mathrm{H_2}}}{x_{\mathrm{CH_4}} + x_{\mathrm{CO}} + x_{\mathrm{H_2}} + x_{\mathrm{CO_2}} + x_{\mathrm{N_2}}} \tag{1.1}$$

$$\eta_{CG} = \frac{\dot{n}_{FR,out}(x_{\mathrm{CH_4}} \cdot LHV_{\mathrm{CH_4}} + x_{\mathrm{CO}} \cdot LHV_{\mathrm{CO}} + x_{\mathrm{H_2}} \cdot LHV_{\mathrm{H_2}})}{\dot{m}_{FS} \cdot LHV_{FS}} \tag{1.2}$$

With x_i being the mole fraction of species i, LHV the lower heating value, and $\dot{n}_{FR,out}$ and $\dot{m}_{FS}$ being the product gas output and the feedstock input, respectively.

Oxygen Carrier The preparation, manufacturing, and selection of OC materials is an ongoing research topic also for chemical looping combustion (CLC) (e.g. [107, 108]). However, results for important OC properties like OC life time obtained under CLC conditions might not be valid for CLG [83]. Additionally, aspects important for CLC like high oxygen carrying capacity or reactivity are not so important in CLG where only limited feedstock oxidation is wanted. Goel *et al.* [109] studied properties like reactivity, H_2-production performance, sintering temperature, and mechanical strength of 9 low-cost OC derived from waste streams or natural minerals. Currently, synthetic OC are only utilized in lab-scale analysis [65, 110] and are therefore produced only in small quantities. Only one report of continuous CLC with an overall amount of more than $1000\,\mathrm{kg}$ of synthetic Ca-Mn-based OC exists [111]. Di Giuliano *et al.* [70] argue for further research in synthetic OC production and performance to enhance the CLG/CLC process, but acknowledge that with scale-up of synthetic OC production, other factors like cost, safety, material availability, and environmental impact become

[3] Although autothermal reforming is possible, it requires an ASU to provide pure oxygen which would negate the whole purpose of CLG.

important. Considering the current situation, scale-up of CLG has to happen first with readily available natural minerals like ilmenite or waste materials like steel converter slag, creating the market for better performing synthetic OC.

There is also research to screen for OCs producing a very low amount of tars. Hildor *et al.* [104] report on specific tar generation from a continuous CLG process utilizing steel converter slag and ilmenite to convert biomass in a $10\,\mathrm{kW_{th}}$ lab scale unit, while Larsson *et al.* [112] use ilmenite as an additive to a sand bed to reduce tar production in the 2-4 $\mathrm{MW_{th}}$ Chalmers gasifier. An enhanced natural olivine which was impregnated with additional iron also showed reduced tar production in continuous biomass gasification [113]. Other studies focus on the conversion of model components like toluene [114] or benzene [104, 115] to compare different OC in terms of tar conversion performance.

For chemical looping processes in fluidized beds several characteristics must be considered with regards to the OC for successful deployment. According to Adanez *et al.* [116] these are:

- **Oxygen carrying capacity:** The amount of oxygen an OC can transport. This determines the minimum solid circulation rate of the OC material between the two reactors in order to supply a certain amount of oxygen to the process. The actually usable part of the theoretically possible transport capacity depends on the gas composition of the FR.
- **Thermodynamic properties:** Depending on the equilibrium state of the metal oxide, full oxidation, partial oxidation, or no oxidation of the feedstock is possible. For initial assessment an Ellingham diagram can be used [117].
- **Reactivity:** The higher the reactivity, the faster the conversion of the OC inside the reactor and the less residence time is required for full conversion. The reactivity can change during operation.
- **Stability:** The OC material experiences mechanical stress and is subject to erosion inside the reactor system. Therefore a certain fraction is lost as fines through cyclones and must be replaced by a make-up stream. The mechanical stability determines the amount of the make up stream required for steady state operation
- **Carbon Deposition:** OC material can be the location for carbon deposition from the gas phase. As this carbon is transported towards the AR it contributes to unwanted carbon slip and should therefore be avoided.
- **Fluidization properties:** The formation of larger agglomerates poses risks to fluidized bed operation and must therefore be avoided. Formed agglomerates must be removed from the bottom of the reactor and be replaced with fresh OC. Depending on the feedstock-ash-OC interaction, the bed temperature, and the fluidization regime, the tendency of agglomerates forming inside the bed changes.
- **Cost:** OC cost should be low as they impact the OPEX. Currently synthetic OC are not competitive with natural minerals or waste materials.
- **Toxicity:** Especially copper or nickel based OCs pose a risk to humans and the environment making handling and disposal of spent OC costly.

According to Mayer *et al.* [118] OC materials can be grouped into three categories based on their reactivity and thermodynamic properties:

1. Materials with high reactivity in AR and FR.
2. Materials with low reactivity inside the FR which can be fully oxidized inside the AR.
3. Materials which can release molecular oxygen depending on O_2 partial pressure. The so called chemical looping with oxygen uncoupling (CLOU) effect requires surplus oxygen on the AR outlet in order to oxidize the OC sufficiently but has the advantage of close to full feedstock conversion inside the FR.

The important OC parameters for this dissertation are the oxygen transport capacity R_{OC} of the OC material, measuring how much oxygen can be transported per OC mass, and the oxidation degree X_S, measuring the actual oxidation of the OC in the process, as defined by [112]:

$$R_{OC} = \frac{m_{OC,ox} - m_{OC,red}}{m_{OC,ox}} \tag{1.3}$$

$$X_S = \frac{m_{OC} - m_{OC,red}}{R_{OC} \cdot m_{OC,ox}} \tag{1.4}$$

In this definition, R_{OC} is the oxygen transport capacity of the OC material, X_S is the oxidation degree of the OC, $m_{OC,red}$ and $m_{OC,ox}$ are the mass of the fully reduced and oxidized state respectively, while the mass of the OC leaving the reactor is m_{OC}.

Process Control For process control in externally heated lab scale reactor setups, the adjustment of the thermal load, i.e. the feedstock feed rate, is often used to control the oxygen to fuel equivalence ratio λ and thus the gasification process while keeping the solid circulation constant (e.g. [119, 120]). A similar approach is to reduce the solids circulation and thus the oxygen transport as demonstrated by Pissot *et al.* [121]. However, the heat transfer is also effected by the circulation resulting in lower FR temperature which is primarily controlled by the solid circulation between the reactors. Larsson *et al.* [112] are the first to state the requirement to uncouple the oxygen transport from the solid flow to circumvent the resulting changes in power, solid circulation, and reactor inventory. The dilution of the OC with silica sand has been tested multiple times showing its feasibility for setups where energy can be supplied in another way than the feedstock input in the FR [121, 122]. Nonetheless, for good process control in autothermal CLG a more flexible approach is required, as the adjustment of OC-sand ratio requires the partial replacement of hot bed material in the system. The subsequently required splitting into the two solid fractions is difficult and expensive and makes this method unsuitable for commercial application. Although, it is theoretically possible to find an OC with the optimal oxygen carrying capacity, utilizing this as process control method would limit the degrees of freedom during operation as oxygen transport would still be coupled to solid circulation. Moreover, solid circulation is the major control factor of the FR temperature.

The important parameters for investigations of process control are the air to fuel equivalence ratio λ, showing the amount of oxygen supplied to the process in relation to the oxygen required for full feedstock conversion:

$$\lambda = \frac{\dot{m}_{O,AR}}{\dot{m}_{FS} \cdot R_{FS}} \tag{1.5}$$

and the oxygen carrier to fuel equivalence ratio ϕ defined by [112]:

$$\phi = \frac{R_{OC} \cdot \dot{m}_{OC} \cdot X_{s,AR}}{\dot{m}_{FS} \cdot R_{FS}} \tag{1.6}$$

quantifying how much oxygen is actually available inside the OC circulation stream in relation to the required oxygen for full feedstock conversion with the mass streams $\dot{m}_{FS}$ and the oxygen requirements for full oxidation R_{FS}.

The key performance indicators (KPIs) which are optimized using process control are the cold gas efficiency (CGE) η_{CG}, measuring the fraction of feedstock energy contained as chemical energy in FR of-gas (Equation 1.2) and the carbon conversion X_C, being the fraction of feedstock carbon converted into gaseous species inside the reactors:

$$X_{C,FR} = \frac{\dot{n}_{gas,FR} \cdot (x_{CH_4} + x_{CO} + x_{CO_2}) \cdot M_C - \dot{m}_{CO_2,fluidization} \cdot \frac{M_C}{M_{CO2}}}{\dot{m}_{FS} \cdot w_{C,FS}} \tag{1.7}$$

with the AR carbon conversion being calculated from CO_2 only:

$$X_{C,AR} = \frac{\dot{n}_{gas,AR} \cdot x_{CO_2} \cdot M_C - \dot{m}_{CO_2,fluidization} \cdot \frac{M_C}{M_{CO2}}}{\dot{m}_{FS} \cdot w_{C,FS}} \tag{1.8}$$

M denotes the molar mass of the species i and $w_{C,FS}$ the carbon fraction inside the feedstock.

1.3.2 Limitations of Current Research

So far, all continuous CLG experiments performed have been conducted with external electrical reactor heating, with the exception of the experiments in the Chalmers 2-4 $\mathrm{MW_{th}}$ gasifier [112, 121, 123]. However, operation with external reactor heating is not feasible for commercial applications. Here, only autothermal process operation is economically feasible and all heat supplied to the gasification reactor must be supplied by the circulating OC material. Furthermore, the Chalmers gasifier suffers from a severe over dimension of the AR which is used to supply heat for commercial purpose and is therefore also fed with the feedstock. Moreover, the produced syngas is also routed into the AR for safe conversion and venting, returning the chemical energy of the syngas to the reactor system instead of removing it for utilization. Hence, results from these experiments give no holistic picture of the process. Nonetheless, the experiments still yield useful insights into the FR side of the process, but not into the stand-alone process and interaction of AR and FR.

Under autothermal process conditions, the free selection of process parameters is restricted by the requirement that both reactors must be in heat balance. Therefore, hydrodynamic constraints have an impact on obtainable reactor temperature and thus reaction chemistry, which in turn affects the syngas quality and overall process performance. Here, the interplay of these operation variables is crucial, as insufficient transport of OC and the corresponding transport of sensible heat between the reactors cannot be offset by increased reactor heating and will affect the maximal attainable FR temperature and therefore the gasifier performance. Moreover, interpretation of data obtained from small-scale experiments might lead to wrong conclusions (e.g. finding that iron based OC should not be considered for CLG because of lower reactivity [114]) because only part of the process is reproduced during the experiments.

1.4 Research Question

Just merging the information of partially contradicting insights from various research categories will likely not produce very good process and plant designs. For this reason, experimental studies are needed on a scale at which all the relevant effects can be studied together and their interdependence and relative importance can be assessed. This requires autothermal experiments at an industrial relevant scale to gain a holistic insight into the process to answer the following overarching research question:

> *Is it possible to operate the chemical looping gasification process under autothermal conditions, what are the efficiencies that can be achieved and what are the key parameters of the process?*

To gather data to answer this research question under the limited operation range of the CLG process with autothermal conditions, experiments are required in the range of approx. $1\,\mathrm{MW_{th}}$, where autothermal operation becomes feasible. They have been conducted in the $1\,\mathrm{MW_{th}}$ modular pilot plant at the Institute of Energy System and Technology at the Technical University of Darmstadt previously used for Carbonate Looping [124, 125], CLC [111, 126–130], and High Temperature Winkler (HTW$^{\mathrm{TM}}$) Gasification [53, 131–133]. The experiments were done under the restriction of utilizing the existing reactors and infrastructure and a readily available OC material to be able to obtain the required quantity, i.e. a natural mineral or a waste material. For biomass feedstocks the selection is wider because wood, straw, leaves, husks and other biomass streams are available in large quantities and commercial technologies like pelleting or chipping and milling for preparation exist.

The rather general research question has been broken into multiple aspects of which four are part of this cumulative dissertation:

1. Which process control and operation range is applicable to achieve high cold gas efficiency during autothermal CLG?

   In order to prepare the existing pilot plant for the experiments this question needs to be answered as several design choices are influenced by the process control concept. It has been shown that the

decoupling of the oxygen transport from the solid circulation is required [112] and possible [121, 122] in order to be able to control the oxygen to fuel equivalence ratio. The suggestion of sub-stoichiometric operation of the AR has not been investigated but was proposed as well [112]. Simulation of the existing control concepts of circulation adjustment, sand dilution, and the novel sub-stoichiometric AR operation in the boundary conditions obtainable in the existing pilot plant were performed to find the most viable method for the pilot plant and are described in the Research Paper I of this dissertation. Research Paper IV validates the concept in actual implementation.

2. What is an appropriate design for an autothermal chemical looping gasifier in the $1\,\mathrm{MW_{th}}$ scale?

   The existing experimental facility had to be adapted in order to be able to run the process safely. The design choices open up a certain range of operation, which are discussed with the corresponding limitations. The design, limitations resulting from these design choices, corresponding operational strategies, and improvements for greenfield plants are discussed in Research Paper II.

3. What is the actual OC material circulation rate during gasification and how can it be measured?

   For future plant design the sizing of the equipment largely depends on the required solid circulation. Multiple methods exist to estimate the solid circulation like stopping loop seal fluidization [134] or adding feedstock batch wise [135] and calculating solid circulation from the system responses of reactor inventory decline and oxygen consumption inside the AR respectively. However, these methods impact the hydrodynamic and therefore only give an approximate representation of real steady-state process conditions. Other methods use moving equipment inside the solid stream [136] or use particle properties, fluidization and pressure drop [137] to estimate solid circulation. Estimation of solid circulation based on an oxygen balance around the FR in an natural gas fired CLC unit was first described by Ohlemüller *et al.* [111]. However, application to systems using solid feedstock and thus exhibiting carbon slip and containing other reacting material inside the OC stream was not conducted. Therefore, this approach was generalized for dual fluidized bed processes and expanded to include additional analysing equipment in Research Paper III and used to determine solid circulation during the experiments.

4. What efficiency and syngas quality regarding composition and tar content are obtainable?

   Assessing the viability of the process not only requires demonstrating technical possibility, but should also consider the obtainable efficiency and product quality. The most important trends concerning CGE, carbon conversion, syngas quality, and tar production are investigated in detail. The limitations of the data caused by the high relative heat loss are discussed. The individual KPIs obtained during the experimental operation of the autothermal CLG pilot plant are analysed in Research Paper V and compared with literature data to show the benefits of the process.

2 Synthesis

This chapter summarizes the findings of the research papers presented in this dissertation in Chapter 3. It roughly follows the research process from initial simulation in Section 2.1 to gather first insights of the process on the projected scale followed by the design of the experimental facility in Section 2.2. The largest part is dedicated to the experiments and the resulting insights into the CLG process (Section 2.3).

2.1 Mass and Energy Balance of the Chemical Looping Gasification Process

In any gasification technology where oxygen is supplied to the gasifier, accurate control of the oxygen to fuel equivalence ratio is critical to balance the exothermic oxidation reactions with the endothermic gasification reactions to produce a high calorific syngas. For gasification technologies using steam/oxygen or air as gasification agents this is straightforward through the control of the oxygen containing gas stream. However, in CLG the oxygen is transported with the solid bed material, which is also used to supply the required heat to sustain the process temperature.

In Research Paper I an existing process model for CLC in Aspen Plus [138, 139] is extended to include biomass pyrolysis and used for the calculation of heat and mass balances to investigate possible approaches to control oxygen input. It utilizes equilibrium calculation and therefore neglects detailed reaction kinetics. However, it is still useful for the comparison and investigation of basic process control strategies.

For the process control of CLG, the concept of reducing solid circulation, and thus oxygen input, is investigated as a reference. It has a very low FR temperature ($T_{FR} < 750\,^{\circ}\mathrm{C}$), which has a strong negative impact on gas quality, and is therefore discarded, confirming the need to decouple oxygen transport from solid transport [112]. The dilution of OC material with sand (while keeping solid circulation constant), which has already been shown experimentally to be able to control the oxygen to fuel equivalence ratio [121, 122], is simulated and shows a much higher FR temperature ($T_{FR} > 980\,^{\circ}\mathrm{C}$) for the same CGE and λ. Therefore, this approach should be preferred during experiments, as it is expected to give much better gas quality with higher syngas fraction and lower tar load.

As a novel approach which was not published before, neither as experimental nor theoretical investigation, the limitation of the air feed to the AR was investigated. With this approach not enough oxygen is present to fully oxidize all the OC particles inside the AR. Hence, the OC particles cannot fully contribute to the oxygen transport, but behave partially like an inert (e.g. sand) as they cycle through the system. Pröll *et al.* [140]

report on OC particles cycling through the system in a reduced form when restricting AR air flow. However, Pröll *et al.* [140] also reduce solid circulation and therefore heat transport between the reactors which is the dominating effect in oxygen limitation [140]. Solid circulation is kept constant during calculation and gives a resulting $T_{FR} > 920\,^{\circ}\mathrm{C}$ for even higher cold gas efficiency at the same λ than for sand dilution and solid circulation reduction approaches. The main difference between dilution with sand and sub-stoichiometric AR operation is in the operational flexibility gained from the reduced OC bed material which can be used to transport oxygen when required for process control. Moreover, solid handling reduces in complexity, as only one solid material requires feeding equipment and no tailoring of particle size distribution (PSD), particle density, and attrition behaviour is necessary. Although carbon slip can be expected in the case of solid feedstock [141, 142], this is not a problem as equilibrium calculations show no formation of CO inside the AR and reaction of oxygen with carbon is generally preferred to OC oxidation [143–145]. Therefore, the approach with sub-stoichiometric AR operation is used for initial investigation of optimization strategies as presented in Research Paper I.

The investigation of possible optimization shows the general trade-off which has to be considered in autothermal gasification. Gas quality is better (i.e. higher syngas content, lower tar yield) if FR temperature is high. The CGE decreases with increasing temperature because the required energy to reach a higher FR is provided by syngas oxidation. The influence of steam to biomass feedstock ratio, OC circulation, temperature of fluidization media, and AR temperature on CGE and FR temperature are analysed in Research Paper I. The insights from the equilibrium simulation neglecting heat losses and reactor hydrodynamic can give an initial qualitative idea of optimization avenues, however, reaction kinetics, hydrodynamic constraints, and heat losses will affect the quantitative values obtainable in experiments.

2.2 Design of the Chemical Looping Pilot Plant

Based on the model already utilized for the investigations in Research Paper I with the addition of detailed ilmenite reaction kinetics [146] as in the CLC model from Ohlemüller *et al.* [139], mass and energy balances were calculated for the existing $1\,\mathrm{MW_{th}}$ modular pilot plant. Heat losses for the reactors were assumed to be $\dot{Q}_{loss,AR} = 50\,\mathrm{kW}$ and $\dot{Q}_{loss,FR} = 60\,\mathrm{kW}$ falling in the range previously estimated for the reactor system [127, 129]. Moreover, reactor hydrodynamics were considered with calculations of solid entrainment according to Kunii & Levenspiel [147] implemented in the process model as described by Ohlemüller *et al.* [138, 139]. Variation of reactor temperature, temperature difference between the reactors, amount of AR fluidization medium and feedstock input were used to asses the likely operation range of the reactor system and peripheral systems during experiments. The hydrodynamic regime of both reactors was found to be in the transition between turbulent and circulating as visualized in the grace diagram in Figure 2.1, indicating that stable operation as CFB reactors is possible. During the design phase the natural ore ilmenite was selected as a suitable OC which belongs to category 2 according to Mayer *et al.* [118]. Although, thermo-gravimetric analysis

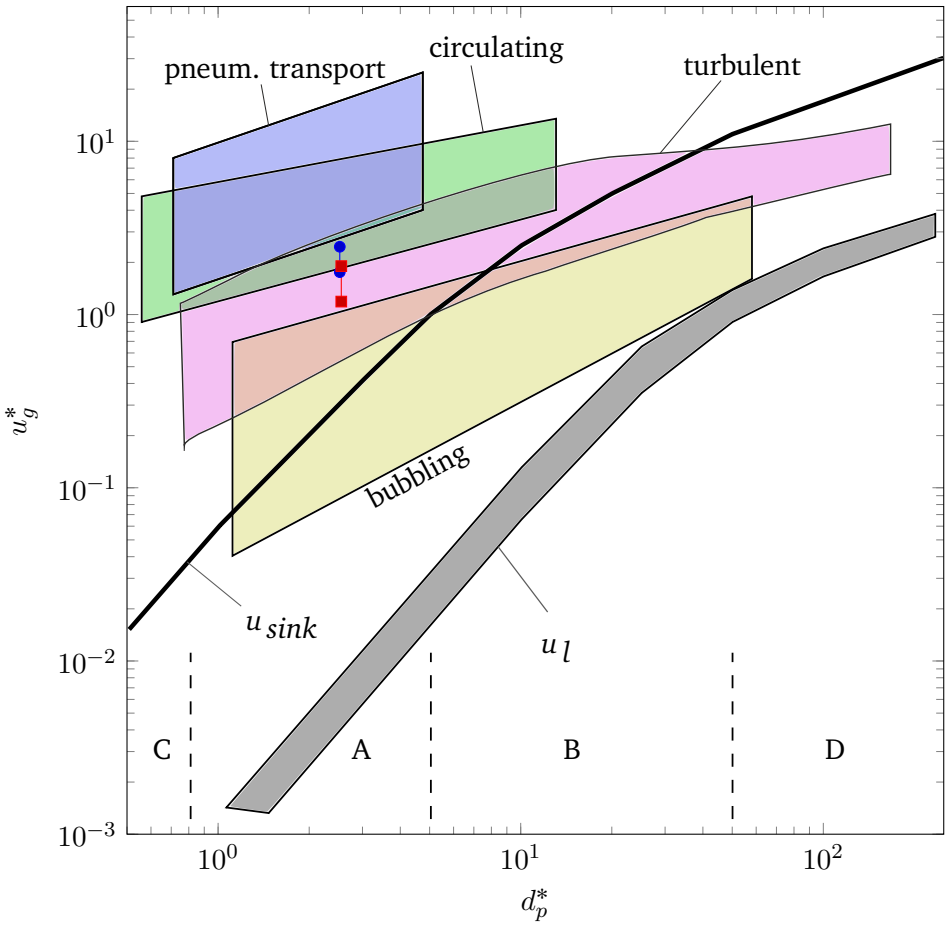

Figure 2.1: Grace diagram indicating the operation regimes of the FR and AR

show lower reactivity of ilmenite compared to other OC (e.g. nickel based [114, 148]) it is still considered a primary option [149] for chemical looping. The main influence on this decision were the operation experience with ilmenite [126–129], the availability in the required quantity and PSD, its non-toxicity, and the initial screening results from OC feedstock ash interaction [94–96].

With the stream results from the process simulation of the core reactor system the reactor periphery was designed. Already existing equipment was evaluated and in case it was found inadequate, modifications were designed, implemented, and commissioned. A schematic of the resulting pilot plant configuration is given in Figure 2.2, with sections of major subsystems or rework highlighted. The modifications include a flue gas recirculation for the AR to be able to control the oxygen input towards the AR without impacting the reactor hydrodynamic. The implemented control loops are described in Research Paper IV. In addition, a new syngas handling line with dedusting, induced draught fan, thermal oxidiser and a new steam fluidisation line for the FR was designed to prepare the existing pilot plant for the autothermal CLG experiments. A hazard and operability study (HAZOP) study was performed including all systems in operation during CLG to ensure safe operation.

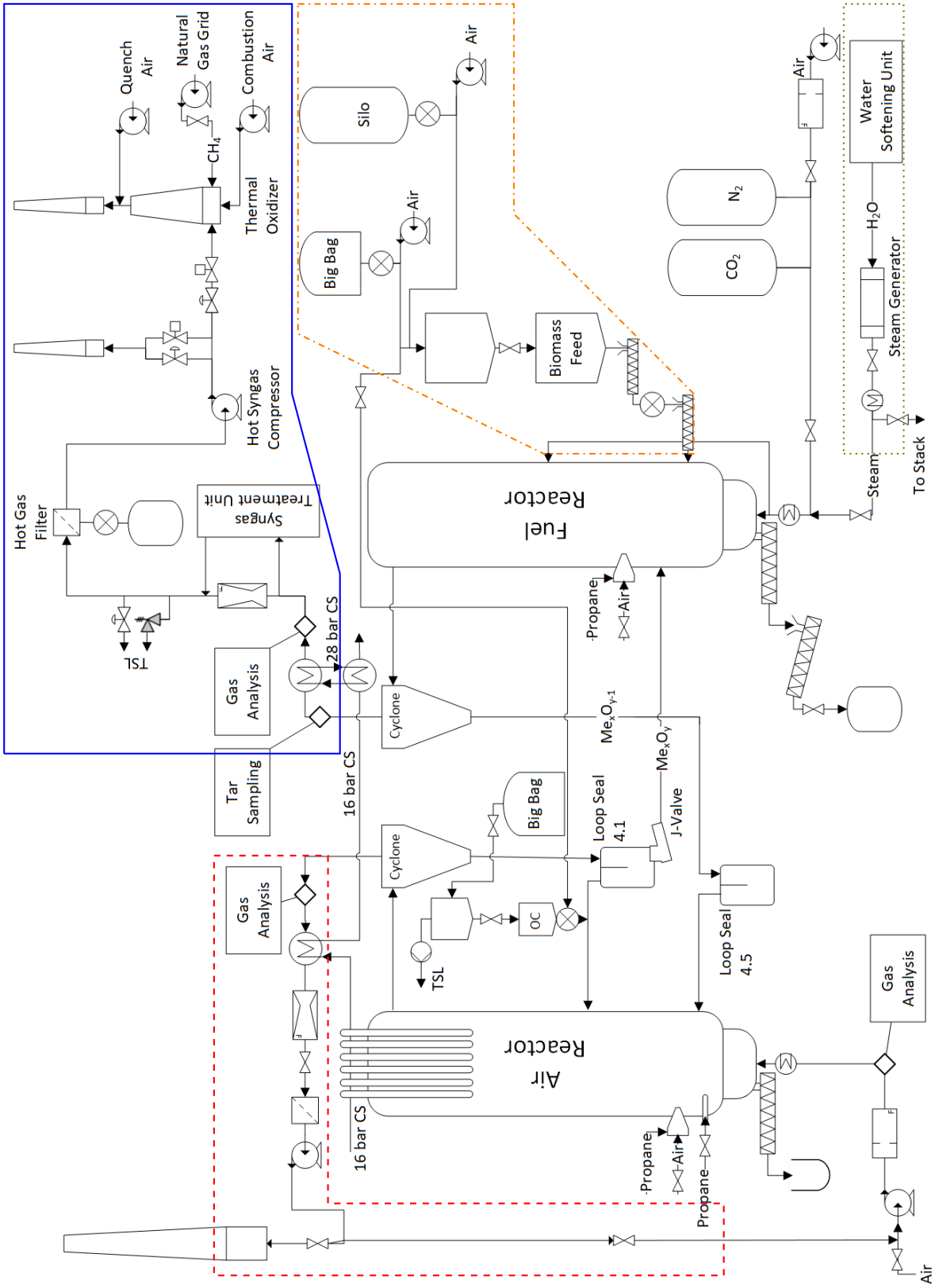

Figure 2.2: Schematic of the CLG pilot plant showing the main subsystems. CS: cooling system, OC: oxygen carrier, TSL: to safe location. syngas handling: ⎯, flue gas handling: - -, biomass feeding: -·-, steam supply: ····.

A dedicated section in Research Paper II discusses topics of interest for autothermal CLG operation like tar production, KPIs, and OC lifetime. Especially the life time of the OC material cannot be easily inferred from smaller laboratory reactors due to the fact that the circulation time, i.e. the redox-cycle-time, increases with reactor size. It is unknown whether chemical, mechanical, or thermal stress are the major contributor to attrition and thus limiting lifetime. However, it is clear that the mechanical and thermal stresses for the autothermal CLG pilot plant are greater than for the externally heated lab-scale units due to the difference in size and the greater temperature difference between the reactors. The influence of important operation variables (thermal load P_{th}, oxygen carrier to fuel ratio ϕ, solid circulation $\dot{m}_{OC}$, bed pressure drop Δp, and second stage fluidization) which can be varied inside the described experimental facility are discussed as well, giving an operation strategy for the maximization of the KPIs.

- The variation of P_{th} is straight forward through the control of feedstock conveying equipment. The heat losses of the pilot plant depend on the surface area (which is not varied) and on the operating temperature. Therefore higher thermal input leads to lower relative heat losses if the temperature is kept constant, and thus higher CGEs can be obtained. Reactor hydrodynamics are influenced by the corresponding volatiles and the steam to biomass ratio and ϕ changes with the variation of the feedstock input.
- The OC to fuel equivalence ratio ϕ is controlled via the oxygen availability inside the AR which can be adjusted by varying the amounts of air and recirculated AR flue gas used as fluidization medium. A higher value of ϕ (while keeping everything else constant) results in a higher temperature inside AR and FR. The production of CH4 and tars is reduced with higher ϕ, however, so is the CGE.
- The global solids circulation $\dot{m}_{OC}$ can be adjusted via the variable J-Valve fluidization. Increasing $\dot{m}_{OC}$ reduces the ΔT between the reactors and thus increases the FR temperature while decreasing the AR temperature. However, it has a direct impact on reactor hydrodynamics in the form of solid inventory measured via bed pressure drop Δp. To keep Δp constant, fluidization must be adjusted. Therefore control of $\dot{m}_{OC}$ is more difficult.
- The bed pressure drop Δp is influenced by the reactor hydrodynamics and the total solid inventory. The total inventory is controlled via OC make up and bed material removal. Increasing solid inventory allows for the reduction of fluidization while keeping the solid circulation constant. Higher Δp is beneficial for the conversion of the feedstock and leads to better gas quality.
- Second stage fluidization can be used to increase the residence time of feedstock particles in the lower region in the bed enhancing conversion and gas quality. It can be controlled via the variable routing of the fluidization medium of the FR to a second inlet at one fifth of the reactor height. This is considered a backup option if conversion is not sufficient and was not required during experiments.

2.3 Autothermal Chemical Looping Experiments

2.3.1 Materials

Oxygen Carrier As OC material the natural mineral Norwegian ilmenite was used. During experiments, two different PSDs, as depicted in Figure 2.3, were used. The finer material has approx. $20\,\%$ of particles smaller $50\,\mu\mathrm{m}$ which was shown to lead to significant solid losses in previous experiments [128, 129] leading to increased make-up rates cooling down the reactor system. The coarse material exhibits only $20\,\%$ of particles smaller $200\,\mu\mathrm{m}$, which will lead to lower entrainment from the reactors and thus lower solid circulation. A perfectly matched PSD is not commercially available and sieving proofed to be economically infeasibly for the pilot tests. The oxygen carrying capacity for the ilmenite was determined to be $R_{OC} = 3.7\,\%$.

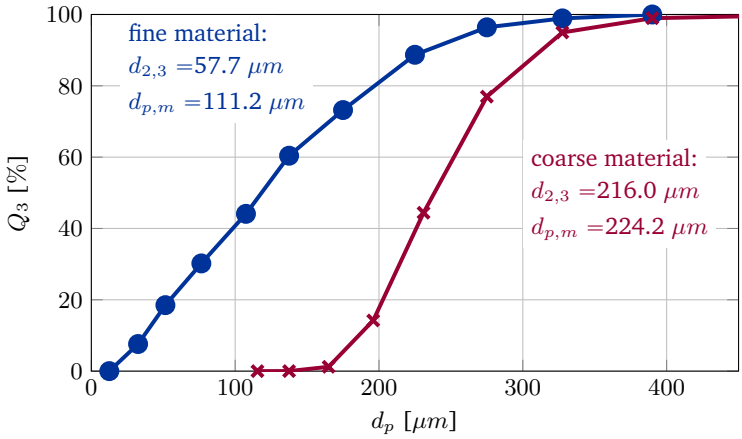

Figure 2.3: Particle size distribution of the ilmenite used as oxygen carrier material during experiments.

Feedstock The experiments were carried out with three different biogenic feedstocks as given in Table 2.1 in three dedicated test campaigns. The industrial wood pellets (IWP) were purchased from Eckhard GmbH and confirm to the norm ENplus A1 and are used as easily available reference feedstock. The pine forest residue (PFR) was sourced from foresting operations in Sweden and pelleted by AB Torkapparater. The wheat straw was obtained from farms in Sweden and also processed by AB Torkapparater including dosing of additives and pelleting.

2.3.2 Process Control

The autothermal CLG experiments were performed with the sub-stoichiometric AR as process control scheme and the performance is evaluated in Research Paper IV. After attaining sufficient reactor temperature and stable hydrodynamics and biomass feed during the experiments, the oxygen input towards the AR was restricted to achieve higher CGE. During the three periods where the switch to the sub-stoichiometric AR operation was initiated, a characteristic system response with a duration of $2\,\mathrm{h}$ to $4\,\mathrm{h}$ could be observed. These periods

Table 2.1: Proximate and ultimate analysis of feedstock used during experiments. LHV: lower heating value, PA: proximate analysis, UA: ultimate analysis, d.b.: dry base, IWP: industrial wood pellets, PFR: pine forest residue.

	Component	IWP	PFR	WSP
PA [wt.-%]	Moisture	8.3	4.4	10.8
	Ash (d.b.)	0.3	2.3	4.709
	Volatiles (d.b.)	84.6	80.3	77.02
	Fixed carbon (d.b.)	15.1	17.4	18.27
UA [wt.-%]	C (d.b.)	50.7	51.1	47.65
	H (d.b.)	6.1	6.1	5.7
	N (d.b.)	0.33	0.44	0.53
	O (d.b.)	42.5	40.1	41.15
	S (d.b.)	0.008	0.025	0.105
	Cl (d.b.)	0.008	0.010	0.076
LHV [MJ kg^{-1}]		17.2	18.30	15.3

are investigated in Research Paper IV. The hydrodynamic behaviour of the system was not impacted due to the partial substitution of AR fluidization air with AR off-gas as described in Research Paper II. The observed characteristic behaviour of the system response is depicted in Figure 2.4:

- The oxygen output of the AR drops immediately to zero, indicating the sub-stoichiometric conditions.
- The temperatures inside both reactors start decreasing as less oxygen is available for exothermic reactions to occur. Therefore less OC particles, and subsequently syngas species, are oxidized.
- The CGE starts increasing, because less syngas is oxidized by the OC.
- The H_2:CO ratio increases. As ilmenite reaction kinetics lead to a preferred oxidation of H_2 [146] it is postulated that the reduction in OC lattice oxygen availability effects the H_2 oxidation to a higher degree.

With the exception of the first characteristic system response all changes occur over the transient period until a new stable operation point is reached. The cause of the long transient period is twofold. Firstly, the refractory lining of the reactor adds enormous thermal inertia to the system, leading to slow temperature changes, and secondly, the OC acts as an oxygen reservoir which can be depleted until a new steady state is reached. During this depletion, the oxygen release of the OC inside the FR is higher than the uptake inside the AR, where oxygen is only available sub-stoichiometrically. Thus the syngas oxidation occurs to a larger extent than the oxidation of OC particles until the new state with lower reduction, and thus slower kinetics [146], is reached. The cyclic reduction and oxidation and the effect of sub-stoichiometric process control is visualized in Figure 2.5 where the overall X_S at both reactor outputs decreases as well as the difference of oxidation degree between the reactors ΔX_S.

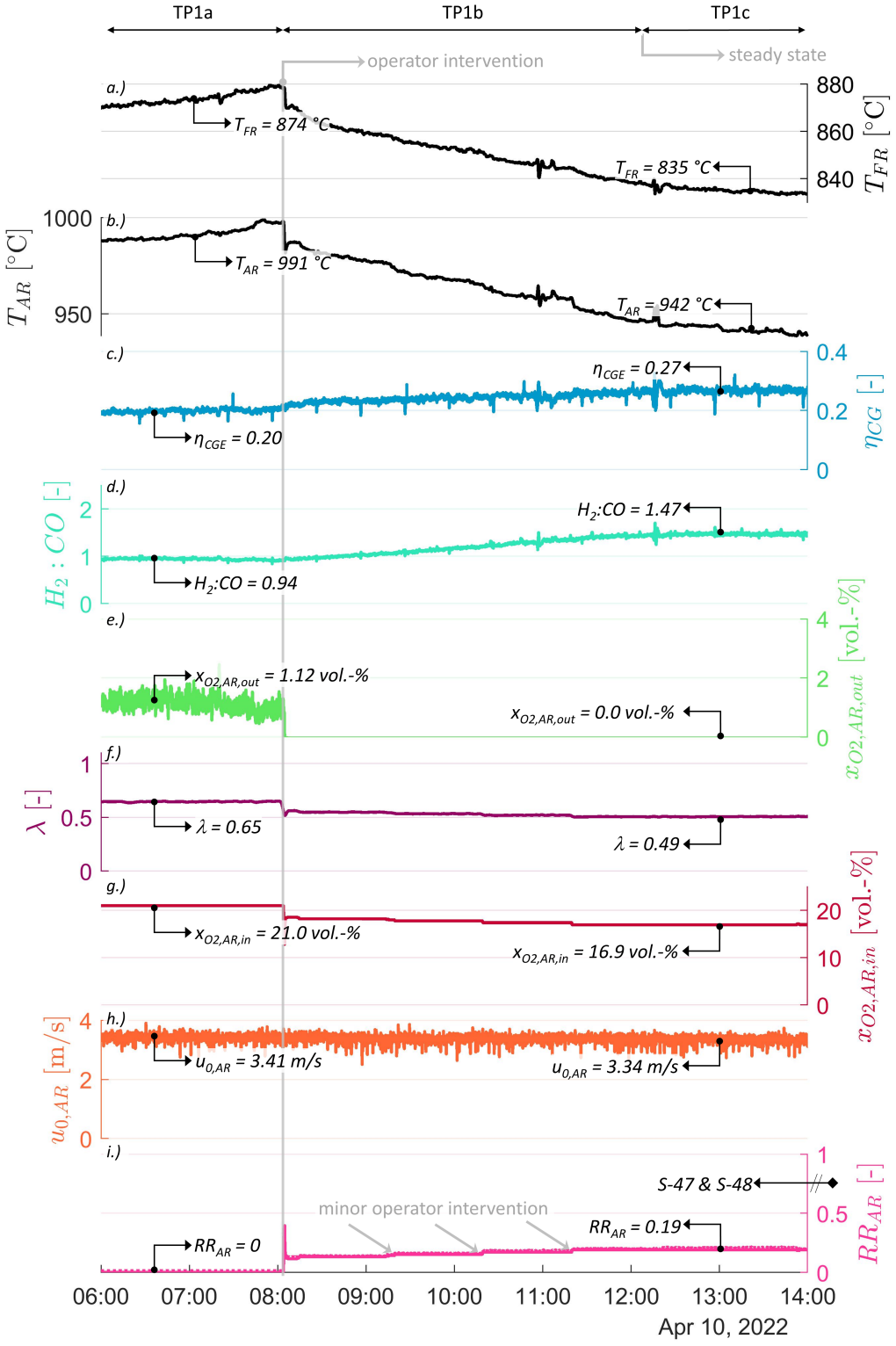

Figure 2.4: Characteristic system response of the CLG process when restricting oxygen input into the AR.

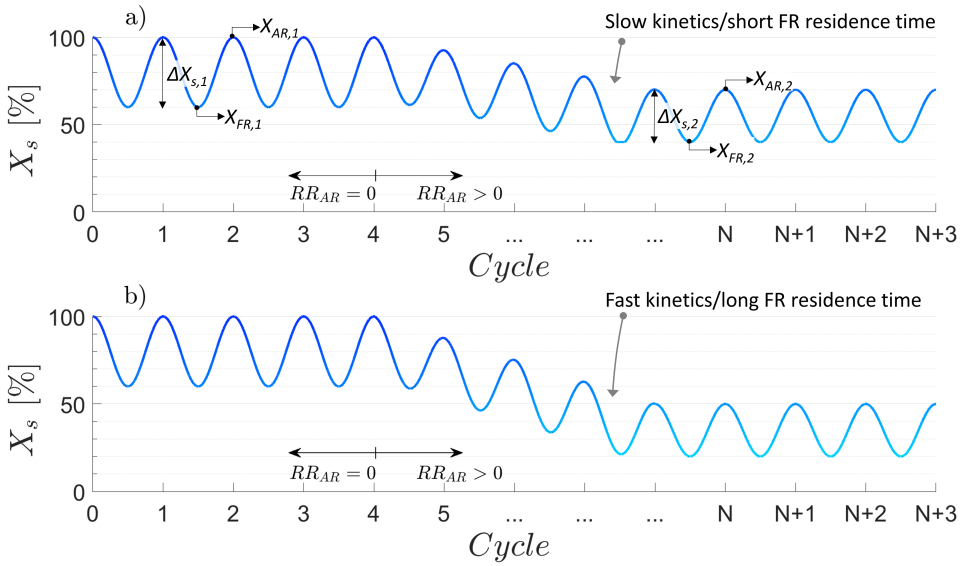

Figure 2.5: Effect of the sub stoichiometric process control on the cyclic reduction and oxidation of the OC material which is oxidized in the AR and reduced in the FR.

2.3.3 Solid Flux Measurement

The effect of the OC acting as a storage reservoir for oxygen can be confirmed by solid samples, taken during plant operation from the loop seals. The oxidation degree X_S is determined as described in Research Paper III by oxidation with air and correction for carbon content. The results are depicted in Figure 2.6. The effect

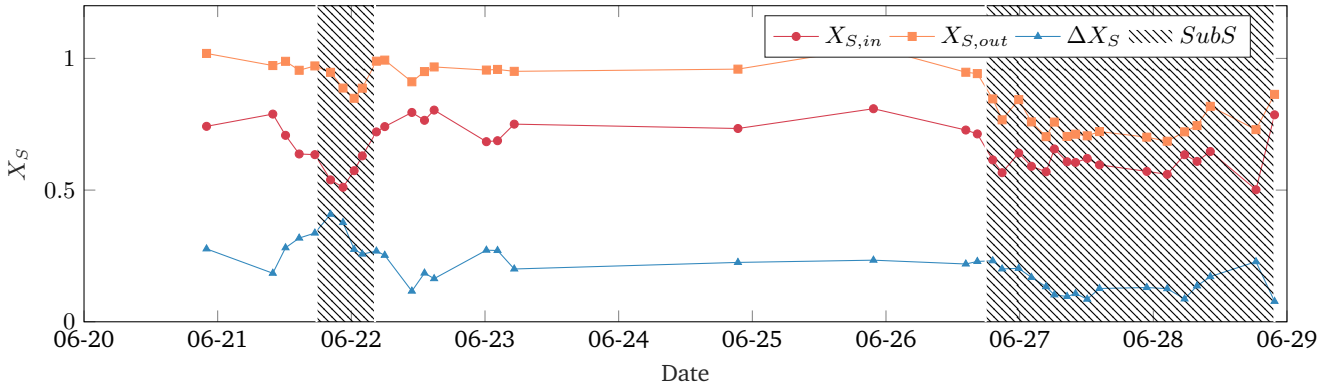

Figure 2.6: Variation of oxidation degree in loop seal samples during the second test campaign. The background pattern depicts times at which the oxygen input into the AR was fully consumed by the OC.

of the process control on the oxidation state of the OC is clearly visible. For the periods where all oxygen input into the AR is consumed (marked by the pattern in Figure 2.6) the oxidation degree at the AR outlet decreases. Moreover, during the second period with reduced oxygen input (from 06-26 onwards) the ΔX_S is also clearly reduced compared to the operation before.

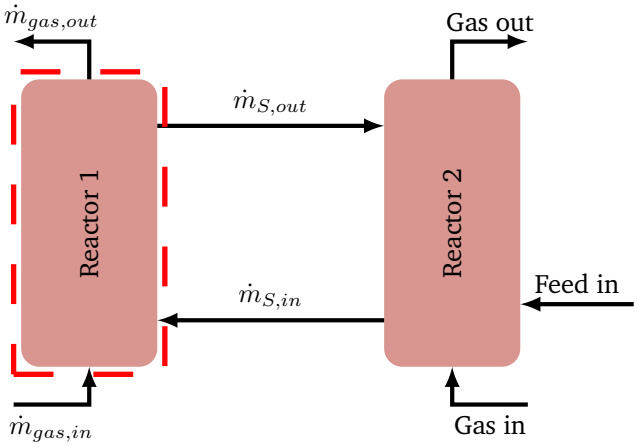

Figure 2.7: Schematic of a dual fluidized bed process indicating relevant streams.

During the test campaign depicted in Figure 2.6 the two different OC PSDs were utilized to investigate the effect of different hydrodynamic behaviour of finer and coarser PSD (for more details see [150, 151]). Initially the coarse ilmenite was used until it was switched to the fine ilmenite on 06-26 and the second, longer period wit sub-stoichiometric process control was achieved. As the PSD affects solids entrainment and hence solids circulation, it also affects heat and oxygen transport between the reactors. Therefore, the solid material transported between the reactors is important for the process heat balance and the sizing of equipment, so accurate knowledge is desirable.

The amount of oxygen transported from AR towards the FR $\dot{m}_{O,AR\rightarrow FR}$ is:

$$\dot{m}_{O,AR\rightarrow FR} = \dot{m}_{OC} \cdot R_{OC} \cdot \Delta X_S \tag{2.1}$$

As ΔX_S can be obtained from loop seal samples and the oxygen supply to the process $\dot{m}_{O,AR\rightarrow FR}$ can be determined from measured gas flows and compositions, the circulation rate $\dot{m}_{OC}$ can be calculated using a balance equation with the material constant R_{OC}. Ohlemüller *et al.* [111] describe using a balance equation around the FR together with information from the sampled solid material for CLC with natural gas. This Approach can be expanded to any dual fluidized bed reactor process as depicted in Figure 2.7. This allows for application to the CLG process where solid biomass feedstocks are used together with the solid bed material. The following equation was derived for the solid flux $\dot{m}_S$:

$$\dot{m}_S = \frac{\dot{m}_{Gas,in}(y_{i,in} - \sum_{j\neq i} y_{j,in} \cdot x_{i,out}) - \dot{m}_{Gas,out}(y_{i,out} - \sum_{j\neq i} y_{j,out} \cdot x_{i,out})}{x_{i,out} - x_{i,in}} \tag{2.2}$$

Careful selection of the reference state can lead to $x_{i,out} = 0$ simplifying calculation and the required laboratory analysis. Moreover, guidelines for the selection of species for the balance equation should take the following criteria into account:

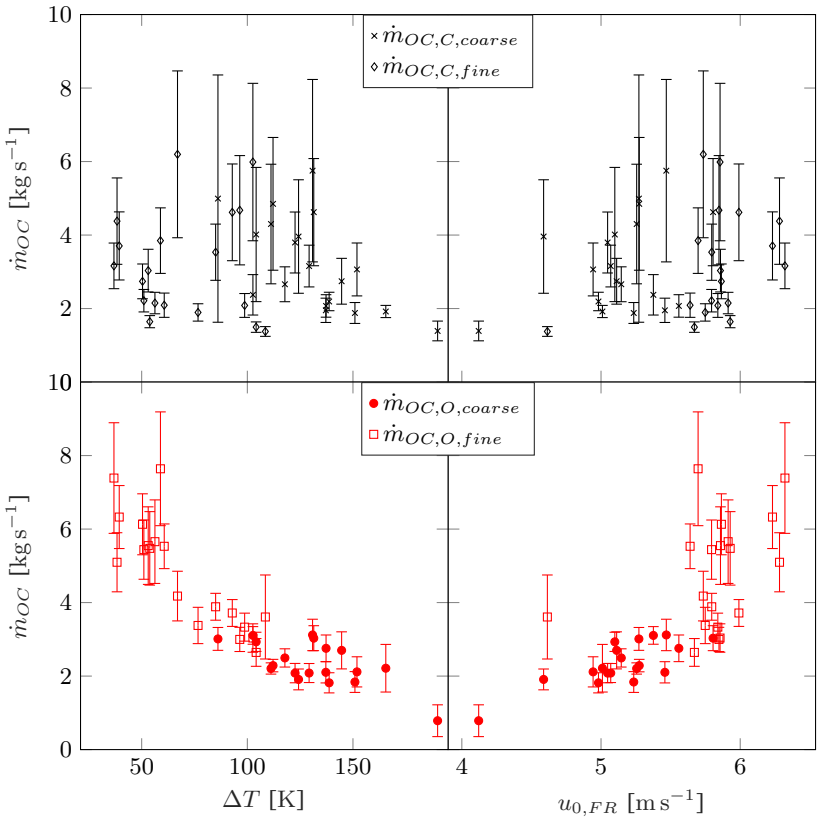

Figure 2.8: Solid circulation over temperature difference and fuel reactor gas velocity.

- Sample analysis: A species for which the mass fraction inside the sample can easily be analysed
- Process: A species which is only present in a few components in the gas phase, reducing the online analysis effort
- Reactions: A species which is quickly consumed or released inside the reactor reducing the possible impact during transient states

The application of the method is demonstrated in Research Paper III on experimental data from CLG experiments using oxygen as the balanced species which is transported as part of the OC lattice and carbon as the species which is transported in addition to the OC as unwanted carbon slip. The measured solid circulation is in the range of $1.8\,\mathrm{kg\,s^{-1}}$ to $5.7\,\mathrm{kg\,s^{-1}}$ or related to thermal input $1.2\,\mathrm{kg\,s^{-1}\,MW^{-1}}$ to $4.3\,\mathrm{kg\,s^{-1}\,MW^{-1}}$. The sampling procedure of the solid samples is described in detail, together with the description of the preparation and the analysis of the samples. Based on the measurement uncertainty of the individual methods and on the equipment utilized for the analysis the propagation of errors was calculated. The resulting values for $\dot{m}_S$ and the uncertainty are compared to other markers indicating changes in solid circulation like temperature difference between the reactors and fluidization velocity inside the FR (Figure 2.8). It was found that the carbon based determination of the solid circulation showed no clear correlation to the markers whereas the oxygen based calculation showed clear correlation. This indicates that the carbon—which is not part of the

OC lattice—could not be sampled representatively with the employed sampling setup. However, the oxygen calculation yields results in the correct quantitative range exhibiting the expected qualitative trends, indicating its usefulness.

Based on the results of the investigation of the solid flux measurement based on solid samples, it was determined that the sampling method should be selected with regards to the species and that species transported as part of the solid lattice show superior performance in terms of reliability and time required in steady-state operation. This is oxygen for CLG. Uncertainty decreases as the mass fraction of the balanced species released from the solid stream increases with an uncertainty of $20\,\%$ or below for the oxygen based calculation during the presented experiments. Moreover, the method does not impact the hydrodynamic state of the system and can therefore be applied during steady state operation. This opens up the possibility to analyse the influence of the solid circulation on other KPIs. As high circulation results in high FR temperatures the effect of circulation on syngas quality is dominated by the temperature effect.

2.3.4 Process Efficiency and Syngas Quality

Research Paper V examines the KPIs for the experiments with woody biomasses (IWP and PFR), while insights from the tests with wheat straw are included in a separate journal article [151]. KPIs and syngas quality are assessed for eight steady-state balance points where solid samples, gas sample bags and tar samples give a holistic insight into the process. Additionally, 708 periods of $20\,\mathrm{min}$ each were averaged showing system behaviour and trends during operation. For these periods, CGE (η_{CG}), carbon conversion (X_C), and syngas yield (Y_{SG}) are calculated and analysed against FR temperature and $\lambda_{FR,eff}$ to see important dependencies. The composition of the permanent gases in the syngas is investigated in parallel.

The cold gas efficiency as depicted in Figure 2.9 is calculated from online gas analysis (H_2, CO, and CH_4) as they are the species of interest for further valorization of the product gas stream with higher hydrocarbons, which contain an appreciable amount of energy, being neglected. A significant amount of energy has to be generated by the conversion of syngas species to obtain the required temperature in autothermal operation, resulting in the visible low CGE. Figure 2.9 b shows two trends C to D and E to F for η_{CG}. They both show the same behaviour at slightly different levels of η_{CG}: with increasing $\lambda_{AR,eff}$ η_{CG} increases. At approx. $\lambda_{AR,eff} = 0.3$, η_{CG} levels off and decreases again. The initial increase of η_{CG} is a result of the temperature increase, which in turn leads to a higher fraction of fixed carbon which is converted to syngas species. However, with increasing temperatures this effect lessens until the higher carbon conversion cannot offset the required syngas conversion to sustain the higher temperature. The different levels of the trends are a result of a difference in thermal load P_{th}. In Figure 2.9 a the trends are not that clear.

Compared to literature data (e.g. [83, 85, 105]) the CGE as depicted in Figure 2.9 is lower, which is caused by the high relative heat loss of the pilot plant. However, when comparing the experimentally obtained CGE to the one predicted during the design phase (Research Paper II) which is in the range of 0.38 to 0.53, it is clear that much higher CGEs are not possible in the $1\,\mathrm{MW_{th}}$ modular pilot plant. As the experiments presented

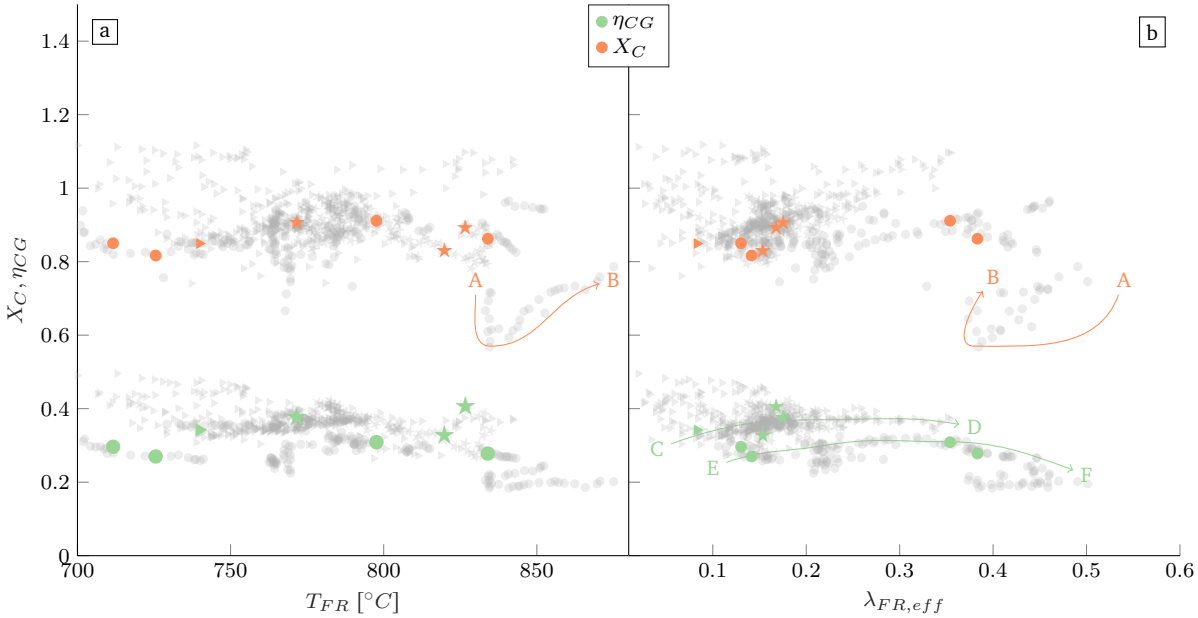

Figure 2.9: Cold gas efficiency and carbon conversion over a: FR temperature and b: FR efficient λ. Feedstock/bed material: • - IWP/fine ilmenite, ▸ - PFR/coarse ilmenite, ★ - PFR/fine ilmenite.

are the first ever autothermal operation of the CLG process, no prior operating experience exists and the plant was not operated at optimized conditions. Moreover, the temperatures assumed during simulation could not be reached as high amounts of heat were extracted due to constructional limitations of the existing AR cooling lances increasing the heat losses. Therefore, the char gasification happens at lower temperatures which slows reaction kinetics and therefore reduces the energy that is transferred to the gas phase. This can also be seen in Figure 2.10 where the carbon conversion is split according to the individual reactors. Here, with increasing temperature the expected reduction of carbon slip occurs, i.e. more carbon gets converted inside the FR and less is transported towards the AR with subsequent combustion inside the AR. The clear trend of the AR carbon conversion $X_{C,AR}$ with temperature seems to indicate that very low carbon slip can be reached for temperatures in the range of $900\,^{\circ}\mathrm{C}$ to $950\,^{\circ}\mathrm{C}$. Nonetheless, as char gasification occurs primarily inside the dense zone of the fluidized bed (i.e. at the bottom), the preheating temperature of the fluidization medium/gasification agent steam will also have an effect as it influences the local reactor temperature.

The reactor temperature also plays a crucial role for the generation of tars as depicted in Figure 2.11. There is a difference in tar production between the employed feedstocks which might be caused by difference in multiple factors like moisture [79], carbon content, or the inclusion of bark and pine needle [58] in the PFR pellets. Compared to the literature data included in Figure 2.11, the data suggests that CLG generates less gravimetric tars and therefore a cleaner syngas than DFBG or steam/oxygen gasification. The reason is likely the catalytic reforming of tars on the ilmenite [112, 152].

The gas chromatography (GC) tars as depicted in Figure 2.12 show different compositions than the ones reported by Condori *et al.* [83] for similar feedstock in a $1.5\,\mathrm{kW}$ lab scale unit. The one ring aromatics Benzene

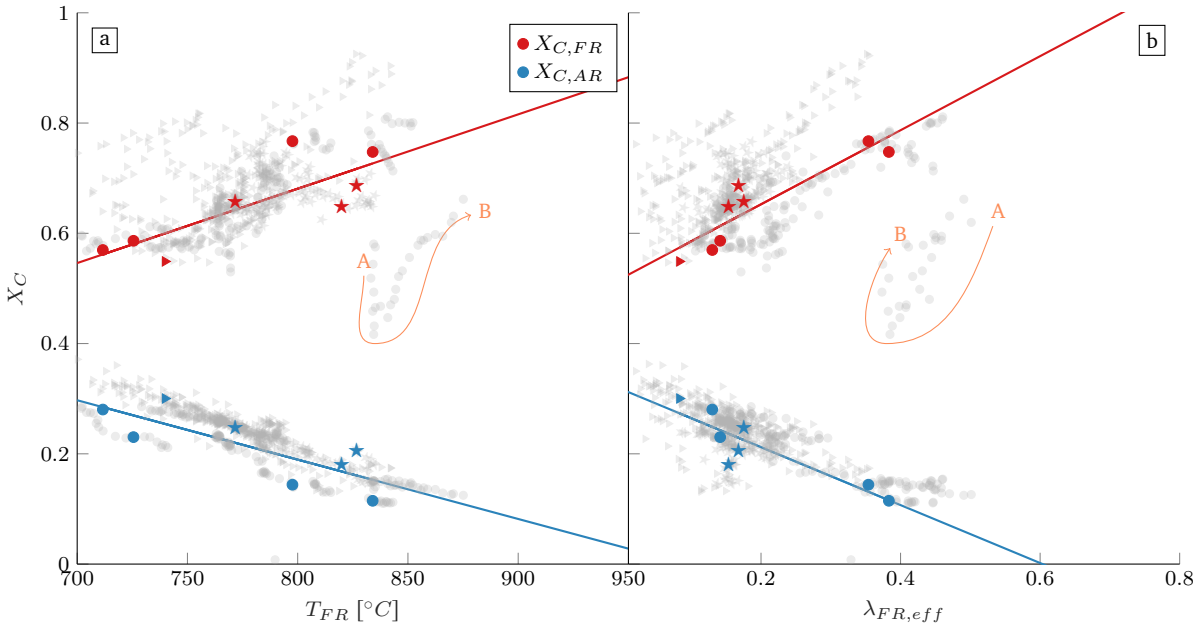

Figure 2.10: Carbon conversion over a: FR temperature and b: FR efficient λ. Feedstocks/bed material: • - IWP/fine ilmenite, ▸ - PFR/coarse ilmenite, ★ - PFR/fine ilmenite.

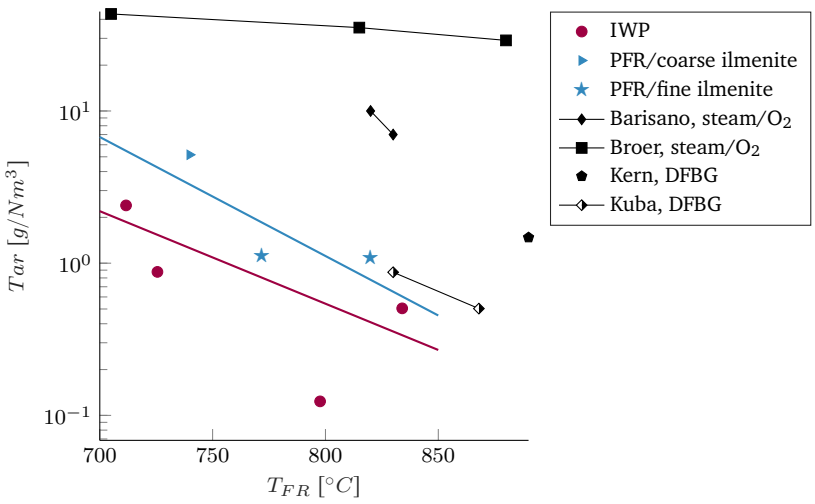

Figure 2.11: Gravimetric tar on a dry gas basis. Feedstocks: • - IWP/fine ilmenite, ▸ - PFR/coarse ilmenite, ★ - PFR/fine ilmenite, Barsiano et al. [153], Broer et al. ("Heavy Tars") [154] , Kern et al. [155], Kuba et al. [79].

and Toluene make up the majority of the GC tars detected during the pilot-scale experiments whereas it is mostly Naphthalene in the lab-scale unit [83]. It is likely that these difference are caused by the difference in temperature [81] as the reactor temperature in the small-scale unit is higher and more uniform which means that initial pyrolysis occurs at higher temperatures.

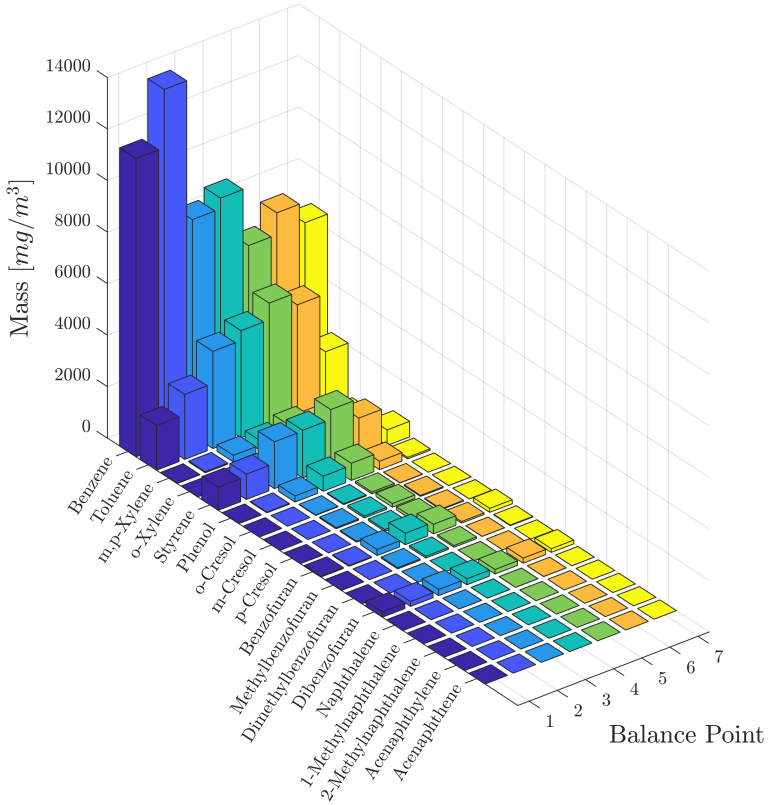

Figure 2.12: Tars as measured by gas chromatography for the balance points.

The inherent trade-off between efficiency and syngas quality can be observed from the experimental data. Low temperature means low quality syngas and low carbon conversion, and high temperature means low CGE. However, the utilization of ilmenite as bed material enhances the process performance in terms of syngas quality when compared to other gasification processes. Further optimizations like different OC material, reactor inventory, and feed location are discussed in Research Paper V. Although no optimization could be performed during the experiments, the KPIs were found to be comparable to other experiments of similar scale with different gasification technologies.

2.4 Conclusion

Coming back to the research questions formulated in Section 1.4 the overarching question can be answered positively: during the experiments more than $100\,\mathrm{t}$ of biogenic feedstock were converted in over $400\,\mathrm{h}$ of CLG operation, demonstrating that the process can be operated under autothermal conditions. The produced syngas was analysed via continuous online analysis of major permanent gas components with additional collection of offline samples for the measurement of higher hydrocarbons by gas sample bags and tar protocol, and bed material samples taken from loop seals, filter, and bottom product for solid material analysis. The data

from subsequent processing of the collected off-line samples were incorporated with the online measurement data in a thorough investigation of KPIs and effects important for large scale operation of the CLG process.

To the four aspects which are part of this cumulative dissertation the following answers were found (details are in the individual publications in Chapter 3):

1. An industrially applicable process control scheme for the autothermal CLG process with sub-stoichiometric AR conditions was successfully employed during the experiments. The scheme was able to control the process and the effect on the OC was studied in detail. The control concept opens up a free choice of OC materials without the need to find an OC with the correct oxygen carrying capacity R_{OC} for the process, as the control concept allows the use of all materials with R_{OC} above the minimum required for the process.

2. An experimental facility for the investigation of the CLG and DFBG process including all relevant documentation was designed and commissioned and first operation experience was generated. It consists of two interconnected CFB reactors with an internal solid circulation for the AR and a global solid circulation which is controlled via J-valve. Although not optimized for the process it allowed for the investigation of the CLG process under autothermal conditions.

3. Solid circulation rates have been determined utilizing a new method based on solid samples collected from the loop seals. The method is applicable to all dual fluidized bed processes and the presented investigation shows an uncertainty of approx. $20\,\%$. The actual solid circulation during the experiments was in the range of $1.2\,\mathrm{kg\,s^{-1}\,MW^{-1}}$ to $4.3\,\mathrm{kg\,s^{-1}\,MW^{-1}}$ with higher circulation being beneficial to syngas quality.

4. CGEs up to 0.5, which is slightly below the range estimated during initial design, could be obtained during the experiments although no optimizations were performed. Carbon conversion is more concentrated inside the FR when FR temperatures are higher, showing the necessity of process control to keep solid circulation and thus heat transport high.

   Gas quality is better than for gases obtained with other gasification technologies. Gravimetric tar productions below $1\,\mathrm{g\,N^{-1}\,m^{-3}}$ make CLG a prime candidate for syngas production where low tar loads are required. Optimization of reactor temperature and inventory will reduce the amount of tars even further.

2.5 Outlook

The results of the experiments present a unique dataset usable as a reference basis for validation of either CFD or process simulation. In fact, a first CLG process model has been validated against the experimental data [156]. Investigation of different feedstock like municipal solid waste or various types of industrial and plastic

wastes and the co-gasification of such feedstocks are important topics in the transformation towards a circular economy. CLG with solid recovered fuel is a prime candidate for near term investigation as there is a good reference base with other gasification technologies and waste streams are available in the required quantity for commercial application. The results encourage further development and upscaling of the CLG technology where the next step in upscaling would be the erection and operation of a demonstration plant optimized for the process.

Other OC materials, especially waste materials like steel converter slag, show promising results and superior performance in lab scale units which should be verified at an industrially relevant scale. For commercial application lower OC life times might be acceptable if waste materials can be sourced cheaper than natural minerals and/or show superior syngas quality. The $1\,\mathrm{MW_{th}}$ modular pilot plant in the configuration for CLG is a prime location to investigate these issues at a scale where the results can be easily transferred to a commercial scale.

The solid samples taken during the three test campaigns pose an interesting collection of OC samples showing the evolution of the OC properties over longer periods under industrially relevant conditions, i.e. thermal and chemical stress as expected in an commercial unit. Further investigation in atomic composition and crystal lattice structure of the samples can give information on the changes expected to happen to OC material during the process and on implications to reaction kinetics and oxygen transport capacity. Moreover, migration pathways and barriers as well as interaction between bed material and feedstock ash under the conditions of the autothermal process can be investigated as well.

References

1. United Nations. *Paris Agreement* Dec. 12, 2015. https://treaties.un.org/pages/ViewDetails.aspx?src=TREATY&mtdsg_no=XXVII-7-d&chapter=27&clang=_en.
2. Friedlingstein, P. *et al.* Global Carbon Budget 2021. *Earth System Science Data* **14,** 1917–2005. ISSN: 1866-3516. doi:10.5194/essd-14-1917-2022. https://essd.copernicus.org/articles/14/1917/2022/ (2023) (Apr. 26, 2022).
3. United Nations Framework Convention on Climate Change (UNFCCC). *Kyoto Protocol* Dec. 10, 1997. https://unfccc.int/sites/default/files/resource/docs/cop3/l07a01.pdf (2023).
4. BP. Statistical Review of World Energy 2022 (2022).
5. Calvin, K. *et al. IPCC, 2023: Climate Change 2023: Synthesis Report. Contribution of Working Groups I, II and III to the Sixth Assessment Report of the Intergovernmental Panel on Climate Change [Core Writing Team, H. Lee and J. Romero (Eds.)]. IPCC, Geneva, Switzerland.* (Intergovernmental Panel on Climate Change (IPCC), July 25, 2023). doi:10.59327/IPCC/AR6-9789291691647. https://www.ipcc.ch/report/ar6/syr/ (2023).
6. Vogt, W. *Road to Survival* (W. Sloane Associates, 1948).
7. *Global Handbook of Quality of Life: Exploration of Well-Being of Nations and Continents* (eds Glatzer, W., Camfield, L., Møller, V. & Rojas, M.) ISBN: 978-94-017-9177-9. doi:10.1007/978-94-017-9178-6. https://link.springer.com/10.1007/978-94-017-9178-6 (2023) (Springer Netherlands, Dordrecht, 2015).
8. Easterlin, R. A. The Worldwide Standard of Living Since 1800. *Journal of Economic Perspectives* **14,** 7–26. ISSN: 0895-3309. doi:10.1257/jep.14.1.7. https://pubs.aeaweb.org/doi/10.1257/jep.14.1.7 (2023) (Feb. 1, 2000).
9. Jevons, W. S. *The Coal Question: An Inquiry Concerning the Progress of the Nation, and the Probable Exhaustion of Our Coal-Mines* (Macmillan and CO, London, 1865).
10. *Greenhouse Gas Emissions from Transport in Europe* https://www.eea.europa.eu/ims/greenhouse-gas-emissions-from-transport (2023).
11. Styring, P., Quadrelli, E. A. & Armstrong, K. *Carbon Dioxide Utilisation* ISBN: 978-0-444-62746-9. doi:10.1016/C2012-0-02814-1. https://linkinghub.elsevier.com/retrieve/pii/C20120028141 (2023) (Elsevier, 2015).
12. Bush, M. J. *Climate Change and Renewable Energy: How to End the Climate Crisis* ISBN: 978-3-030-15424-0. doi:10.1007/978-3-030-15424-0. https://link.springer.com/10.1007/978-3-030-15424-0 (2023) (Springer International Publishing, Cham, 2020).
13. *Waste to Energy: Opportunities and Challenges for Developing and Transition Economies* (ed Karagiannidis, A.) ISBN: 978-1-4471-2306-4. doi:10.1007/978-1-4471-2306-4. https://link.springer.com/10.1007/978-1-4471-2306-4 (2023) (Springer London, London, 2012).
14. Lee, R. P., Keller, F. & Graebner, M. Beyond *Plastics-to-Plastics* to *Waste-to-Products* : Opportunities for Closing the Carbon Cycle via Chemical Recycling. *Chemie Ingenieur Technik* **95,** 1228–1232. ISSN: 0009-286X, 1522-2640. doi:10.1002/cite.202300013. https://onlinelibrary.wiley.com/doi/10.1002/cite.202300013 (2023) (Aug. 2023).
15. Higman, C. & van der Burgt, M. *Gasification* 2nd ed. 435 pp. ISBN: 978-0-7506-8528-3 (Gulf Professional Pub./Elsevier Science, Amsterdam ; Boston, 2008).

16. *Climate Change 2022 - Mitigation of Climate Change: Working Group III Contribution to the Sixth Assessment Report of the Intergovernmental Panel on Climate Change* 1st ed. (ed Intergovernmental Panel On Climate Change (Ipcc)) ISBN: 978-1-00-915792-6. doi:10.1017/9781009157926. https://www.cambridge.org/core/product/identifier/9781009157926/type/book (2023) (Cambridge University Press, Aug. 17, 2023).

17. Anderson, K. & Peters, G. The Trouble with Negative Emissions. *Science* **354,** 182–183. ISSN: 0036-8075, 1095-9203. doi:10.1126/science.aah4567. https://www.science.org/doi/10.1126/science.aah4567 (2023) (Oct. 14, 2016).

18. Cramer, W., Kicklighter, D. W., Bondeau, A., Iii, B. M., Churkina, G., Nemry, B., Ruimy, A., Schloss, A. L. & Intercomparison, T. P. O. T. P. N. M. Comparing Global Models of Terrestrial Net Primary Productivity (NPP): Overview and Key Results. *Global Change Biology* **5,** 1–15. ISSN: 1354-1013, 1365-2486. doi:10.1046/j.1365-2486.1999.00009.x. https://onlinelibrary.wiley.com/doi/10.1046/j.1365-2486.1999.00009.x (2023) (Apr. 1999).

19. Ito, A. A Historical Meta-analysis of Global Terrestrial Net Primary Productivity: Are Estimates Converging? *Global Change Biology* **17,** 3161–3175. ISSN: 1354-1013, 1365-2486. doi:10.1111/j.1365-2486.2011.02450.x. https://onlinelibrary.wiley.com/doi/10.1111/j.1365-2486.2011.02450.x (2023) (Oct. 2011).

20. Pan, S. *et al.* Impacts of Climate Variability and Extremes on Global Net Primary Production in the First Decade of the 21st Century. *Journal of Geographical Sciences* **25,** 1027–1044. ISSN: 1009-637X, 1861-9568. doi:10.1007/s11442-015-1217-4. http://link.springer.com/10.1007/s11442-015-1217-4 (2023) (Sept. 2015).

21. McKendry, P. Energy Production from Biomass (Part 1): Overview of Biomass. *Bioresource Technology* **83,** 37–46. ISSN: 09608524. doi:10.1016/S0960-8524(01)00118-3. https://linkinghub.elsevier.com/retrieve/pii/S0960852401001183 (2023) (May 2002).

22. Field, C. B., Behrenfeld, M. J., Randerson, J. T. & Falkowski, P. Primary Production of the Biosphere: Integrating Terrestrial and Oceanic Components. *Science* **281,** 237–240. ISSN: 0036-8075, 1095-9203. doi:10.1126/science.281.5374.237. https://www.science.org/doi/10.1126/science.281.5374.237 (2023) (July 10, 1998).

23. *Bioenergy Options for a Cleaner Environment in Developed and Developing Countries* 1st ed (ed Sims, R. E. H.) 184 pp. ISBN: 978-0-08-044351-5 (Elsevier, Amsterdam ; Boston, 2004).

24. Ladanai, S. & Vinterbäck, J. Global Potential of Sustainable Biomass for Energy. ISSN: ISSN 1654-9406. https://www.worldbioenergy.org/uploads/WBA_Global%20Potential.pdf (2023) (2009).

25. Smith, W. K., Zhao, M. & Running, S. W. Global Bioenergy Capacity as Constrained by Observed Biospheric Productivity Rates. *BioScience* **62,** 911–922. ISSN: 1525-3244, 0006-3568. doi:10.1525/bio.2012.62.10.11. https://academic.oup.com/bioscience/article-lookup/doi/10.1525/bio.2012.62.10.11 (2023) (Oct. 2012).

26. Beringer, T., Lucht, W. & Schaphoff, S. Bioenergy Production Potential of Global Biomass Plantations under Environmental and Agricultural Constraints: BIOENERGY PRODUCTION POTENTIAL OF GLOBAL BIOMASS PLANTATIONS. *GCB Bioenergy* **3,** 299–312. ISSN: 17571693. doi:10.1111/j.1757-1707.2010.01088.x. https://onlinelibrary.wiley.com/doi/10.1111/j.1757-1707.2010.01088.x (2023) (Aug. 2011).

27. Smeets, E., Faaij, A., Lewandowski, I. & Turkenburg, W. A Bottom-up Assessment and Review of Global Bio-Energy Potentials to 2050. *Progress in Energy and Combustion Science* **33,** 56–106. ISSN: 03601285. doi:10.1016/j.pecs.2006.08.001. https://linkinghub.elsevier.com/retrieve/pii/S0360128506000359 (2023) (Feb. 2007).

28. Haberl, H., Beringer, T., Bhattacharya, S. C., Erb, K.-H. & Hoogwijk, M. The Global Technical Potential of Bio-Energy in 2050 Considering Sustainability Constraints. *Current Opinion in Environmental Sustainability* **2,** 394–403. ISSN: 18773435. doi:10.1016/j.cosust.2010.10.007. https://linkinghub.elsevier.com/retrieve/pii/S1877343510001132 (2023) (Dec. 2010).

29. Haberl, H., Erb, K.-H., Krausmann, F., Running, S., Searchinger, T. D. & Kolby Smith, W. Bioenergy: How Much Can We Expect for 2050? *Environmental Research Letters* **8,** 031004. ISSN: 1748-9326. doi:10.1088/1748-9326/8/3/031004. https://iopscience.iop.org/article/10.1088/1748-9326/8/3/031004 (2023) (Sept. 1, 2013).

30. Klein, D., Humpenöder, F., Bauer, N., Dietrich, J. P., Popp, A., Leon Bodirsky, B., Bonsch, M. & Lotze-Campen, H. The Global Economic Long-Term Potential of Modern Biomass in a Climate-Constrained World. *Environmental Research Letters* **9,** 074017. ISSN: 1748-9326. doi:10.1088/1748-9326/9/7/074017. https://iopscience.iop.org/article/10.1088/1748-9326/9/7/074017 (2023) (July 1, 2014).

31. Wu, W., Hasegawa, T., Ohashi, H., Hanasaki, N., Liu, J., Matsui, T., Fujimori, S., Masui, T. & Takahashi, K. Global Advanced Bioenergy Potential under Environmental Protection Policies and Societal Transformation Measures. *GCB Bioenergy* **11,** 1041–1055. ISSN: 1757-1693, 1757-1707. doi:10.1111/gcbb.12614. https://onlinelibrary.wiley.com/doi/10.1111/gcbb.12614 (2023) (Sept. 2019).

32. Dornburg, V. *et al.* Bioenergy Revisited: Key Factors in Global Potentials of Bioenergy. *Energy & Environmental Science* **3,** 258. ISSN: 1754-5692, 1754-5706. doi:10.1039/b922422j. http://xlink.rsc.org/?DOI=b922422j (2023) (2010).

33. Slade, R., Bauen, A. & Gross, R. Global Bioenergy Resources. *Nature Climate Change* **4,** 99–105. ISSN: 1758-678X, 1758-6798. doi:10.1038/nclimate2097. https://www.nature.com/articles/nclimate2097 (2023) (Feb. 2014).

34. Errera, M., Dias, T. C., Maya, D. & Lora, E. Global Bioenergy Potentials Projections for 2050. *Biomass and Bioenergy* **170,** 106721. ISSN: 09619534. doi:10.1016/j.biombioe.2023.106721. https://linkinghub.elsevier.com/retrieve/pii/S0961953423000193 (2023) (Mar. 2023).

35. Haberl, H., Erb, K. H., Krausmann, F., Gaube, V., Bondeau, A., Plutzar, C., Gingrich, S., Lucht, W. & Fischer-Kowalski, M. Quantifying and Mapping the Human Appropriation of Net Primary Production in Earth's Terrestrial Ecosystems. *Proceedings of the National Academy of Sciences* **104,** 12942–12947. ISSN: 0027-8424, 1091-6490. doi:10.1073/pnas.0704243104. https://pnas.org/doi/10.1073/pnas.0704243104 (2023) (July 31, 2007).

36. Krausmann, F., Erb, K.-H., Gingrich, S., Haberl, H., Bondeau, A., Gaube, V., Lauk, C., Plutzar, C. & Searchinger, T. D. Global Human Appropriation of Net Primary Production Doubled in the 20th Century. *Proceedings of the National Academy of Sciences* **110,** 10324–10329. ISSN: 0027-8424, 1091-6490. doi:10.1073/pnas.1211349110. https://pnas.org/doi/full/10.1073/pnas.1211349110 (2023) (June 18, 2013).

37. International Energy Agency. *Net Zero Roadmap: A Global Pathway to Keep the 1.5 °C Goal in Reach - 2023 Update* (Paris, 2023). https://www.iea.org/reports/net-zero-roadmap-a-global-pathway-to-keep-the-15-0c-goal-in-reach (2023).

38. Ipcc. *Global Warming of 1.5°C: IPCC Special Report on Impacts of Global Warming of 1.5°C above Pre-industrial Levels in Context of Strengthening Response to Climate Change, Sustainable Development, and Efforts to Eradicate Poverty* 1st ed. ISBN: 978-1-00-915794-0. doi:10.1017/9781009157940. https://www.cambridge.org/core/product/identifier/9781009157940/type/book (2023) (Cambridge University Press, June 9, 2022).

39. Reid, W. V., Ali, M. K. & Field, C. B. The Future of Bioenergy. *Global Change Biology* **26,** 274–286. ISSN: 1354-1013, 1365-2486. doi:10.1111/gcb.14883. https://onlinelibrary.wiley.com/doi/10.1111/gcb.14883 (2023) (Jan. 2020).

40. World Bioenergy Association. *Global Bioenergy Statistics 2022* (2023). https://www.worldbioenergy.org/uploads/221223%20WBA%20GBS%202022.pdf (2023).

41. Adams, P., Bridgwater, T., Lea-Langton, A., Ross, A. & Watson, I. in *Greenhouse Gases Balances of Bioenergy Systems* 107–139 (Elsevier, 2018). ISBN: 978-0-08-101036-5. doi:10.1016/B978-0-08-101036-5.00008-2. https://linkinghub.elsevier.com/retrieve/pii/B9780081010365000082 (2023).

42. FAO. *UNIFIED BIOENERGY TERMINOLOGY* (Rome, Dec. 2004). https://www.fao.org/3/j4504e/j4504e00.pdf (2023).

43. Kemper, T. G. in *Bailey's Industrial Oil and Fat Products* (ed Shahidi, F.) 1st ed., 1–38 (Wiley, Feb. 17, 2020). ISBN: 978-0-471-38460-1. doi:10.1002/047167849X.bio013.pub2. https://onlinelibrary.wiley.com/doi/10.1002/047167849X.bio013.pub2 (2023).

44. International Energy Agency. *Biofuels for Transport: An International Perspective* ISBN: 978-92-64-01513-5. doi:10.1787/9789264015135-en. https://www.oecd-ilibrary.org/energy/biofuels-for-transport_9789264015135-en (2023) (OECD, May 11, 2004).

45. Firrisa, M. T., Van Duren, I. & Voinov, A. Energy Efficiency for Rapeseed Biodiesel Production in Different Farming Systems. *Energy Efficiency* **7,** 79–95. ISSN: 1570-646X, 1570-6478. doi:10.1007/s12053-013-9201-2. http://link.springer.com/10.1007/s12053-013-9201-2 (2023) (Feb. 2014).

46. McKendry, P. Energy Production from Biomass (Part 2): Conversion Technologies. *Bioresource Technology* **83,** 47–54. ISSN: 09608524. doi:10.1016/S0960-8524(01)00119-5. https://linkinghub.elsevier.com/retrieve/pii/S0960852401001195 (2023) (May 2002).

47. Galazka, J. M., Tian, C., Beeson, W. T., Martinez, B., Glass, N. L. & Cate, J. H. D. Cellodextrin Transport in Yeast for Improved Biofuel Production. *Science* **330,** 84–86. ISSN: 0036-8075, 1095-9203. doi:10.1126/science.1192838. https://www.science.org/doi/10.1126/science.1192838 (2023) (Oct. 2010).

48. Liu, J.-C., Chang, W.-J., Hsu, T.-C., Chen, H.-J. & Chen, Y.-C. Direct Fermentation of Cellulose to Ethanol by Saccharomyces Cerevisiae Displaying a Bifunctional Cellobiohydrolase Gene from Orpinomyces Sp. Y102. *Renewable Energy* **159,** 1029–1035. ISSN: 09601481. doi:10.1016/j.renene.2020.05.118. https://linkinghub.elsevier.com/retrieve/pii/S0960148120308223 (2023) (Oct. 2020).

49. Basu, P. *Biomass Gasification, Pyrolysis and Torrefaction* ISBN: 978-0-12-812992-0. doi:10.1016/C2016-0-04056-1. https://linkinghub.elsevier.com/retrieve/pii/C20160040561 (2023) (Elsevier, 2018).

50. Alobaid, F., Busch, Jan-Peter, Stroehle, Jochen & Epple, Bernd. *Investigations on Torrefied Biomass for Co-Combustion in Pulverised Coal-Fired Furnaces* July 2012.

51. Brown, R. C. The Role of Pyrolysis and Gasification in a Carbon Negative Economy. *Processes* **9,** 882. ISSN: 2227-9717. doi:10.3390/pr9050882. https://www.mdpi.com/2227-9717/9/5/882 (2021) (May 18, 2021).

52. Mourant, D., Lievens, C., Gunawan, R., Wang, Y., Hu, X., Wu, L., Syed-Hassan, S. S. A. & Li, C.-Z. Effects of Temperature on the Yields and Properties of Bio-Oil from the Fast Pyrolysis of Mallee Bark. *Fuel* **108,** 400–408. ISSN: 00162361. doi:10.1016/j.fuel.2012.12.018. https://linkinghub.elsevier.com/retrieve/pii/S0016236112010411 (2023) (June 2013).

53. Langner, E., Kaltenmorgen, J., Heinze, C., Ströhle, J. & Epple, B. Fluidized Bed Gasification of Solid Recovered Fuels in a 500 kWth Pilot Plant. *Fuel* **344,** 127901. ISSN: 00162361. doi:10.1016/j.fuel.2023.127901. https://linkinghub.elsevier.com/retrieve/pii/S0016236123005148 (2023) (July 2023).

54. Pissot, S., Berdugo Vilches, T., Thunman, H. & Seemann, M. Dual Fluidized Bed Gasification Configurations for Carbon Recovery from Biomass. *Energy & Fuels* **34,** 16187–16200. ISSN: 0887-0624, 1520-5029. doi:10.1021/acs.energyfuels.0c02781. https://pubs.acs.org/doi/10.1021/acs.energyfuels.0c02781 (2021) (Dec. 17, 2020).

55. Karl, J. & Pröll, T. Steam Gasification of Biomass in Dual Fluidized Bed Gasifiers: A Review. *Renewable and Sustainable Energy Reviews* **98,** 64–78. ISSN: 13640321. doi:10.1016/j.rser.2018.09.010. https://linkinghub.elsevier.com/retrieve/pii/S1364032118306567 (2019) (Dec. 2018).

56. Larsson, A., Kuba, M., Berdugo Vilches, T., Seemann, M., Hofbauer, H. & Thunman, H. Steam Gasification of Biomass – Typical Gas Quality and Operational Strategies Derived from Industrial-Scale Plants. *Fuel Processing Technology* **212,** 106609. ISSN: 03783820. doi:10.1016/j.fuproc.2020.106609. https://linkinghub.elsevier.com/retrieve/pii/S0378382020309000 (2020) (Feb. 2021).

57. Bolhàr-Nordenkampf, M., Rauch, R., Bosch, K. & Aichernig, C. Biomass CHP Plant Güssing – Using Gasification for Power Generation (2003).

58. Larsson, A., Gunnarsson, I. & Tengberg, F. The GoBiGas Project Demonstration of the Production of Biomethane from Biomass via Gasification. doi:10.13140/RG.2.2.27352.55043. http://rgdoi.net/10.13140/RG.2.2.27352.55043 (2022) (2018).

59. Fan, L., Li, F. & Ramkumar, S. Utilization of Chemical Looping Strategy in Coal Gasification Processes. *Particuology* **6,** 131–142. ISSN: 16742001. doi:10.1016/j.partic.2008.03.005. https://linkinghub.elsevier.com/retrieve/pii/S1674200108000552 (2019) (June 2008).

60. Fan, L.-S. *Chemical Looping Systems for Fossil Energy Conversions* 420 pp. ISBN: 978-0-470-87252-9 (Wiley-AIChE, Hoboken, NJ, 2010).

61. *German Biofuel Firm Choren Declares Insolvency | Reuters* https://www.reuters.com/article/biof-gra-de-weu-europe-meal-oils-eny-pro-idAFLDE7670QA20110708/ (2023).

62. *Energy from Organic Materials (Biomass): A Volume in the Encyclopedia of Sustainability Science and Technology, Second Edition* (ed Kaltschmitt, M.) ISBN: 978-1-4939-7812-0. doi:10.1007/978-1-4939-7813-7. http://link.springer.com/10.1007/978-1-4939-7813-7 (2020) (Springer New York, New York, NY, 2019).

63. *Directive (EU) 2018/2001 of the European Parliament and of the Council of 11 December 2018 on the Promotion of the Use of Energy from Renewable Sources (Recast) (Text with EEA Relevance.)* Dec. 11, 2018. http://data.europa.eu/eli/dir/2018/2001/oj/eng (2023).

64. Aneke, M. & Wang, M. Potential for Improving the Energy Efficiency of Cryogenic Air Separation Unit (ASU) Using Binary Heat Recovery Cycles. *Applied Thermal Engineering* **81,** 223–231. ISSN: 13594311. doi:10.1016/j.applthermaleng.2015.02.034. https://linkinghub.elsevier.com/retrieve/pii/S1359431115001428 (2023) (Apr. 2015).

65. Qasim, M., Ayoub, M., Ghazali, N. A., Aqsha, A. & Ameen, M. Recent Advances and Development of Various Oxygen Carriers for the Chemical Looping Combustion Process: A Review. *Industrial & Engineering Chemistry Research* **60,** 8621–8641. ISSN: 0888-5885, 1520-5045. doi:10.1021/acs.iecr.1c01111. https://pubs.acs.org/doi/10.1021/acs.iecr.1c01111 (2023) (June 23, 2021).

66. De Vos, Y., Jacobs, M., Van Der Voort, P., Van Driessche, I., Snijkers, F. & Verberckmoes, A. Development of Stable Oxygen Carrier Materials for Chemical Looping Processes—A Review. *Catalysts* **10,** 926. ISSN: 2073-4344. doi:10.3390/catal10080926. https://www.mdpi.com/2073-4344/10/8/926 (2023) (Aug. 12, 2020).

67. Yu, Z., Yang, Y., Yang, S., Zhang, Q., Zhao, J., Fang, Y., Hao, X. & Guan, G. Iron-Based Oxygen Carriers in Chemical Looping Conversions: A Review. *Carbon Resources Conversion* **2,** 23–34. ISSN: 25889133. doi:10.1016/j.crcon.2018.11.004. https://linkinghub.elsevier.com/retrieve/pii/S2588913318300279 (2023) (Apr. 2019).

68. Lin, Y. *et al.* Review of Biomass Chemical Looping Gasification in China. *Energy & Fuels* **34,** 7847–7862. ISSN: 0887-0624, 1520-5029. doi:10.1021/acs.energyfuels.0c01022. https://pubs.acs.org/doi/10.1021/acs.energyfuels.0c01022 (2020) (July 16, 2020).

69. Mendiara, T., García-Labiano, F., Abad, A., Gayán, P., de Diego, L., Izquierdo, M. & Adánez, J. Negative CO2 Emissions through the Use of Biofuels in Chemical Looping Technology: A Review. *Applied Energy* **232,** 657–684. ISSN: 03062619. doi:10.1016/j.apenergy.2018.09.201. https://linkinghub.elsevier.com/retrieve/pii/S0306261918315186 (2019) (Dec. 2018).

70. Di Giuliano, A., Capone, S., Anatone, M. & Gallucci, K. Chemical Looping Combustion and Gasification: A Review and a Focus on European Research Projects. *Industrial & Engineering Chemistry Research* **61,** 14403–14432. ISSN: 0888-5885, 1520-5045. doi:10.1021/acs.iecr.2c02677. https://pubs.acs.org/doi/10.1021/acs.iecr.2c02677 (2023) (Oct. 5, 2022).

71. Nguyen, N. M., Alobaid, F., Dieringer, P. & Epple, B. Biomass-Based Chemical Looping Gasification: Overview and Recent Developments. *Applied Sciences* **11,** 7069. ISSN: 2076-3417. doi:10.3390/app11157069. https://www.mdpi.com/2076-3417/11/15/7069 (2023) (July 30, 2021).

72. Dai, J. & Whitty, K. J. Chemical Looping Gasification and Sorption Enhanced Gasification of Biomass: A Perspective. *Chemical Engineering and Processing - Process Intensification* **174,** 108902. ISSN: 02552701. doi:10.1016/j.cep.2022.108902. https://linkinghub.elsevier.com/retrieve/pii/S0255270122001180 (2023) (Apr. 2022).

73. Güleç, F. & Okolie, J. A. Decarbonising Bioenergy through Biomass Utilisation in Chemical Looping Combustion and Gasification: A Review. *Environmental Chemistry Letters.* ISSN: 1610-3653, 1610-3661. doi:10.1007/s10311-023-01656-5. https://link.springer.com/10.1007/s10311-023-01656-5 (2023) (Oct. 3, 2023).

74. Goel, A., Moghaddam, E. M., Liu, W., He, C. & Konttinen, J. Biomass Chemical Looping Gasification for High-Quality Syngas: A Critical Review and Technological Outlooks. *Energy Conversion and Management* **268,** 116020. ISSN: 01968904. doi:10.1016/j.enconman.2022.116020. https://linkinghub.elsevier.com/retrieve/pii/S0196890422008135 (2023) (Sept. 2022).

75. Miao, Z., Jiang, E. & Hu, Z. Review of Agglomeration in Biomass Chemical Looping Technology. *Fuel* **309,** 122199. ISSN: 00162361. doi:10.1016/j.fuel.2021.122199. https://linkinghub.elsevier.com/retrieve/pii/S0016236121020755 (2023) (Feb. 2022).

76. Jiang, H., Huo, R., Zhang, Z., Lin, Y., Zhao, Z., Huang, Z., Fang, Y. & Li, H. Removal of Pollution from the Chemical Looping Process: A Mini Review. *Fuel Processing Technology* **221,** 106937. ISSN: 03783820. doi:10.1016/j.fuproc.2021.106937. https://linkinghub.elsevier.com/retrieve/pii/S0378382021002150 (2023) (Oct. 2021).

77. Xu, D., Tong, A. & Fan, L.-S. State of Scale-Up Development in Chemical Looping Technology for Biomass Conversions: A Review and Perspectives. *Waste and Biomass Valorization* **13,** 1363–1383. ISSN: 1877-2641, 1877-265X. doi:10.1007/s12649-021-01563-2. https://link.springer.com/10.1007/s12649-021-01563-2 (2023) (Mar. 2022).

78. Osman, M., Khan, M. N., Zaabout, A., Cloete, S. & Amini, S. Review of Pressurized Chemical Looping Processes for Power Generation and Chemical Production with Integrated CO2 Capture. *Fuel Processing Technology* **214,** 106684. ISSN: 03783820. doi:10.1016/j.fuproc.2020.106684. https://linkinghub.elsevier.com/retrieve/pii/S0378382020309759 (2023) (Apr. 2021).

79. Kuba, M. & Hofbauer, H. Experimental Parametric Study on Product Gas and Tar Composition in Dual Fluid Bed Gasification of Woody Biomass. *Biomass and Bioenergy* **115,** 35–44. ISSN: 09619534. doi:10.1016/j.biombioe.2018.04.007. https://linkinghub.elsevier.com/retrieve/pii/S0961953418300965 (2023) (Aug. 2018).

80. Gogulancea, V., Rolfe, A., Jaffar, M., Brandoni, C., Atsonios, K., Detsios, N., Dieringer, P. & Huang, Y. Technoeconomic and Environmental Assessment of Biomass Chemical Looping Gasification for Advanced Biofuel Production. *International Journal of Energy Research* **2023** (ed Gürel, A. E.) 1–17. ISSN: 1099-114X, 0363-907X. doi:10.1155/2023/6101270. https://www.hindawi.com/journals/ijer/2023/6101270/ (2023) (July 22, 2023).

81. Milne, T. A., Evans, R. J. & Abatzaglou, N. *Biomass Gasifier "Tars": Their Nature, Formation, and Conversion* NREL/TP-570-25357, ON: DE00003726, 3726 (Nov. 1, 1998), NREL/TP-570–25357, ON: DE00003726, 3726. doi:10.2172/3726. http://www.osti.gov/servlets/purl/3726/ (2020).

82. Palma, C. F. Modelling of Tar Formation and Evolution for Biomass Gasification: A Review. *Applied Energy,* 13. doi:10.1016/j.apenergy.2013.04.082 (2013).

83. Condori, O., García-Labiano, F., de Diego, L. F., Izquierdo, M. T., Abad, A. & Adánez, J. Biomass Chemical Looping Gasification for Syngas Production Using Ilmenite as Oxygen Carrier in a 1.5 kWth Unit. *Chemical Engineering Journal* **405,** 126679. ISSN: 13858947. doi:10.1016/j.cej.2020.126679. https://linkinghub.elsevier.com/retrieve/pii/S1385894720328072 (2020) (Feb. 2021).

84. Condori, O., García-Labiano, F., de Diego, L. F., Izquierdo, M. T., Abad, A. & Adánez, J. Syngas Production via Biomass Chemical Looping Gasification (BCLG) in a 50 kWth Unit Using Ilmenite as Oxygen Carrier. *Proceedings of the Fluidized Bed Conversion Conference 2022,* 10 (2022).

85. Condori, O., García-Labiano, F., de Diego, L. F., Izquierdo, M. T., Abad, A. & Adánez, J. Biomass Chemical Looping Gasification for Syngas Production Using LD Slag as Oxygen Carrier in a 1.5 kWth Unit. *Fuel Processing Technology* **222,** 106963. ISSN: 03783820. doi:10.1016/j.fuproc.2021.106963. https://linkinghub.elsevier.com/retrieve/pii/S0378382021002411 (2022) (Nov. 2021).

86. Hildor, F., Leion, H., Linderholm, C. J. & Mattisson, T. Steel Converter Slag as an Oxygen Carrier for Chemical-Looping Gasification. *Fuel Processing Technology* **210,** 106576. ISSN: 03783820. doi:10.1016/j.fuproc.2020.106576. https://linkinghub.elsevier.com/retrieve/pii/S0378382020308675 (2021) (Dec. 2020).

87. Ma, T., Fan, C., Hao, L., Li, S., Song, W. & Lin, W. Biomass-Ash-Induced Agglomeration in a Fluidized Bed. Part 1: Experimental Study on the Effects of a Gas Atmosphere. *Energy & Fuels* **30,** 6395–6404. ISSN: 0887-0624, 1520-5029. doi:10.1021/acs.energyfuels.6b00164. https://pubs.acs.org/doi/10.1021/acs.energyfuels.6b00164 (2023) (Aug. 18, 2016).

88. Ma, T., Fan, C., Hao, L., Li, S., Jensen, P. A., Song, W., Lin, W. & Dam-Johansen, K. Biomass Ash Induced Agglomeration in Fluidized Bed. Part 2: Effect of Potassium Salts in Different Gas Composition. *Fuel Processing Technology* **180,** 130–139. ISSN: 03783820. doi:10.1016/j.fuproc.2018.08.004. https://linkinghub.elsevier.com/retrieve/pii/S0378382018310993 (2023) (Nov. 2018).

89. Fernández, M. J. Sintering Reduction of Herbaceous Biomass When Blended with Woody Biomass_ Predictive and Combustion Tests, 10. doi:10.1016/j.fuel.2018.11.115 (2019).

90. Grimm, A., Öhman, M., Lindberg, T., Fredriksson, A. & Boström, D. Bed Agglomeration Characteristics in Fluidized-Bed Combustion of Biomass Fuels Using Olivine as Bed Material. *Energy & Fuels* **26,** 4550–4559. ISSN: 0887-0624, 1520-5029. doi:10.1021/ef300569n. https://pubs.acs.org/doi/10.1021/ef300569n (2021) (July 19, 2012).

91. Di Giuliano, A., Malsegna, B., Lucantonio, S. & Gallucci, K. Experimental Assessments of Pyrolytic and Fluid-Dynamic Interactions between Pretreated Residual Biomasses and Fluidized Beds Made up of Oxygen Carriers for Chemical Looping Gasification. *Advanced Powder Technology* **34,** 104010. ISSN: 09218831. doi:10.1016/j.apt.2023.104010. https://linkinghub.elsevier.com/retrieve/pii/S0921883123000730 (2023) (May 2023).

92. Balland, M. Biomass Ash Fluidised-Bed Agglomeration: Hydrodynamic Investigations, 19 (2017).

93. Vamvuka, D., Zografos, D. & Alevizos, G. Control Methods for Mitigating Biomass Ash-Related Problems in Fluidized Beds. *Bioresource Technology* **99,** 3534–3544. ISSN: 09608524. doi:10.1016/j.biortech.2007.07.049. https://linkinghub.elsevier.com/retrieve/pii/S0960852407006086 (2021) (June 2008).

94. Di Giuliano, A., Funcia, I., Pérez-Vega, R., Gil, J. & Gallucci, K. Novel Application of Pretreatment and Diagnostic Method Using Dynamic Pressure Fluctuations to Resolve and Detect Issues Related to Biogenic Residue Ash in Chemical Looping Gasification. *Processes* **8,** 1137. ISSN: 2227-9717. doi:10.3390/pr8091137. https://www.mdpi.com/2227-9717/8/9/1137 (2020) (Sept. 11, 2020).

95. Di Giuliano, A., Lucantonio, S. & Gallucci, K. Devolatilization of Residual Biomasses for Chemical Looping Gasification in Fluidized Beds Made up of Oxygen-Carriers. *Energies* **14,** 311. ISSN: 1996-1073. doi:10.3390/en14020311. https://www.mdpi.com/1996-1073/14/2/311 (2021) (Jan. 8, 2021).

96. Di Giuliano, A., Lucantonio, S., Malsegna, B. & Gallucci, K. Pretreated Residual Biomasses in Fluidized Beds for Chemical Looping Gasification: Experimental Devolatilizations and Characterization of Ashes Behavior. *Bioresource Technology* **345,** 126514. ISSN: 09608524. doi:10.1016/j.biortech.2021.126514. https://linkinghub.elsevier.com/retrieve/pii/S0960852421018563 (2021) (Feb. 2022).

97. Di Giuliano, A., Gallucci, M., Malsegna, B., Lucantonio, S. & Gallucci, K. Pretreated Residual Biomasses in Fluidized Beds for Chemical Looping Gasification: Analysis of Devolatilization Data by Statistical Tools. *Bioresource Technology Reports* **17,** 100926. ISSN: 2589014X. doi:10.1016/j.biteb.2021.100926. https://linkinghub.elsevier.com/retrieve/pii/S2589014X21003042 (2022) (Feb. 2022).

98. Wang, P., Means, N., Shekhawat, D., Berry, D. & Massoudi, M. Chemical-Looping Combustion and Gasification of Coals and Oxygen Carrier Development: A Brief Review. *Energies* **8,** 10605–10635. ISSN: 1996-1073. doi:10.3390/en81010605. http://www.mdpi.com/1996-1073/8/10/10605 (2019) (Sept. 24, 2015).

99. Purnomo, V., Mei, D., Soleimanisalim, A. H., Mattisson, T. & Leion, H. Effect of the Mass Conversion Degree of an Oxygen Carrier on Char Conversion and Its Implication for Chemical Looping Gasification. *Energy & Fuels* **36,** 9768–9779. ISSN: 0887-0624, 1520-5029. doi:10.1021/acs.energyfuels.2c00944. https://pubs.acs.org/doi/10.1021/acs.energyfuels.2c00944 (2023) (Sept. 1, 2022).

100. Bayham, S. C. *et al.* Iron-Based Coal Direct Chemical Looping Combustion Process: 200-h Continuous Operation of a 25-kW $_{th}$ Subpilot Unit. *Energy & Fuels* **27,** 1347–1356. ISSN: 0887-0624, 1520-5029. doi:10.1021/ef400010s. https://pubs.acs.org/doi/10.1021/ef400010s (2023) (Mar. 21, 2013).

101. Kim, H. R. Coal Direct Chemical Looping Combustion Process: Design and Operation of a 25-kWth Sub-Pilot Unit, 15 (2013).

102. Hedayati, A., Soleimanisalim, A. H., Linderholm, C. J., Mattisson, T. & Lyngfelt, A. Experimental Evaluation of Manganese Ores for Chemical Looping Conversion of Synthetic Biomass Volatiles in a 300 W Reactor System. *Journal of Environmental Chemical Engineering* **9,** 105112. ISSN: 22133437. doi:10.1016/j.jece.2021.105112. https://linkinghub.elsevier.com/retrieve/pii/S2213343721000907 (2021) (Apr. 2021).

103. Hedayati, A., Soleimanisalim, A. H., Mattisson, T. & Lyngfelt, A. Thermochemical Conversion of Biomass Volatiles via Chemical Looping: Comparison of Ilmenite and Steel Converter Waste Materials as Oxygen Carriers. *Fuel* **313,** 122638. ISSN: 00162361. doi:10.1016/j.fuel.2021.122638. https://linkinghub.elsevier.com/retrieve/pii/S0016236121025059 (2022) (Apr. 2022).

104. Hildor, F., Soleimanisalim, A. H., Seemann, M., Mattisson, T. & Leion, H. Tar Characteristics Generated from a 10 kWth Chemical-Looping Biomass Gasifier Using Steel Converter Slag as an Oxygen Carrier. *Fuel* **331,** 125770. ISSN: 00162361. doi:10.1016/j.fuel.2022.125770. https://linkinghub.elsevier.com/retrieve/pii/S0016236122025972 (2023) (Jan. 2023).

105. Condori, O., Abad, A., Izquierdo, M. T., de Diego, L. F., García-Labiano, F. & Adánez, J. Assessment of the Chemical Looping Gasification of Wheat Straw Pellets at the 20 kWth Scale. *Fuel* **344,** 128059. ISSN: 00162361. doi:10.1016/j.fuel.2023.128059. https://linkinghub.elsevier.com/retrieve/pii/S0016236123006725 (2023) (July 2023).

106. Mendiara, T., Pérez-Astray, A., Izquierdo, M., Abad, A., De Diego, L., García-Labiano, F., Gayán, P. & Adánez, J. Chemical Looping Combustion of Different Types of Biomass in a 0.5 kWth Unit. *Fuel* **211,** 868–875. ISSN: 00162361. doi:10.1016/j.fuel.2017.09.113. https://linkinghub.elsevier.com/retrieve/pii/S0016236117312218 (2023) (Jan. 2018).

107. Luo, S., Zeng, L. & Fan, L.-S. Chemical Looping Technology: Oxygen Carrier Characteristics. *Annual Review of Chemical and Biomolecular Engineering* **6,** 53–75. ISSN: 1947-5438, 1947-5446. doi:10.1146/annurev-chembioeng-060713-040334. http://www.annualreviews.org/doi/10.1146/annurev-chembioeng-060713-040334 (2020) (July 24, 2015).

108. Samprón, I., De Diego, L. F., García-Labiano, F. & Izquierdo, M. T. Effect of the Fe Content on the Behavior of Synthetic Oxygen Carriers in a 1.5 kW Biomass Chemical Looping Gasification Unit. *Fuel* **309,** 122193. ISSN: 00162361. doi:10.1016/j.fuel.2021.122193. https://linkinghub.elsevier.com/retrieve/pii/S001623612102069X (2023) (Feb. 2022).

109. Goel, A., Ismailov, A., Moghaddam, E. M., He, C. & Konttinen, J. Evaluation of Low-Cost Oxygen Carriers for Biomass Chemical Looping Gasification. *Chemical Engineering Journal* **469,** 143948. ISSN: 13858947. doi:10.1016/j.cej.2023.143948. https://linkinghub.elsevier.com/retrieve/pii/S1385894723026797 (2023) (Aug. 2023).

110. Zhao, H., Tian, X., Ma, J., Chen, X., Su, M., Zheng, C. & Wang, Y. Chemical Looping Combustion of Coal in China: Comprehensive Progress, Remaining Challenges, and Potential Opportunities. *Energy & Fuels* **34,** 6696–6734. ISSN: 0887-0624, 1520-5029. doi:10.1021/acs.energyfuels.0c00989. https://pubs.acs.org/doi/10.1021/acs.energyfuels.0c00989 (2023) (June 18, 2020).

111. Ohlemüller, P., Reitz, M., Ströhle, J. & Epple, B. Investigation of Chemical Looping Combustion of Natural Gas at 1 MWth Scale. *Proceedings of the Combustion Institute* **37,** 4353–4360. ISSN: 15407489. doi:10.1016/j.proci.2018.07.035. https://linkinghub.elsevier.com/retrieve/pii/S154074891830453X (2023) (2019).

112. Larsson, A., Israelsson, M., Lind, F., Seemann, M. & Thunman, H. Using Ilmenite To Reduce the Tar Yield in a Dual Fluidized Bed Gasification System. *Energy & Fuels* **28,** 2632–2644. ISSN: 0887-0624, 1520-5029. doi:10.1021/ef500132p. https://pubs.acs.org/doi/10.1021/ef500132p (2020) (Apr. 17, 2014).

113. Virginie, M., Adánez, J., Courson, C., de Diego, L., García-Labiano, F., Niznansky, D., Kiennemann, A., Gayán, P. & Abad, A. Effect of Fe–Olivine on the Tar Content during Biomass Gasification in a Dual Fluidized Bed. *Applied Catalysis B: Environmental* **121–122,** 214–222. ISSN: 09263373. doi:10.1016/j.apcatb.2012.04.005. https://linkinghub.elsevier.com/retrieve/pii/S0926337312001403 (2020) (June 2012).

114. Mendiara, T., Johansen, J. M., Utrilla, R., Geraldo, P., Jensen, A. D. & Glarborg, P. Evaluation of Different Oxygen Carriers for Biomass Tar Reforming (I): Carbon Deposition in Experiments with Toluene. *Fuel* **90,** 1049–1060. ISSN: 00162361. doi:10.1016/j.fuel.2010.11.028. https://linkinghub.elsevier.com/retrieve/pii/S0016236110006435 (2023) (Mar. 2011).

115. Zhen, H. *et al.* Chemical Looping Gasification of Benzene as a Biomass Tar Model Compound Using Hematite Modified by Ni as an Oxygen Carrier. *Applications in Energy and Combustion Science* **15,** 100172. ISSN: 2666352X. doi:10.1016/j.jaecs.2023.100172. https://linkinghub.elsevier.com/retrieve/pii/S2666352X23000614 (2023) (Sept. 2023).

116. Adanez, J., Abad, A., Garcia-Labiano, F., Gayan, P. & de Diego, L. F. Progress in Chemical-Looping Combustion and Reforming Technologies. *Progress in Energy and Combustion Science* **38,** 215–282. ISSN: 03601285. doi:10.1016/j.pecs.2011.09.001. https://linkinghub.elsevier.com/retrieve/pii/S0360128511000505 (2019) (Apr. 2012).

117. Fan, L.-S., Zeng, L. & Luo, S. Chemical-Looping Technology Platform. *AIChE Journal* **61,** 2–22. ISSN: 00011541. doi:10.1002/aic.14695. http://doi.wiley.com/10.1002/aic.14695 (2020) (Jan. 2015).

118. Mayer, K., Penthor, S., Pröll, T. & Hofbauer, H. The Different Demands of Oxygen Carriers on the Reactor System of a CLC Plant – Results of Oxygen Carrier Testing in a 120 kWth Pilot Plant. *Applied Energy* **157,** 323–329. ISSN: 03062619. doi:10.1016/j.apenergy.2015.07.053. https://linkinghub.elsevier.com/retrieve/pii/S030626191500882X (2020) (Nov. 2015).

119. Wei, G., He, F., Huang, Z., Zheng, A., Zhao, K. & Li, H. Continuous Operation of a 10 kW $_{th}$ Chemical Looping Integrated Fluidized Bed Reactor for Gasifying Biomass Using an Iron-Based Oxygen Carrier. *Energy & Fuels* **29,** 233–241. ISSN: 0887-0624, 1520-5029. doi:10.1021/ef5021457. https://pubs.acs.org/doi/10.1021/ef5021457 (2020) (Jan. 15, 2015).

120. Shen, T., Wu, J., Shen, L., Yan, J. & Jiang, S. Chemical Looping Gasification of Coal in a 5 kW $_{th}$ Interconnected Fluidized Bed with a Two-Stage Fuel Reactor. *Energy & Fuels* **32,** 4291–4299. ISSN: 0887-0624, 1520-5029. doi:10.1021/acs.energyfuels.7b03111. https://pubs.acs.org/doi/10.1021/acs.energyfuels.7b03111 (2023) (Apr. 19, 2018).

121. Pissot, S., Vilches, T. B., Maric, J. & Seemann, M. *Chemical Looping Gasification in a 2-4 MWth Dual Fluidized Bed Gasifier* in. 23rd International Conference on Fluidized Bed ConversionSeoul, South Korea (2018), 10.

122. Ge, H., Guo, W., Shen, L., Song, T. & Xiao, J. Biomass Gasification Using Chemical Looping in a 25 kW Th Reactor with Natural Hematite as Oxygen Carrier. *Chemical Engineering Journal* **286,** 174–183. ISSN: 13858947. doi:10.1016/j.cej.2015.10.092. https://linkinghub.elsevier.com/retrieve/pii/S138589471501503X (2020) (Feb. 2016).

123. Berdugo Vilches, T., Lind, F., Rydén, M. & Thunman, H. Experience of More than 1000 h of Operation with Oxygen Carriers and Solid Biomass at Large Scale. *Applied Energy* **190,** 1174–1183. ISSN: 03062619. doi:10.1016/j.apenergy.2017.01.032. https://linkinghub.elsevier.com/retrieve/pii/S0306261917300405 (2023) (Mar. 2017).

124. Hilz, J., Helbig, M., Haaf, M., Daikeler, A., Ströhle, J. & Epple, B. Long-Term Pilot Testing of the Carbonate Looping Process in 1 MWth Scale. *Fuel* **210,** 892–899. ISSN: 00162361. doi:10.1016/j.fuel.2017.08.105. https://linkinghub.elsevier.com/retrieve/pii/S0016236117310967 (2022) (Dec. 2017).

125. Haaf, M., Peters, J., Hilz, J., Unger, A., Ströhle, J. & Epple, B. Combustion of Solid Recovered Fuels within the Calcium Looping Process – Experimental Demonstration at 1 MWth Scale. *Experimental Thermal and Fluid Science* **113,** 110023. ISSN: 08941777. doi:10.1016/j.expthermflusci.2019.110023. https://linkinghub.elsevier.com/retrieve/pii/S0894177719319259 (2020) (May 2020).

126. Ströhle, J., Orth, M. & Epple, B. Design and Operation of a 1 MWth Chemical Looping Plant. *Applied Energy* **113,** 1490–1495. ISSN: 03062619. doi:10.1016/j.apenergy.2013.09.008. https://linkinghub.elsevier.com/retrieve/pii/S030626191300754X (2019) (Jan. 2014).

127. Ströhle, J., Orth, M. & Epple, B. Chemical Looping Combustion of Hard Coal in a 1 MWth Pilot Plant Using Ilmenite as Oxygen Carrier. *Applied Energy* **157,** 288–294. ISSN: 03062619. doi:10.1016/j.apenergy.2015.06.035. https://linkinghub.elsevier.com/retrieve/pii/S030626191500793X (2020) (Nov. 2015).

128. Ohlemüller, P., Busch, J.-P., Reitz, M., Ströhle, J. & Epple, B. Chemical-Looping Combustion of Hard Coal: Autothermal Operation of a 1 MWth Pilot Plant. *Journal of Energy Resources Technology* **138,** 042203. ISSN: 0195-0738, 1528-8994. doi:10.1115/1.4032357. https://asmedigitalcollection.asme.org/energyresources/article/doi/10.1115/1.4032357/373072/ChemicalLooping-Combustion-of-Hard-Coal (2019) (July 1, 2016).

129. Ohlemüller, P., Ströhle, J. & Epple, B. Chemical Looping Combustion of Hard Coal and Torrefied Biomass in a 1 MW Th Pilot Plant. *International Journal of Greenhouse Gas Control* **65,** 149–159. ISSN: 17505836. doi:10.1016/j.ijggc.2017.08.013. https://linkinghub.elsevier.com/retrieve/pii/S1750583617302190 (2019) (Oct. 2017).

130. Ohlemüller, P. G. *Untersuchung von Chemical-Looping-Combustion im Megawatt-Maßstab* 1. Auflage. 175 pp. ISBN: 978-3-7369-9959-6 (Cuvillier Verlag, Göttingen, 2019).

131. Herdel, P., Krause, D., Peters, J., Kolmorgen, B., Ströhle, J. & Epple, B. Experimental Investigations in a Demonstration Plant for Fluidized Bed Gasification of Multiple Feedstock's in 0.5 MW Th Scale. *Fuel* **205,** 286–296. ISSN: 00162361. doi:10.1016/j.fuel.2017.05.058. https://linkinghub.elsevier.com/retrieve/pii/S0016236117306336 (2019) (Oct. 2017).

132. Krause, D., Herdel, P., Ströhle, J. & Epple, B. HTW™-Gasification of High Volatile Bituminous Coal in a 500 kWth Pilot Plant. *Fuel* **250,** 306–314. ISSN: 00162361. doi:10.1016/j.fuel.2019.04.014. https://linkinghub.elsevier.com/retrieve/pii/S001623611930571X (2019) (Aug. 2019).

133. Heinze, C., May, J., Langner, E., Ströhle, J. & Epple, B. High Temperature Winkler Gasification of Rhenish Lignite in an Optimized 500 kWth Pilot Plant. *Fuel* **333,** 126289. ISSN: 00162361. doi:10.1016/j.fuel.2022.126289. https://linkinghub.elsevier.com/retrieve/pii/S0016236122031131 (2023) (Feb. 2023).

134. Larsson, A., Seemann, M., Neves, D. & Thunman, H. Evaluation of Performance of Industrial-Scale Dual Fluidized Bed Gasifiers Using the Chalmers 2–4-MW $_{th}$ Gasifier. *Energy & Fuels* **27,** 6665–6680. ISSN: 0887-0624, 1520-5029. doi:10.1021/ef400981j. https://pubs.acs.org/doi/10.1021/ef400981j (2020) (Nov. 21, 2013).

135. Linderholm, C., Schmitz, M. & Lyngfelt, A. Estimating the Solids Circulation Rate in a 100-kW Chemical Looping Combustor. *Chemical Engineering Science* **171,** 351–359. ISSN: 00092509. doi:10.1016/j.ces.2017.05.025. https://linkinghub.elsevier.com/retrieve/pii/S0009250917303378 (2022) (Nov. 2017).

136. Ludlow, J. C., Monazam, E. R. & Shadle, L. J. Improvement of Continuous Solid Circulation Rate Measurement in a Cold Flow Circulating Fluidized Bed. *Powder Technology* **182,** 379–387. ISSN: 00325910. doi:10.1016/j.powtec.2007.06.031. https://linkinghub.elsevier.com/retrieve/pii/S0032591007003312 (2022) (Mar. 2008).

137. Stollhof, M., Penthor, S., Mayer, K. & Hofbauer, H. Estimation of the Solid Circulation Rate in Circulating Fluidized Bed Systems. *Powder Technology* **336,** 1–11. ISSN: 00325910. doi:10.1016/j.powtec.2018.05.033. https://linkinghub.elsevier.com/retrieve/pii/S0032591018304054 (2022) (Aug. 2018).

138. Ohlemüller, P., Alobaid, F., Gunnarsson, A., Ströhle, J. & Epple, B. Development of a Process Model for Coal Chemical Looping Combustion and Validation against 100 kWth Tests. *Applied Energy* **157,** 433–448. ISSN: 03062619. doi:10.1016/j.apenergy.2015.05.088. https://linkinghub.elsevier.com/retrieve/pii/S0306261915007217 (2019) (Nov. 2015).

139. Ohlemüller, P., Alobaid, F., Abad, A., Adanez, J., Ströhle, J. & Epple, B. Development and Validation of a 1D Process Model with Autothermal Operation of a 1 MW Th Chemical Looping Pilot Plant. *International Journal of Greenhouse Gas Control* **73,** 29–41. ISSN: 17505836. doi:10.1016/j.ijggc.2018.03.013. https://linkinghub.elsevier.com/retrieve/pii/S1750583617308381 (2019) (June 2018).

140. Pröll, T., Bolhàr-Nordenkampf, J., Kolbitsch, P. & Hofbauer, H. Syngas and a Separate Nitrogen/Argon Stream via Chemical Looping Reforming – A 140kW Pilot Plant Study. *Fuel* **89,** 1249–1256. ISSN: 00162361. doi:10.1016/j.fuel.2009.09.033. https://linkinghub.elsevier.com/retrieve/pii/S0016236109004608 (2019) (June 2010).

141. Huseyin, S., Wei, G.-q., Li, H.-b., He, F. & Huang, Z. Chemical-Looping Gasification of Biomass in a 10 kWth Interconnected Fluidized Bed Reactor Using Fe2O3/Al2O3 Oxygen Carrier. *Journal of Fuel Chemistry and Technology* **42,** 922–931. ISSN: 18725813. doi:10.1016/S1872-5813(14)60039-6 (Aug. 2014).

142. Markström, P., Linderholm, C. & Lyngfelt, A. Chemical-Looping Combustion of Solid Fuels – Design and Operation of a 100kW Unit with Bituminous Coal. *International Journal of Greenhouse Gas Control* **15,** 150–162. ISSN: 17505836. doi:10.1016/j.ijggc.2013.01.048. https://linkinghub.elsevier.com/retrieve/pii/S1750583613000790 (2019) (July 2013).

143. Guo, Q., Cheng, Y., Liu, Y., Jia, W. & Ryu, H.-J. Coal Chemical Looping Gasification for Syngas Generation Using an Iron-Based Oxygen Carrier. *Industrial & Engineering Chemistry Research* **53,** 78–86. ISSN: 0888-5885, 1520-5045. doi:10.1021/ie401568x. https://pubs.acs.org/doi/10.1021/ie401568x (2020) (Jan. 8, 2014).

144. Song, Q., Xiao, R., Deng, Z., Zhang, H., Shen, L., Xiao, J. & Zhang, M. Chemical-Looping Combustion of Methane with CaSO4 Oxygen Carrier in a Fixed Bed Reactor. *Energy Conversion and Management* **49,** 3178–3187. ISSN: 01968904. doi:10.1016/j.enconman.2008.05.020. https://linkinghub.elsevier.com/retrieve/pii/S0196890408002197 (2020) (Nov. 2008).

145. Ryu, H.-J., Bae, D.-H. & Jin, G.-T. Effect of Temperature on Reduction Reactivity of Oxygen Carrier Particles in a Fixed Bed Chemical-Looping Combustor. *Korean Journal of Chemical Engineering* **20,** 960–966. ISSN: 0256-1115, 1975-7220. doi:10.1007/BF02697306. http://link.springer.com/10.1007/BF02697306 (2020) (Sept. 2003).

146. Abad, A., Adánez, J., Cuadrat, A., García-Labiano, F., Gayán, P. & de Diego, L. F. Kinetics of Redox Reactions of Ilmenite for Chemical-Looping Combustion. *Chemical Engineering Science* **66,** 689–702. ISSN: 00092509. doi:10.1016/j.ces.2010.11.010. https://linkinghub.elsevier.com/retrieve/pii/S000925091000672X (2019) (Feb. 2011).

147. Kunii, D. & Levenspiel, O. *Fluidization Engineering* 2. 491 pp. ISBN: 978-0-409-90233-4 (Butterworth-Heinemann, Boston, 1991).

148. Mendiara, T., Johansen, J. M., Utrilla, R., Jensen, A. D. & Glarborg, P. Evaluation of Different Oxygen Carriers for Biomass Tar Reforming (II): Carbon Deposition in Experiments with Methane and Other Gases. *Fuel* **90,** 1370–1382. ISSN: 00162361. doi:10.1016/j.fuel.2010.12.034. https://linkinghub.elsevier.com/retrieve/pii/S0016236110006940 (2023) (Apr. 2011).

149. Bartocci, P., Abad, A., Flores, A. C. & de las Obras Loscertales, M. Ilmenite: A Promising Oxygen Carrier for the Scale-up of Chemical Looping. *Fuel* **337,** 126644. ISSN: 00162361. doi:10.1016/j.fuel.2022.126644. https://linkinghub.elsevier.com/retrieve/pii/S0016236122034688 (2023) (Apr. 2023).

150. Dieringer, P., Marx, F., Ströhle, J. & Epple, B. System Hydrodynamics of a 1 MWth Dual Circulating Fluidized Bed Chemical Looping Gasifier. *Energies.* ISSN: 1996-1073. doi:10.3390/en16155630. https://www.mdpi.com/1996-1073/16/15/5630 (2023).

151. Dieringer, P., Marx, F., Lebendig, F., Müller, M., Di Guiliano, A., Galucci, K., Ströhle, J. & Epple, B. Fate of Ilmenite as Oxygen Carrier during 1 MWth Chemical Looping Gasification of Biogenic Residues. *Applications in Energy and Combustion Science,* 100227. ISSN: 2666352X. doi:10.1016/j.jaecs.2023.100227. https://linkinghub.elsevier.com/retrieve/pii/S2666352X23001164 (2023) (Nov. 2023).

152. Min, Z., Asadullah, M., Yimsiri, P., Zhang, S., Wu, H. & Li, C.-Z. Catalytic Reforming of Tar during Gasification. Part I. Steam Reforming of Biomass Tar Using Ilmenite as a Catalyst. *Fuel* **90,** 1847–1854. ISSN: 00162361. doi:10.1016/j.fuel.2010.12.039. https://linkinghub.elsevier.com/retrieve/pii/S001623611000699X (2021) (May 2011).

153. Barisano, D. *et al.* Steam/Oxygen Biomass Gasification at Pilot Scale in an Internally Circulating Bubbling Fluidized Bed Reactor. *Fuel Processing Technology* **141,** 74–81. ISSN: 03783820. doi:10.1016/j.fuproc.2015.06.008. https://linkinghub.elsevier.com/retrieve/pii/S037838201530028X (2021) (Jan. 2016).

154. Broer, K. M., Woolcock, P. J., Johnston, P. A. & Brown, R. C. Steam/Oxygen Gasification System for the Production of Clean Syngas from Switchgrass. *Fuel* **140,** 282–292. ISSN: 00162361. doi:10.1016/j.fuel.2014.09.078. https://linkinghub.elsevier.com/retrieve/pii/S0016236114009478 (2021) (Jan. 2015).

155. Kern, S., Pfeifer, C. & Hofbauer, H. Gasification of Wood in a Dual Fluidized Bed Gasifier: Influence of Fuel Feeding on Process Performance. *Chemical Engineering Science* **90,** 284–298. ISSN: 00092509. doi:10.1016/j.ces.2012.12.044. https://linkinghub.elsevier.com/retrieve/pii/S000925091200735X (2023) (Mar. 2013).

156. Detsios, N., Atsonios, K., Grammelis, P., Dieringer, P., Ströhle, J., Nikkanen, V. & Orfanoudakis, N. A Comparative Analysis and Assessment of Dual Fluidized Bed and Chemical Looping Gasification: Design Considerations for Commercial Use and Applicability in BTL Schemes. *Proceedings of the 31st European Biomass Conference and Exhibition* **5-8 June 2023,** 6 Pages. ISSN: 2282-5819. doi:10.5071/31STEUBCE2023-4AO.5.2. http://www.etaflorence.it/proceedings?detail=19897 (2023) (2023).

3 Research Papers

3.1 First Research Paper

Process Control Strategies in Chemical Looping Gasification – A Novel Process for the Production of Biofuels Allowing for Net Negative CO2 Emissions

Authors: Paul Dieringer, Falko Marx, Falah Alobaid, Jochen Ströhle, Bernd Epple
Journal: Applied Sciences
Date: 2020-06-22
ISSN: 2076-3417
DOI: 10.3390/app10124271

applied sciences

MDPI

Article

Process Control Strategies in Chemical Looping Gasification—A Novel Process for the Production of Biofuels Allowing for Net Negative CO_2 Emissions

Paul Dieringer *, Falko Marx, Falah Alobaid, Jochen Ströhle and Bernd Epple

Institute for Energy Systems & Technology, Technical University Darmstadt, Otto-Berndt-Str. 2, 64287 Darmstadt, Germany; falko.marx@est.tu-darmstadt.de (F.M.); falah.alobaid@est.tu-darmstadt.de (F.A.); jochen.stroehle@est.tu-darmstadt.de (J.S.); bernd.epple@est.tu-darmstadt.de (B.E.)

* Correspondence: paul.dieringer@est.tu-darmstadt.de; Tel.: +49-6151-16-22692

Received: 20 May 2020; Accepted: 12 June 2020; Published: 22 June 2020

Abstract: Chemical looping gasification (CLG) is a novel gasification technique, allowing for the production of a nitrogen-free high calorific synthesis gas from solid hydrocarbon feedstocks, without requiring a costly air separation unit. Initial advances to better understand the CLG technology were made during first studies in lab and bench scale units and through basic process simulations. Yet, tailored process control strategies are required for larger CLG units, which are not equipped with auxiliary heating. Here, it becomes a demanding task to achieve autothermal CLG operation, for which stable reactor temperatures are obtained. This study presents two avenues to attain autothermal CLG behavior, established through equilibrium based process simulations. As a first approach, the dilution of active oxygen carrier materials with inert heat carriers to limit oxygen transport to the fuel reactor has been investigated. Secondly, the suitability of restricting the air flow to the air reactor in order to control the oxygen availability in the fuel reactor was examined. Process simulations show that both process control approaches facilitate controlled and de-coupled heat and oxygen transport between the two reactors of the chemical looping gasifier, thus allowing for efficient autothermal CLG operation. With the aim of inferring general guidelines on how CLG units have to be operated in order to achieve decent synthesis gas yields, different advantages and disadvantages associated to the two suggested process control strategies are discussed in detail and optimization avenues are presented.

Keywords: chemical looping; biomass gasification; process control; process simulation

1. Introduction

The reduction of greenhouse gas emissions (GHGE) in order to reach the unilateral goals agreed upon in the UNFCCC Paris Agreement is one of the major challenges of civilization in the 21st century. While notable advances in the energy sector have been achieved in recent years [1,2], the de-carbonization of the transport sector, which is responsible for almost one quarter of the European GHGE emissions [3] and consumes 36% of the global final energy [1], signifies a key issue on the path to a closed carbon cycle. Especially the replacement of conventional fuels in the heavy freight transport and aviation industry, where electrification is currently not viable, remains a major hurdle. When considering the European Union's Renewable Energy Directive (RED II) [4], which set a target of a share of 14% renewable energy in the transport sector by 2030, while at the same time alleviating negative impacts on food availability and prices, it is clear that significant advances in renewable fuel generation are required.

The production of so-called advanced or second-generation biofuels through thermochemical conversion of biomass-based residues is an auspicious pathway to achieve these goals. Gasification is

a mature thermochemical biomass conversion process, although its primary use is the generation of heat and electricity, while the synthesis of advanced biofuels through the gasification route has not been implemented in an industrial scale, yet [5].

Commonly, biomass gasification is achieved through utilizing air or pure oxygen in the gasifier. Albeit, pure oxygen is typically used in gasification processes embedded in biomass-to-biofuel process chains, since a nitrogen-free, high calorific value syngas is required for fuel synthesis [6]. The provision of this oxygen requires an air separation unit (ASU), which is associated with high capital and operational costs, hence adversely affecting the energetic plant efficiency and process economics [6,7]. Alternatively, steam [8–10] or carbon dioxide [10–12] can be deployed as the gasification medium. Yet, either of the two suffers from slow gasification kinetics [6,13,14] and strong process endothermicity [6,15], limiting the process efficiency. To circumvent this, the dual fluidized bed gasification (DFBG) technology achieves feedstock gasification in two connected reactors; a gasifier in which steam gasification of the deployed feedstock is attained, and a combustor in which the residual char is combusted facilitating full char conversion and the provision of heat, which is transported to the gasifier using an inert circulating bed material [16–18].

A similar gasification concept allowing for decent fuel conversions, without requiring an ASU is the chemical looping gasification (CLG) process, where biomass gasification is also carried out in two separate reactors (see Figure 1) [15,19–22]. Just as the related chemical looping combustion (CLC) process, CLG is realized using two coupled fluidized bed reactors, in order to attain good heat and mass transport characteristics [21,23,24]. Here, steam or carbon dioxide provide bed fluidization and gasification (see Equations (1) and (2)) of the feedstock in the fuel reactor (FR) [15,24]. Additional oxygen for the partial (see Equation (3)) or full (see Equations (4)–(6)) oxidation of gaseous hydrocarbon species, enhancing gasification kinetics and reducing the process endothermicity, is supplied through a circulating oxygen carrier (OC, Me_xO_y) [19,21,24]. Furthermore, the homogeneous water gas shift (WGS) reaction (Equation (7)) takes place inside the gas phase.

$$C + CO_2 \rightarrow 2\,CO \tag{1}$$

$$C + H_2O \rightarrow CO + H_2 \tag{2}$$

$$Me_xO_y + CH_4 \rightarrow Me_xO_{y-1} + 2\,H_2 + CO \tag{3}$$

$$4Me_xO_y + CH_4 \rightarrow 4\,Me_xO_{y-1} + 2\,H_2O + CO_2 \tag{4}$$

$$Me_xO_y + CO \rightarrow Me_xO_{y-1} + CO_2 \tag{5}$$

$$Me_xO_y + H_2 \rightarrow Me_xO_{y-1} + H_2O \tag{6}$$

$$CO + H_2O \leftrightarrow H_2 + CO_2 \tag{7}$$

The required oxygen transport to the FR is facilitated through a repeated regeneration of the OC (see. Equation (8)) in the air reactor (AR) with oxygen contained in the inlet air [15,20,24]. Moreover, unconverted char is combusted in the air reactor (see. Equation (9)), leading to a full conversion of the deployed feedstock [23,25].

$$Me_xO_{y-1} + 0.5\,O_2 \rightarrow Me_xO_y \tag{8}$$

$$C + O_2 \rightarrow CO_2 \tag{9}$$

The latter reaction is generally undesired, as a high carbon conversion is targeted inside the FR, in order to maximize the carbon capture efficiency of the process [23,26,27]. In literature, carbon capture efficiencies in the range of 90–99% are reported for CLC [26,28,29]. As approximately one third of the carbon contained in the feedstock is transferred into the valorized end-product (e.g., liquid Fischer-Tropsch fuels) in process chains employing CLG for syngas generation, this means that up to 65% of the carbon contained in the feedstock can be captured and stored, constituting negative

emissions in case biogenic feedstocks are being employed. Yet, in reality figures falling short of this value can be expected, as a fraction of the feedstock carbon will be lost in the AR in the form of CO_2.

Apart from the oxygen transport, the continuous solid circulation between the two reactors provides the required heat transport from the AR, in which the exothermic re-oxidation of the OC occurs, to the FR, where the endothermic gasification reactions take place [15,19,23], thus allowing for stable elevated reactor temperatures.

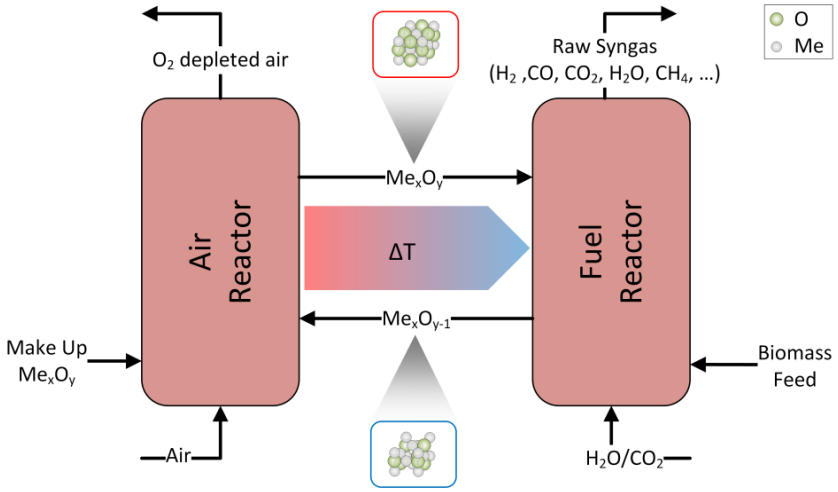

Figure 1. Schematic of chemical looping gasification (CLG) process.

CLG not only offers excellent characteristics in terms of feedstock flexibility [24], but is especially well suited for biomass-based feedstocks [30,31], commonly exhibiting a reactive char and containing a large fraction of volatiles. This means that high char conversions can be achieved through the gasification reaction with steam or CO_2, while volatiles are converted to the desired syngas species through their partial oxidation on the OC surface (see Equation (3)). Furthermore, it is reported that iron containing materials [32–35] can facilitate the cracking and oxidation of tars, which are known to be formed in significant amounts during biomass gasification [36].

While the role of the gasification agent is similar in CLC and CLG (i.e., char gasification), the oxygen carrier is meant to only partially oxidize the gaseous species in CLG, yielding a raw product gas with a high heating value [23,37], instead of a heat release from the AR, which is used for heat and power generation in CLC [24,38,39]. This shift from CLC to CLG is achieved through lowering the oxygen-to-fuel equivalence ratio in the FR to values below unity. An autothermal CLG process, maximizing the chemical energy contained in the raw syngas without relying on external heating, is obtained when the net heat release from the process equals zero (neglecting heat losses).

Although one might hence deduce that the transition from CLC to CLG is straightforward, there are major differences between the two processes. While large OC circulation rates are favorable in CLC, as they allow for a high oxygen availability in the FR, which favors fuel combustion [40–43] and provide for a large heat transport from the AR to the FR [41,44,45], the former is not desired in CLG. Here, the oxygen availability in the FR has to be limited in order to prevent the full oxidation of the employed feedstock. However, even more so than in CLC, CLG requires large heat transportation rates from the AR and FR due to the less pronounced occurrence of full oxidation reactions (Equations (4)–(6)), at the cost of highly endothermic partial oxidation reactions (Equation (3)) in the FR. This leads to a fundamental challenge in terms of process control, as both, heat and oxygen transfer between the two reactors, have to be controlled independently in order to attain an autothermal CLG process. Initial advances to reach this target were made by Ge et al. [37], diluting an active OC material with an inert, thus obtaining stable reactor temperatures for a lab-scale CLG unit. Yet, due to the significance of this inherent challenge, an in-depth analysis of this issue is required. Therefore, this work takes a holistic

approach to this matter, employing process simulations in order to establish suitable process control measures to attain an autothermal CLG process. In the following, the developed process model will be introduced in Section 2, before general process control and optimization strategies are presented and discussed in detail in Section 3. To round off these elucidations, the most crucial findings and an outlook on future research topics are given in Section 4 of this article.

2. Modelling Methods

2.1. Description of the Process Model

The deployed Aspen Plus™ model, shown in Figure 2, is largely adopted from a previous study by Ohlemüller et al. [25]. Here, the chemical reactions occurring in the AR and FR are modelled in two separate reactors, whereas gas-solid and solid-solid separation is achieved through cyclones and separators, respectively. In order to reduce model complexity, the AR and FR were modelled as equilibrium RGIBBS reactors in this work, as this simplification allows for a basic description of the most crucial phenomena required for process control and obviates the necessity of accurate kinetic data. To account for the solid circulation in chemical looping processes, a constant mass stream of solids continuously cycles through the system (OCR-TOAR/OCO-TOFR), after being added to the system after initiation of the simulation (INIT).

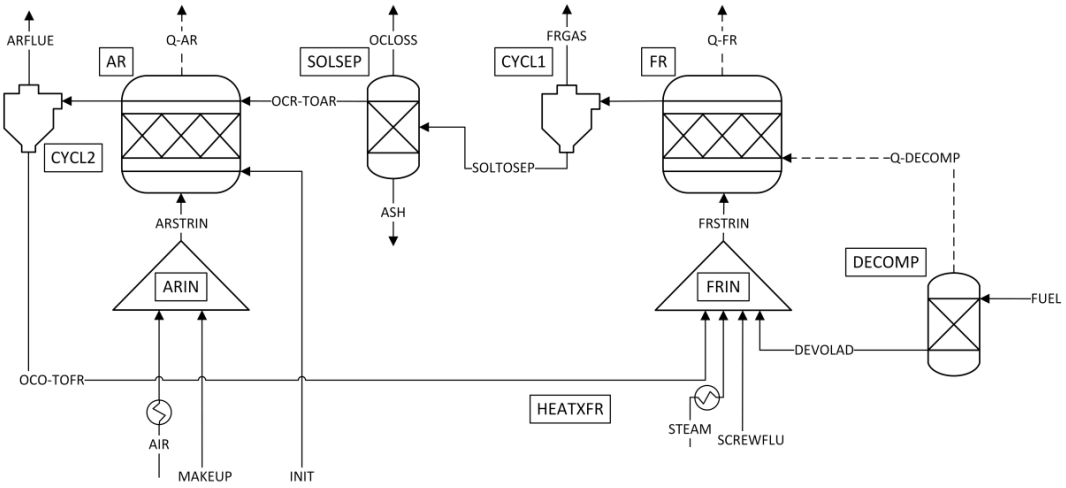

Figure 2. Flow sheet of the Aspen Plus™ CLG process model.

For completeness and comprehensibility reasons, all components and streams are briefly described in the following:

- Prior to any calculation, an initial solid mass flow is given into the system (INIT), to model the circulating solid OC mass. Instead of estimating the actual solid loss, the approach of Ohlemüller et al. [25], setting the total OC loss (OCLOSS) to 1% of the circulating mass to achieve fast flowsheet conversion, was adopted. The same amount of fresh solids was constantly fed to the AR (MAKEUP), to achieve constant solid circulation.
- For both reactors, cyclones are employed to achieve solid-gas separation. The FR products are separated into a gas (FRGAS) and solid (SOLTOSEP) stream, via CYCL1 (separation efficiency 100%). Similarly, the AR products are separated into a gas (ARFLUE) and solid stream (OCO-TOFR) in CYLC2 (separation efficiency 100%).
- All streams entering the process are fed at ambient temperature (T_0 = 25 °C), except for the stream STEAM, which is fed as saturated steam (120 °C).

- The steam and the air entering the FR/AR are preheated to a designated inlet temperature ($T_{air,AR}$, $T_{H2O,FR}$). If not stated otherwise, the inlet temperature of both streams (STEAM, AIR) when entering the FR/AR is set to 400 °C.
- As Aspen Plus™ is not equipped to handle solid fuels, the biomass feedstock (FUEL) is fed to the decomposer (DECOMP), where it is decomposed into its pyrolysis products (DEVOLAD). The heat of pyrolysis (Q-DECOMP) is transferred to the fuel reactor. A detailed description of the decomposer block is given in Section 2.2.
- The pyrolysis products (DEVOLAD), the gasification agent (STEAMX), the OC recycled from the AR (OCO-TOFR), and the CO_2 required for solid feeding and loop seal fluidization (SCREWFLU) are mixed (FRIN) before entering the fuel reactor.
- Subsequently, the educts entering the fuel reactor (FR) are converted into reaction products according to the chemical equilibrium at the given boundary conditions (T_{FR}, P_{FR} = 1 atm).
- The solids leaving CYCL1 are separated into the OC fed to the AR (OCR-TOAR) and a stream containing carbon and ash (SOL) in the solids separation (SOLSEP). This separation signifies the removal of bed material (i.e., OC, ash and unconverted feedstock) from the FR via sluicing during operation. Additionally, a fraction of the oxygen carrier material is removed from the system (OCLOSS), to model OC losses via sluicing and attrition.
- The OC makeup stream (MAKEUP) and the inlet air (AIRX) are mixed (ARIN) before being fed to the AR.
- Inside the air reactor (AR) the reduced OC and the unreacted char react with the oxygen contained in the air according to the chemical equilibrium at the given boundary conditions (T_{AR}, P_{AR} = 1 atm).

2.2. Decomposer

Generally, the conversion of a fuel during gasification is described by three subsequent mechanisms: drying, pyrolysis and gasification [6]. While the gasification step is modelled in the FR, the former two mechanisms are modelled in the decomposer block in this study. As drying solely encompasses the release of moisture from the fuel [6,46], the main focus of this section is placed on fuel pyrolysis. Ohlemüller et al. [25] applied the pyrolysis model of Matthesius et al. [47] to predict the pyrolysis product composition from coal proximate and ultimate analysis parameters. Although it is reported that the basic mechanism of coal and biomass pyrolysis are similar [6,7], it was decided to employ a pyrolysis model specifically tailored for biomass feedstocks, as this study is focused on the conversion of biomass-based fuels. Neves et al. [48] devised a pyrolysis model for biomass feedstock built on the basis of an extensive experimental database. Similar to the pyrolysis model by Matthesius et al. [47], this model solely requires information on the feedstock composition (C, H, O and char content) to estimate the final chemical composition of the organics after pyrolysis, allowing for its straight forward implementation into the existing Aspen Plus™ model. Cuadrat et al. [49] found that the formation of tar and larger hydrocarbons (>C1) is negligible in the presence of ilmenite and steam/CO_2. Therefore, the assumption by Ohlemüller et al. [25] and Mendiara et al. [50] that tars and larger hydrocarbons are directly converted to methane and carbon monoxide was also adopted in this study. Moreover, oxygen and hydrogen contained in the char were converted to syngas, resulting in a char solely consisting of carbon. As the FR is modelled based on chemical equilibrium, these simplifications do not have an impact on the final simulation results.

By applying these assumptions, the product compositions after pyrolysis were calculated on the basis of the proximate and ultimate analysis of wood pellets, being the model feedstock for all subsequent considerations (see Table 1).

Table 1. Summary of the Ultimate and Proximate analysis for industrial wood pellets.

Ultimate Analysis	wt-%	Proximate Analysis	wt-%
C (d.a.f.)	50.8	Moisture	6.5
H (d.a.f.)	6	Ash (d.b.)	0.7
N (d.a.f.)	0.07	Volatile matter (d.b.)	85.1
O (d.a.f.)	43.2	Fixed carbon (d.b.)	14.2
S (d.a.f.)	0.008		
Cl (d.a.f.)	0.006		
Net calorific value [MJ/kg]	17.96		

Since the pyrolysis product composition is highly temperature dependent [6,7,48], a constant temperature representing the FR temperature during CLG was selected as the input for the pyrolysis model ($T_{devol.}$ = 900 °C). A summary of the final product composition after de-volatilization, which was implemented into the process model, is given in Table 2.

Table 2. Mass yields [wt-%] for DECOMP Aspen Plzus® block for industrial wood pellets according to pyrolysis model of Neves et al. [48] (T = 900 °C).

Component	wt-%	Component	wt-%
ASH	0.65	H_2O	14.06
CO	55.20	N_2	0.06
C	11.92	CO_2	3.11
CH_4	13.55	H_2S	0.01
H_2	1.43		

2.3. Boundary Conditions

For all subsequent simulations, the biomass input was selected in such a way, that the thermal load, P_{th}, of the chemical looping gasifier amounted to 1 MW. In terms of the circulating solid materials, the deployed oxygen carrier material is ilmenite, for which is has been established that the major redox stages are FeO + TiO_2, Fe_3O_4, TiO_2 and Fe_2TiO_5 [51]. These redox stages were modelled as $FeTiO_3$ (for FeO + TiO_2), Fe_3O_4, TiO_2, and Fe_2O_3 + TiO_2 (for Fe_2TiO_5). Deeper redox stages (e.g., FeO) were also considered in the process model, yet were not found to be formed in notable amounts. The inert solid sand was modelled through pure SiO_2. The FR and AR are operated under atmospheric pressure. Moreover, the air reactor temperature was set to 1050 °C, if not stated otherwise. The fuel reactor temperature results from the energy balance of the process, requiring that both reactors are in heat balance ($\dot{Q}_{FR} = 0$, $\dot{Q}_{AR} \geq 0$). As the kinetic syngas inhibition of char gasification reactions [8,12] is not considered in the RGIBBS equilibrium calculation, full char conversion is attained inside the FR for all temperatures considered in this study. Although this simplification signifies a deviation from reality, it does not impact the general inferences which will be elaborated on hereinafter. For the steam to biomass ratio in the FR a value of 0.9, reported for a 2–4 MW_{th} chemical looping gasifier in literature [52], was selected if not stated otherwise. During CLC/CLG operation CO_2 is required for fuel feeding and inerting. This stream of CO_2, entering the fuel reactor, was selected in such a way that the CO_2 to biomass ratio amounts to 0.2, to take into account that the CO_2 input through the feeding section increases with increased thermal load. The two remaining process variables, the air mass flow entering the AR and the circulating oxygen carrier mass, were adjusted in such a way that autothermal CLG operation was achieved. A summary of all boundary conditions is given in Table A1 in Appendix A.

3. Results and Discussion

3.1. Attaining CLG Behavior

Generally, shifting from a combustion to a gasification process is achieved through lowering the air/oxygen-to-fuel ratio of the process, thereby decreasing the ratio of fully to partially oxidized gas species leaving the process and hence increasing the heating value of the product gas [6,53,54]. Here, the critical parameter is the so called air-to-fuel equivalence ratio given by the ratio of oxygen fed to the AR, $\dot{m}_{O,AR}$, and the oxygen required for full feedstock combustion, $\dot{m}_{O,stoich}$:

$$\lambda = \frac{\dot{m}_{O,AR}}{\dot{m}_{O,stoich}}. \quad (10)$$

According to this definition, (close to) full combustion of the feedstock is attained for air-to-fuel equivalence ratios larger than unity ($\lambda > 1$), while gasification processes require sub-stoichiometric oxygen feeding (i.e., $\lambda < 1$).

Due to the dissection of the gasification/combustion reaction into two separate reactors in chemical looping processes, there is no direct contact between the air entering the AR and the fuel entering the FR. Hence, the application of an alternative parameter, the oxygen-carrier-to-fuel equivalence ratio, ϕ', relating the amount of oxygen carried by the OC to the FR to the oxygen required for stoichiometric combustion, has been suggested [43]:

$$\phi' = \frac{R_{OC} \cdot \dot{m}_{OC}}{\dot{m}_{O,stoich}}. \quad (11)$$

Here, R_{OC} denotes the oxygen transport capacity of the given oxygen carrier material. While this parameter accurately relates the two quantities for CLC, where the OC always leaves the AR in a (close to) fully oxidized state, this is not necessarily the case in CLG. Therefore, a slightly altered oxygen-carrier-to-fuel equivalence ratio, ϕ, considering the possibility of a partially reduced OC leaving the AR, has been proposed for gasification applications [35]:

$$\phi = \frac{R_{OC} \cdot \dot{m}_{OC} \cdot X_{s,AR}}{\dot{m}_{O,stoich}}, \quad (12)$$

where $X_{s,AR}$ signifies the oxidation degree of the oxygen carrier at the AR outlet, given by [24,35]:

$$X_{s,AR} = \frac{m_{OC,AR} - m_{OC,red}}{R_{OC} \cdot m_{OC,ox}}. \quad (13)$$

Here, $m_{OC,red}$ and $m_{OC,ox}$ are the mass of an OC sample in a fully reduced and oxidized state respectively, while $m_{OC,AR}$ is the mass of the OC sample leaving the AR. For ilmenite the fully reduced oxygen carrier is approximated by $FeTiO_3$, the fully oxidized state is approximated by $Fe_2O_3 + 2TiO_2$, and $Fe_3O_4 + 3TiO_2$ denotes an intermediate redox state ($X_s = 0.67$).

In order to assess how λ and ϕ have to be adjusted in order to obtain an efficient CLG process, one should first assess the general impact of these two parameters on the process. Due to the relative fast kinetics of the OC re-oxidation [55–57], the oxygen carrier is often assumed to leave the AR in a (close to) fully oxidized state for $\lambda > 1$ in chemical looping processes. In contrast, sub-stoichiometric air-to-fuel equivalence ratios ($\lambda < 1$) only lead to a partial re-oxidation of the OC in the AR. Following the same logic, the OC material can be assumed to leave the FR in a (close to) fully reduced state in case $\phi < 1$, whereas partial reduction is attained for $\phi > 1$. From these deductions, it becomes clear that "standard" CLC operation is attained for $\lambda > 1$ and $\phi > 1$, [42,43]. Here, a highly oxidized OC leaves the AR, before being partially reduced in the FR, which is illustrated in Figure 3a.

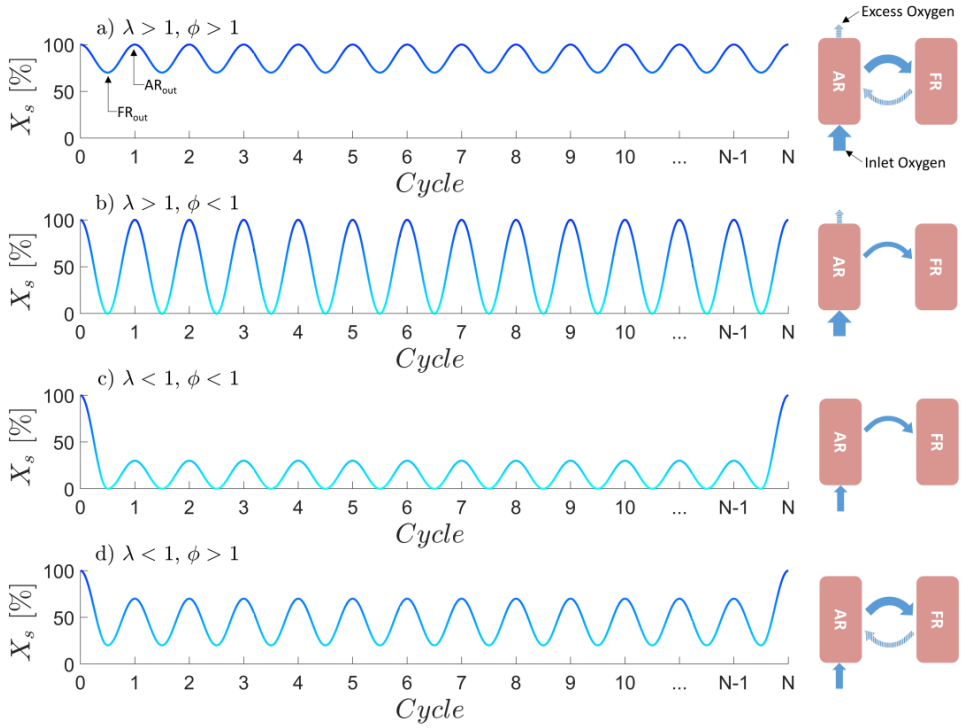

Figure 3. Different chemical looping modes (**a**–**d**) dependent on the air-to-fuel equivalence ratio λ and the oxygen-carrier-to-fuel equivalence ratio ϕ.

When targeting pronounced syngas formation, the oxygen release in the FR has to be limited, so that full feedstock oxidation is prevented [35,52]. The most obvious avenue that can be pursued to achieve this is lowering ϕ below unity. When doing so, the employed air-to-fuel equivalence ratio λ determines how much oxygen is transported between the two reactors per gram of OC. In case of $\lambda > 1$, which is illustrated in Figure 3b, the oxygen carrier undergoes a full redox cycle and hence the full oxygen transport capacity of the OC material (i.e., R_{OC}) is exploited. On the other hand, $\lambda < 1$ means that in equilibrium the OC leaves the AR in a partially reduced state, hence also reducing the mass specific oxygen transport of the OC (see Figure 3c). Lastly, one might also consider a process with $\lambda < 1$ and $\phi > 1$, as shown Figure 3d. In order to attain a steady-state process exhibiting these characteristics, full reduction of the oxygen carrier has to be prevented in the FR (e.g., kinetically), so that a fraction of oxygen is transported back to the AR. This means that in contrast to the former approaches, this case cannot be attained in equilibrium-like conditions. While this approach might also be feasible for CLG operation in theory, straight forward measures allowing for a controlled oxygen release in the FR are not at hand. Consequently, lowering the oxygen-to-fuel-ratio in the FR (i.e., $\phi < 1$) is the most promising avenue to attain CLG behavior. When aiming for large syngas yields, ϕ has to assume values below unity, while values exceeding unity are targeted in CLC [42,43]. In the following, different effective control strategies to achieve this reduction in ϕ, required for pronounced syngas formation in the FR, while at the same time achieving an autothermal process, will be investigated.

In order to simplify the subsequent considerations, a standard parameter to describe gasification processes, the cold gas efficiency (CGE), η_{CG}, will be deployed hereinafter. It describes which amount of chemical energy from the fuel is transferred to the gaseous FR product gas during gasification [6,7].

$$\eta_{CG} = \frac{\dot{n}_{gas,FR} \cdot (x_{CH4,FR} \cdot LHV_{CH4} + x_{CO,FR} \cdot LHV_{CO,FR} + x_{H2,FR} \cdot LHV_{H2})}{\dot{m}_{fuel} \cdot LHV_{fuel}} \quad (14)$$

Here, $\dot{n}_{gas,FR}$ and $\dot{m}_{fuel}$ denote the mole flow of the product gas stream and the fuel input into the FR, respectively. *LHV* is the lower heating value of the fuel (mass basis) and the gas species (molar basis) and x_i is the mole fraction of the gas species.

3.2. Reduction of OC Circulation

One approach to obtain CLG behavior, which has been suggested by Pissot et al. [52], is reducing the amount of OC cycled through the system ($\dot{m}_{OC}$), hence reducing ϕ. This approach can be deduced directly from Equation (12). Due to the resulting lower oxygen transport to the FR, syngas formation is favored, as less oxygen for full oxidation of the feedstock is provided by the OC. The simulation results for this approach are given in Figure 4. When considering the gas composition (Figure 4a) of the streams leaving the air and fuel reactor, various trends are visible. As expected, the syngas content in the gaseous FR products increases with decreasing OC circulation rate, which can directly be attributed to the lower oxygen/fuel ratio in the FR. Consequently, steam and CO_2 formation decrease. Yet, it has to be noted that substantial syngas concentrations are only attained for $\phi < 1$, which requires significant reductions in the OC circulation rate, when compared to CLC, where OC-to-fuel equivalence ratios as high as 8 [27] and 25 [40] are reported in literature for solid and gaseous fuels, respectively. For the gas concentrations leaving the AR, a strong impact of ϕ on the effluent oxygen is visible. As the inlet air mass flow was not varied ($\lambda = 1.2$), this observation is clear, as less O_2 is removed from the gas stream due to the lower OC circulation for $\phi < 1$. Furthermore, the CO_2 content in the AR product is predicted to be insignificant, indicating a complete char conversion, which is expected in chemical equilibrium. When considering Figure 4b, showing the solid composition after the fuel and air reactor, it can be seen that the OC leaves the AR and FR in a fully oxidized (Fe_2O_3 + TiO_2) and reduced ($FeTiO_3$) state, respectively for $\phi < 1$, whereas the OC is only partially reduced (indicated through the presence of Fe_3O_4) in the FR in case ϕ exceeds unity. Hence, the fraction of $FeTiO_3$ leaving the FR strongly increases with decreasing OC circulation, signifying a higher degree of reduction of the OC, due to the lower oxygen availability. As expected one consequently obtains chemical looping combustion behavior (see Figure 3a) for oxygen-carrier-to-fuel equivalence ratios greater than unity ($\phi > 1$), whereas chemical looping gasification behavior (see Figure 3b) is attained for $\phi < 1$.

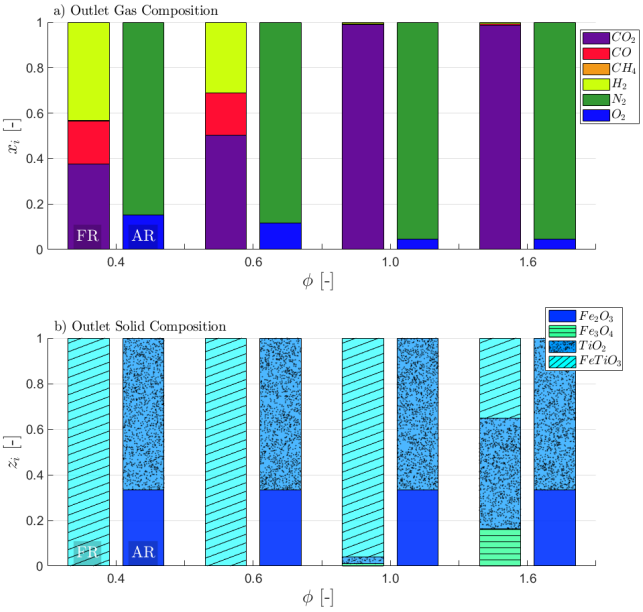

Figure 4. Simulation results for CLG operation through reduced oxygen carrier (OC) circulation. Dry molar gas composition (**a**) and molar solid composition (**b**) as a function of ϕ for varying OC circulation rates ($\lambda = 1.2$).

Based on these findings, one can conclude that a successful shifting from CLC to CLG for a given air-to-fuel ratio can be attained through a reduction in the OC circulation, which can also be seen in Figure 5a, showing a linear dependence between the two parameters. This means that for a change of ϕ from 1.0 to 0.5, the OC circulation rate has to be halved. However, lower solid circulation rates also result in a proportional decrease in the heat transport from the AR to the FR and hence a drop-off in FR temperatures [35,58]. While a moderate decrease in fuel reactor temperatures with decreasing OC circulation rate is visible for $\phi > 1$, for which complete feedstock conversion is attained in the FR, this decrease becomes more prominent for $\phi < 1$, where gasification reactions in the FR are dominant, hence increasing the endothermicity of reactions occurring in the FR. Consequently, FR temperatures fall below 800 °C for $\phi < 0.5$, where the availability of circulating OC material for sensible heat transport between the FR and AR is halved, when compared to $\phi = 1$ and more importantly the syngas content in the FR products is significant (see Figure 4a). This increase in syngas content also goes in hand with a decrease in the total net heat release from the CLG process ($\dot{Q}_{net}$), which can be calculated from the difference in the enthalpies of the streams entering ($_{in}$) and leaving ($_{out}$) the air and fuel reactor (see Equation (15)), as the enthalpy of the FR products increases.

$$\dot{Q}_{net} = \sum_{FR,in} \dot{m}_i \cdot h_i - \sum_{FR,out} \dot{m}_i \cdot h_i + \sum_{AR,in} \dot{m}_i \cdot h_i - \sum_{AR,out} \dot{m}_i \cdot h_i \quad (15)$$

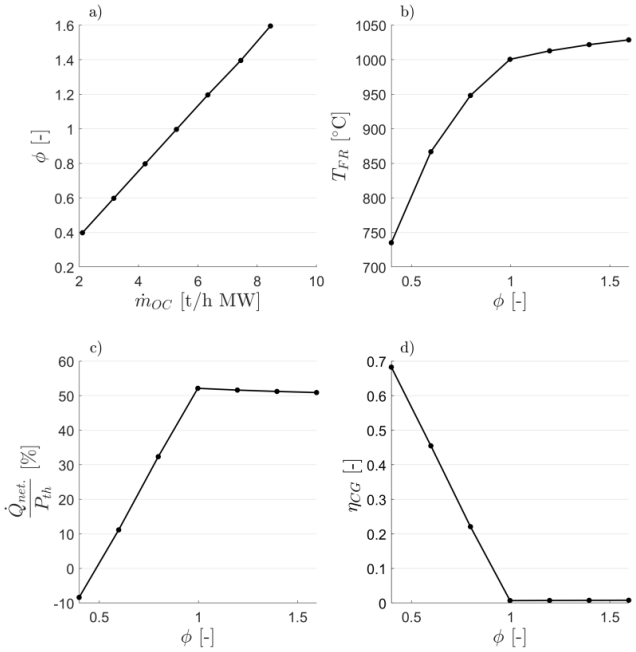

Figure 5. Simulation results for CLG operation through reduced OC circulation. OC-to-fuel ratio as a function of the OC circulation rate (**a**). Fuel reactor temperature (**b**), relative net process heat (**c**), and cold gas efficiency (**d**) for different values of ϕ (λ = 1.2).

The decrease in net process heat release with decreasing ϕ, indicating the retaining of chemical energy in the FR products, also becomes visible upon consideration of Figure 5c, depicting the relative net heat release of the process for the different OC-to-fuel ratios. For the given boundary conditions, an autothermal process, for which syngas yields are maximized without relying on external heat addition ($\dot{Q}_{net} = 0$) is attained for an OC to fuel ratio of approx. 0.5. The resulting cold gas efficiency for this operating point amounts to approx. 60% (see Figure 5d) at a FR temperature of 775 °C. Although the equilibrium model predicts full char and volatile conversions for these temperatures (see Figures 4a

and 5d), char, volatile, and tar conversion are known to be kinetically governed processes in chemical looping systems [25,55,56,59], leading to product compositions deviating strongly from equilibrium composition [35,52]. Due to this reason, temperature differences in the range of 50 to 100 °C are generally targeted in dual fluidized bed gasification [16], in order to obtain sufficiently high gasifier temperatures, allowing for decent char, volatile, and tar conversions. Accordingly, FR temperatures in the range of 850–950 °C are desired in CLG, in order to attain high carbon capture efficiencies and cold gas efficiencies as well as low syngas tar loads [20,23,37,60,61].

These considerations underline that, although the desired reduction in ϕ is possible, attaining an efficient autothermal CLG process through a reduction in the OC circulation rate is not a recommendable strategy as it entails low fuel reactor temperatures, due to the dual-purpose of the OC circulation (i.e., oxygen and heat transport). Consequently, alternative approaches, allowing for a decoupling of oxygen and heat transport between the AR and FR and hence increased FR temperatures are required, in order to attain a CLG process exhibiting the desired characteristics.

3.3. Dilution of OC with Inert Bed Material

One strategy allowing for a decoupling of oxygen and heat transport between air and fuel reactor, which has been discussed in literature, is employing a mixture of an active OC material and a solid inert species (e.g., sand) [35,37,52]. Here, the inert fraction serves purely as a heat carrier, transferring sensible heat between the two reactors, without participating in the occurring reactions, while the active OC fraction fulfills its dual purpose of oxygen and heat transport. Consequently, this approach is a combination of CLG and dual fluidized bed gasification, which solely employs inert bed materials for heat transport. Following this logic, Ge et al. [37] found that through accurately tailoring the mixing ratio of inert silica sand and hematite, serving as an OC, FR temperatures can be stabilized at elevated levels (i.e., >900 °C), while at the same time ensuring a controlled oxygen transport to the FR, resulting in large syngas yields.

In terms of the impact of the variation in OC-to-fuel ratio on gas compositions achieved through this dilution of the OC material with an inert, similar observations are obtained (see Figure 6a). This means syngas formation increases steadily for $\phi < 1$. Moreover, the OC carrier composition, shown in Figure 3b, follows similar trends as observed for a plain reduction in the OC circulation rate (see Section 3.2), with a fully reduced OC leaving the FR for $\phi < 1$ (see Figure 3b), whereas only partial reduction is observed for $\phi > 1$ (see Figure 3a). Yet, the fraction of active OC material clearly decreases with decreasing ϕ, due to the dilution with silica sand.

As the total amount of circulating solids is kept constant, the mass of circulating OC material is inversely proportional to the dilution factor. This means that there exists a linear relationship between the solid fraction of the inert material (z_{SiO2}) and ϕ, which is visible in Figure 7a. Hence, for a given solid circulation rate, shifting from CLC to CLG can be attained through increased inert dilution. The positive effect of inert addition on FR temperatures becomes apparent upon consideration of Figure 7b. In contrast to a direct reduction in the OC circulation rate, the substitution of a fraction of the active metal oxide with an inert heat carrier allows for a sustaining of FR temperatures above 980 °C even for OC to fuel ratios as low as 0.5. Due to this increase in FR temperatures, the average temperature of the CLG process increases, leading to a slightly increased ϕ of approx. 0.55 for which autothermal operation is attained (see Figure 7c) (Higher process temperatures increase the heating demands of the educts entering the FR and AR and hence reduce the OC-to-fuel ratios for which autothermal operation can be obtained). Therefore, the cold gas efficiency obtained for autothermal operation for the given approach is also marginally reduced (see Figure 7d), when compared to the approach discussed in Section 3.2. Yet, it has to be noted that due to the intensified heat transport between the AR and FR, significantly smaller reactor temperature gradients are required for the given approach. Consequently, AR temperatures can be lowered without jeopardizing char conversions in the FR, thus reducing average process temperatures and allowing for strongly increased cold gas efficiencies (see also Section 3.5). Another advantage of this approach is that a catalytic material,

not participating in oxygen transport (e.g., olivine), could be employed for OC dilution instead of sand, allowing for improved syngas characteristics with regard to tar content.

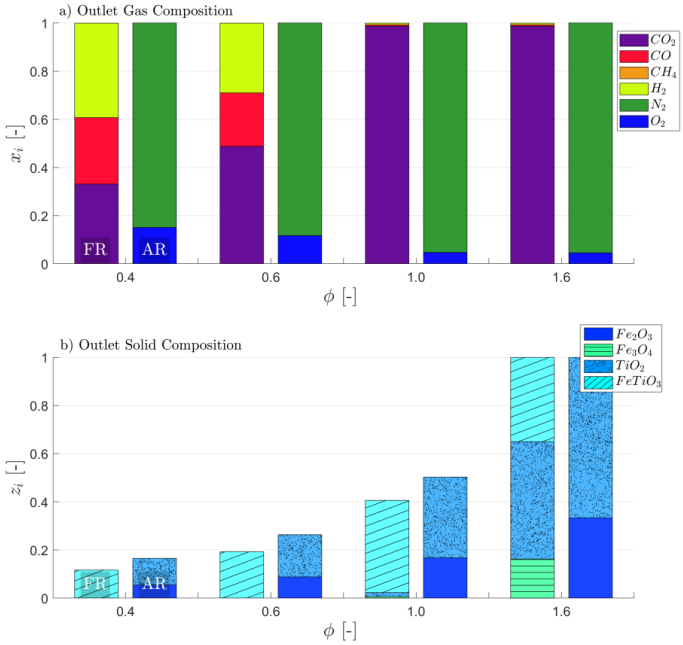

Figure 6. Simulation results for CLG operation through OC dilution with inert SiO_2 sand. Dry molar gas composition (**a**) and molar solid composition (**b**) as a function of ϕ for varying OC circulation rates (λ = 1.2, $\dot{m}_{OC} + \dot{m}_{SiO2} = const.$).

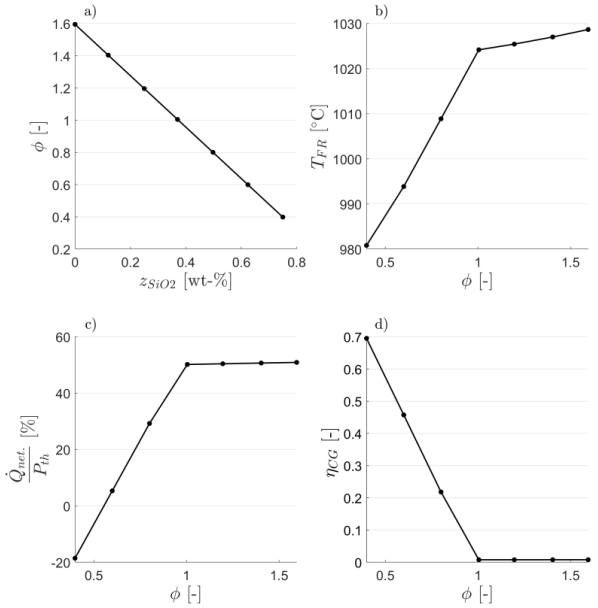

Figure 7. Simulation results for CLG operation through OC dilution with inert SiO_2 sand. OC-to-fuel ratio as a function of the inert concentration of the circulating solid mixture (**a**). Fuel reactor temperature (**b**), relative net process heat (**c**), and cold gas efficiency (**d**) for different values of ϕ (λ = 1.2, $\dot{m}_{OC} + \dot{m}_{SiO2} = const$).

Despite the presented advantages, Larsson et al. [35] found that, albeit slightly reducing tar loads, the addition of an active OC (ilmenite) to an inert circulating bed material in a dual-fluidized bed gasifier (for $\phi < 0.2$), entails a continuous drop in cold gas efficiency. This was explained by the fact that ilmenite addition does not enhance char conversion significantly, while its presence leads to a partial oxidation of the product gas. On the other hand, Pissot et al. [52] found that dilution of an active OC bed with up to 90% of an inert material does not entail visible enhancements in the cold gas efficiency of the CLG process, while it has a visible negative impact on carbon conversion. This shows that the mixing of an inert and an active OC material can have different effects on the process depending on the governing boundary conditions. Another drawback of this approach is that, albeit the addition of solids allows for an adjustment of ϕ during operation, it leads to a large system inertia, making it an arduous task to quickly react to disturbances. Moreover, a fraction of the solid material has to be removed from the system for ash removal in a continuously operated CLG unit. Economic considerations require a separation of these materials for further processing, recycling, and disposal. Clearly, the presence of a third component (i.e., sand, olivine) further complicates this task. Lastly, it is known that the operation of a fluidized bed with multiple bed materials of different characteristics brings about additional challenges in terms of material fluidization, entrainment, and attrition, as well as bed segregation [62]. Due to these reasons it was also suggested to employ materials of a low oxygen transport capability (R_O), such as LD-slag, containing a large inactive fraction not participating in the oxygen transport, which fulfills the purpose of the inert heat carrier [52]. Through this, oxygen carrier circulation rates providing sufficient heat transport between the reactors can be targeted, without obtaining OC-to-fuel equivalence ratios above unity. Yet, for this approach the main challenge is finding suitable OC materials exhibiting an oxygen transport capability in the desired range, high activity towards hydrocarbon conversion, and good chemical and mechanical stability.

3.4. Reduction of Air-to-Fuel Equivalence Ratio

To allow for a less restricted material selection and avoid solid inert addition, an alternative strategy to decouple oxygen and heat transport between the AR and FR is required. In order to achieve this, Larson et al. [35] suggested the deployment of a secondary system in which the OC is pre-reduced before entering the FR. This means that, as shown in Figure 3c, a partially reduced OC enters the FR ($X_s < 1$), thus entailing a lower OC-to-fuel ratio (see Equation (12)). Instead of employing a secondary reactor to accomplish this, one can also operate the AR in a sub-stoichiometric fashion ($\lambda < 1$), thereby preventing full re-oxidation of the OC in the AR. This means that in order to attain CLG conditions, the amount of air fed into the air reactor can be reduced, while retaining a constant OC circulation. As a consequence, the OC steadily reaches a lower degree of oxidation, hence lowering its oxygen release in the FR, until steady state is reached (more details see Appendix B). This approach has already been pursued in a 140 kW_{th} chemical looping reforming unit, employing methane as a fuel [44]. The suggested concept becomes more lucid when considering the simulation results shown in Figure 8. Clearly, the amount of fully reduced ilmenite leaving the air and fuel reactor increases when decreasing the air input into the AR for $\phi < 1$ (see Figure 8b). While the same is true for the solids leaving the FR for all presented CLG approaches, a strong increase in the $FeTiO_3$ and Fe_3O_4 content in the AR products is obtained when reducing λ below unity. This can be explained by the fact that the oxygen available in the air reactor is insufficient to fully re-oxidize the OC, signified through an O_2–free product gas from the AR for $\phi < 1$ (see Figure 8a). Consequently, a pure stream of N_2 containing small concentrations of Argon and other minor compounds is produced in the AR [44]. Since substantial quantities of OC are cycled through the system in a fully reduced state, they effectively act as an inert, meaning that they transfer sensible heat, but do not participate in the occurring chemical reactions through oxygen release and uptake. However, in practice the reduced OC could potentially function as a catalytic site for tar cracking and methane reforming and favor the formation of syngas [32–35], thereby enhancing the process characteristics. Another advantage of the given approach is that an undiluted OC can be employed, which simplifies the required solid-gas and solid-solid (ash-OC-char) separation and the

operation of the CLG unit with regard to the fluidization behavior. Moreover, the net heat duty of the process can be tailored promptly and easily through an adjustment of the air flow to the AR, allowing for quick responses to disturbances (e.g., variations in feedstock composition).

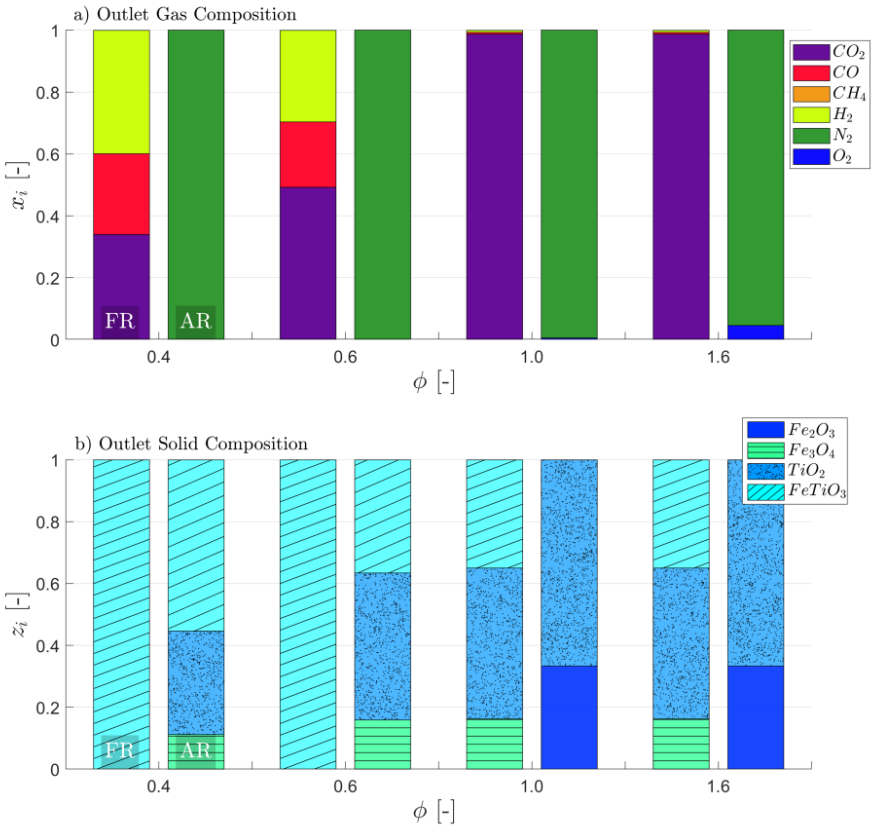

Figure 8. Simulation results for CLG operation through reducing λ. Dry molar gas composition (**a**) and molar solid composition (**b**) as a function of ϕ ($\dot{m}_{OC} = const.$).

The impact of the air-to-fuel equivalence ratio (λ) on ϕ is shown in Figure 9a. In CLC mode ($\lambda > 1$), where full OC oxidation is achieved in the AR (i.e., $X_{s,AR} = 1$), ϕ assumes a constant value, given by the amount of oxygen which is transported by a fully oxidized OC for a given circulation rate, regardless of the deployed air-to-fuel ratio (see Equation (12)). In contrast, lowering λ to values below unity to attain CLG operation means that ϕ and λ are equal, as the oxygen transport to the FR is limited by the oxygen availability in the AR:

$$\phi = \begin{cases} \lambda & \text{for } \lambda < 1 \\ \frac{R_{OC} \cdot \dot{m}_{OC}}{\dot{m}_{O,stoich}} = const. & \text{for } \lambda \geq 1 \end{cases} \tag{16}$$

The discontinuity of this relation for $\lambda = 1$ can be explained by the fact that when surpassing this value, a transient shift from CLC (see Figure 3a) to CLG (see Figure 3c) behavior (or vice versa) occurs, which goes in hand with a continuous decrease (resp. increase) in the oxidation degree of the oxygen carrier, before steady state sets in (more details see Appendix B).

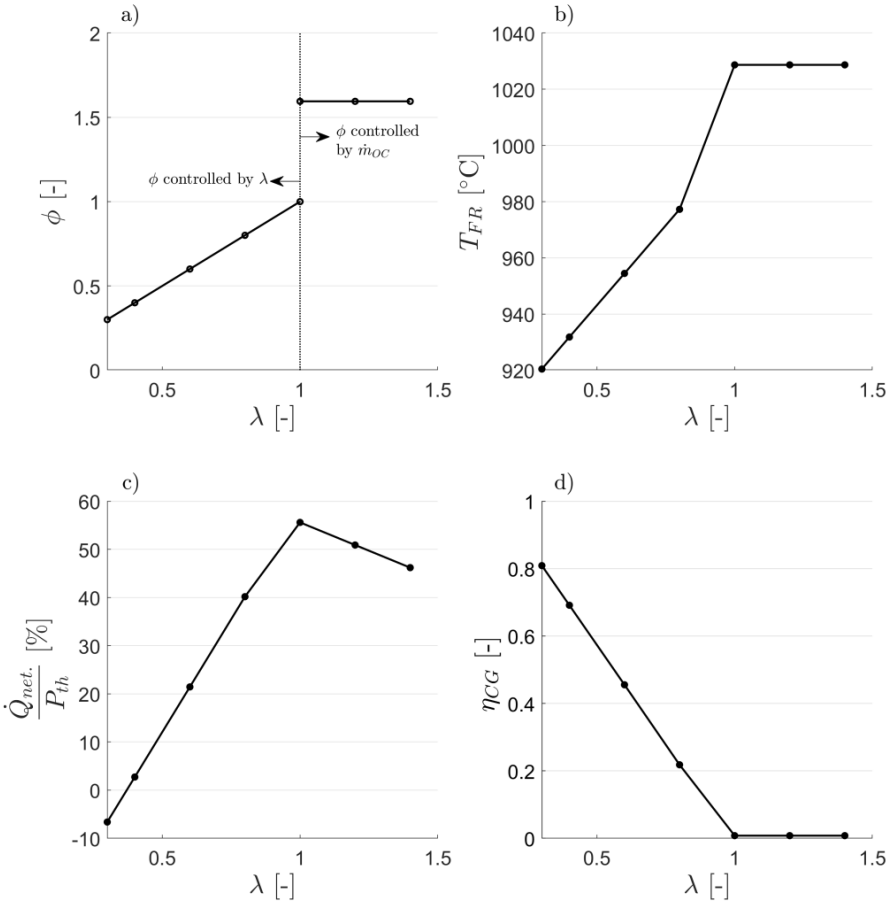

Figure 9. Simulation results for CLG operation through reducing λ. OC-to-fuel ratio as a function of the air-to-fuel equivalence ratio λ (**a**). Fuel reactor temperature (**b**), relative net process heat (**c**), and cold gas efficiency (**d**) for different values of λ ($\dot{m}_{OC} = const.$).

In terms of FR temperatures, Figure 9b shows that the given approach leads to a successful retaining of FR temperatures above 900 °C, even for ϕ-values as low as 0.4, due to the transportation of sensible heat by the OC. Moreover, the given approach yields more beneficial results in terms of the process heat balance, which can be seen in Figure 9c. Clearly, autothermal CLG operation is attained for $\phi = 0.37$, which means cold gas efficiencies exceeding 70% can be achieved (see Figure 9d). This is the case as in contrast to the previous approaches (see Sections 3.2 and 3.3), the AR is not operated in air excess during CLG operation, reducing the loss of sensible heat through the AR off-gases. This means that if one would reduce the air feed to the AR to the minimum extent required for full OC re-oxidation for the CLG approach employing inert dilution (see Section 3.3), enhanced cold gas efficiencies could be attained. Nonetheless, the given approach clearly shows advantages in terms of process control due to its flexibility, the possibility of freely selecting a suitable OC material (i.e., no specific limits on R_O), without having to consider material mixtures, and the availability of a catalytically active reduced OC material, instead of an inert solid, cycling through the system. Moreover, the chemical strain on the OC material is reduced as the change in oxidation degree for each redox cycle is lower, when compared to the former approaches, relying on full reduction and oxidation in the FR and AR, respectively (see Figure 3b,c), which should have beneficial effects on the OC lifetime.

However, one issue that might arise due to the operation of the AR in an sub-stoichiometric fashion is related to the fact that during operation a fraction of the feedstock char leaves the FR unconverted and hence travels to the AR with the circulating OC material [23,26,27]. This so called "carbon slip"

leads to competing reactions between the OC material and the residual char, in case the AR is operated with $\lambda < 1$. Yet, simulations show that in an oxygen deficient atmosphere carbon conversion is favored to OC re-oxidation in chemical equilibrium. Moreover, CO formation shows to be negligible (more details see Appendix C). Due to the fast kinetics of both char conversion and OC re-oxidation, it can be expected that equilibrium-like conditions are attained in the AR and hence all residual char is fully oxidized to CO_2 in the AR. This hypothesis is also supported by chemical looping experiments in small scale fixed bed reactors, during which it was established that in the beginning of the re-oxidation stage oxygen preferentially reacts with deposited carbon before re-oxidizing the OC [21,63,64]. Nonetheless, experiments showing that this is also the case in a continuously operated CLG unit and that CO formation is negligible are required to establish that full char conversion without substantial CO formation in the AR can be attained for this approach. Another issue related to this approach is the potential deep reduction of the OC, which could potentially entail problems related to intensified OC attrition or bed agglomeration. Although the process model does not predict substantial formation of deeper reduction stages (e.g., FeO) in the FR, such phases, related to bed agglomeration, have been found to be formed in CLC under highly reducing conditions [51,65,66]. Therefore, the gravity of this issue should be further investigated in experimental studies.

3.5. Optimizing CLG Efficiency

In the previous section it was established that OC-to-fuel equivalence ratios smaller than unity are required in the FR. Moreover, it was demonstrated only when decoupling heat and oxygen transfer between the AR and FR, $\phi < 1$ and FR temperatures above 850 °C can be obtained for an autothermal CLG process. Thermodynamically speaking, it does not make a difference how this decoupling of heat and oxygen transport is attained, which is why the following considerations will focus on the CLG approach presented in Section 3.4, employing a reduction in the air-to-fuel equivalence ratio to achieve CLG behavior.

When optimizing gasification processes, the trade-off between maximizing the carbon conversion in the gasifier and at the same time attaining high cold gas efficiencies is at the core of many optimization strategies. This is also the case in CLG, where $\eta_{CGE} = 1$ and complete char conversion is desired, yet not attainable. While large carbon capture efficiencies are obtained in cases where the char is gasified in the fuel reactor to a large extent, which is promoted by high FR temperatures [20,23,37], large steam/biomass ratios [20,37], and high OC-to-fuel ratios (if sufficient char residence times are provided) [27,52], cold gas efficiencies are maximized by the minimization of the oxidation of H_2 and hydrocarbons in the FR [35]. Although full oxidation of syngas in the FR should be limited to achieve large CGEs, formation of steam and CO_2 in the FR is required to a certain extent to obtain autothermal CLG conditions. The degree to which this formation of fully oxidized gas species is required is determined by the criterion of the CLG process being in heat balance ($\dot{Q}_{net} = 0$). This means that the heat release attained through full feedstock oxidation has to balance the heat demand of pre-heating of all inlet streams to the given reactor temperatures, the heat of reaction for endothermic gasification reactions, and the heat losses of the CLG unit. This has also been shown in the previous sections where despite assuming chemical equilibrium (i.e., full feedstock conversion), cold gas efficiencies deviating strongly from unity were obtained for autothermal boundary conditions (see Figures 5, 7 and 9).

Therefore, one approach to enhance the cold gas efficiency in CLG is a reduction in the inlet gas flows entering the air and fuel reactor. Since the air mass flow entering the AR is required to control ϕ, this leaves the steam mass flow entering the FR as a free variable which can be altered to enhance cold gas efficiencies. The effect of a reduction in the steam to biomass ratio on the net heat release of the process is shown in Figure 10a. It is visible that, with a decreasing steam to biomass ratio, the air-to-fuel equivalence ratio for which an autothermal process is attained decreases. Due to the direct correlation between the oxygen availability and cold gas efficiency in CLG (see Figure 10b), this also means that the CGE obtained for autothermal operation increases with decreasing steam/biomass ratio, so that the CGE is raised from 72.5 to 77.1%, when decreasing the steam/biomass ratio from 0.9 to 0.3. However,

it is obvious that the reduction of the steam to biomass ratio would also entail a drop in carbon capture efficiencies of the process, as less steam is available for char gasification and the kinetic inhibition effect of syngas increases with decreasing steam concentrations (entailing larger syngas partial pressures) in the FR [8,12,67,68]. This becomes most obvious for a steam to biomass ratio of 0, for which char conversions in the FR would be diminutive in a real gasifier, due to the slow kinetics of heterogeneous solid-solid OC-feedstock reactions [67–69]. As this drop in char conversion is not predicted by the equilibrium model, the negative effect on process efficiency with decreasing steam to biomass ratio cannot be evaluated in this study. However, sufficient steam availability clearly is a prerequisite in CLG, when targeting large char conversions and hence carbon capture efficiencies.

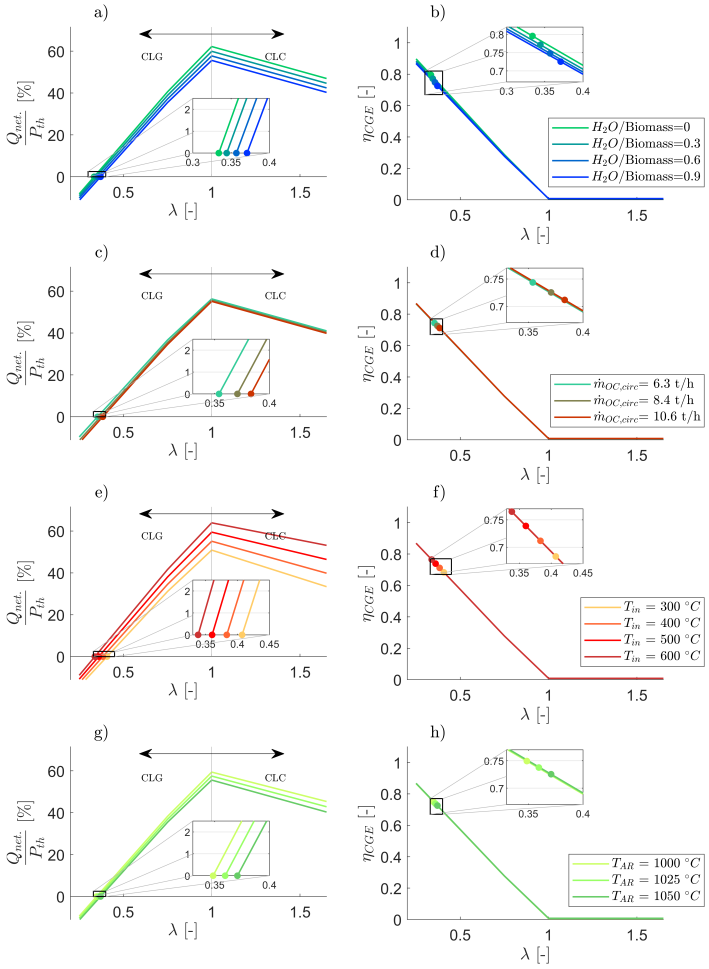

Figure 10. Net heat release and cold gas efficiency for CLC/CLG process as a function of the air to fuel equivalence ratio for different steam to biomass ratios (**a**,**b**), OC circulation rates (**c**,**d**), gas inlet temperatures (**e**,**f**), and air reactor temperatures (**g**,**h**). Circles mark the cold gas efficiency for autothermal CLG operation ($\dot{m}_{OC} = const.$, so $\phi = \lambda$ for $\lambda < 1$ and $\phi = const. > 1$ for $\lambda > 1$).

Another possible measure to enhance CGEs are variations in the circulation rate of the OC, which is shown in Figure 10c,d. Clearly, larger solid circulation rates enhance the heat transport between the reactors and hence entail higher FR temperatures [16]. However, due to material attrition, solid loss, which necessitates continuous make-up feeding, also scales with the circulation rate. As shown in Figure 10d, the effect of this material loss on the process heat balance is comparatively small, thus its effect on the cold gas efficiency is low. However, the model predicts an increase in FR temperatures

from 892 to 951 °C, when increasing the circulation rate from 6.3 to 10.6 t/h. This means that generally, large solid circulation rates are desired in CLG units, as large FR temperatures are beneficial for volatile and char conversion [20,23,37]. Yet, it has to be kept in mind that the solid circulation in dual fluidized bed systems requires solid entrainment from the fluidized bed riser, which can be increased through an increase in gas velocities (i.e., increase in steam/biomass ratio), smaller particle diameters or smaller reactor diameters [16]. Moreover, intensified solid circulation also increases the occurrence of a "carbon slip" to the AR, due to the lower residence times of the char particles in the FR [27,28,70]. This means that the OC circulation rate can only be varied within a given range.

Increasing the inlet temperature of the steam and air entering the FR and AR respectively, thereby decreasing the heat demand for heating up of the gases inside the reactor, is a further strategy to boost cold gas efficiencies. As shown in Figure 10e, this approach allows for a reduction of the air-to-fuel equivalence ratio from 0.38 to 0.34 when increasing inlet temperatures from 400 °C to 600 °C. Hence, maximizing inlet gas temperatures through heat recuperation is a key task in CLG in order to optimize the process efficiency, which is illustrated by the increase in the CGE from 68.3 to 76.5%, when increasing gas inlet temperatures from 300 to 600 °C (see Figure 10f). Due to the absence of corrosive compounds and the high process temperatures, the hot off-gases leaving the AR are ideal for steam generation and heat recuperation. On the other hand, special syngas coolers are being used to recuperate sensible heat from syngas streams for steam production [71–73], highlighting that efficient gas pre-heating using heat from process off-gases is possible in CLG.

Furthermore, variations in the AR temperatures can be considered, in order to enhance CLG process efficiencies. Generally speaking, a reduction in average process temperatures is beneficial for the process heat release, as pre-heating demands for all educts (i.e., inlet gases & feedstock material) are being reduced as a consequence, thus allowing for intensified heat extraction for a given air-to-fuel ratio (see Figure 10g). As visible in Figure 10h, a slight increase in the CGE by 2.4 percentage points can be attained for autothermal CLG operation when lowering AR temperatures from 1050 to 1000 °C. Yet, it has to be kept in mind that in chemical looping processes, air and fuel reactor temperatures are coupled, which means that a drop in FR temperatures is an inevitable effect of reduced AR temperatures. For the given boundary conditions, FR temperatures are projected to directly correlate with AR temperatures, which means that for the given reduction in AR temperatures from 1050 to 1000 °C, a corresponding drop in FR temperatures from 928 to 880 °C entails. This means that when attempting to prevent the ensuing drop in FR temperatures, related to negative effects on volatile and carbon conversion, OC circulation rates have to be increased accordingly as a counter-measure.

Although these insights allow for a first glimpse on process optimization approaches, it becomes clear that a detailed consideration of reaction kinetics and reactor hydrodynamics is quintessential, when aiming for a holistic optimization of the CLG process, as both phenomena have a pronounced effect on the process parameters. As it is well known that the conversion of char and other hydrocarbons is kinetically governed [25,55,56,59], the impact of reactor temperature, residence time, and gas concentrations on reaction kinetics need to be established in detail, allowing for accurate predictions of the governing reactions in a realistic environment. Moreover, reactor hydrodynamics are a crucial factor in chemical looping systems [74,75], making it a pre-requisite to consider them in advanced CLG process models. Through considering these phenomena, it thus becomes feasible to assess to which extent the preceding approaches can be utilized to obtain a CLG process exhibiting not only a high cold gas efficiency, but also excellent carbon capture efficiencies. Nonetheless, the preceding explanations offer valuable insights on the fundamental challenges associated with the autothermal CLG process, which require catering to, when implementing the technology in large scale.

4. Conclusions

In the course of this study, an equilibrium process model for the chemical looping gasification of biomass, using ilmenite ore as the oxygen carrier, was deployed to establish adequate process control techniques to attain autothermal behavior for gasifiers of any scale. It was shown that

pursuing continuous CLG operation leads to unique challenges in terms of the OC circulation, which is responsible for both, oxygen and heat transport between the air and fuel reactor. While high OC circulation is generally beneficial in CLC to achieve complete fuel conversion in the FR and prevent a drop in FR temperatures, CLG faces an essential dilemma. Here, large OC circulation rates are necessary to fulfill the process heat balance (i.e., retain constant temperatures in the FR), whereas significantly lower circulation rates are required in terms of the necessary oxygen transport. Hence, heat and oxygen transport have to be de-coupled. Based on model calculations, two strategies to achieve autothermal CLG behavior through a de-coupling of oxygen and heat transport were presented. One eligible option is the dilution of the OC with an inert solid (e.g., sand), allowing for an accurate tailoring of the mixture's heat capacity and oxygen transport capability through its composition. As an alternative, the oxygen transport to the FR can be controlled through the oxygen availability (i.e., air supply) in the AR, leading to a deeply reduced oxygen carrier cycling through the system, not being fully re-oxidized in the AR. While both approaches lead to stable autothermal CLG behavior with sufficiently high FR temperatures, the latter strategy possesses certain advantages in terms of process control and fuel reactor chemistry, based on which it was deemed more suitable for large-scale operation. Regardless of the deployed approach, it was shown that restricting oxygen release in the FR is key in controlling CLG operation, where large cold gas efficiencies are desired. As partial oxidation of the feedstock is necessary in order to fulfill the heat balance of an autothermal process, this means that heat losses and heat sinks in the chemical looping gasifier have to be minimized, so that the oxygen input into the FR can be reduced, thus boosting syngas yields. Possible strategies to achieve this are gas pre-heating, variations in the OC circulation, alterations in the average CLG process temperature, and a reduction in the H_2O/biomass ratio in the FR.

Certainly, the presented findings encourage a deeper investigation of the chemical looping gasification of biomass on a numerical level, as only through the deployment of elaborate models considering hydrodynamics and reaction kinetics in-depth inferences regarding the process efficiency are facilitated. Moreover, they also call for experimental investigations of the suggested process control strategies. Especially the suggested continuous CLG operation with a deeply reduced OC, not being fully re-oxidized in the AR, means setting foot on a new terrain. Here, the suitability of the presented approach is decided by the fact whether positive (e.g., pronounced methane reforming ability, increased syngas selectivity & tar cracking) or negative effects (e.g., intensified attrition, reactivity loss, particle agglomerations) prevail.

Author Contributions: Conceptualization, J.S. and P.D.; methodology, P.D.; writing—original draft preparation, P.D.; writing—review and editing, F.M., J.S. and F.A.; visualization, P.D.; supervision, B.E. All authors have read and agreed to the published version of the manuscript.

Funding: This work has received funding of the European Union's Horizon 2020-Research and Innovation Framework Programme under grant agreement No. 817841 (Chemical Looping gasification foR sustainAble production of biofuels-CLARA).

Acknowledgments: The authors would like to thank the Technical University of Darmstadt, enabling the open-access publication of this paper.

Conflicts of Interest: The authors declare no conflict of interest. The funders had no role in the design of the study; in the collection, analyses, or interpretation of data; in the writing of the manuscript, or in the decision to publish the results.

Nomenclature

Symbol	Explanation	Unit
h_i	Enthalpy of stream i	kJ/kg
$\dot{m}_i$	Mass flow of component/element i	kg/h
M_i	Molar mass of component/element i	g/mole
$\dot{n}_i$	Mole flow of component/element i	kmole/h
P	Power	kW
p	Pressure	bar
R_{OC}	Oxygen transport capacity of oxygen carrier	-
$\dot{m}_{air,AR}$	Mass flow of air entering the AR	kg/h
T	Temperature	°C
x_i	Mass/mole fraction in gas phase	-
X_i	Conversion of component i	-
$Y_{i,j}$	Mass yield of component/element i from substance j	-
z_i	Mass/mole fraction in solid phase	-
η_{CC}	Carbon capture efficiency	-
η_{CGE}	Cold gas efficiency	-
λ	Air-to-fuel equivalence ratio	-
ϕ	Oxygen carrier-to-fuel equivalence ratio	-

Subscript	Explanation
AR	Air reactor
devol.	Devolatilization.
FR	Fuel reactor
init	Initial
net	net
O	Oxygen
OC	Oxygen Carrier
ox	Oxidation
red	Reduction
s	Solid
stoich	Stoichiometric
th	Thermal

Abbreviation	Explanation
AR	Air Reactor
ASU	Air Separation Unit
CGE	Cold Gas Efficiency
CLC	Chemical Looping Combustion
CLG	Chemical Looping Gasification
FR	Fuel Reactor
GHGE	Greenhouse Gas Emissions
LHV	Lower Heating Value
OC	Oxygen Carrier
RED II	European Union Renewable Energy Directive
WGS	Water-Gas-Shift

Appendix A. Boundary Conditions for CLG Process Model

A summary of all model boundary conditions employed for the simulations presented in Section 3.2, Section 3.3 and Section 3.4 is given in Table A1.

Table A1. Boundary conditions for 1 MW_{th} CLC/CLG process model for different CLG approaches.

Parameter	Approach 1 *	Approach 2 *	Approach 3 *	Unit
T_{FR}	730–1030	980–1030	930–1030	°C
T_{AR}	1050	1050	1050	°C
p_{FR}/p_{AR}	1.013	1.013	1.013	bar
$\dot{m}_{fuel}$	200.4	200.4	200.4	kg/h
$\dot{m}_{H2O,FR}$	180.4	180.4	180.4	kg/h
$\dot{m}_{CO2,FR}$	40.1	40.1	40.1	kg/h
$\dot{m}_{air,AR}$	1362.6	1362.6	454–1590	kg/h
$T_{CO2,FR}$	25	25	25	°C
$T_{H2O,FR}/T_{air,AR}$	400	400	400	°C
$\dot{m}_{OC,init}$	2.11–8.45	8.45	8.45	t/h
z_{SiO2}	0	0–75	0	wt-%

* CLG approach I: Reduction in OC circulation rate (see Section 3.2), CLG approach 2: Dilution with solid inert (see Section 3.3), CLG approach 3: Reduction of air inlet into AR (see Section 3.4).

Appendix B. Shifting from CLC to CLG Operation through Variations in the Air-to-Fuel Equivalence Ratio

As described in Section 3.4, the oxygen availability in the FR is solely dependent on the circulation rate of the OC and the oxygen transport capability of the OC material (R_O), when operating the AR in air excess ($\lambda > 1$) in CLC, as the OC material is fully oxidized inside the AR. When subsequently reducing λ to values below unity from a steady state CLC operating point (see Figure A1a), the limited air availability in the AR leads to a transient phase during which the OC undergoes a continuous drop in the oxidation degree with each redox cycle, as more oxygen is consumed in the FR (combustion conditions) than is being supplied in the AR. As soon as the oxidation degree in the FR approaches 0, the oxygen availability in the subsequent redox cycle is determined by the oxygen supply in the AR. Hence, ϕ is equal to λ from this point onwards. As indicated in Figure A1a, this means that steady state CLG conditions are attained as a consequence. When on the other hand starting off with steady state CLG operation ($\lambda < 1$) before increasing λ beyond unity, the OC undergoes a transient phase during which its oxidation degree increases with each redox cycle, since more oxygen is supplied in the AR than is being consumed in the FR. As soon as the amount of oxygen transported by the OC is sufficient to fully oxidize the deployed feedstock, CLC conditions are attained. It has to be noted that this can be the case before steady state is reached (see Figure A1b). This means that despite the described discontinuity in the relation between λ and ϕ for $\lambda = 1$, a rapid switch in the OC-to-fuel ratio will not occur during operation, as the transition from CLC to CLG or vice versa will occur smoothly via a transient phase during which the oxidation degree of the OC adapts to the newly set boundary conditions.

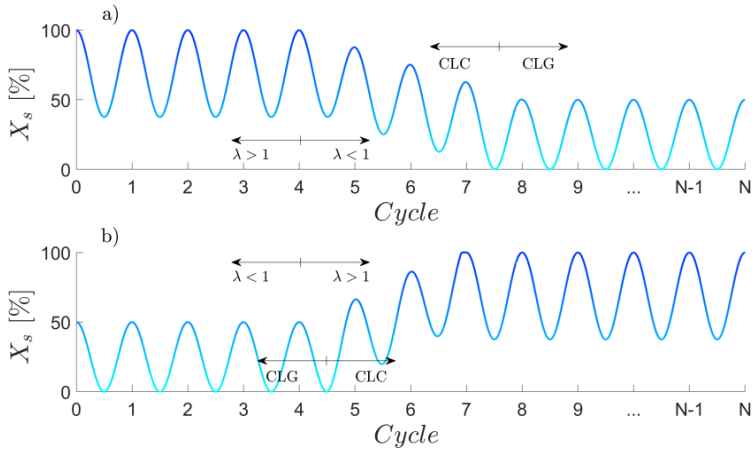

Figure A1. Progression of the OC oxidation degree when shifting from CLC ($\lambda > 1$) to CLG ($\lambda < 1$) mode through variations of the air-to-fuel equivalence ratio. (**a**) Shift from CLC to CLG, (**b**) shift from CLG to CLG.

Appendix C. Char Conversion in an Sub-Stoichiometrically Operated AR

In order to establish how a mixture of unconverted char and a fully reduced OC behaves in an sub-stoichiometric oxygen containing atmosphere in the AR, a mixture of char (5 mole-%) and a reduced OC (78 mole-% $FeTiO_3$, 6 mole-% Fe_2O_3 and 11 mole-% TiO_2) were reacted with different amounts of air in an RGIBBS reactor of varying temperature (900–1100 °C). The results for an AR temperature of 1000 °C are shown in Figure A2. It is visible that char conversion occurs prior to OC re-oxidation, as the char fraction is zero regardless of the deployed air-to-fuel ratio. Moreover, the chemical equilibrium predicts a further reduction of the OC in case the amount of oxygen contained in the inlet air is insufficient for char conversion. Certainly, this behavior can only be observed in case of sufficiently long reaction times (rarely given in a fluidized bed), since solid-solid reactions between OC and char particles are known to exhibit slow kinetics [67–69]. This means that when attempting full char conversion, the inlet air entering the AR has to be sufficient to provide full carbon combustion. When this is the case, it can be assumed that full char conversion is attained inside the AR. In terms of the CO content at the reactor outlet it can be seen that full CO conversion to CO_2 is achieved regardless of the utilized air-to-fuel ratio, indicated by negligible concentrations of CO in the AR outlet (see Figure A2).

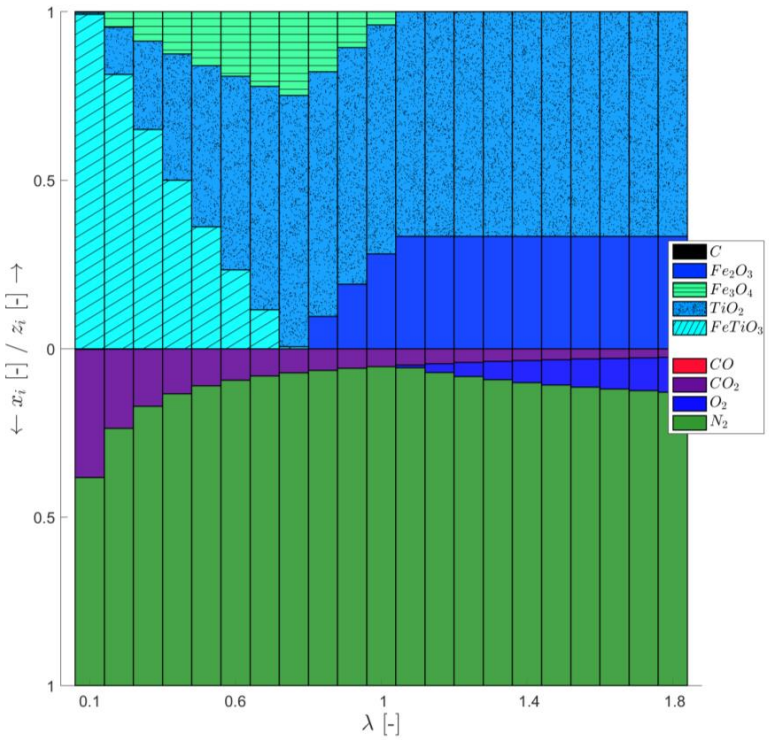

Figure A2. Solid and gas composition at chemical equilibrium for TAR = 1000 °C at varying air-to-fuel equivalence ratio λ (Inlet solid composition: 78 mole-% $FeTiO_3$, 6 mole-% Fe_2O_3 and 11 mole-% TiO_2).

References

1. International Energy Agency (IEA). *Key World Energy Statistics 2018*; International Energy Agency: Paris, France, 2018.
2. Energy Information Administration. Statistics Data Browser—Electricity Generation from Renewables by Source. Available online: https://www.iea.org/statistics/ (accessed on 23 August 2019).
3. European Commission. Transport Emissions—A European Strategy for Low-Emission Mobility. Available online: https://ec.europa.eu/clima/policies/transport_en (accessed on 23 August 2019).
4. EUR-Lex. Directive (EU) 2018/2001 of the European Parliament and of the Council of 11 December 2018 on the Promotion of the Use of Energy from Renewable Sources (Text with EEA Relevance). Available online: https://eur-lex.europa.eu/legal-content/en/TXT/?uri=CELEX:32018L2001 (accessed on 12 June 2020).
5. Carrasco, J.E.; Monti, A.; Tayeb, J.; Kiel, J.; Girio, F.; Matas, B.; Santos Jorge, R. *Strategic Research and Innovation Agenda 2020*; EERA: Brussels, Belgium, 2020; p. 82.

6. De, S.; Agarwal, A.K.; Moholkar, V.S.; Thallada, B. *Coal and Biomass Gasification: Recent Advances and Future Challenges*; Springer: Berlin/Heidelberg, Germany, 2018.
7. Higman, C.; Van der Burgt, M. *Gasification*, 2nd ed.; Gulf Professional Publishing: Houston, TX, USA; Elsevier Science: Amsterdam, The Netherlands, 2008.
8. Barrio, M.; Gbel, B.; Rimes, H.; Henriksen, U.; Hustad, J.E.; Srensen, L.H. Steam gasification of wood char and the effect of hydrogen inhibition on the chemical kinetics. In *Progress in Thermochemical Biomass Conversion*; Bridgwater, A.V., Ed.; Blackwell Science Ltd.: Oxford, UK, 2001; pp. 32–46.
9. Hansen, L.K.; Rathmann, O.; Olsen, A.; Poulsen, K. *Steam Gasification of Wheat Straw, Barley Straw, Willow and Giganteus*; Risø National Laboratory: Roskilde, Denmark, 1997.
10. Klose, W.; Wolki, M. On the intrinsic reaction rate of biomass char gasification with carbon dioxide and steam. *Fuel* **2005**, *84*, 885–892. [CrossRef]
11. Ollero, P.; Serrera, A.; Arjona, R.; Alcantarilla, S. The CO_2 gasification kinetics of olive residue. *Biomass Bioenergy* **2003**, *24*, 151–161. [CrossRef]
12. Barrio, M.; Hustad, J.E. CO_2 Gasification of birch char and the effect of CO inhibition on the calculation of chemical kinetics. In *Progress in Thermochemical Biomass Conversion*; Bridgwater, A.V., Ed.; Blackwell Science Ltd.: Oxford, UK, 2001; pp. 47–60.
13. Basu, P. *Biomass Gasification and Pyrolysis*; Elsevier: Amsterdam, The Netherlands, 2010.
14. Ge, H.; Zhang, H.; Guo, W.; Song, T.; Shen, L. System simulation and experimental verification: Biomass-based integrated gasification combined cycle (BIGCC) coupling with chemical looping gasification (CLG) for power generation. *Fuel* **2019**, *241*, 118–128. [CrossRef]
15. Huang, Z.; Zhang, Y.; Fu, J.; Yu, L.; Chen, M.; Liu, S.; He, F.; Chen, D.; Wei, G.; Zhao, K.; et al. Chemical looping gasification of biomass char using iron ore as an oxygen carrier. *Int. J. Hydrogen Energy* **2016**, *41*, 17871–17883. [CrossRef]
16. Karl, J.; Pröll, T. Steam gasification of biomass in dual fluidized bed gasifiers: A review. *Renew. Sust. Energ. Rev.* **2018**, *98*, 64–78. [CrossRef]
17. Xu, G.; Murakami, T.; Suda, T.; Matsuzawa, Y.; Tani, H. The superior technical choice for dual fluidized bed gasification. *Ind. Eng. Chem. Res.* **2006**, *45*, 2281–2286. [CrossRef]
18. Aigner, I.; Pfeifer, C.; Hofbauer, H. Co-gasification of coal and wood in a dual fluidized bed gasifier. *Fuel* **2011**, *90*, 2404–2412. [CrossRef]
19. Huang, Z.; He, F.; Feng, Y.; Zhao, K.; Zheng, A.; Chang, S.; Wei, G.; Zhao, Z.; Li, H. biomass char direct chemical looping gasification using NiO-modified iron ore as an oxygen carrier. *Energy Fuels* **2014**, *28*, 183–191. [CrossRef]
20. Ge, H.; Guo, W.; Shen, L.; Song, T.; Xiao, J. Biomass gasification using chemical looping in a 25 kW_{th} reactor with natural hematite as oxygen carrier. *Chem. Eng. J.* **2016**, *286*, 174–183. [CrossRef]
21. Guo, Q.; Cheng, Y.; Liu, Y.; Jia, W.; Ryu, H.-J. Coal chemical looping gasification for syngas generation using an iron-based oxygen carrier. *Ind. Eng. Chem. Res.* **2014**, *53*, 78–86. [CrossRef]
22. Huang, Z.; He, F.; Feng, Y.; Zhao, K.; Zheng, A.; Chang, S.; Li, H. Synthesis gas production through biomass direct chemical looping conversion with natural hematite as an oxygen carrier. *Bioresour. Technol.* **2013**, *140*, 138–145. [CrossRef] [PubMed]
23. Huseyin, S.; Wei, G.; Li, H.; He, F.; Huang, Z. Chemical-looping gasification of biomass in a 10 kW_{th} interconnected fluidized bed reactor using Fe_2O_3/Al_2O_3 oxygen carrier. *J. Fuel Chem. Technol.* **2014**, *42*, 922–931. [CrossRef]
24. Adanez, J.; Abad, A.; Garcia-Labiano, F.; Gayan, P.; De Diego, L.F. Progress in chemical-looping combustion and reforming technologies. *Prog. Energy Combust. Sci.* **2012**, *38*, 215–282. [CrossRef]
25. Ohlemüller, P.; Alobaid, F.; Abad, A.; Adanez, J.; Ströhle, J.; Epple, B. Development and validation of a 1D process model with autothermal operation of a 1 MW_{th} chemical looping pilot plant. *Int. J. Greenh. Gas Control* **2018**, *73*, 29–41. [CrossRef]
26. Markström, P.; Linderholm, C.; Lyngfelt, A. Chemical-looping combustion of solid fuels—Design and operation of a 100 kW unit with bituminous coal. *Int. J. Greenh. Gas Control* **2013**, *15*, 150–162. [CrossRef]
27. Cuadrat, A.; Abad, A.; García-Labiano, F.; Gayán, P.; De Diego, L.F.; Adánez, J. Effect of operating conditions in Chemical-Looping Combustion of coal in a 500 Wth unit. *Int. J. Greenh. Gas Control* **2012**, *6*, 153–163. [CrossRef]

28. Pérez-Vega, R.; Abad, A.; García-Labiano, F.; Gayán, P.; De Diego, L.F.; Adánez, J. Coal combustion in a 50 kWth chemical looping combustion unit: Seeking operating conditions to maximize CO_2 capture and combustion efficiency. *Int. J. Greenh. Gas Control* **2016**, *50*, 80–92. [CrossRef]
29. Ströhle, J.; Orth, M.; Epple, B. Chemical looping combustion of hard coal in a 1 MW_{th} pilot plant using ilmenite as oxygen carrier. *Appl. Energy* **2015**, *157*, 288–294. [CrossRef]
30. Cao, Y.; Casenas, B.; Pan, W.-P. Investigation of chemical looping combustion by solid fuels. 2. Redox reaction kinetics and product characterization with coal, biomass, and solid waste as solid fuels and CuO as an oxygen carrier. *Energy Fuels* **2006**, *20*, 1845–1854. [CrossRef]
31. Leion, H.; Mattisson, T.; Lyngfelt, A. Solid fuels in chemical-looping combustion. *Int. J. Greenh. Gas Control* **2008**, *2*, 180–193. [CrossRef]
32. Virginie, M.; Adánez, J.; Courson, C.; De Diego, L.F.; García-Labiano, F.; Niznansky, D.; Kiennemann, A.; Gayán, P.; Abad, A. Effect of Fe–olivine on the tar content during biomass gasification in a dual fluidized bed. *Appl. Catal. B Environ.* **2012**, *121–122*, 214–222. [CrossRef]
33. Kuhn, J.N.; Zhao, Z.; Felix, L.G.; Slimane, R.B.; Choi, C.W.; Ozkan, U.S. Olivine catalysts for methane and tar-steam reforming. *Appl. Catal. B Environ.* **2008**, *81*, 14–26. [CrossRef]
34. Mendiara, T.; Johansen, J.M.; Utrilla, R.; Geraldo, P.; Jensen, A.D.; Glarborg, P. Evaluation of different oxygen carriers for biomass tar reforming (I): Carbon deposition in experiments with toluene. *Fuel* **2011**, *90*, 1049–1060. [CrossRef]
35. Larsson, A.; Israelsson, M.; Lind, F.; Seemann, M.; Thunman, H. Using ilmenite to reduce the tar yield in a dual fluidized bed gasification system. *Energy Fuels* **2014**, *28*, 2632–2644. [CrossRef]
36. Milne, T.A.; Evans, R.J.; Abatzaglou, N. *Biomass Gasifier "Tars": Their Nature, Formation, and Conversion*; National Renewable Energy Laboratory: Golden, CO, USA, 1998.
37. Ge, H.; Guo, W.; Shen, L.; Song, T.; Xiao, J. Experimental investigation on biomass gasification using chemical looping in a batch reactor and a continuous dual reactor. *Chem. Eng. J.* **2016**, *286*, 689–700. [CrossRef]
38. Leion, H.; Jerndal, E.; Steenari, B.-M.; Hermansson, S.; Israelsson, M.; Jansson, E.; Johnsson, M.; Thunberg, R.; Vadenbo, A.; Mattisson, T.; et al. Solid fuels in chemical-looping combustion using oxide scale and unprocessed iron ore as oxygen carriers. *Fuel* **2009**, *88*, 1945–1954. [CrossRef]
39. Fan, L.-S. *Chemical Looping Systems for Fossil Energy Conversions*; Wiley-AIChE: Hoboken, NJ, USA, 2010.
40. Mayer, K.; Penthor, S.; Pröll, T.; Hofbauer, H. The different demands of oxygen carriers on the reactor system of a CLC plant—Results of oxygen carrier testing in a 120 kW_{th} pilot plant. *Appl. Energy* **2015**, *157*, 323–329. [CrossRef]
41. Ohlemüller, P.G. *Untersuchung von Chemical-Looping-Combustion im Megawatt-Maßstab*; Cuvillier: Göttingen, Germany, 2019.
42. De Diego, L.F.; Garcı´a-Labiano, F.; Gayán, P.; Celaya, J.; Palacios, J.M.; Adánez, J. Operation of a 10 kW_{th} chemical-looping combustor during 200h with a CuO–Al_2O_3 oxygen carrier. *Fuel* **2007**, *86*, 1036–1045. [CrossRef]
43. Adánez, J.; Gayán, P.; Celaya, J.; De Diego, L.F.; García-Labiano, F.; Abad, A. Chemical Looping Combustion in a 10 kW_{th} Prototype Using a CuO/Al_2O_3 Oxygen Carrier: Effect of Operating Conditions on Methane Combustion. *Ind. Eng. Chem. Res.* **2006**, *45*, 6075–6080. [CrossRef]
44. Pröll, T.; Bolhàr-Nordenkampf, J.; Kolbitsch, P.; Hofbauer, H. Syngas and a separate nitrogen/argon stream via chemical looping reforming—A 140 kW pilot plant study. *Fuel* **2010**, *89*, 1249–1256. [CrossRef]
45. Ohlemüller, P.; Busch, J.-P.; Reitz, M.; Ströhle, J.; Epple, B. Chemical-Looping Combustion of Hard Coal: Autothermal Operation of a 1 MW_{th} Pilot Plant. *J. Energy Resour. Technol.* **2016**, *138*, 042203. [CrossRef]
46. Mallick, D.; Mahanta, P.; Moholkar, V.S. Co-gasification of coal and biomass blends: Chemistry and engineering. *Fuel* **2017**, *204*, 106–128. [CrossRef]
47. Matthesius, G.A.; Morris, R.M.; Desai, M.J. Prediction of the volatile matter in coal from ultimate and proximate analyses. *J. S. Afr. Inst. Min. Metall.* **1987**, *5*, 157–161.
48. Neves, D.; Thunman, H.; Matos, A.; Tarelho, L.; Gómez-Barea, A. Characterization and prediction of biomass pyrolysis products. *Prog. Energy Combust. Sci.* **2011**, *37*, 611–630. [CrossRef]
49. Cuadrat, A.; Abad, A.; Gayán, P.; De Diego, L.F.; García-Labiano, F.; Adánez, J. Theoretical approach on the CLC performance with solid fuels: Optimizing the solids inventory. *Fuel* **2012**, *97*, 536–551. [CrossRef]

50. Mendiara, T.; Pérez-Astray, A.; Izquierdo, M.T.; Abad, A.; De Diego, L.F.; García-Labiano, F.; Gayán, P.; Adánez, J. Chemical Looping Combustion of different types of biomass in a 0.5 kW_{th} unit. *Fuel* **2018**, *211*, 868–875. [CrossRef]
51. Leion, H.; Lyngfelt, A.; Johansson, M.; Jerndal, E.; Mattisson, T. The use of ilmenite as an oxygen carrier in chemical-looping combustion. *Chem. Eng. Res. Des.* **2008**, *86*, 1017–1026. [CrossRef]
52. Pissot, S.; Vilches, T.B.; Maric, J.; Seemann, M. Chemical looping gasification in a 2–4 MWth dual fluidized bed gasifier. In Proceedings of the 23rd International Conference on Fluidized Bed Conversion, Seoul, South Korea, 13 May 2018.
53. Li, K.; Zhang, R.; Bi, J. Experimental study on syngas production by co-gasification of coal and biomass in a fluidized bed. *Int. J. Hydrogen Energy* **2010**, *35*, 2722–2726. [CrossRef]
54. Narváez, I.; Orío, A.; Aznar, M.P.; Corella, J. Biomass gasification with air in an atmospheric bubbling fluidized bed. effect of six operational variables on the quality of the produced raw gas. *Ind. Eng. Chem. Res.* **1996**, *35*, 2110–2120. [CrossRef]
55. Abad, A.; Adánez, J.; Cuadrat, A.; García-Labiano, F.; Gayán, P.; De Diego, L.F. Kinetics of redox reactions of ilmenite for chemical-looping combustion. *Chem. Eng. Sci.* **2011**, *66*, 689–702. [CrossRef]
56. Zafar, Q.; Abad, A.; Mattisson, T.; Gevert, B. Reaction kinetics of freeze-granulated NiO/$MgAl_2O_4$ oxygen carrier particles for chemical-looping combustion. *Energy Fuels* **2007**, *21*, 610–618. [CrossRef]
57. Mattisson, T.; Lyngfelt, A.; Cho, P. The use of iron oxide as an oxygen carrier in chemical-looping combustion of methane with inherent separation of CO_2. *Fuel* **2001**, *80*, 1953–1962. [CrossRef]
58. Ohlemüller, P.; Ströhle, J.; Epple, B. Chemical looping combustion of hard coal and torrefied biomass in a 1 MW_{th} pilot plant. *Int. J. Greenh. Gas Control* **2017**, *65*, 149–159. [CrossRef]
59. Dennis, J.S.; Scott, S.A. In situ gasification of a lignite coal and CO_2 separation using chemical looping with a Cu-based oxygen carrier. *Fuel* **2010**, *89*, 1623–1640. [CrossRef]
60. He, F.; Huang, Z.; Li, H.; Zhao, Z. Biomass Direct Chemical Looping Conversion in a Fluidized Bed Reactor with Natural Hematite as an Oxygen Carrier. In Proceedings of the Asia-Pacific Power and Energy Engineering Conference (IEEE), Wuhan, China, 28–31 March 2011; pp. 1–7.
61. Zhao, H.; Guo, L.; Zou, X. Chemical-looping auto-thermal reforming of biomass using Cu-based oxygen carrier. *Appl. Energy* **2015**, *157*, 408–415. [CrossRef]
62. Kunii, D.; Levenspiel, O. *Fluidization Engineering*, 2nd ed.; Butterworth-Heinemann: Boston, MA, USA, 1991.
63. Song, Q.; Xiao, R.; Deng, Z.; Zhang, H.; Shen, L.; Xiao, J.; Zhang, M. Chemical-looping combustion of methane with $CaSO_4$ oxygen carrier in a fixed bed reactor. *Energy Convers. Manag.* **2008**, *49*, 3178–3187. [CrossRef]
64. Ryu, H.-J.; Bae, D.-H.; Jin, G.-T. Effect of temperature on reduction reactivity of oxygen carrier particles in a fixed bed chemical-looping combustor. *Korean J. Chem. Eng.* **2003**, *20*, 960–966. [CrossRef]
65. Cuadrat, A.; Abad, A.; Adánez, J.; De Diego, L.F.; García-Labiano, F.; Gayán, P. Behavior of ilmenite as oxygen carrier in chemical-looping combustion. *Fuel Process. Technol.* **2012**, *94*, 101–112. [CrossRef]
66. Cho, P.; Mattisson, T.; Lyngfelt, A. Carbon Formation on Nickel and Iron Oxide-Containing Oxygen Carriers for Chemical-Looping Combustion. *Ind. Eng. Chem. Res.* **2005**, *44*, 668–676. [CrossRef]
67. Leion, H.; Lyngfelt, A.; Mattisson, T. Effects of Steam and CO_2 in the Fluidizing Gas when Using Bituminous Coal in Chemical-Looping Combustion. In Proceedings of the 20th International Conference on Fluidized Bed Combustion, Xi'an, China, 18–21 May 2009; pp. 608–611.
68. Leion, H.; Mattisson, T.; Lyngfelt, A. The use of petroleum coke as fuel in chemical-looping combustion. *Fuel* **2007**, *86*, 1947–1958. [CrossRef]
69. Brown, T.A.; Dennis, J.S.; Scott, S.A.; Davidson, J.F.; Hayhurst, A.N. Gasification and chemical-looping combustion of a lignite char in a fluidized bed of iron oxide. *Energy Fuels* **2010**, *24*, 3034–3048. [CrossRef]
70. Mendiara, T.; De Diego, L.F.; García-Labiano, F.; Gayán, P.; Abad, A.; Adánez, J. Behaviour of a bauxite waste material as oxygen carrier in a 500 Wth CLC unit with coal. *Int. J. Greenh. Gas Control* **2013**, *17*, 170–182. [CrossRef]
71. Herdel, P.; Krause, D.; Peters, J.; Kolmorgen, B.; Ströhle, J.; Epple, B. Experimental investigations in a demonstration plant for fluidized bed gasification of multiple feedstock's in 0.5 MW_{th} scale. *Fuel* **2017**, *205*, 286–296. [CrossRef]
72. Weidenfeller, D.J.; Kulik, R.; Rothenpieler, K.; Stückrath, K.; Hetzer, J. Design, Simulation and Practical Experience of the Largest Syngas Cooler in Operation for Coal Gasification. In Proceedings of the 8th International Freiberg Conference, Cologne, Germany, 12–16 June 2016.

73. Schmidtsche Schack, ARVOS GmbH. *Schmidtsche Schack®Solutions for Gasification Plants*. Available online: https://www.schmidtsche-schack.com/products/syngas-cooler#c255 (accessed on 17 June 2020).
74. Bischi, A.; Langørgen, Ø.; Morin, J.-X.; Bakken, J.; Ghorbaniyan, M.; Bysveen, M.; Bolland, O. Hydrodynamic viability of chemical looping processes by means of cold flow model investigation. *Appl. Energy* **2012**, *97*, 201–216. [CrossRef]
75. Markström, P.; Lyngfelt, A. Designing and operating a cold-flow model of a 100 kW chemical-looping combustor. *Powder Technol.* **2012**, *222*, 182–192. [CrossRef]

3.2 Second Research Paper

Design of a 1 MW_{th} Pilot Plant for Chemical Looping Gasification of Biogenic Residues

Authors: Falko Marx, Paul Dieringer, Jochen Ströhle, Bernd Epple
Journal: Energies
Date: 2021-04-30
ISSN: 1996-1073
DOI: 10.3390/en14092581

energies

MDPI

Article

Design of a 1 MW_{th} Pilot Plant for Chemical Looping Gasification of Biogenic Residues

Falko Marx *, Paul Dieringer, Jochen Ströhle and Bernd Epple

Institute for Energy Systems & Technology, Technische Universität Darmstadt, Otto-Berndt-Str. 2, 64287 Darmstadt, Germany; paul.dieringer@est.tu-darmstadt.de (P.D.); jochen.stroehle@est.tu-darmstadt.de (J.S.); bernd.epple@est.tu-darmstadt.de (B.E.)
* Correspondence: falko.marx@est.tu-darmstadt.de; Tel.: +49-6151-16-23002

Abstract: Chemical looping gasification (CLG) is a promising process for the thermochemical solid to liquid conversion route using lattice oxygen, provided by a solid oxygen carrier material, to produce a nitrogen free synthesis gas. Recent advances in lab-scale experiments show that CLG with biomass has the possibility to produce a carbon neutral synthesis gas. However, all experiments have been conducted in externally heated units, not enabling autothermal operation. In this study, the modification of an existing pilot plant for demonstrating autothermal operation of CLG is described. Energy and mass balances are calculated using a validated chemical looping combustion process model extended for biomass gasification. Based on six operational cases, adaptations of the pilot plant are designed and changes discussed. A reactor configuration using two circulating fluidized bed reactors with internal solid circulation in the air reactor is proposed and a suitable operating strategy devised. The resulting experimental unit enables a reasonable range of operational parameters within restrictions imposed from autothermal operation.

Keywords: chemical looping; biomass; gasification; fluidized bed; autothermal; pilot plant

Citation: Marx, F.; Dieringer, P.; Ströhle, J.; Epple, B. Design of a 1 MW_{th} Pilot Plant for Chemical Looping Gasification of Biogenic Residues. *Energies* **2021**, *14*, 2581. https://doi.org/10.3390/en14092581

Academic Editor: Andrea Di Carlo

Received: 31 March 2021
Accepted: 28 April 2021
Published: 30 April 2021

1. Introduction

The reduction of greenhouse gas emissions is one of the major challenges in the 21th century. The European Commission sets a minimum share of 14% as a goal for renewable transport fuels produced from non food or feed sources in 2030 [1] in order to combat global warming according to the UNFCCC Paris Agreement. This is a major increase from the less than 0.1% share of renewable transport fuels in 2018 in the European Union (including food grade sources) [2] and necessitates the development of second generation biofuels. Moreover, first generation biofuels mostly utilize biochemical conversion from sugar and starch or physicochemical conversion from plant oil or fat for the production of drop in fuels [3]. However, these processes cannot be used efficiently for the production of second generation biofuels from EU approved biogenic sources—as they are low in sugar, starch, oil and fat and high in cellulosis and lignin—so new production processes are needed.

However, efficient technological pathways for the production of second generation exist only partially and not in an entire process chain, in the form of thermochemical conversion through gasification, methanol or Fischer–Tropsch synthesis and subsequent refining. Gasification, the starting point of the process chain for solid to liquid conversion, is presently used for the generation of heat and electricity [4] and very little for the production of liquid biofuels [5]. It is a well known process which converts solid feedstock in to a high caloric syngas and is considered to have a high potential for the decarbonization of hard to electrify aviation and maritime transport sectors. Additionally, the energy required for the conversion is provided by the biomass feedstock giving the potential of a total carbon neutral drop-in fuel.

As the feedstocks considered by the European Union [1] include seasonally varying types of biomass like husk and straw, as well as more continually sourceable foresting residue, sewage sludge, and biogenic household waste, fluidized bed gasification with its good feedstock flexibility seems a suitable process. Moreover, the good heat and mass transfer characteristics of fluidized bed facilitate complete conversion of the feedstock into syngas, thus achieving a high carbon conversion [6,7] and process efficiency [7,8]. Furthermore, as fuel synthesis requires an N_2-free syngas and thus gasification without the presence of N_2 [9], the subsequent syngas cleaning gives rise to easy carbon capture with storage or utilization making the carbon footprint of the product negative. The N_2-free gasification environment is usually created by the provision of pure oxygen provided by an air separation unit (ASU) [9,10], but in fluidized bed gasification another possibility exists to create an N_2-free atmosphere: dual fluidized bed gasification (DFBG) utilizes two reactors to split the gasification process from the oxidation or combustion process used to generate the necessary heat while avoiding the expensive ASU. Nonetheless, as heated solid bed material circulating between the two reactors is used to transfer the energy for the process, the transport of some amounts of carbon from the feedstock to the gasification reactor is necessary for the combustion reactor to generate the required heat, giving a substantial amount of CO_2-emission from the process.

The chemical looping gasification (CLG) process operates in a similar manner using two coupled fluidized bed reactors. However, instead of transporting residual feedstock from the gasification reactor to one operated with air, it employs a metal oxide to transport oxygen from a reactor operated with air towards the gasification, thus giving the benefit of a process with virtually no CO_2 emission. So far all experiments with continuous operation of the process were conducted in lab and pilot scale with external heating [11–15] and a maximum thermal load of 25 kW [16,17]. Furthermore, autothermal operation has not been demonstrated and problems of process scale up have not been identified and alleviated. Therefore the existing 1 MW chemical looping combustion (CLC) pilot plant located at Technische Universität Darmstadt is modified for the operation and investigation of the CLG process with biomass.

In this work, the design and modifications of the 1 MW pilot plant are described. Starting from the underlying, fundamental gasification process, the existing infrastructural restrictions, and the planed operation range, mass and energy balances are calculated and required adjustments identified and implemented.

2. Theory

2.1. Gasification Fundamentals

Fluidized bed CLG of solid feedstocks comprises, after initial drying and devolatilization, the following main reactions:

$$C + CO_2 \longleftrightarrow 2\,CO \qquad \Delta H = 172.4\,\mathrm{kJ\,mol^{-1}} \qquad \text{Bodouard reaction} \qquad \text{(R1)}$$

$$C + H_2O \longleftrightarrow CO + H_2 \qquad \Delta H = 131.3\,\mathrm{kJ\,mol^{-1}} \qquad \text{char reforming} \qquad \text{(R2)}$$

$$CO + H_2O \longleftrightarrow CO_2 + H_2 \qquad \Delta H = -41.1\,\mathrm{kJ\,mol^{-1}} \qquad \text{water gas shift} \qquad \text{(R3)}$$

$$C + 2\,H_2 \longleftrightarrow CH_4 \qquad \Delta H = -74.8\,\mathrm{kJ\,mol^{-1}} \qquad \text{methanation} \qquad \text{(R4)}$$

Further important reactions between the commonly used gasification agent H_2O [9] and the formed methane is the steam methane reforming reaction:

$$CH_4 + H_2O \longleftrightarrow CO + 3\,H_2 \qquad \Delta H = 206.1\,\mathrm{kJ\,mol^{-1}} \qquad \text{steam methane reforming} \qquad \text{(R5)}$$

$$CH_4 + 2\,H_2O \longleftrightarrow CO_2 + 4\,H_2 \qquad \Delta H = 165\,\mathrm{kJ\,mol^{-1}} \qquad \text{steam methane reforming} \qquad \text{(R6)}$$

where reaction (R6) is the combination of reactions (R3) and (R5).

The influence of reactions (R5) and (R6) largely depends on the formed methane from devolatilization and reaction (R4). These reactions require a high amount of heat, as indicated by the reaction enthalpies, thus greatly contributing to the overall endothermic re-

action inside the fuel reactor (FR). Moreover, it is clear that higher gasification temperatures lead to lower amounts of CH_4.

Reactions (R1) and (R2) necessitate a high amount of heat which cannot be balanced by the exothermic reactions (R3) and (R4) and has to be supplied for the gasification process. This heat can either be provided in situ through the oxidation of part of the feedstock (syngas species, volatiles and char) or externally e.g., through supply of a bed material heated in a second reactor enabling an autothermal process. The CLG process, schematically shown in Figure 1, employs both routes to supply the gasification energy. The solid oxygen carrier (OC) material supplies sensible heat to the fuel reactor (FR) while also providing lattice oxygen for the oxidation of part of the feedstock.

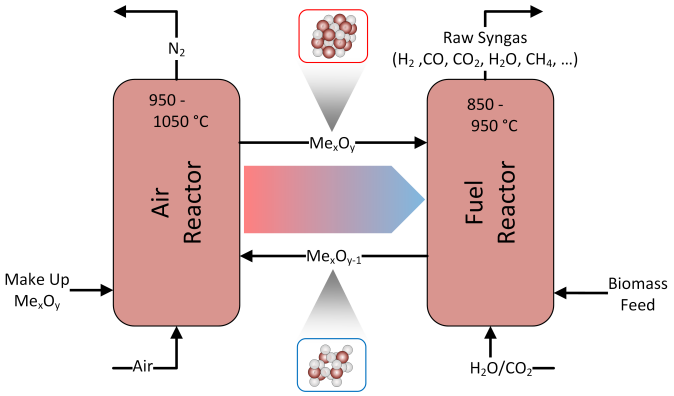

Figure 1. Schematic of the CLG process showing the cyclic reduction and oxidation of an OC material which is oxidized in the air reactor (AR) and reduced in the fuel reactor (FR).

However, additional reactions have to be considered when the bed material is a chemically active part of the feedstock conversion. In the FR where the OC material is reduced the reactions are:

$$\mathrm{Me}_x\,\mathrm{O}_y + \mathrm{CH_4} \longrightarrow \mathrm{Me}_x\mathrm{O}_{y-1} + 2\,\mathrm{H_2} + \mathrm{CO} \quad \text{(R7)}$$

$$4\,\mathrm{Me}_x\,\mathrm{O}_y + \mathrm{CH_4} \longrightarrow 4\,\mathrm{Me}_x\mathrm{O}_{y-1} + 2\,\mathrm{H_2O} + \mathrm{CO_2} \quad \text{(R8)}$$

$$\mathrm{Me}_x\,\mathrm{O}_y + \mathrm{CO} \longrightarrow \mathrm{Me}_x\mathrm{O}_{y-1} + \mathrm{CO_2} \quad \text{(R9)}$$

$$\mathrm{Me}_x\,\mathrm{O}_y + \mathrm{H_2} \longrightarrow \mathrm{Me}_x\mathrm{O}_{y-1} + \mathrm{H_2O} \quad \text{(R10)}$$

$$m\,\mathrm{Me}_x\,\mathrm{O}_y + \mathrm{C}_m\,\mathrm{H}_n \longrightarrow m\,\mathrm{Me}_x\,\mathrm{O}_{y-1} + \mathrm{mCO} + \mathrm{n}/2\,\mathrm{H_2O} \quad \text{(R11)}$$

$$2\,\mathrm{Me}_x\,\mathrm{O}_y + \mathrm{C} \longrightarrow 2\,\mathrm{Me}_x\,\mathrm{O}_{y-1} + \mathrm{CO_2} \quad \text{(R12)}$$

Solid–solid reactions between char and OC (R12) are generally slower than the heterogeneous gas solid reactions (R7) to (R10) and can therefore be neglected [18,19] except for very high reaction temperatures [20]. The reduced OC is then transported to the air reactor (AR), where it is oxidized with air in an exothermic reaction:

$$\mathrm{Me}_x\,\mathrm{O}_{y-1} + 0.5\,\mathrm{O_2} \longrightarrow \mathrm{Me}_x\mathrm{O}_y \quad \text{(R13)}$$

$$\mathrm{C} + \mathrm{O_2} \longrightarrow \mathrm{CO_2} \quad \text{(R14)}$$

Inside the AR the combustion of char, reaction (R14) is favored above the oxidation of OC through reaction (R13) [20–22], so residual char transported with the OC from the FR to the AR will be combusted before the oxidation of the OC, adding to the full feedstock conversion and supplying additional heat to the exothermic re-oxidation, (R13). However, (R14) is undesired during CLG, as it reduces the major advantage of a virtually CO_2-free flue gas stream from the AR when compared to DFBG.

CLG has been demonstrated to work as a continuous process in externally heated bench and lab-scale units up to 25 kW [17]. Large-scale experiments at Chalmers

University [23] suffer from the necessity of the AR to supply hot water for building heating and thus the requirement of significant fuel feeding to the AR. Therefore, exhibiting a severe mismatch of reactor dimension of factor 3 to 6 [24] while not depending on (R13) for heat release inside the AR. Hence, these experiments cannot be considered autothermal or even CLG, creating a need for experiments in a bigger scale to confirm the possibility and investigate the performance of autothermal CLG.

Process parameters considered important during the design are the cold gas efficiency:

$$\eta_{CG} = \frac{\dot{n}_{FR,out}(X_{CH_4} \cdot LHV_{CH_4} + X_{CO} \cdot LHV_{CO} + X_{H_2} \cdot LHV_{H_2})}{\dot{m}_{FS} \cdot LHV_{FS}} \quad (1)$$

with X_i being the mole fraction of species i, LHV the lower heating value, and $\dot{n}_{FR,out}$ and $\dot{m}_{FS}$ being the product gas output and the feedstock input, respectively. The oxygen carrier to fuel equivalence ratio is defined by [25]:

$$\phi = \frac{R_{OC} \cdot \dot{m}_{OC} \cdot X_{s,AR}}{\dot{m}_{O,stoich}} \quad (2)$$

$$X_{s,AR} = \frac{m_{OC,AR} - m_{OC,red}}{R_{OC} \cdot m_{OC,ox}} \quad (3)$$

In this definition the oxygen required for full feedstock conversion is $m_{O,stoich}$, R_{OC} is the oxygen transport capacity of the OC material, $X_{s,AR}$ is the oxidation degree of the OC, $m_{OC,red}$ and $m_{OC,ox}$ are the mass of the fully reduced and oxidized state respectively, while the mass of the OC leaving the AR is $m_{OC,AR}$. For gasification ϕ has to be smaller than unity to prevent the full oxidation of the feedstock [25,26]. However, syngas formation is observed even for values of $\phi > 1$ [27]. Values of $\phi < 1$ can be achieved by reducing the mass flow $\dot{m}_{OC}$ or the OC oxidation, i.e., $m_{OC,AR} - m_{OC,red}$. The first option has the disadvantage of also influencing the heat transport $\dot{Q}$ between the reactors:

$$\dot{Q} = \dot{m}_{OC} \cdot c_p \cdot \Delta T \quad (4)$$

with c_p, the heat capacity of the OC and ΔT, the temperature difference of OC particles entering and leaving the FR. The influence of the OC oxidation on c_p is small and can be compensated by adjustments of $\dot{m}_{OC}$ during practical application of option two.

Additionally the fraction of syngas in the dry product gas is defined as:

$$x_{SG} = \frac{X_{CO} + X_{H_2}}{X_{CH_4} + X_{CO} + X_{H_2} + X_{CO_2} + X_{H_2S} + X_{N_2}} \quad (5)$$

2.2. Bed Materials for Chemical Looping Gasification

The selection and testing of bed materials is a crucial task when designing a CLG process. Eight criteria for CLC are given by Adanez et al. [28] and repeated here with notes on how they apply to CLG:

1. Oxygen transport capacity: as gasification processes limit the supply of oxygen below the stoichiometric ratio required for full feedstock conversion, a high oxygen transport capacity is not so important as the process is limited by the sensible heat transported and not the oxygen [16,26]. For CLC the supply of excess oxygen is not critical, for CLG it must be limited without impairing the transport of sensible heat as otherwise, the temperature in the FR would drop, negatively influencing the gasification [26].
2. Thermodynamic suitability: the bed material must be able to oxidise the feedstock at least partially while not releasing molecular oxygen. Thus chemical looping with oxygen uncoupling (CLOU) materials cannot be used for CLG.
3. High reactivity over multiple reduction-oxidation cycles: activation over multiple cycles can increase or decrease reactivity.

4. Stability: the expected lifetime of the bed material should be as long as possible, as losses through attrition need to be compensated by a make-up stream. This make-up stream requires heating to process temperature, thus always leading to an efficiency drop. Measurement and calculation of OC lifetime is not straightforward and can vary by a factor of 3.2 for one experiment depending on the method used [29].
5. Carbon deposition: carbon transport towards the AR with subsequent combustion negatively impacts carbon utilization and capture efficiency. However, Adanez et al. [28] note that no carbon deposition has been found in relevant studies.
6. Fluidization properties: formation of agglomerates or low melting compounds with parts of the feedstock must be avoided. This becomes difficult if a herbaceous feedstock—high in ash and alkali metals—is used and might require mitigation measures like pre-treatment [30,31] or feedstock mixing [32].
7. Cost: the current production cost for synthetic materials make them non competitive when compared to naturally occurring minerals or waste materials.
8. Toxicity: deployment of environmental friendly and non-toxic OC material avoids special and costly requirements during handling and disposal of deactivated OC material.

Moreover, the design for pilot and demonstration plants need to consider an additional point:

9. Availability: the selected material must be available in the required quantity. Synthesized OC materials are not available on a commercial scale yet. So a natural ore or a waste material must be used.

Especially OC materials which are categorized as materials for syngas production [33–35] are problematic as they are either synthetic materials not available in the required quantities, expensive or toxic to humans and the environment. However, even materials with full oxidization capability for combustion can be used for the production of high calorific syngas when suitable control concepts are employed [11,16,26]. While lots of operating experience with bed materials for DFBG in the range above 1 MW exists [36], there is little experience with OC materials in the same power range [23,25]. However, even those experiments do not give a good indication of their process performance, as the AR—or rather combustor, as it is always fed with fuel—used is oversized by a factor of 3 to 6 [24], effectively creating a reservoir of OC and sensible heat more dependent on the required energy for heating supply than the CLG process. Moreover, higher attrition rates of e.g., ilmenite are reported for CLG when compared with CLC [11] but if the effects are the same in a bigger CLG plant is still an open question. Due to the small size of lab-scale reactors, the OC material undergoes more oxidation/reduction cycles per hour, thus giving higher stress from chemical conversion when compared to the mechanical stress from the transport through the reactors and coupling elements.

Depending on the requirements of the targeted application for the syngas, a last point is to be considered when selecting the OC bed material:

10. Catalytic properties: selecting a material (or additive) which catalytically reduces the formation of unwanted components like tars [37,38] and CH_4 [39] or binds elements to the solid fraction (e.g., sulphur in form of gypsum) as a primary method. Secondary gas cleaning methods might therefore not be necessary or can be designed much smaller.

Tar production is of major concern for subsequent syngas treatment especially for biomass gasification where tar production is high [40]. Bed height, bed material, temperatures, velocities, feedstock, and feedstock feeding location [37] have an influence on the production of tars. Existing kinetic models for the prediction of tar production are not applicable as they are developed for a very specific process and reactor size [15], need fitting against the actual reactor performance [41], or are not reliable in the prediction of tars formed [42–44]. Furthermore, no model was developed for CLG yet.

3. Process Design

In the following, the CLG technology fundamentals described in Section 2 are combined with boundary conditions from the existing pilot plant as well as feedstock properties and hydrodynamic characteristics yielding a process design suitable for the demonstration of autothermal CLG in the existing 1 MW_{th} pilot plant.

3.1. Existing Pilot Plant

The heart of the CLG pilot plant consists of two refractory lined circulating fluidized bed (CFB) reactors which are coupled using two loop seals and one J-valve and have properties indicated in Table 1. The CFB400-reactor of the pilot plant has been used as gasifier for High Temperature Winkler (HTW^{TM}) gasification [45,46] and as FR in the CLG-related processes for chemical looping combustion, while the CFB600-reactor has been used as AR [47–51]. Thus major components can be reused for CLG by combining elements from the CLC and the HTW^{TM} process configurations. Nonetheless, major adaptations are made, as the HTW^{TM} configuration is build for lower fluidization velocities and with 0.5 MW_{th} [45] also for lower thermal input.

Table 1. Reactor properties of the 1 MW CLG pilot plant.

Reactor	AR—CFB600	FR—CFB400	Unit
Height	8.66	11.35	m
Inner diameter	0.59	0.28 to 0.4	m
Outer diameter	1.3	1.0	m
Temperature	1050	950	°C
Fuel feeding	in bed (propane lance), return leg of LS 4.5 (solids)	in bed via screw (solids)	

Furthermore, as electrical preheating temperatures of fluidization media are limited to 400 °C, process stream heating has to be done inside the reactors, negatively impacting cold gas efficiency which would be optimized in an industrial plant using heat integration. The cooling system sets a limit of 1 MW_{th} which can be safely handled for CLC. However, as a major part of the energy of the feedstock remains as heating value in the product gas, feedstock input above the 1 MW_{th} is possible for CLG.

Therefore the following case has been set as design specifications for the investigations of CLG for which mass and energy balances were calculated, required changes to the pilot plant identified and modifications designed.

- As the cooling system is designed to handle a thermal load of 1 MW safely, the design power of the pilot plant is is set to 1 MW_{th}.
- Ilmenite as OC: For the selected thermal power, a total inventory of about 1000 kg was used during CLC experiments in the pilot plant [50], and the same can be expected for CLG. Thus, of the points listed in Section 2.2, the availability is a major concern for experiments in that scale, and a natural ore or a widely available waste material had to be selected. Recent studies show promising results for ilmenite in continuous units [11], and operating experience with ilmenite in the pilot plant exists [49,50]. Moreover, ilmenite has been shown to catalytically reduce tars [25,52].
- Temperatures for the AR of 1050 °C and 950 °C are considered the maximum viable temperatures. Higher FR temperatures will yield a higher H_2/CO ratio at the expense of lower cold gas efficiency. So slightly lower FR temperatures might be desired in industrial application. Moreover, as OC ash interaction may lead to problems at high temperatures [31] and the temperature difference between the reactors is an important parameter for process control [26], the FR temperature is not fixed and considered an important variable in the planned experiments.
- Industrial wood pellets as feedstock as described in Section 3.2.

3.2. Feedstocks

As model feedstock for the calculation of the heat and mass balances and the design of modifications, industrial wood pellets have been selected, as they are widely available and allow for easy comparison with existing gasification technologies in pilot and demonstration scale where wood based materials are gasified [36]. Additionally, wheat straw, as a seasonal varying biomass source, and pine forest residue, as a more constant source, are selected as feedstocks from the EU-approved list [1] for experimental investigations.

Initial investigations of wheat straw by Di Giuliano et al. [31] indicate that it is a difficult feedstock for CLG, due to its low ash softening point and the possibility to cause agglomerates and bed defluidization, so that it requires at least some pre-treatment. However, as fluidization velocities in the CFB reactors are two magnitudes higher than the investigated fluidization velocities, the required pre-treatment cannot be directly inferred, but a higher fluidization velocity seems to lower the required pre-treatment effort [31]. Moreover, reaction kinetics for pelletized wheat straw in various bed materials are similar to pellets of pine forest residue [53] opening up possibilities to switch between these feedstocks during gasifier operation. Nevertheless, additional investigations on the pre-treatment of wheat straw are needed to be able to give accurate information on the fuel properties—which are indicated in Table 2 for the planed feedstocks—as they vary with pre-treatment. It is assumed that pre-treatment of wheat straw will make handling and gasification easier, as it reduces agglomeration tendencies (additivation, torrefaction) and water content (drying, torrefaction). Thus, raw wheat straw is the most difficult to gasify and can be used as a lower end in feedstock quality.

Table 2. Proximate and ultimate analysis of feedstocks.

	Component	Wood Pellets	Pine Forest Residue	Wheat Straw
Proximate Analysis in wt. − %	Moisture	6.5	7	7
	Ash (d.b.)	0.7	1.86	7.5
	Volatiles (d.b.)	85.1	78.86	81.5
	Fixed carbon (d.b.)	14.2	12.28	11
Ultimate Analysis in wt. − %	C (d.a.f.)	50.8	52.7	48.2
	H (d.a.f.)	6	6.4	6.5
	N (d.a.f.)	0.07	0.39	0.43
	O (d.a.f.)	43.2	40.5	44.9
	S (d.a.f.)	0.008	0.05	0.11
	Cl (d.a.f.)	0.006	0.007	0.05
Net calorific value in MJ kg^{-1}		17.96	18.41	17.12

3.3. Heat and Mass Balances

Heat and mass balances for the pilot plant were calculated considering reaction kinetics of ilmenite and reactor hydrodynamics using a validated Aspen Plus^{TM} model for CLC [51] extended to cover biomass gasification via a Langmuir–Hinschelwood mechanism [26]. However, instead of an equilibrium model used by Dieringer et al. [26], the more realistic original reaction kinetics for ilmenite were used for the OC gas reaction. As a starting point, the CLC case was selected in terms of reactor dimensions, temperatures, solid inventories, pressure, and loop seal (LS) fluidization. The feedstock flow $\dot{m}_{FS}$ (industrial wood pellets) was selected as 1 MW_{th}, and the heat losses were assumed to be 110 kW which falls in the reported range of 60 kW to 200 kW [48,50]. Furthermore, heat losses are considered to be dependent on reactor temperature and independent of feedstock input. LS fluidization with CO_2 is set to 84.2 kg h^{-1} based on previous operating experience [49,50]. To obtain autothermal operation at these conditions, the oxygen availability inside the AR was varied through the inlet feed rate of air into the AR, while the heat transport between both reactors was controlled through the global metal oxide solid circulation rate ($\dot{m}_{OC,AR,out}$, $\dot{m}_{OC,FR,out}$), until both reactors were in heat balance. The hydrodynamic constraints related

to the required solid entrainment (calculated as suggested by Kunii and Levenspiel [54], described in detail elsewhere [51,55]) from each reactor were achieved by varying the steam inlet flow $\dot{m}_{H_2O}$ and flue gas recirculation inlet flow $\dot{m}_{AR,reci}$ for the FR and AR, respectively, while setting internal solid circulation to zero. All boundary conditions are listed in Table 3, and the corresponding results are in Table 4. The listed streams are visualized in the reactor configuration in Figure 2.

Table 3. Boundary conditions for the simulation of autothermal CLG operations of the 1 MW pilot plant.

Property	Value	Unit	Property	Value	Unit
$d_{p,50}$	154	µm	$T_{Gas,in}$	400	°C
Δp_{FR}	61	mbar	Δp_{AR}	90	mbar
p_{FR}	1	bar	p_{AR}	1	bar
d_{FR}	0.28 to 0.4	m	d_{AR}	0.59	m
h_{FR}	11.35	m	h_{AR}	8.66	m

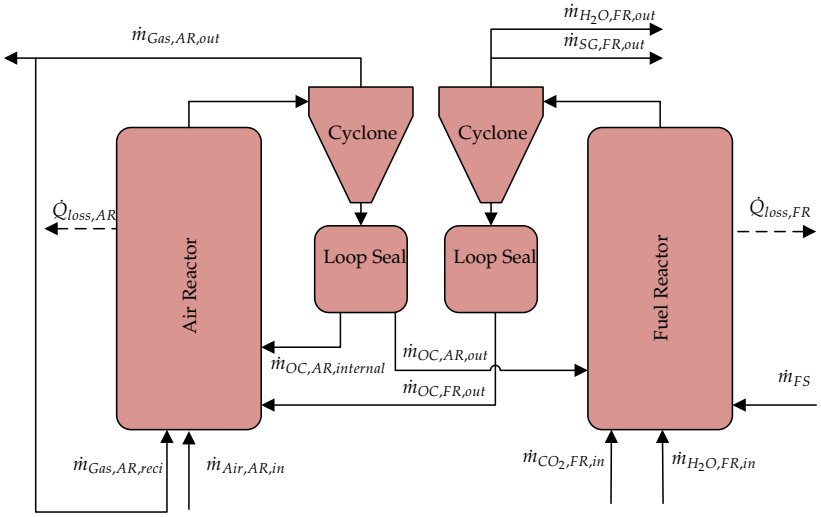

Figure 2. Streams for the calculation of mass and energy balances of the CLG process.

In small scale units where the energy is supplied via furnace heating, the oxygen supply can be controlled via the circulation. However, in the 1 MW pilot plant the heat is supplied only via the circulation of the bed material. From the results of the Reference case, it can be seen that the transport of oxygen must be limited in order to obtain a good gasification process, while the solid circulation must remain high as indicated by the substantial amount of recirculated gas fed to the reactor. Thus, a new control method for the oxygen transport must be realised, decoupling the transport of oxygen from the transport of sensible heat as described by Dieringer et al. [26]. Moreover, the superficial gas velocity u_0 in the AR is below the range of a CFB, as shown in Figure 3, while the calculated solid flux G_S is also below the range commonly observed in commercial CFB units [56]. Indeed, past operation of the AR showed good performance with superficial gas velocities of approximately 3.5 m s^{-1} to 5 m s^{-1}. In the pilot plant, the installation of a (partial) flue gas recirculation for the AR is used to increase u_0 while also supplying the inert fluidization medium required for the process control. Increasing the solids discharge from the AR—while keeping the global solids circulation constant—creates the need for an internal solid circulation in the AR—where material not transported through the J-valve is returned via the LS—which is not common in smaller units. In fact, most lab- and bench-scale units have internal solids recirculation for the FR to enhance carbon conversion [57] or no solids recirculation at all [11,17]. Nonetheless, this solution comes with a penalty, as additional

fluidization medium is needed and has to be heated to process temperature. However, reducing the diameter of an existing, refractory lined reactor is costly and time consuming, so the efficiency penalty has to be accepted; yet it also opens the possibility to use the start-up burner for fast temperature adjustments in-between experimental set points without severe impact on reactor hydrodynamics. In a commercial unit, the diameter would be designed according to process specification and corresponding hydrodynamics, requiring the flue gas recirculation only for process control. Nonetheless, this initial estimation shows that CLG is possible in the existing 1 MW pilot plant.

Table 4. Simulation results for autothermal CLG operations of the 1 MW pilot plant. Stream names correspod to Figure 2. Boundary conditions deviating from the reference case are underlined. The first block contains the thermodynamic and hydrodynamic constraints and results, the second block contains the process streams (in some cases with composition). The third block gives information on solid composition for the FR, while the last block shows general process performance parameters.

Stream	Reference	HT1	HT2	HF	HP1	HP2	Unit
T_{AR}	1025	1050	1050	1025	1025	1025	°C
T_{FR}	900	900	950	900	900	900	°C
$\dot{m}_{FS}$	200.4	200.4	200.4	200.4	240.48	280.56	$kg\,h^{-1}$
$u_{0,AR}$	3.42	3.12	3.97	5.03	5.01	5.01	$m\,s^{-1}$
$u_{0,FR}$	6.25	5.46	7.64	5.67	6.23	6.75	$m\,s^{-1}$
$\dot{Q}_{loss,AR}$	48.5	49.4	49.9	49.3	50.5	49.6	kW
$\dot{Q}_{loss,FR}$	59.8	61.8	59.8	61.3	59.4	61.2	kW
$\dot{m}_{OC,AR,out}$	7180	5690	9979	6244	7257	8285	$kg\,h^{-1}$
$\dot{m}_{OC,FR,out}$	7130	5649	9906	6175	7199	8236	$kg\,h^{-1}$
$\dot{m}_{OC,AR,internal}$	0	0	0	12,120	10,994	9971	$kg\,h^{-1}$
$\dot{m}_{Air,AR,in}$	640	600	745	730	760	802	$kg\,h^{-1}$
$\dot{m}_{Gas,AR,out}$	950.6	854.6	1062.7	1404.3	1413.6	1425.5	$kg\,h^{-1}$
— $X_{CO_2,AR}$	0.111	0.117	0.096	0.098	0.111	0.122	
— $X_{O_2,AR}$	0.004	0.003	0.005	0.005	0.004	0.003	
$\dot{m}_{AR,reci}$	360.7	296.3	391.2	744.3	708.2	672.8	$kg\,h^{-1}$
$\dot{m}_{H_2O,FR,in}$	301.53	237.04	383.83	247.14	263.4	276.94	$kg\,h^{-1}$
$\dot{m}_{CO_2,FR,in}$	84.2	84.2	84.2	84.2	84.2	84.2	$kg\,h^{-1}$
$\dot{m}_{H_2O,FR,out}$	362.9	294.5	451.5	318.8	337.9	354.0	$kg\,h^{-1}$
$\dot{m}_{Syngas,FR,out}$	271.1	267.0	287.8	280.5	307.3	334.3	$kg\,h^{-1}$
— $X_{CO_2,FR}$	0.466	0.439	0.543	0.531	0.440	0.377	
— $X_{CO,FR}$	0.304	0.317	0.240	0.277	0.324	0.354	
— $X_{CH_4,FR}$	0.092	0.099	0.057	0.072	0.095	0.113	
— $X_{H_2,FR}$	0.139	0.145	0.160	0.119	0.141	0.156	
— $X_{H_2S,FR}$	5.26×10^{-5}	5.22×10^{-5}	5.13×10^{-5}	5.38×10^{-5}	5.48×10^{-5}	5.56×10^{-5}	
$\dot{n}_{Solid,FR,out}$	14.84	11.54	20.60	13.38	15.09	16.90	$mol\,h^{-1}$
— $X_{C,out}$	0.04	0.05	0.03	0.05	0.05	0.05	
— $X_{Fe_2O_3,out}$	0.09	0.06	0.10	0.13	0.09	0.07	
— $X_{FeTiO_3,out}$	0.68	0.76	0.66	0.57	0.68	0.74	
— $X_{TiO_2,out}$	0.18	0.12	0.21	0.25	0.18	0.14	
$\dot{n}_{Solid,FR,in}$	15.55	12.11	21.70	14.43	15.93	17.54	$mol\,h^{-1}$
— $X_{Fe_2O_3,in}$	0.17	0.16	0.18	0.23	0.19	0.15	
— $X_{FeTiO_3,in}$	0.48	0.53	0.47	0.30	0.44	0.55	
— $X_{TiO_2,in}$	0.35	0.31	0.35	0.46	0.37	0.30	
— $X_{Fe_3O_4,in}$	0.00	0.00	0.00	0.00	0.00	0.00	
η_{CG}	0.474	0.505	0.384	0.396	0.475	0.531	
x_{SG}	0.443	0.462	0.400	0.396	0.465	0.511	
ϕ	0.585	0.412	0.836	0.729	0.537	0.412	

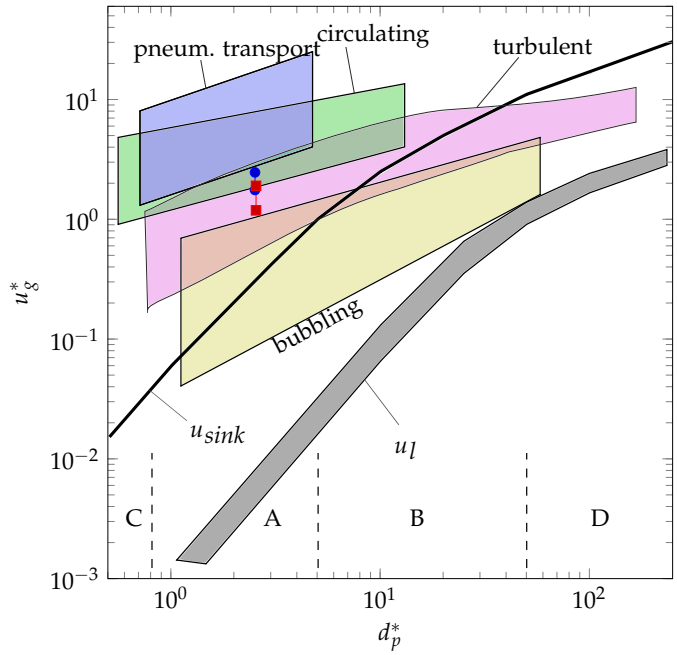

Figure 3. Grace diagram indicating the operation regimes of the FR —●— and AR —■—.

In order to asses the exact limits and to find the corresponding bottle necks where adaptations are needed, some variations on the boundary conditions have been made to be able to decide on equipment alteration and to generate data for the subsequent detailed design. While the simulation of the reference case yields a cold gas efficiency η_{CG} of 0.474, values above 0.8 are reported for externally heated continuous units with a slight increase of η_{CG} with increasing FR temperature [11]. Thus, two additional points with increased AR temperature (HT1) and increase of both reactor temperatures (HT2) were considered to test the feasibility of higher temperatures in the 1 MW pilot plant. The low superficial gas velocity for the AR was raised to $u_{0,AR} = 5\,\mathrm{m\,s^{-1}}$ by increasing the flow of fluidization medium (HF) to see the effect and possibility at higher inlet and outlet streams. This case was also used as a basis for an increase in fuel input to 1.2 MW (HP1) and 1.4 MW (HP2) to reduce the relative impact of heat loss and test the limits of the syngas handling equipment. During experimental operation, the AR superficial velocity would be targeted at slightly above the minimum discharge needed for either stable operation or required by the process—whichever is higher—in order to keep the negative impact of heat demand by fluidization medium low. However, for design purposes, the upper end of the range has to be considered.

From the variation of the reactor temperatures, it is clear that increasing the AR temperature is beneficial to process efficiency, while also increasing the FR, negatively impacts the process performance. For HT1 the increased heating demand in the AR is counteracted by the reduced solids circulation ($\dot{m}_{OC,FR,out}$ and $\dot{m}_{OC,AR,out}$) needed to supply the heat for the gasification process and thus reducing the overall amount of required fluidization medium ($\dot{m}_{Air,AR,in}$, $\dot{m}_{AR,reci}$ and $\dot{m}_{H_2O,FR,in}$) to achieve this lowered solids circulation. The higher FR temperature in HT2 leads to a syngas composition higher in H_2 and lower in CH_4 which is desired, but also requiring significantly higher solids circulation. The corresponding heating requirement of fluidization medium negatively impacts process efficiency. The influence on the syngas quality is caused not only by the raise in gasification temperature, but also in the added steam content from fluidization, influencing reactions (R3), (R5) and (R6). The biggest effect has the increase of the oxygen carrier to fuel equivalence ratio ϕ which raises the relative contribution of oxidation reactions (R8) to (R12).

The increase in AR solids entrainment through higher fluidization velocity (HF) essentially decouples the reactor hydrodynamics of both reactors. Here the model constraint of no internal solids circulation $\dot{m}_{OC,AR,internal}$ is omitted. Instead, the superficial gas velocity $u_{0,AR}$ is targeted at $5\,\mathrm{m\,s^{-1}}$. The higher heat demand for the fluidization medium here has to be supplied by exothermic reaction (R13) leading to a higher degree of OC oxidation as indicated by the increase in ϕ. Consequently, the solids circulation between the reactors is lowered as more oxygen is supplied per OC mass. This leads to lower fluidization requirements and heat demand in the FR reducing the negative impact of the higher fluidization velocity in the AR. Increasing the feedstock input $\dot{m}_{FS}$ while keeping the AR hydrodynamic constant (HP1 and HP2) positively influences process efficiency, as the relative increase in FR fluidization medium required for solids discharge is only about half of the relative increase in feedstock. Thus, only a relatively small part of the additional feedstock is used to cover the energy requirement of the additional fluidization medium, while most of the additional feedstock energy is available for the conversion into syngas making a positive impact on syngas content and cold gas efficiency. This positive influence is mostly caused by more beneficial reactor hydrodynamics and lower relative heat losses of the reactors.

The simulated cases shed light on the process range the reactors can be operated without major modifications, and also highlights the huge impact of heat loss and heat demand in this scale of experiments. It shows that higher FR temperatures in case HT2 require higher fluidization and bigger size of downstream syngas equipment than significant increases in feedstock input (HP2) making this the more critical case to be considered during design. Although the syngas quality increases with higher FR temperature, the cold gas efficiency is drastically reduced, which is in contrast to the observations from Condori et al. [11]. This discrepancy can be explained by the external heating in the lab-scale plant, which can thus compensate the higher heating demands of the process streams. The positive effect of high temperatures for process streams entering the reactors has been shown [26], highlighting the need of good heat recovery and integration for the process. Moreover, the simulated process conditions make clear that individual variations of process parameters like steam to biomass ratio, or oxygen carrier to fuel equivalence ratio ϕ as done by Condori et al. [11] are not possible if no external heating is available. Instead, the CFB mode and the defined solid discharge required for the heat transport also lower the steam to biomass ratio and oxygen carrier to fuel equivalence ratio, as can be seen by the feedstock increase (HP1, HP2). Furthermore, the predicted influence of these combined changes is not necessarily the same as the one observed in small-scale experiments. This can bee seen by the increase of X_{CH_4} with increasing feedstock input, where the accompanying changes in steam to biomass ratio and oxygen carrier to fuel equivalence ratio lead to lower CH_4 in the experiments described by Condori et al. [11].

Confirmation or refutation of either the trends experimentally observed in small scale units or simulated for the existing pilot plant necessitates experiments in the $1\,\mathrm{MW}_{th}$ range where autothermal operation—instead of external electrical heating—becomes necessary. Here, the requirements imposed by autothermal operation of the process limit the range of applicable parameter variation as they are interdependent. Therefore, the existing pilot plant is modified to provide the experimental data needed.

4. Plant Design

The flow sheet in Figure 4 shows a simplified configuration of the designed pilot plant, including major components and important subsystems. Some of the components already available from CLC and HTW^{TM} can be reused, while other subsystems are new or altered. For all subsystems affected by the new CLG process and the alterations a HAZOP analysis has been performed to ensure safe operation.

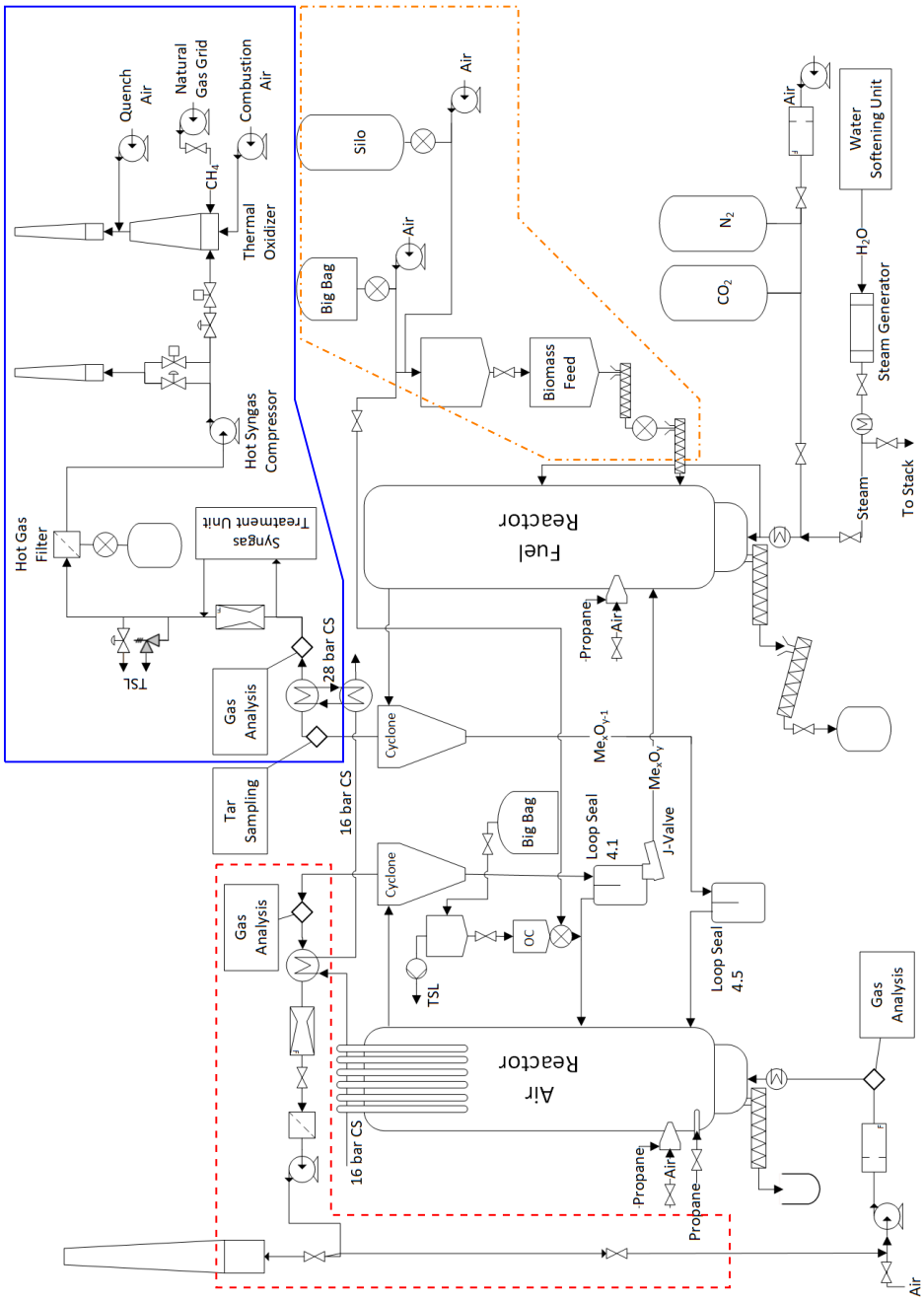

Figure 4. Schematic of the CLG pilot plant showing the main subsystems. CS: cooling system, OC: oxygen carrier, TSL: to safe location. syngas handling: —, flue gas handling: - -, biomass feeding: -..-.

4.1. Reactor System

The reactor system (Figure 5) comprises of the two CFB reactors, two LS and a J-Valve as coupling elements. The total inventory of bed material during CLG operation with ilmenite is about 1000 kg with approximately 250 kg in the AR, 80 kg in the FR, and the rest in the coupling elements. Transport of sensible heat to the FR is not facilitated by internal solid circulation and additional fluidization medium would be required, cooling down the reactor and negatively impacting on process efficiency. Thus, no internal circulation is implemented for the FR. Moreover, process simulations show only reduced OC leaving

the reactor [26] giving no benefit of returning it from the cyclone to the reactor. However, the Gibbs reactor model employed in this study leads to full conversion, while in reality a mixture of different phases will always be present. Nonetheless, the prevalence of highly reduced phases in both FR and AR has been confirmed in continuous experiments [11].

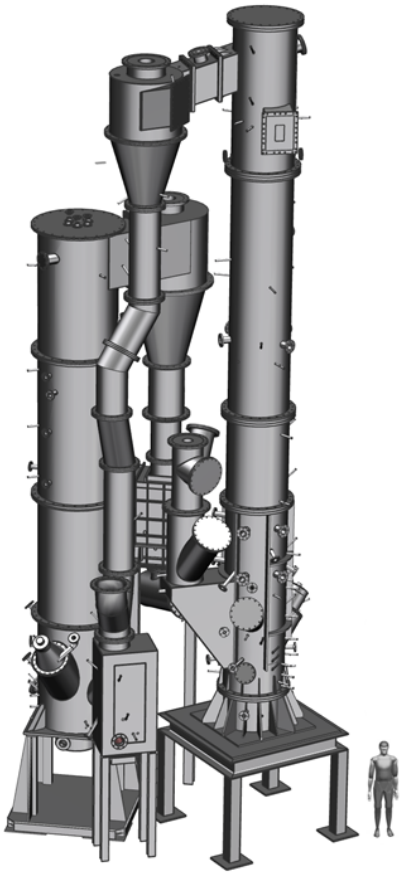

Figure 5. CLG reactor configuration including the main coupling elements.

Although many lab-scale reactor designs feature a FR operating in bubbling mode (e.g., [11,14,17,58]), the used CFB mode of the FR has the advantage of improved gas-solid mixing and thus featuring higher rates of carbon conversion [57], while the requirement ranges for the size and shape of the feedstock is wider [10] opening up possibilities for more feedstocks. Furthermore, the higher solids concentration in the freeboard may enhance tar cracking and methane reforming by supply of additional oxygen and catalytic sites in this region. However, increasing superficial velocities too much will lead to pneumatic transport in the FR (Figure 3) and unstable reactor hydrodynamics.

The disadvantage of having no internal solid recirculation for the FR is the transport of all discharged feedstock particles towards the AR. Furthermore, for the pilot plant, the minimization of heat losses is considered more important than the minimization of carbon slip towards the AR as relative heat losses for the pilot plant are in the range of 0.1 to 0.2. So minimization of coupling elements is used instead of carbon recovery via a carbon stripper. However, carbon slip is assumed to be a minor problem as the biomasses considered for the experiments contain low amounts of fixed carbon [9]. The feeding location is lowered into the dense region of the bed when compared to previous CLC experiments [49] where high carbon slip for hard coal was experienced, which should reduce the carbon slip as char gasification in the densest region is enhanced. Moreover,

carbon slip is more pronounced in small reactors and the sometimes utilized carbon strippers might not be required in bigger units [59]. Nonetheless, to maximize residence time of char particles inside the dense region, a variable amount of fluidization medium can be rerouted directly before the wind box of the FR to a second stage fluidization located at approx. one fifth of the reactor height. This increases bed density in the lower region and residence time of OC particles while keeping a high solids discharge in the CFB operation is possible by increasing the reactor inventory. The exact influence must be determined via experimental operation.

Investigations in the FR are the most crucial, as the formation of tars make the process and reactor design more critical to subsequent equipment than the re-oxidation in the AR. Therefore, it is advantageous for experimental operation to handle imbalances of solids discharge between the reactors inside the AR instead of the FR where it would negatively impact temperature and possibly lead to poorer syngas quality. The feedstock input directly in the dense zone of the bed should also reduce the amount of tars formed during initial devolatilization [37].

4.2. Flue Gas Handling

The flue gas composition from the AR is measured by an on-line gas analysis before the flue gas is cooled down in a heat exchanger to approx. 230 °C (Figure 4, red box). The flow rate is measured using a venturi before the fines passing the cyclone are separated by a filter giving a dust-free flue gas. The following induced draft fan is used to control the pressure in the reactor and vents the flue gas via a stack. Part of the flue gas can be recirculated via a controlled butterfly valve to adjust the inlet of the AR fluidization. The variation of flue gas recirculation allows to adjust the superficial gas velocity $u_{0,AR}$ and thereby the entrainment of particles from the AR while keeping the OC to fuel equivalence ratio ϕ constant. This is a small but significant adjustment in converting from a CLC plant to a CLG plant as it allows to control the overall process as described in [26].

4.3. Syngas Handling

Major modifications are needed for the FR off-gases (Figure 4, blue box) when converting a CLC unit into a CLG unit, as all parts need to be designed with the consideration of explosive atmospheres . Moreover, commonly used heat exchangers are either prone to clogging with tars on cold surfaces or the syngas cooling rate is to low, allowing for recombination of syngas species. The process simulation from Section 3.3 show high syngas streams that need to be safely handled and greatly exceed the capacity of the syngas removal deployed for HTW^{TM} gasification [45,46]. The only component reusable is the cooler, a patented tube-in-tube gas liquid heat exchanger from SCHMIDT'SCHE SCHACK consisting of four tubes cooling the gas to approx. 380 °C very fast and without recirculation zones [60] avoiding the recombination of syngas to longer hydro-carbons. The cooling water is pressurised to 28 bar to be able to raise temperature levels to 200 °C in order to avoid excessive condensation of tars inside the tubes of the raw gas cooler.

After the cooler the syngas is available for cleaning. Here part of the syngas can be routed to a syngas treatment unit for cleaning and separation of CO_2, so that it is subsequently available for synthesis. Moreover, test rigs for the fine cleaning of the syngas and the synthesis of higher hydro-carbons are added, creating the unique possibility to investigate the whole solid to liquid value chain.

The return line from the syngas treatment unit consisting of all streams not used for synthesis is merged back, and the gas is routed to a hot gas filter for the removal of solids, resulting in a dust free syngas stream to the hot syngas compressor used to control the pressure in the FR. From here the syngas is transported to a thermal oxidizer for safe venting. The option of a second stack where the FR off gas can be vented is included for start up, shut down and to allow for a restart of the thermal oxidizer in case of failures without the full shut down of the pilot plant. The additional valves before the hot gas filter

are installed for safety pressure relief in case the switching between the thermal oxidizer and the second stack fails.

The described syngas line differs substantially from the ones deployed in either industrial scale or lab-scale. While in industrial plants all produced syngas would be cleaned, only the amount of syngas needed for research in gas cleaning is processed in the pilot plant to reduce the cost of the deployed gas cleaning equipment. In lab-scale the small quantities of formed syngas allow for untreated release to a safe location in the environment, which is not possible for streams in the size of the pilot plant, entailing the need for the thermal oxidizer.

All properties of the syngas stream leaving the FR are of major importance for further process development. Thus, sample and measurement sites consisting of an isokinetic dust and tar sampling port, a psychrometric water content measurement, and an on-line gas analysis are integrated into the syngas line. The isokinetic sampling of dust and tars is done before the raw syngas is cooled while ports for the measurement of the water content and gas composition are located before and after the cooler and can be connected as required.

4.4. Solid Feeding

4.4.1. Feedstock

The pilot plant is equipped with various entry points for solid feedstocks (Figure 4, orange box) like a big bag station, a container station (not shown on Figure 4) and a silo capable of introducing pulverized and pelletized feedstocks which are transported pneumatically to a fuel container purged with CO_2. This container discontinuously feeds fuel to a second, weighted container from which the fuel is fed continuously, controlled via screws and a hopper directly in to the bed of the FR. Both containers are pressurised to the bed pressure of the FR at the location of the feed screw to avoid the back flow of syngas into the fuel feeding system. The screw feeder is cooled with thermal oil to ensure that gasification temperatures are only reached in the bed and no gasification occurs inside the screw.

4.4.2. Oxygen Carrier

Initial filling of loop seals with OC is done via a weighted dosing container, a hopper, a screw conveyor, and a series of tubs connected to the stand-pipes. OC materiel is fed into the return leg of LS 4.1 for reactor filling and make-up dosing to compensate losses caused by agglomeration and attrition.

4.5. Cooling and Preheating

The cooling system is designed to handle the full 1 MW of heat released during CLC and therefore has enough capacity for further increase of feedstock as discussed previously. However, for bigger units, where process heat would be used to generate steam and preheat the input streams, changes might be required when compared to CLC to optimize the heat integration. Nonetheless, this is no concern for the pilot plant, where steam generation and preheating is done via independently powered systems. Yet, it limits also the operation range of the pilot plant—seen on simulated case HT2—where higher outlet stream temperatures always lead to a severe process penalty. For the pilot plant, this penalty cannot be alleviated by heat recovery for the preheating of inlet streams. Here the option of higher preheating temperatures would require a substantial increase of heat exchanger surface, for which no space is available at the existing site. Furthermore, the existing electrical infrastructure is already at its limit, so increasing the electrical preheating power is not feasible.

Increasing the fuel input necessitates deeper investigation of the limitation of safe operation in terms of the cooling system, especially when considering that most of the 1000 kg OC material is in a highly reduced state during operation. Here the safety relevant quantity is not the total amount of feedstock input or the reduced OC, but the possible amount of oxygen input to the AR. The oxygen input will first fully oxidise the OC inside the AR, possibly with much higher power than the nominal feedstock input which will set a limit only after full oxidation inside the AR has been reached. Here mitigation measures are an over design of the cooling system and a limitation of oxygen input to safely handable amounts.

4.6. On Line Measurements

4.6.1. Gas Analysis

The main product of the gasification process, the synthesis gas from the FR, is extracted and analyzed continuously as sown in Figure 6 via a heated probe which includes a filter (1), that can be back flushed with CO_2 to prevent blockage.

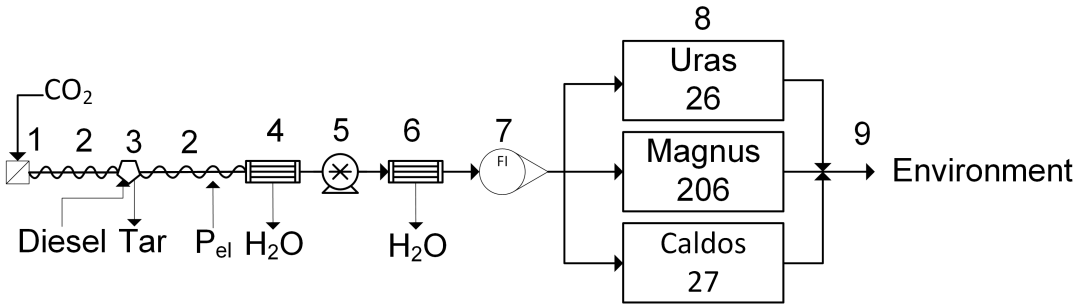

Figure 6. Schematic of the gas analysis equipment: (1) heated probe with filter, (2) heated tube, (3) tar removal (only for FR), (4) condenser for water removal, (5) pump, (6) condeser for water removal, (7) rotameter, (8) measurement equipment, (9) safe location in the environment.

The gas then passes in a heated tube (2)—to prevent the condensation of remaining tars—to a tar removal unit with diesel as solvent (3) and a first condenser unit (4) where the majority of the water and higher hydro-carbons are removed. The measurement gas pump (5) transports the gas through a second condenser unit to remove the rest of the water (6) which is followed by a rotameter (7) measuring the sampling gas flow. The sampling gas is distributed to the commercially available gas analysing equipment from ABB (8) given in Table 5 before being released to a safe location in the environment (9).

O_2 is measured via its paramagnetic quality in an Magnos 206 analyzer while H_2 is determined via thermal conductivity in a Caldos 27 unit. The components CO_2, CO, CH_4, SO_2 and NO are measured by an spectroscopic non-dispersive infra red (NDIR) sensor in an Uras 26 analyzer.

For the AR both gas analysis lines differ in the heated probe which does not include a tar removal unit. The measurement ranges of the equipment is different, as can be seen in Table 5 and H_2 and CH_4 is not measured. At the inlet of the AR, the composition is of interest to control the oxygen feed to the process and the amount of recirculated flue gas.

The water content is measured in both reactor outlets via a psychrometric Hygrophil H4320 unit from Bartec with the sampling gas extraction as shown in Figure 7. The gas is extracted via a heated probe (1) and transported in an electrically heated tube (2) to the analyzer (3) which includes a CO_2-driven ejector pump to facilitate the gas transport. The gas is released to the environment afterwards (4).

Table 5. Listing of gas analysis equipment for all reactors.

Reactor	Equipment	Measurement Principle	Component	Range	Error	Unit
FR	Magnos 206	paramagnetic	O_2	0 to 25	0.9	vol. − %
	Caldos 27	thermal conductivity	H_2	0 to 40	1.8	vol. − %
	Uras 26	NDIR	CO_2	0 to 100	3.0	vol. − %
	Uras 26	NDIR	CO	0 to 40	1.2	vol. − %
	Uras 26	NDIR	CH_4	0 to 20	0.6	vol. − %
	Uras 26	NDIR	SO_2	0 to 5	0.15	vol. − %
	Uras 26	NDIR	NO	0 to 1000	30	ppm
	Hygrophil H4320	psychrometric	H_2O	2 to 100	0.3	vol. − %
AR outlet	Magnos 206	paramagnetic	O_2	0 to 25	0.9	vol. − %
	Uras 26	NDIR	CO_2	0 to 30	0.9	vol. − %
	Uras 26	NDIR	CO	0 to 5	0.15	vol. − %
	Uras 26	NDIR	SO_2	0 to 4000	120	ppm
	Uras 26	NDIR	NO	0 to 1000	30	ppm
	Hygrophil H4320	psychrometric	H_2O	2 to 100	0.3	vol. − %
AR inlet	Magnos 206	paramagnetic	O_2	0 to 25	0.9	vol. − %
	Uras 26	NDIR	CO_2	0 to 100	3.0	vol. − %
	Uras 26	NDIR	CO	0 to 5	0.15	vol. − %
	Uras 26	NDIR	SO_2	0 to 5	0.15	vol. − %
	Uras 26	NDIR	NO	0 to 1000	30	ppm

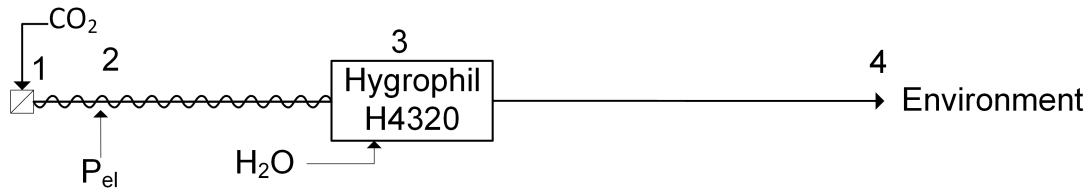

Figure 7. Schematic of the water content analysis equipment: (1) heated probe with filter, (2) heated tube, (3) psychrometric analyzer, (4) safe location in the environment.

Both water content measurements and the three gas analysis are integrated in the process control system of the pilot plant with all measurements available in real time and as trend lines.

4.6.2. Temperature and Pressure

The pilot is equipped with temperature and pressure in all inlet and outlet streams of the reactors including the LS fluidization. Multiple additional measurement sites for pressure and temperature are installed along the reactor height to acquire more insight in the reactor state during operation. The pressure sensors for the AR are differential pressure transducers with the other side open to atmosphere while at the FR all pressure measurements are purged with CO_2 and are mostly differential pressure transducers measuring between different reactor heights. This allows us to control the bed hight and density and to control the influence of the second stage fluidization.

4.6.3. Flow Measurements

The flow rates of all streams entering the reactors and coupling elements are measured either with an orifice plate, a rotameter or are controlled via a mass flow controller. The main streams leaving the reactors are measured via two venturi with side streams for off-line analysis, process control or the syngas treatment unit measured inside the respective analysis or control equipment. The mass flow of solids entering the system is measured via load cells and the corresponding trend line gradients.

4.7. Off-Line Sampling

4.7.1. Solid Sampling

The bottom product removal of the AR transfers the material to an open barrel and is immediately accessible for inspection and sampling, while for the FR it is transferred to a sealed and CO_2-purged container which can be replaced periodically during operation to allow for the collection of samples. The same is implemented for filter dust sampling. The AR filter is equipped with a hopper and an open barrel, while the FR filter has an additional CO_2 purge and the container is sealed.

Both loop seals allow for the collection of solid samples for off-line analysis. The OC samples enable the determination of the exact phase composition of the circulating OC and to balance the reactors individually. Moreover, knowledge of the oxidation level before and after the reactors allows for an additional method for the quantification of solid circulation.

4.7.2. Gas and Tar Sampling

More gas species like COS and higher hydrocarbons can be measured using Fourier transform infrared (FTIR) spectroscopy which can be connected at different locations. These measurements are not considered important during pilot plant operation but are important for the evaluation of the process. At the FTIR a port for gas sample bags and gas mice exists to enable off-line gas analysis.

Additionally, isokinetic sampling is possible in the synthesis gas line allowing for dust and tar sample collection according to tar protocol/CEN TS 15439. Velocity is measured by an S-Pitot tube 550 mm downstream of the sampling lance, both located in the center line of a refractory lined tube. The dust loaded syngas sample stream is transfered via a heated lance towards a heated filter and through six impinger bottles where five are filled with isopropanol as solvent and the last is empty. The impinger bottles are tempered to 40 °C (impinger 1, 2 and 4) and −20 °C (impinger 2, 5 and 6). The sample volume is measured inside a comercially available ST5 isokinetic sampler from Dado lab, which also adjusts the sample volume flow based on the pitot measurement.

5. Plant Operation

The simulations from Section 3.3 show that autothermal CLG experiments are needed to obtain further insights into the process, which are of high relevance for industrial deployment. The modified pilot plant (Section 4) renders these experiments feasible allowing for the generation of the following, required information:

5.1. Literature, describing the demonstration of autothermal operation of the CLG process, is not yet available. While autothermal CLC has been successfully demonstrated [49,51] the higher prevalence of endothermic reactions impose the need for higher heat transfer to the FR and different control strategies [26].

5.2. Continuous CLG of residual biomass has been successfully demonstrated in lab-scale [11,15,16]. Nonetheless, upscaling to higher thermal loads is necessary to obtain data for reliable simulations and design of industrial scale units.

5.3. Due to their interdependence, the key performance indicators achievable in autothermal operation are unknown. This affects the cold gas efficiency η_{CG}, the carbon conversion η_{CC}, the syngas yield x_{SG} and the syngas quality (tars, CH_4, etc.). For example, in electrically heated systems the cold gas efficiency η_{CG} can be theoretically driven to 100% by supplying enough heat through the furnace. However, the exact amount of external heat supplied is seldom reported. The carbon slip depends amongst other on reactor size [59] and data for bigger scale units is not existent.

5.4. Tar production can presently not be accurately predicted as no model was developed for CLG yet. Especially bed height and feeding location are also dependent on reactor size and their influence cannot be quantified [37]. The pilot plant experiments will give important insight on this matter in industrial like conditions, allowing for inferences for future upscaling endeavours.

5.5. OC life time is difficult to asses with currently available data, as the time of circulation and thus of re-oxidation cycles increases with increasing reactor size while the mechanical erosion is dependent on the transport velocity only. The exact contribution of the two effects is unknown and thus it is likely that the size of the reactor will have an influence on the OC life time.

5.6. Assessment of economic feasibility of the CLG process requires data from bigger scale units to make accurate predictions for e.g., sizing of components and process performance.

For the demonstration of autothermal CLG (item 5.1.) a suitable control concept for the oxygen carrier to fuel equivalence ratio ϕ based on a sub-stoichiometric AR operation (reduced OC oxidation, see Equations (2) and (3)) according to Dieringer et al. [26] is implemented. The corresponding operating strategy considering pilot plant limitations is described in the following.

Chemical Looping Gasification Operation

The start-up sequence of the pilot plant is preheating with electrically heated air, preheating with propane burner, OC filling plus propane burner, CFB combustion, CLC as described in [47]. Afterwards the switch to CLG is achieved by a reduction of air input to the AR while increasing flue gas recirculation, thus reducing ϕ to values smaller than unity. After stable CLG operation is attained, optimization of individual key performance indicators is targeted during experiments. The devised experimental operation of the pilot plant (described hereafter) allows to directly obtain data for items 5.2. and 5.3. while information for items 5.4. and 5.5. can be inferred from additional off-line analysis. Item 5.6. builds on this data but needs additional information, e.g., component and material pricing, which cannot be generated in the pilot plant. The main operation variables through which the process can be controlled are:

- Thermal load: Increasing the thermal load above 1 MW_{th} decreases the relative heat loss as it depends on reactor temperature and not on thermal load. Therefore, a higher fraction of the feedstock input, $\dot{m}_{FS}$, can be converted into syngas increasing process efficiency. The feedstock input rate $\dot{m}_{FS}$ is directly proportional to the thermal load, but an adjustment requires corresponding changes in fluidization imposed by reactor hydrodynamics and heat balance influencing the steam to biomass ratio. Nonetheless, the simulations in Section 3.3 show also an increase of CH_4 production with increasing thermal load, indicating a tendency to form hydrocarbons including tars.
  The limit for the thermal input is set by the maximum possible feedstock input and the syngas handling and cooling, as higher loads result in a higher amount of product gas which has to be handled safely. During operation a high thermal load is targeted at all operation points to obtain high η_{CG}.
- The OC to fuel equivalence ratio ϕ determines the net heat release from the process. A higher value of ϕ (while keeping everything else constant) results in a higher temperature inside AR and FR. However, the cold gas efficiency η_{CG} will decrease with higher ϕ as does the production of CH_4 and tars. The control of ϕ is straightforward through the control of the oxygen availability inside the AR.
  For experimental investigation the variation of temperatures is important. However, higher temperatures increase the load on the cooling system. Here the limits have to be considered during operation, and a reduction in thermal load (leading to smaller process streams and further decreasing η_{CG}) may be required in order to be able to reach higher gasification temperatures. Moreover, the refractory lining of the AR and/or the ash melting behaviour of the feedstock inside the FR limit the maximum admissible reactor temperatures.
  Actual control of ϕ is achieved via the variable amounts of air and recirculated AR flue gas fed to the AR to obtain a sub-stoichiometric environment inside the AR as it is the most suitable method for large scale operation described in detail by Dieringer et al. [26].

- The global solids circulation $\dot{m}_{OC}$ can be controlled via adjustment of J-valve and FR fluidization and transports sensible heat required in the FR. Depending on the operating state of the AR internal solids recirculation, fluidization of the AR needs adjustment as well to obtain hydrodynamic equilibrium between the reactors. Yet, $\dot{m}_{OC}$ is not directly accessible during pilot plant operation but can be inferred qualitatively from the temperature difference between the reactors. Higher solids circulation reduces the temperature difference ΔT between AR and FR. An accurate determination of $\dot{m}_{OC}$ is possible only indirectly via the oxygen content in the solid samples taken from the loop seals.
  Increasing global solids circulation reduces not only ΔT but also η_{CG} as more fluidization medium and corresponding heating is required. Furthermore, OC residence time inside the reactors is reduced when the solids circulation increases and as higher superficial gas velocities are employed, carbon slip towards the AR might increase. The variable to be controlled is the gasification temperature inside the FR while the limit of the AR temperature might require adjustment via ϕ.

The OC to fuel equivalence ratio ϕ and the global solids circulation $\dot{m}_{OC}$ are used to investigate the inevitable trade-off between cold gas efficiency and syngas quality in the form of produced CH_4, higher hydrocarbons, and tar. In contrast, the maximization of the thermal load is used to boost the process performance η_{CG} for all operation points by allowing for a smaller value of ϕ while at the same time guaranteeing autothermal operation.

While the variables above are used to adjust and stabilize the process and to investigate general trends, two more adjustable parameters exist which can be used to influence the syngas quality:

- Bed pressure drop Δp: The simulations in Section 3.3 are done with a fixed pressure drop Δp for both reactors. However, during operation of the pilot plant, Δp can be varied and is dependent on the exact distribution of bed material between the reactors (controlled by the governing hydrodynamic boundary conditions) as well as the total amount of bed material inside the reactor system. Increasing the pressure drop inside the FR will increase OC particle residence time inside the reactor (and the amount of OC per feedstock input). This will also increase the entrainment from the FR and thereby the solid circulation. However, increasing Δp allows for the reduction of fluidization medium, while keeping the entrainment constant, thus improving process efficiency. Reduction of tar and CH_4 content in syngas is facilitated by the increased availability of catalytic sites for conversion.
  The OC make up stream is used to control the overall amount of OC inside the reactor system, while its distribution is influenced by small adjustments to fluidization medium. The required changes in fluidization are small compared to the changes needed for the operation variables discussed above. The range of Δp is limited by the reactor hydrodynamics and the characteristics of corresponding pripheral equipment (e.g., maximum load of AR primary air fan).
- Second stage fluidization can be varied to enhance the residence time of the feedstock inside the dense zone of the FR as describes in Section 4.1. Rerouting part of the fluidization medium to the second stage fluidization will reduce entrainment and solid circulation, if the total amount of steam is kept constant and can be counteracted by additional bed material. Qualitative effects on synthesis gas are the same as for the bed pressure drop Δp, however, the quantitative influence may vary.

The feedstock types given in Table 2 are an additional parameter for experimental variation. However, the feedstock is not usable as process control variable and is therefore not included in the list above. Furthermore, the other variables must be used to adjust for feedstock variation to keep the process stable.

6. Conclusions

In this article, the design pathway of a 1 MW_{th} chemical looping gasification (CLG) pilot plant, allowing for autothermal, semi-industrial process investigation, has been described in detail. Starting from a process model, considering fundamental CLG characteristics, a suitable operational mode and associated necessary adaptions for an existing 1 MW_{th} chemical looping combustion (CLC) pilot plant have been established. Subsequently, it has been illustrated which inherent interconnections and trade-offs associated to CLG can be further analyzed in such an experimental setup and which strategies towards an optimized process setup, replicable in industry scale, can be pursued with it. These are:

- Calculation of heat and mass balances for autothermal CLG show a significantly reduced range of freely selectable operation parameters (operation temperatures, steam to biomass feed ratio, and oxygen carrier to fuel equivalence ratio), when compared to externally heated lab-scale units, due to the requirements of autothermal operation.
- Process control under autothermal condition can be achieved via three parameters: thermal load, oxygen carrier to fuel equivalence ratio, and global solid circulation. However, due to restrictions imposed by reactor hydrodynamics and autothermal operation, changes in one parameter must be balanced by changes in at least one of the other two. Moreover, the global solids circulation is adjusted indirectly via fluidization velocities and can only be inferred qualitatively from the reactor temperature difference during operation.
- Attempting to attain high cold gas efficiency and good syngas quality through higher gasification temperature inevitably results in high relative heat losses, as heat integration is not reasonably achievable in the 1 MW_{th} scale and the existing unit. This leads to an unavoidable trade-off between cold gas efficiency and syngas quality, e.g., CH_4 and tar content which has to be accepted during experiments.
- Data which are not reliably obtainable from simulation, like tar formation or oxygen carrier (OC) life time, yet are fundamental for scale-up and economic considerations becomes available by conducting experiments in an industry relevant scale in the designed pilot plant.

In summary, future endeavours aiming towards industrial application of CLG are facilitated, through the described design of a 1 MW_{th} CLG pilot plant. Here, the experimental facility lays the foundation to generate a unique robust dataset containing essential information required for up-scaling of CLG to industry size, thus propelling the technology towards market maturity.

Author Contributions: conceptualization, F.M., J.S. and P.D.; simulation, P.D. and F.M.; writing—original draft preparation, F.M.; writing—review and editing, P.D., J.S. and F.M.; visualization, F.M. and P.D.; supervision, B.E. All authors have read and agreed to the published version of the manuscript.

Funding: This work has received funding of the European Union's Horizon 2020—Research and Innovation Framework Programme under grant agreement No. 817841 (Chemical Looping gasification foR sustainAble production of biofuels—CLARA).

Acknowledgments: The authors gratefully acknowledge the support given by Harald Tremmel and Karl Voigtländer from AICHERNIG Engineering GmbH during HAZOP analysis.

Conflicts of Interest: The authors declare no conflict of interest.

Abbreviations

The following abbreviations are used in this manuscript:

AR	air reactor
ASU	air separation unit
CFB	circulating fluidized bed
CLC	chemical looping combustion
CLG	chemical looping gasification
CLOU	chemical looping with oxygen uncoupling
DFBG	dual fluidized bed gasification
FR	fuel reactor
FTIR	Fourier transform infrared
HTW^{TM}	High Temperature Winkler
LS	loop seal
NDIR	non-dispersive infra red
OC	oxygen carrier

Symbols

LHV	MJ kg^{-1}, MJ mol^{-1}	lower heating value
R_{OC}		oxygen transport capacity
T	K, °C	temperature
X		mole fraction
ΔH	J mol^{-1}	reaction enthalpy
Δp	Pa, bar	differential pressure
ϕ		oxygen carrier to fuel equivalence ratio
$\dot{Q}$	W	heat flow
$\dot{m}$	kg s^{-1}	mass flow
$\dot{n}$	mol s^{-1}	molar flow
η_{CG}		cold gas efficiency
c_p	J kg^{-1} K^{-1}	specific heat
$d_{p,50}$	m	mean particle diameter
d	m	diameter
h	m	height
m	kg	mass
p	Pa, bar	pressure
u	m s^{-1}	velocity
x_{SG}		syngas content

Subscripts

AR	Air Reactor
FR	Fuel Reactor
FS	Feed Stock
OC	Oxygen Carrier
O	Oxygen
$internal$	internal recirculation
in	stream entering reactor
$loss$	loss
out	stream leaving reactor
ox	oxidized
$reci$	recirculation
red	reduced
$stoich$	stoichiometric

References

1. Directive (EU) 2018/2001 of the European Parliament and of the Council of 11 December 2018 on the Promotion of the Use of Energy from Renewable Sources. p. 128. Available online: https://eurovent.eu/?q=articles/review-directive-eu-20182001-promotion-use-energy-renewable-sources-gen-115400 (accessed on 19 December 2020).

2. International Energy Agency. Data & Statistics. 2020. Available online: https://www.iea.org/data-and-statistics?country=EU28&fuel=Energy20transition20indicators&indicator=Biotrans (accessed on 19 December 2020).
3. Kaltschmitt, M. (Ed.) *Energy from Organic Materials (Biomass): A Volume in the Encyclopedia of Sustainability Science and Technology*, 2nd ed.; Springer: New York, NY, USA, 2019. [CrossRef]
4. Carrasco, J.E.; Monti, A.; Tayeb, J.; Kiel, J.; Girio, F.; Matas, B.; Santos Jorge, R. Strategic Research and Innovation Agenda 2020. EERA Technical Report. 2020. Available online: http://www.eera-bioenergy.eu/wp-content/uploads/pdf/EERABioenergySRIA2020.pdf=AOvVaw012VUhnaqiUbL-yP76cz6s (accessed on 19 December 2020).
5. Molino, A.; Larocca, V.; Chianese, S.; Musmarra, D. Biofuels Production by Biomass Gasification: A Review. *Energies* **2018**, *11*, 811. [CrossRef]
6. Gómez-Barea, A.; Leckner, B. Estimation of Gas Composition and Char Conversion in a Fluidized Bed Biomass Gasifier. *Fuel* **2013**, *107*, 419–431. [CrossRef]
7. Thomsen, T.P.; Sárossy, Z.; Gøbel, B.; Stoholm, P.; Ahrenfeldt, J.; Frandsen, F.J.; Henriksen, U.B. Low Temperature Circulating Fluidized Bed Gasification and Co-Gasification of Municipal Sewage Sludge. Part 1: Process Performance and Gas Product Characterization. *Waste Manag.* **2017**, *66*, 123–133. [CrossRef]
8. Arena, U.; Zaccariello, L.; Mastellone, M.L. Fluidized Bed Gasification of Waste-Derived Fuels. *Waste Manag.* **2010**, *30*, 1212–1219. [CrossRef]
9. De, S.; Agarwal, A.K.; Moholkar, V.S.; Thallada, B. (Eds.) *Coal and Biomass Gasification: Recent Advances and Future Challenges*; Energy, Environment, and Sustainability; Springer: Singapore, 2018. [CrossRef]
10. Higman, C.; van der Burgt, M. *Gasification*, 2nd ed.; Gulf Professional Pub.: Boston, MA, USA; Elsevier: Amsterdam, The Netherlands, 2008.
11. Condori, O.; García-Labiano, F.; de Diego, L.F.; Izquierdo, M.T.; Abad, A.; Adánez, J. Biomass Chemical Looping Gasification for Syngas Production Using Ilmenite as Oxygen Carrier in a 1.5 kWth Unit. *Chem. Eng. J.* **2021**, *405*, 126679. [CrossRef]
12. Huseyin, S.; Wei, G.Q.; Li, H.B.; He, F.; Huang, Z. Chemical-Looping Gasification of Biomass in a 10 kWth Interconnected Fluidized Bed Reactor Using Fe_2O_3/Al_2O_3 Oxygen Carrier. *J. Fuel Chem. Technol.* **2014**, *42*, 922–931. [CrossRef]
13. Guo, Q.; Cheng, Y.; Liu, Y.; Jia, W.; Ryu, H.J. Coal Chemical Looping Gasification for Syngas Generation Using an Iron-Based Oxygen Carrier. *Ind. Eng. Chem. Res.* **2014**, *53*, 78–86. [CrossRef]
14. Wei, G.; He, F.; Huang, Z.; Zheng, A.; Zhao, K.; Li, H. Continuous Operation of a 10 kW_{th} Chemical Looping Integrated Fluidized Bed Reactor for Gasifying Biomass Using an Iron-Based Oxygen Carrier. *Energy Fuels* **2015**, *29*, 233–241. [CrossRef]
15. Samprón, I.; de Diego, L.F.; García-Labiano, F.; Izquierdo, M.T.; Abad, A.; Adánez, J. Biomass Chemical Looping Gasification of Pine Wood Using a Synthetic Fe_2O_3/Al_2O_3 Oxygen Carrier in a Continuous Unit. *Bioresour. Technol.* **2020**, *316*, 123908. [CrossRef] [PubMed]
16. Ge, H.; Guo, W.; Shen, L.; Song, T.; Xiao, J. Experimental Investigation on Biomass Gasification Using Chemical Looping in a Batch Reactor and a Continuous Dual Reactor. *Chem. Eng. J.* **2016**, *286*, 689–700. [CrossRef]
17. Ge, H.; Guo, W.; Shen, L.; Song, T.; Xiao, J. Biomass Gasification Using Chemical Looping in a 25 kW Th Reactor with Natural Hematite as Oxygen Carrier. *Chem. Eng. J.* **2016**, *286*, 174–183. [CrossRef]
18. Brown, T.A.; Dennis, J.S.; Scott, S.A.; Davidson, J.F.; Hayhurst, A.N. Gasification and Chemical-Looping Combustion of a Lignite Char in a Fluidized Bed of Iron Oxide. *Energy Fuels* **2010**, *24*, 3034–3048. [CrossRef]
19. Leion, H.; Mattisson, T.; Lyngfelt, A. The Use of Petroleum Coke as Fuel in Chemical-Looping Combustion. *Fuel* **2007**, *86*, 1947–1958. [CrossRef]
20. Chen, L. The Direct Solid-Solid Reaction between Coal Char and Iron-Based Oxygen Carrier and Its Contribution to Solid-Fueled Chemical Looping Combustion. *Appl. Energy* **2016**, *184*, 9–18. [CrossRef]
21. Leion, H.; Mattisson, T.; Lyngfelt, A. Solid Fuels in Chemical-Looping Combustion. *Int. J. Greenh. Gas Control* **2008**, *2*, 180–193. [CrossRef]
22. Song, Q.; Xiao, R.; Deng, Z.; Zhang, H.; Shen, L.; Xiao, J.; Zhang, M. Chemical-Looping Combustion of Methane with $CaSO_4$ Oxygen Carrier in a Fixed Bed Reactor. *Energy Convers. Manag.* **2008**, *49*, 3178–3187. [CrossRef]
23. Pissot, S.; Vilches, T.B.; Maric, J.; Seemann, M. Chemical Looping Gasification in a 2–4 MWth Dual Fluidized Bed Gasifier. In Proceedings of the 23rd International Conference on Fluidized Bed Conversion, Seoul, Korea, 13–17 May 2018; p. 10.
24. Larsson, A.; Seemann, M.; Neves, D.; Thunman, H. Evaluation of Performance of Industrial-Scale Dual Fluidized Bed Gasifiers Using the Chalmers 2–4-MW_{th} Gasifier. *Energy Fuels* **2013**, *27*, 6665–6680. [CrossRef]
25. Larsson, A.; Israelsson, M.; Lind, F.; Seemann, M.; Thunman, H. Using Ilmenite to Reduce the Tar Yield in a Dual Fluidized Bed Gasification System. *Energy Fuels* **2014**, *28*, 2632–2644. [CrossRef]
26. Dieringer, P.; Marx, F.; Alobaid, F.; Ströhle, J.; Epple, B. Process Control Strategies in Chemical Looping Gasification—A Novel Process for the Production of Biofuels Allowing for Net Negative CO_2 Emissions. *Appl. Sci.* **2020**, *10*, 4271. [CrossRef]
27. Yin, S.; Shen, L.; Dosta, M.; Hartge, E.U.; Heinrich, S.; Lu, P.; Werther, J.; Song, T. Chemical Looping Gasification of a Biomass Pellet with a Manganese Ore as an Oxygen Carrier in the Fluidized Bed. *Energy Fuels* **2018**, *32*, 11.
28. Adanez, J.; Abad, A.; Garcia-Labiano, F.; Gayan, P.; de Diego, L.F. Progress in Chemical-Looping Combustion and Reforming Technologies. *Prog. Energy Combust. Sci.* **2012**, *38*, 215–282. [CrossRef]
29. Linderholm, C.; Knutsson, P.; Schmitz, M.; Markström, P.; Lyngfelt, A. Material Balances of Carbon, Sulfur, Nitrogen and Ilmenite in a 100 kW CLC Reactor System. *Int. J. Greenh. Gas Control* **2014**, *27*, 188–202. [CrossRef]

30. Alabdrabalameer, H.A.; Taylor, M.J.; Kauppinen, J.; Soini, T.; Pikkarainen, T.; Skoulou, V. Big Problem, Little Answer: Overcoming Bed Agglomeration and Reactor Slagging during the Gasification of Barley Straw under Continuous Operation. *Sustain. Energy Fuels* **2020**, *4*, 3764–3772. [CrossRef]
31. Di Giuliano, A.; Funcia, I.; Pérez-Vega, R.; Gil, J.; Gallucci, K. Novel Application of Pretreatment and Diagnostic Method Using Dynamic Pressure Fluctuations to Resolve and Detect Issues Related to Biogenic Residue Ash in Chemical Looping Gasification. *Processes* **2020**, *8*, 1137. [CrossRef]
32. Fernández, M.J. Sintering reduction of herbaceous biomass when blended with woody biomass: Predictive and combustion tests. *Fuel* **2019**, *239*, 1115–1124. [CrossRef]
33. Luo, S.; Zeng, L.; Fan, L.S. Chemical Looping Technology: Oxygen Carrier Characteristics. *Annu. Rev. Chem. Biomol. Eng.* **2015**, *6*, 53–75. [CrossRef] [PubMed]
34. Fan, L.S.; Zeng, L.; Luo, S. Chemical-Looping Technology Platform. *AIChE J.* **2015**, *61*, 2–22. [CrossRef]
35. Zhao, X.; Zhou, H.; Sikarwar, V.S.; Zhao, M.; Park, A.H.A.; Fennell, P.S.; Shen, L.; Fan, L.S. Biomass-Based Chemical Looping Technologies: The Good, the Bad and the Future. *Energy Environ. Sci.* **2017**, *10*, 1885–1910. [CrossRef]
36. Larsson, A.; Kuba, M.; Berdugo Vilches, T.; Seemann, M.; Hofbauer, H.; Thunman, H. Steam Gasification of Biomass—Typical Gas Quality and Operational Strategies Derived from Industrial-Scale Plants. *Fuel Process. Technol.* **2021**, *212*, 106609. [CrossRef]
37. Gómez-Barea, A.; Ollero, P.; Leckner, B. Optimization of Char and Tar Conversion in Fluidized Bed Biomass Gasifiers. *Fuel* **2013**, *103*, 42–52. [CrossRef]
38. Devi, L.; Ptasinski, K.J.; Janssen, F.J. Pretreated Olivine as Tar Removal Catalyst for Biomass Gasifiers: Investigation Using Naphthalene as Model Biomass Tar. *Fuel Process. Technol.* **2005**, *86*, 707–730. [CrossRef]
39. Amin, A.M.; Croiset, E.; Epling, W. Review of Methane Catalytic Cracking for Hydrogen Production. *Int. J. Hydrogen Energy* **2011**, *36*, 2904–2935. [CrossRef]
40. Milne, T.A.; Evans, R.J.; Abatzaglou, N. *Biomass Gasifier "Tars": Their Nature, Formation, and Conversion*; Technical Report NREL/TP-570-25357; United States Department of Energy: Washington, DC, USA, 1998. [CrossRef]
41. Benedikt, F.; Kuba, M.; Schmid, J.C.; Müller, S.; Hofbauer, H. Assessment of Correlations between Tar and Product Gas Composition in Dual Fluidized Bed Steam Gasification for Online Tar Prediction. *Appl. Energy* **2019**, *238*, 1138–1149. [CrossRef]
42. Palma, C.F. Model for Biomass Gasification Including Tar Formation and Evolution. *Energy Fuels* **2013**, *27*, 5. [CrossRef]
43. Wojnicka, B.; Ściążko, M.; Schmid, J.C. Modelling of Biomass Gasification with Steam. *Biomass Conv. Bioref.* **2019**. [CrossRef]
44. Stark, A.K.; Bates, R.B.; Zhao, Z.; Ghoniem, A.F. Prediction and Validation of Major Gas and Tar Species from a Reactor Network Model of Air-Blown Fluidized Bed Biomass Gasification. *Energy Fuels* **2015**, *29*, 2437–2452. [CrossRef]
45. Herdel, P.; Krause, D.; Peters, J.; Kolmorgen, B.; Ströhle, J.; Epple, B. Experimental Investigations in a Demonstration Plant for Fluidized Bed Gasification of Multiple Feedstock's in 0.5 MW Th Scale. *Fuel* **2017**, *205*, 286–296. [CrossRef]
46. Krause, D.; Herdel, P.; Ströhle, J.; Epple, B. HTW™-Gasification of High Volatile Bituminous Coal in a 500 kWth Pilot Plant. *Fuel* **2019**, *250*, 306–314. [CrossRef]
47. Ströhle, J.; Orth, M.; Epple, B. Design and Operation of a 1 MWth Chemical Looping Plant. *Appl. Energy* **2014**, *113*, 1490–1495. [CrossRef]
48. Ströhle, J.; Orth, M.; Epple, B. Chemical Looping Combustion of Hard Coal in a 1 MWth Pilot Plant Using Ilmenite as Oxygen Carrier. *Appl. Energy* **2015**, *157*, 288–294. [CrossRef]
49. Ohlemüller, P.; Busch, J.P.; Reitz, M.; Ströhle, J.; Epple, B. Chemical-Looping Combustion of Hard Coal: Autothermal Operation of a 1 MWth Pilot Plant. *J. Energy Resour. Technol.* **2016**, *138*, 042203. [CrossRef]
50. Ohlemüller, P.; Ströhle, J.; Epple, B. Chemical Looping Combustion of Hard Coal and Torrefied Biomass in a 1 MW Th Pilot Plant. *Int. J. Greenh. Gas Control* **2017**, *65*, 149–159. [CrossRef]
51. Ohlemüller, P.; Alobaid, F.; Abad, A.; Adanez, J.; Ströhle, J.; Epple, B. Development and Validation of a 1D Process Model with Autothermal Operation of a 1 MW Th Chemical Looping Pilot Plant. *Int. J. Greenh. Gas Control* **2018**, *73*, 29–41. [CrossRef]
52. Min, Z.; Asadullah, M.; Yimsiri, P.; Zhang, S.; Wu, H.; Li, C.Z. Catalytic Reforming of Tar during Gasification. Part I. Steam Reforming of Biomass Tar Using Ilmenite as a Catalyst. *Fuel* **2011**, *90*, 1847–1854. [CrossRef]
53. Di Giuliano, A.; Lucantonio, S.; Gallucci, K. Devolatilization of Residual Biomasses for Chemical Looping Gasification in Fluidized Beds Made up of Oxygen-Carriers. *Energies* **2021**, *14*, 311. [CrossRef]
54. Kunii, D.; Levenspiel, O. *Fluidization Engineering*, 2nd ed.; Butterworth-Heinemann Series in Chemical Engineering; Butterworth-Heinemann: Boston, MA, USA, 1991.
55. Ohlemüller, P.; Alobaid, F.; Gunnarsson, A.; Ströhle, J.; Epple, B. Development of a Process Model for Coal Chemical Looping Combustion and Validation against 100 kWth Tests. *Appl. Energy* **2015**, *157*, 433–448. [CrossRef]
56. Grace, J.R.; Avidan, A.A.; Knowlton, T.M. (Eds.) *Circulating Fluidized Beds*, 1st ed.; Blackie Academic & Professional: London, UK; New York, NY, USA, 1997.
57. Schmid, J.C.; Pfeifer, C.; Kitzler, H.; Pröll, T.; Hofbauer, H. A New Dual Fluidized Bed Gasifier Design for Improved in Situ Conversion of Hydrocarbons. In Proceedings of the International Conference on Polygeneration Strategies (ICPS), Vienna, Austria, 30 August–1 September 2011; p. 10.
58. Kronberger, B.; Johansson, E.; Löffler, G.; Mattisson, T.; Lyngfelt, A.; Hofbauer, H. A Two-Compartment Fluidized Bed Reactor for CO_2 Capture by Chemical-Looping Combustion. *Chem. Eng. Technol.* **2004**, *27*, 1318–1326. [CrossRef]

59. Lyngfelt, A.; Leckner, B. A 1000 MWth Boiler for Chemical-Looping Combustion of Solid Fuels—Discussion of Design and Costs. *Appl. Energy* **2015**, *157*, 475–487. [CrossRef]
60. Hetzer, J.; Kulik, R.; Rothenpieler, K.; Stückrath, K.; Weidenfeller, D.J. Design, Simulation and Practical Experience of the Largest Syngas Cooler in Operation for Coal Gasification. In Proceedings of the 8th International Freiberg Conference, Cologne, Germany, 12–16 June 2016.

3.3 Third Research Paper

Solid flux measurement in dual fluidized bed processes based on solid samples

Authors: Falko Marx, Paul Dieringer, Jochen Ströhle, Bernd Epple
Journal: Fuel
Date: 2023-01-31
ISSN: 0016-2361
DOI: 10.1016/j.fuel.2023.127589

Fuel 341 (2023) 127589

Contents lists available at ScienceDirect

Fuel

journal homepage: www.elsevier.com/locate/fuel

Full length article

Solid flux measurement in dual fluidized bed processes based on solid samples ☆

Falko Marx *, Paul Dieringer, Jochen Ströhle, Bernd Epple

Technical University of Darmstadt, Department of Mechanical Engineering, Institute for Energy Systems & Technology, Otto-Bernd-Str. 2, Darmstadt, 64287, Germany

ARTICLE INFO

Keywords:
Chemical looping
Solid flow measurement
Dual fluidized bed

ABSTRACT

Chemical looping gasification is a novel dual fluidized bed technology for the conversion of solid feedstock to a nitrogen-free syngas without the need of pure oxygen. Recently, a pilot plant has been erected to advance chemical looping gasification towards autothermal operation. For autothermal operation, the solids flux between the two reactors becomes important, as it transports the required sensible heat in addition to the oxygen required for the process. As a reliable method to accurately measure the solids flux under process conditions currently does not exist, a method has been devised to measure the solid circulation for dual fluidized bed systems and tested utilizing the process specifics of chemical looping gasification to allow for calibration of online measurement equipment without opening the reactor system. This method utilizes solid samples from coupling elements to calculate the solids flux in chemical looping gasification with an overall uncertainty smaller than 20%.

1. Introduction

Spurred by the increasing pace of climate change, research in carbon neutral and carbon negative processes has increased in order to combat the global warming. One focus is the decarbonization of the transport sector. While for road transport electrification is a viable option, aviation and maritime transport require different approaches. Here, the production of bio-fuels using the well-known Fischer–Tropsch process is one option. However, thermal conversion of biomass into the required syngas for the synthesis step is still not commercialized although efforts have been made for dual fluidized bed gasification [1,2]. One process offering the possibility of virtually no CO_2 emissions, when combined with a suitable separation step during gas cleaning, is CLG, which has seen increasing research activity into scale up. It utilizes a metal oxide powder, which is cyclically oxidized and reduced while being transported back and forth between two fluidized bed reactors, to supply oxygen to the gasification process without the need for an expensive air separation unit.

CLG has been successfully demonstrated in lab scale using coal with synthetic OC materials [3], biomass with synthetic OC [4–6] and with biomass and natural minerals like haematite [7,8] or ilmenite [9]. Even waste materials have been tried as OC materials [10]. Advances towards autothermal operation are being made using simulations [11,12] and by design of a pilot plant [13]. These advances stress the importance of the OC not only for the transport of oxygen, but also for the transport of sensible heat from FR to AR as high heating demands inside the FR cannot be compensated by external electrical reactor heating for successful process deployment. However, reliable measurements of the solids circulation are difficult to obtain. Moreover, the solids transported from the FR towards the AR consist not only of the reduced OC material, but include also a fraction of unconverted feedstock in the form of fixed carbon, called carbon slip, and ash. Methods to obtain quantitative data for the OC circulation between the reactors can be classified as online, offline, invasive and non-invasive [14]. Additionally simulation and cold-flow studies can be used to generate the data afterwards. Nonetheless, for elaborate and expensive experiments as described in [13] the measurement of solid circulation during the experiments and from material samples results in far more reliable data than a posteriori generated data from cold flow models or simulation.

Stollhof et al. [15] investigated methods to estimate the solid circulation rate based on the amount of fluidization medium, particle properties and pressure profile in the reactors which can be applied

☆ This work has received funding of the European Union's Horizon 2020-Research and Innovation Framework Programme under grant agreement No. 817841 (Chemical Looping gasification foR sustainAble production of biofuels — CLARA). The content of this work reflects only the author's view, and the European Commission is not responsible for any use that may be made of the information it contains.

* Corresponding author.
E-mail address: falko.marx@est.tu-darmstadt.de (F. Marx).

https://doi.org/10.1016/j.fuel.2023.127589
Received 24 October 2022; Received in revised form 19 January 2023; Accepted 22 January 2023
Available online 31 January 2023

Abbreviations

AR	Air reactor
CFB	Circulating fluidized bed
CFD	Computational fluid dynamics
CLC	Chemical looping combustion
CLG	Chemical looping gasification
FI	Flow indicator
FR	Fuel reactor
GA	Gas analysis
LS	Loop seal
OC	Oxygen carrier
PA	Proximate analysis
PSD	Particle size distribution
SP	Sample point
UA	Ultimate analysis

Symbols

LHV	Lower heating value (MJkg^{-1}, MJmol^{-1})
R_{OC}	Oxygen transport capacity
T	Temperature (K, °C)
W	Molar mass, atomic mass (kgmol^{-1})
X_S	Oxidation degree
$\dot{m}$	Mass flow (kgs^{-1})
m	Mass (kg)
x	Mass fraction in solid phase
y	Mass fraction in gas phase
N_2	Nitrogen

Subscripts

C	Carbon
Gas	Gas phase
LS	Loop seal
OC	Oxygen carrier
O	Oxygen
S	Solid
e	End of oxidation in stream entering reactor
i	Chemical species
j	Chemical species
out	Stream leaving reactor
ox	Oxidized real start mass including carbon
red	Reduced
$scale$	Weighing scale
s	Start of oxidation
$total$	Sum of all components

Superscripts

f	Hypothetical state at oxidation start

to the hot reactor system. However, a reported deviation of ±40% is discouraging as such deviations in solid circulation could potentially result in a FR temperature drop of more than 150 K [11] negatively impacting conversion and syngas quality. Smaller deviations have been reported using empirical adjustments. However, fitting to a geometrical similar model is required, and temperature influences seem to be difficult to quantify [16]. Direct measurement using impact force of the particle flow is limited by the maximum permissible temperature of the measurement equipment and can therefore not be used under process conditions. However, a recent review by Liu et al. [17] suggests a design which might be possible. Online Measurements using optical sensing have been successfully tested in cold flow configurations [18] and in 2D setups [19]. However, the application to large-scale units operating at high temperatures is not possible as the sensor cannot measure deep inside the 3D flow structure of the solid flux or through the refractory lined reactor walls. Other setups using moving mechanical equipment inside the solid flux [20] seem problematic with regards to the lifetime under the harsh process conditions.

Direct online measurement using the microwave and Doppler effect is an option, but usually requires extensive calibration under process conditions [21], which are not feasible, as the loop has to be broken for calibration. It can be calibrated under cold conditions, but the influence of the temperature cannot be reliably predicted and subsequently compensated, as no data is available yet.

Using tracer particles as described in [14] is likely to be of limited use, as attrition and the continuous removal of agglomerates pose the possibility of the removal of the tracer particle. Magnetic tracer are good for cold flow models [22] but refractory lining and Curie temperature pose problems for hot systems. The injection of cold particles and tracking the corresponding temperature drop with thermocouples [23] seems the most viable tracer method. However, as with most tracer methods it requires a uniformly moving packed bed. It becomes generally more difficult to locate small amounts of tracer particles with growing plant size, as tracers can be easily obscured making the methods less accurate.

The solid circulation can be determined via scaling laws based on measurement in a cold flow model with accumulation measurements inside the coupling elements (e.g. loop seals) or with another method. A perfectly scaled cold flow model is difficult to realize for metal powders, as the cold flow model would need to be filled with Helium or use radioactive materials. Not perfectly scaled cold flow models can give a quantitative measurement in the right order of magnitude, but the exact error created cannot be assessed.

Calculations using CFD require validation of the model to allow for an assessment of the quality of the generated data. However, during endeavours of upscaling such models extrapolate far outside their validation range, as the data to be obtained is the data required for validation. Theoretically, the solid circulation is obtainable via the heat balance. However, accurate knowledge of heat losses can be obtained for indoor laboratory units [24,25] but estimation of heat losses for large scale industry plants through the refractory lined reactor walls under changing ambient outdoor conditions is challenging. Methods using balances around a heat exchanger removing sensible heat from the bed material [26] are applicable to CFB boilers but not in CLG where the bed material is used to heat the FR.

Linderholm et al. describe a method which uses batch wise fuel feeding and measuring of system response time to determine the solid circulation in an externally heated reactor system fed with coal [27]. However, application seems impossible when using fuels high in volatiles like biomasses where changes in fuel feed severely impact reactor hydrodynamic. Furthermore, under autothermal condition the fuel feed is directly impacting system temperature, reactor chemistry, and gas velocity and would therefore significantly alter the solid discharge in CFB reactors. The introduction of a mechanical device to divert and sample the entire solids flow are successfully deployed in small scale units [9]. However, at larger units these become very difficult to operate and the sampled volume impractical to handle. The general applicability of different measurement technologies to industry sized plants is discussed by Liu et al. [17].

This study proposes a new method utilizing solid samples taken from coupling elements and the specifics of the process to obtain the solid circulation from experimental operation with no dependence on reactor geometry. Moreover, the error can be quantified by the calculation of the propagated uncertainties. The underlying calculation and required measurements are presented here in detail.

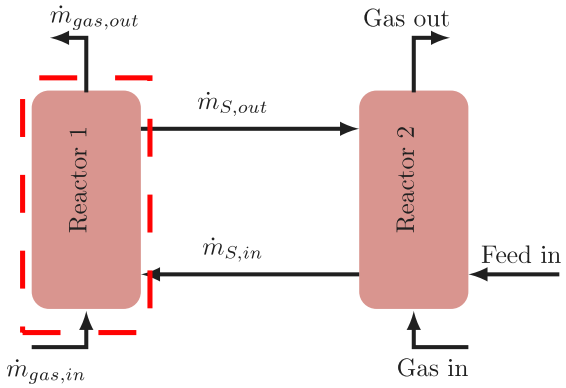

Fig. 1. Schematic of a dual fluidized bed process indicating relevant streams.

2. Method

Coupled fluidized bed reactors are usually used to periodically load or unload a carrier material with a substance (CLG, CLC [28,29], carbonate looping [30–32] etc.) and even where only heat transport is desired (e.g. dual fluidized bed gasification [33]) some amount of reactive material is transported. To determine the solid circulation, a suitable balance around one reactor can be employed to get accurate information on the solids transport between the reactors. The necessary measurement sites for the gaseous streams (e.g. composition, volume flows) are usually part of any reactor setup as they are used for process control. However, such a balance equation requires information on solids flux composition which is usually not available via online measurements and needs to be taken from offline sample analysis.

A general reactor setup is depicted in Fig. 1 with a boundary for the balance around Reactor 1. Usually one reactor has a simpler chemistry (less components) and requires less assumptions (less reactions or equilibrium reactions) or sample analysis and is therefore simpler to balance. The balance itself can be a mass balance or one or multiple elemental (or molecular) balances and depends on the process. As all processes have a difference in composition in the solids flux entering and leaving a reactor, this difference can be used according to the balance equation to calculate the solids flux transported between the reactors.

Assuming substance i is transported in excess with the solids flux $\dot{m}_S$ and released inside Reactor 1 as a gaseous species, the balance equation is:

$$\begin{aligned} 0 =& x_{i,in} \cdot \dot{m}_{S,in} - x_{i,out} \cdot \dot{m}_{S,out} \\ &+ y_{i,in}\dot{m}_{gas,in} - y_{i,out}\dot{m}_{gas,out} \end{aligned} \tag{1}$$

With y_i being the mass fraction of species i in the gas stream, while x_i is the mass fraction in the solids flux expressed as excess quantity. The expression of i as excess quantity, i.e. $\dot{m}_{total} = \dot{m}_S + \dot{m}_i = \dot{m}_S(1 + x_i)$ has the advantages, in case of only one incorporated or released species were $\dot{m}_S$ become equal for inlet and outlet stream. If there is more than one species incorporated or released, the difference of the two solids mass fluxes $\dot{m}_{S,in}$ and $\dot{m}_{S,out}$ must be the difference of all other species j released from or incorporated into the solids flux giving:

$$\begin{aligned} \Delta\dot{m}_S =& -\dot{m}_{S,in} + \dot{m}_{S,out} \\ =& \sum_{j\neq i} y_{j,in} \cdot \dot{m}_{Gas,in} - \sum_{j\neq i} y_{j,out} \cdot \dot{m}_{Gas,out} \end{aligned} \tag{2}$$

And therefore the solids flux entering Reactor 1 can be calculated to be[1]:

$$\dot{m}_S = \frac{\dot{m}_{Gas,in}(y_{i,in} - \sum_{j\neq i} y_{j,in} \cdot x_{i,out}) - \dot{m}_{Gas,out}(y_{i,out} - \sum_{j\neq i} y_{j,out} \cdot x_{i,out})}{x_{i,out} - x_{i,in}} \tag{3}$$

The selection of species i should be done according to:

- sample analysis: a species for which the mass fraction inside the sample can easily be analysed
- process: a species which is only present in a few components in the gas phase, reducing the online analysis effort
- reactions: a species which is fast consumed or released inside the reactor reducing the possible impact during transient states

It should be noted that $\Delta\dot{m}_S$ can be zero for processes where only one species is released or incorporated into the solids flux, with the balance equation simplifying accordingly. Moreover, the reference state for x_i can be selected to be either $x_{i,in}$ or $x_{i,out}$ simplifying the equation and probably the laboratory analysis. For the CLG process either oxygen or carbon can be used to balance the AR. The advantage of using carbon is its good availability to sample analysis, while for oxygen the reference state can be selected as $x_{i,in} = 0$ simplifying the equation.

3. Experimental

3.1. 1 MW_{th} pilot plant

A simplified flow sheet of the 1 MW_{th} experimental facility for autothermal operation of the CLG process is shown in Fig. 2 and described in detail elsewhere [13]. It shows the reactor system including the relevant measurement sites and sampling points in the installed loop seals for this method. The OC is oxidized inside the AR which is operated in a CFB mode. The entrained solids are separated via a cyclone and transported towards the AR loop seal. From the AR loop seal the oxidized OC is then transported via a J-valve into the bed of the FR. Inside the FR (also a CFB) the OC is reduced with the feedstock which is fed into the dense zone of the bed. Entrained solids are separated via cyclone and transported through the FR loop seal back to the AR. The amount of solids transported from the AR loop seal towards the FR i.e. the global solid circulation between the reactors, is controlled via the J-valve fluidization. Any material entrained from the AR which exceeds the solids flux through the J-valve is returned to the AR. The measurement sites relevant for the described method are the measurements of the gas flows (FI), the gas composition (GA), and the SPs which are indicated in the flow sheet. The solids fluxes are sampled inside the loop seal sample points (details provided in Section 3.3). Additional streams entering the reactor system are the feedstock going into the FR and propane for heating and co-firing in the AR. The propane can either be fed directly into the bed or via the start-up burner together with air. The OC material make-up flow, which is fed into the AR loop seal, is neglected during calculation as it is two orders of magnitude smaller than the circulating material.

As AR operation in sub-stoichiometric conditions is required to limit the oxygen availability and thus the syngas conversion inside the FR [11–13], it can be assumed that all oxygen in the air flow fed to the AR is consumed making oxygen a good candidate as the species to be balanced. Moreover, the oxidation degree X_S as defined by [34]:

$$\begin{aligned} X_S &= \frac{m_{OC,LS} - m_{OC,red}}{R_{OC} \cdot m_{oc,ox}} \\ &= 1 - \frac{m_{OC,ox} - m_{OC,LS}}{R_{OC} \cdot m_{oc,ox}} \end{aligned} \tag{4}$$

$$R_{OC} = \frac{m_{OC,ox} - m_{OC,red}}{m_{OC,ox}} \tag{5}$$

[1] Details in Appendix A.1.

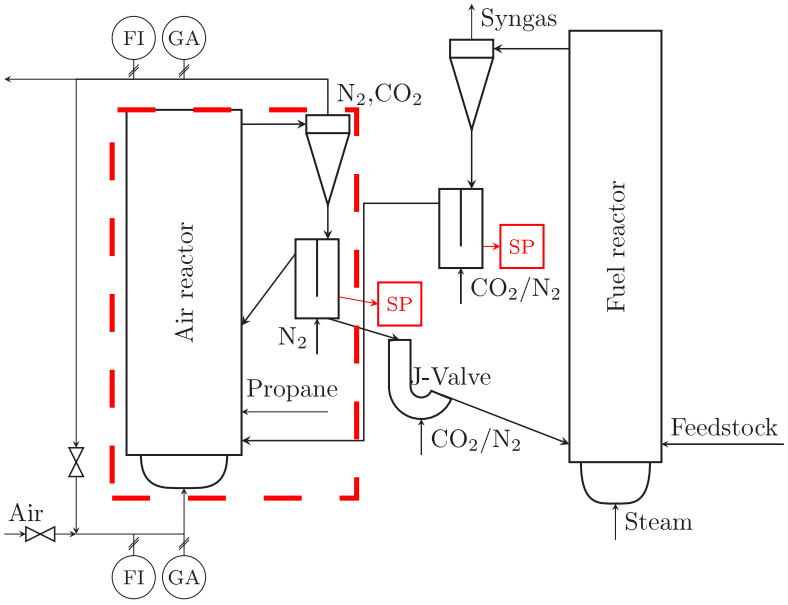

Fig. 2. Schematic of the chemical looping gasification process indicating relevant measurement sites, sample position, and balance boundary. FI: flow indicator GA: gas analysis, SP: sample point.

Table 1
Proximate and ultimate analysis of feedstock used during experiments. LHV: lower heating value, PA: proximate analysis, UA: ultimate analysis.

	Component	Pine forest residue
PA [wt. – %]	Moisture	4.4
	Ash (d.b.)	2.3
	Volatiles (d.b.)	80.3
	Fixed carbon (d.b.)	17.4
UA [wt. – %]	C (d.b.)	51.1
	H (d.b.)	6.1
	N (d.b.)	0.44
	O (d.b.)	40.1
	S (d.b.)	0.025
	Cl (d.b.)	0.010
LHV [MJ kg^{-1}]		19.70

is an interesting parameter, and its determination gives insight into the performance of the OC material and the overall process. Nonetheless, the balance can be done without exact knowledge of X_S by selecting the reference state for the oxygen fraction transported in excess to the FR output fraction. The laboratory analysis of the oxidation of the OC can then be done with a laboratory oven and a weighing scale. For all calculations in this work an $R_{OC} = 0.033$ is used as determined for used ilmenite by [35]. As the undesired carbon slip from FR towards AR results in a systematic error it has to be corrected by the amount of carbon transported, which requires the additional analysis of the carbon content in the samples. However, the occurrence of carbon slip, although unwanted in practical application of CLG, allows the balance to be done using carbon – as the carbon content requires analysis anyway – without the analysis of the oxygen content or oxidation degree of the OC.

The solid–solid reaction of OC and char inside the loop seals is not considered here. Although solid–solid reactions can occur at the conditions inside the loop seals [36], the OC leaving the FR is already highly reduced, and the low amount of fixed carbon in the feedstock(see Table 1) leads to mass fractions of less than 0.5% carbon inside the loop seal. Moreover, the mean residence time inside the loop seal is less than a minute making the effect negligible.

Thus the solid flux can be calculated using the AR and either carbon or oxygen as the main species to balance with the other as an additional species incorporated into the OC flux. With carbon as the main species:

$$\dot{m}_{OC} = \frac{\dot{m}_{Gas,in}(y_{C,in} - y_{O,in} \cdot x_{C,out}) - \dot{m}_{Gas,out}(y_{C,out} - y_{O,out} \cdot x_{C,out})}{x_{C,out} - x_{C,in}} \tag{6}$$

or more specific to the gas analysis equipment working on molecular species:

$$\dot{m}_{OC} = \frac{\begin{aligned}&\dot{m}_{Gas,in}[\frac{W_C}{W_{CO_2}} y_{CO_2,in} - \\ &(y_{O_2,in} + \frac{W_{O_2}}{W_{CO_2}} y_{CO_2,in}) \cdot x_{C,out}] - \\ &\dot{m}_{Gas,out}[\frac{W_C}{W_{CO_2}} y_{CO_2,out} - \\ &(y_{O_2,out} + \frac{W_{O_2}}{W_{CO_2}} y_{CO_2,out}) \cdot x_{C,out}]\end{aligned}}{x_{C,out} - x_{C,in}} \tag{7}$$

with oxygen as main species specific to the gas analysis equipment:

$$\dot{m}_{OC} = \frac{\dot{m}_{Gas,in}(y_{O_2,in} + \frac{W_{O_2}}{W_{CO_2}} y_{CO_2,in}) - \dot{m}_{Gas,out}(y_{O_2,out} + \frac{W_{O_2}}{W_{CO_2}} y_{CO_2,out})}{x_{O,out} - x_{O,in}} \tag{8}$$

Where W is the molar mass of the species, and $\dot{m}_{OC}$ is the OC flux in the reduced state of the process. The additional term results from the fact that oxygen is transported as part of carbon dioxide and reactions between the transported carbon and the provided oxygen. As oxygen is incorporated into the OC flux $\dot{m}_{OC}$, it has to be accounted for in the case of the carbon balance, whereas carbon is not part of the OC so Eq. (3) simplifies.

For the carbon based balance a suitable reference state for x_C is the carbon free oxygen carrier, while for the oxygen based balance the input concentration $x_{O,in}$ is a better reference state. The consequence

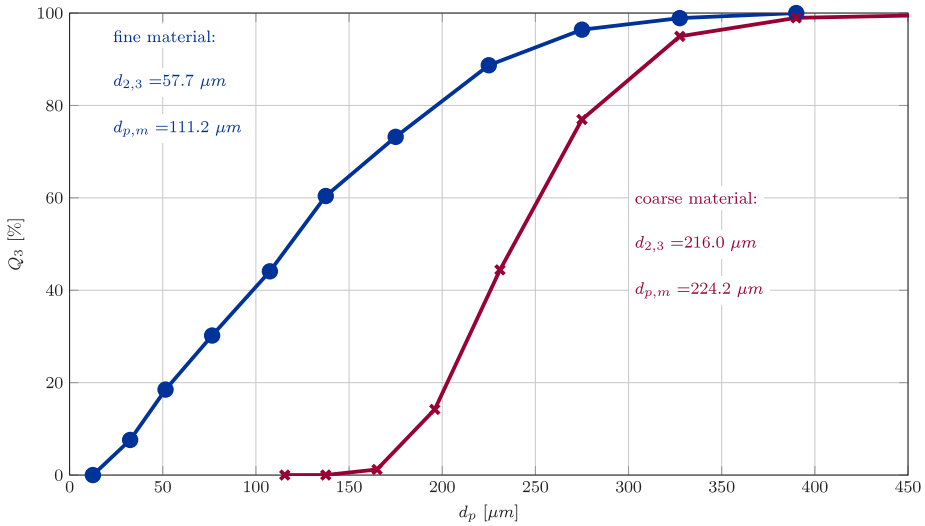

Fig. 3. Particle size distribution of the ilmenite used as oxygen carrier material during experiments.

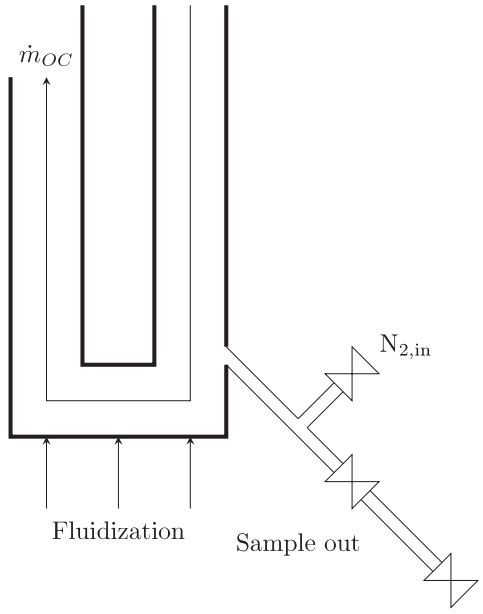

Fig. 4. Simplified schematic of the sampling setup.

of choosing $x_{O,in} = 0$ is a reference state which is dependent on the sample point and varies with the sample taken whereas it is constant for the carbon case.

As oxidation of char is favoured over OC oxidation [36–38], $x_{C,out}$ should be zero and the equation simplifies accordingly. However, during experiments the transport of a small amount of unconverted carbon from FR towards AR is observed, so the AR-outlet sample has to be analysed for carbon content.

Based on Eqs. (7) and (8) and the measurement uncertainties (Table 2), the propagated uncertainties of $\dot{m}_{OC}$ is calculated as described in Appendix A.2.2.

3.2. 1 MW_{th} pilot plant operation

The experimental data result from an experimental test campaign using the 1 MW_{th} CLG pilot plant at Technical University of Darmstadt.

Table 2
Values used for the estimation of the uncertainty (partially from [13]).

	Uncertainty	Unit
$\dot{m}_{Gas,in}$	30	kg h^{-1}
$\dot{m}_{Gas,out}$	30	kg h^{-1}
$y_{O_2,in}$	0,009	
$y_{CO_2,in}$	0,009	
$y_{O_2,out}$	0,009	
$y_{CO_2,out}$	0,009	
$x_{C,in}$	0,0005	
$x_{C,out}$	0,0001	
m_{scale}	1×10^{-10}	kg

The experiments were carried out with pine forest residue as feedstock (analysis in Table 1). Ilmenite with two different PSDs was used as OC material with the PSDs given in Fig. 3. The initial filling of the reactor system (approx. 1000 kg) was done with the coarse material and the make up was also the coarse material. During a period of two days fine ilmenite was used as makeup to increase the solid entrainment from the reactors and thus the solid flux between the reactors to decrease the temperature difference ΔT between the reactors and improve process performance.[2] During the operation of the pilot plant, various operational states of CLC, CLG with propane co-firing in the AR, and autothermal CLG were investigated. Fluidization of the reactor coupling elements was with either N_2 or CO_2, and the distribution of the streams on the AR and FR output streams was analysed. The carbon and oxygen content of all streams is added to the gas input stream for the calculation accordingly.

All stream data used for the calculation of the solid circulation is averaged for a period of 20 min before the sample time to gain the mean mass flows and gas compositions.

3.3. Sampling procedure

The samples were taken from the standpipe of the two loop seals, where a sampling setup according to Fig. 4 was used. In order to ensure

[2] Previous experiments showed high material losses of the fine ilmenite [28, 29]. Additionally the coarse material required no drying prior to usage, resulting in significantly lowered cost. During experiments it was discovered that the required solid circulation could not be reached with the coarse material. Therefore the bed material was gradually replaced with the fine material.

Fig. 5. Set of Samples from air reactor (left) and fuel reactor (right).

samples representing the current process state, the sampling tube was flushed with nitrogen to remove all material in the sampling tube and replace it with new material. The process was observed via infra-red thermometer and was deemed successful when temperatures of 300 °C on the outside were reached. The sample was then discharged from the loop seal via ball valves into a sealed vessel where it was left for cool down for two hours in order to prevent reaction with air oxygen. Afterwards the sample was removed from the system.

It should be noted, that the sample is taken from the outside of the U-shape of the loop seals while most of the solid transport happens on the inside of the U-shape. In fact, depending on loop seal operation a significant zone of stagnant particles has been observed in other units [39]. Therefore, a significant amount of time has to be operated in a steady state for the samples to be truly representative of the operational state. However, the exact time needed is unknown. Nonetheless, under the assumption that the flushing of the sampling setup is successful in removing any stagnant particle zones, the time required in steady-state operation for a representative sample should be in the range required for the whole inventory to cycle once through the system. For the 1 MW_{th} CLG pilot plant with an OC inventory of 1000 kg the time is 4 min to 10 min. Moreover, it is unknown if accumulation of carbon occurs inside the LS or whether the material density influences the distribution inside the LS and thus the representative nature of the samples with regard to the carbon content. Either accumulation or maldistribution might cause a systematic sampling error for the carbon fraction. For the oxygen only the stagnant zones might cause errors, as the oxygen is transported inside the OC lattice structure. However, the nitrogen-flushing during the sampling procedure mitigates errors by stagnant zones.

A typical pair of samples is shown in Fig. 5 where the coarse particles consisting of partially converted feedstock pellets is visible. During the pilot tests the loop seals were sampled over 30 times with a typical sample mass of 0.4 kg to 1.5 kg. Some samples are not considered during the analysis as the sampled mass was below 0.4 kg which is not deemed enough as it indicates a clogged sampling setup and it can therefore not be guaranteed that the sample is representative. All other samples are considered representative for the loop seal and that the actual sample mass has no influence on the accuracy of the method as only small fractions are used for the determination of carbon and oxygen content. Additionally, one sample was discarded as the temperature rise on the sampling setup could not be detected before discharging the material into the sealed sampling container. Therefore the material sampled is at least partially from a previous operating point.

3.4. Sample preparation and analysis

For the analysis of the carbon content the samples were first classified into two particle fractions using a 400 µm sieve. The coarse fraction (containing the majority of the transported carbon) was then crushed to a fine dust in a mortar to be able to process it via a commercially available elemental analysis system (Elementar vario MACRO cube in CHNS setup). The finer fraction was processed in the same system without further preparation. Each fraction was analysed in triplicate with a sample mass of 50 mg using a method providing sufficient oxygen for full oxidation of the carbon and OC material.

From theoretical considerations the carbon content x_c should not exceed 0.5 wt. – % in the FR samples. All samples where x_c exceeds a threshold of 2 wt. – % have therefore been discarded.

For the oxygen balance x_O was determined by oxidizing a sample mass of approx. 5 g in a laboratory oven with the mass being determined before (m_s) and after (m_e) oxidation. The output oxygen fraction is then determined to be[3]:

$$x_{O,out} = \frac{m_{s,out} m_{e,in}}{m_{e,out} \cdot m_{s,in}} - 1 \tag{9}$$

while the input fraction is always zero. The masses m_s have to be corrected for their carbon content x_c which results in a weight loss during oxidation giving:

$$m_s = \frac{m_{s,real}}{1 - x_c}$$

3.5. Evaluation of measurement method

Based on the described method and the experimental setup the evaluation of the proposed method to calculate the solids flux can only be done during hot operation, as it needs reacting material. However, determining its accuracy is difficult as no good reference method exists. Nonetheless, the plausibility of the values obtained can be checked using results from heat and mass balances used for the design of the experimental facility [13] and by correlation with a quantity known to be directly influenced by the global solid circulation, i.e. the temperature difference between the AR and FR. The higher the solid circulation the smaller the temperature difference between the reactors. The reactor setup (Fig. 2) is done in a way that all material discharged from the

[3] Details in Appendix A.1.1.

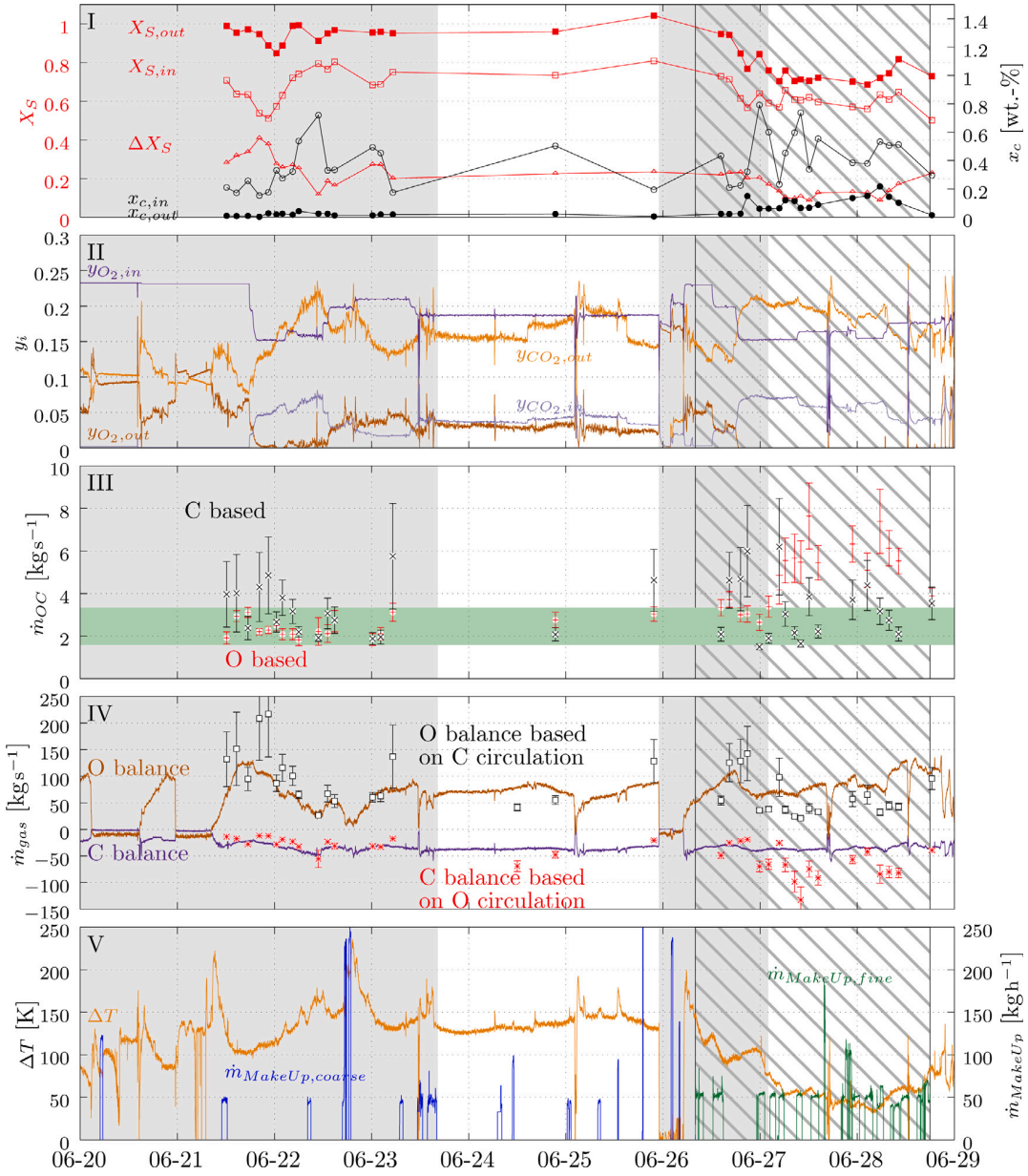

Fig. 6. Experimental results form chemical looping tests in the 1 MW_{th} range. I: Oxidation degree X_S and carbon content x_c of the collected samples. II: Composition of air reactor gas streams. III: Solid circulation using this papers method, the green region marks the range assumed during the design of the experimental facility [13]. IV: Oxygen and carbon balance from online measurement and from solid circulation and sample composition. V: Temperature difference between air and fuel reactor and oxygen carrier make up stream. Grey background: Periods with major operational adjustments to optimize the process. Patterned background: Period with finer bed material and air reactor operation in oxygen deficient atmosphere.

FR is transported towards the AR and therefore equal to the solid circulation. Hence, the solid circulation should show a correlation to FR gas velocity. Moreover, the calculation is done via the carbon balance and via the oxygen balance giving an indication if the carbon is sampled correctly. If both calculations yield the same result the carbon content is sampled representatively and can be used, otherwise the oxygen based value should be preferred.

4. Results and discussion

The carbon content x_c and the oxidation degree X_S in the valid samples as analysed is depicted in Fig. 6, plot I. It shows two distinct regions for the AR samples in terms of carbon content $x_{c,out}$ and oxidation degree $X_{S,out}$. At the start there is very low carbon content in these samples caused by the operation of the AR with excess oxygen and $X_{S,out}$ is close to unity. In the later part (indicated by the patterned background) the AR was operated in an oxygen deficient state as described by [11] which leads to an incomplete conversion of the carbon transported from the FR into the AR and to a reduction in X_S. Additionally the fine material was used as OC make up during the later part.

The data for the relevant reactor state is given in Fig. 6, plot II - V and shows the composition of the reactor inlet and outlet gas (II), the solid circulation as calculated by the method presented in Section 2 (III), the oxygen uptake and carbon release inside the AR based on the balance equations of the streams entering and leaving the reactor (IV),

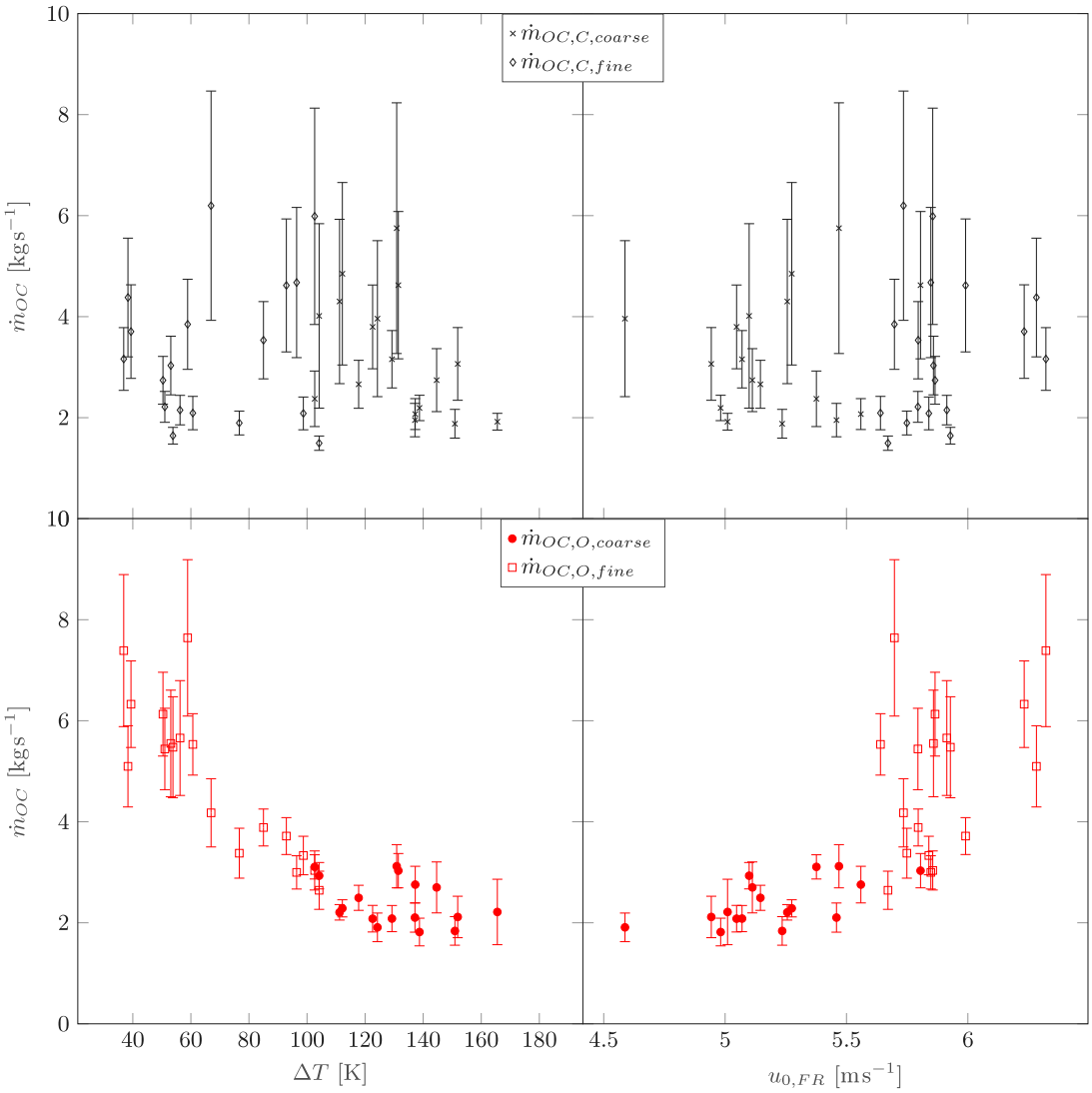

Fig. 7. Solid Circulation over Temperature Difference and fuel reactor gas velocity.

and the temperature difference ΔT between AR and FR with the OC make up stream fed into the reactor (V). The expected range of solid circulation $\dot{m}_{OC}$=1.58 kg s^{-1} to 3.33 kg s^{-1} from the design phase of the experimental facility [13] is indicated in Fig. 6, plot III by the green region.

It can be recognized from the AR gas composition (II) that there are many samples taken during times where major changes in gas composition occur. These are caused by adjustments made to various operation parameters to optimize the CLG process (corresponding times are indicated by the grey background). Here fluctuation of the calculated solid circulation between the two reactors is expected, as the solid circulation is impacted by the adjustments. However, these changes occur over time scales in the range of multiple hours, which is much longer than the required time for the oxygen carrier to cycle through the system, making the method applicable to the data. There exist two longer operation periods where only minor adjustment were performed by the plant operators and where the calculation should yield values with fluctuations not exceeding the uncertainty. However, the high fluctuation of the carbon based calculation Fig. 6, plot III suggests non representative carbon samples. The oxygen based calculation yields results which fall into the expected range of solid circulation [13] and do not fluctuate as much between consecutive samples. It can be asserted, that during the first phases all except one of the measurements are in the expected region. Nonetheless, the outlier was sampled during a system restart with very low circulation and FR gas velocity (see also Fig. 7) and is therefore likely to be correct. In both plots (II & III) the two distinct modes of operation can also be seen. In plot II, the later part – the oxygen deficient state of the AR – is defined by $y_{O_2,out} = 0$ while in plot III there is a significant increase in oxygen based calculated solid circulation $\dot{m}_{OC}$.

The carbon and oxygen balance in Fig. 6, plot IV shows the oxygen uptake and carbon release inside the AR. However, when using the carbon based solid circulation and the change ΔX_S from the samples to calculate the oxygen uptake it does match the uptake from the gas flows inside the uncertainty range only for very few samples. This is also indicative of non representative carbon sampling. As such, the other direction – using the oxygen based solid circulation and the change Δx_c from the samples to calculate the carbon release – does neither match the gas phase calculation.

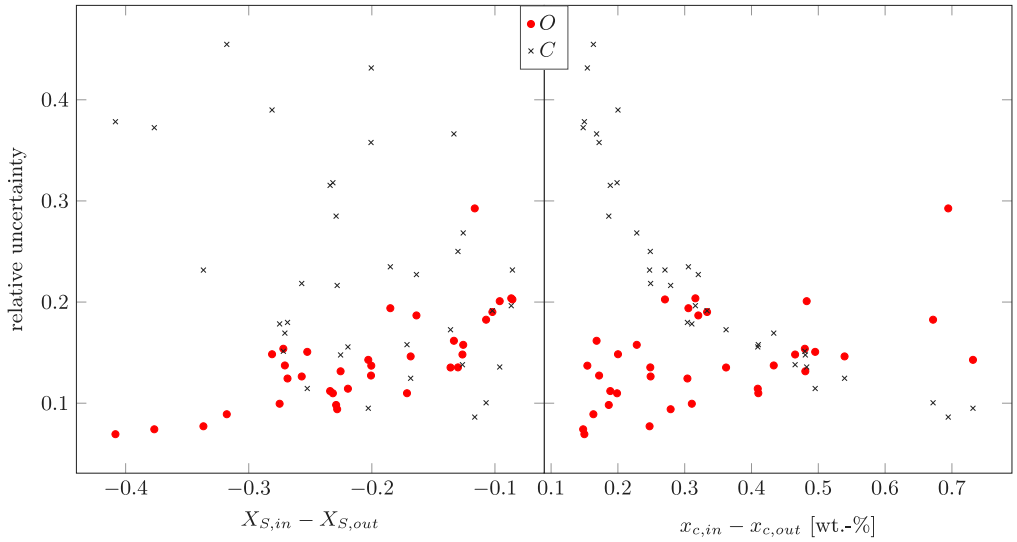

Fig. 8. Relative uncertainty over the difference in the transported species in input and output sample.

In Fig. 6, plot V the temperature difference ΔT between the reactors is given together with the OC make up feed rate $\dot{m}_{OC}$. The feed of coarse material is indicated in blue, while the fine material is red. Again, the two operational states are clearly visible in the plot as there is a decrease in temperature difference between the reactors as soon as the finer material is fed to the system. The total make up of coarse material fed to the reactor system over the period of 152 h depicted is 932 kg with an average feed rate of $\dot{m}_{OC} = 6.1\,\mathrm{kg\,h^{-1}}$. In contrast, the total make up of fine material is 1422 kg over 58 h at an average feed rate of $\dot{m}_{OC} = 24.5\,\mathrm{kg\,h^{-1}}$ replacing the inventory. The removal of bed material is not depicted here.

During the period where the fine OC material was used for make up (indicated by patterned background) the measured solid circulation increases and exceeds the expected range (III). Moreover, when looking at the circulation against the temperature difference between the reactors and the FR gas velocity (Fig. 7) the difference is much smaller with fine OC than with the coarse OC also indicative of the expected and measured higher circulation. The carbon based calculation shows none of the expected trends, further indication that carbon sampling inside the loop seals is not representative. The experimental temperature difference is smaller than the $\Delta T = 100\,\mathrm{K}$ assumed during the design, which is also indicative that the observed solid circulation which is higher than the one assumed during design is true. Moreover, the finer OC material leads to a much higher material discharge from the reactors allowing for a higher solid circulation and thus smaller ΔT which also gives credibility to the measured data. The higher solid circulation also corresponds to higher FR gas velocity as shown in Fig. 7. Therefore, it can be concluded the method gives qualitatively correct and likely also quantitative reliable results when oxygen is used.

Regarding the calculated uncertainty it is clear from Eqs. (7) and (8) that the very small fraction of transported carbon or oxygen during CLG leads to a comparatively high uncertainty, especially when there is very low carbon or high oxygen content in the input sample. Furthermore, as the oxygen transported is in the range 0.6 wt. − % to 1.4 wt. − % whereas the carbon fraction is in the range 0.1 wt. − % to 0.8 wt. − %, uncertainties of the oxygen case based calculation will be lower. The relative uncertainty is depicted in Fig. 8 over the difference of inlet and outlet composition of the transported species ΔX_S and Δx_c. It is immediately visible that the uncertainty of the carbon based calculation is higher than from the oxygen based case. Additionally the oxygen based calculation features lower uncertainty for a higher change in oxidation degree X_S and for lower carbon slip, while the uncertainty of the carbon based calculation shows only the expected dependency on carbon slip where higher carbon slip results in lower uncertainty.

As oxygen is transported inside the OC lattice structure as part of the particle and not as a separate particle – like carbon – it is the better species to use for the calculation. From the evolution of the uncertainty it can be supposed that the method is likely to give better results if the fraction of the transported and balanced species is higher (e.g. with CO_2 in carbonate looping process). Overall the uncertainty from CLG pilot testing is below 20 % using the more reliable species of oxygen which is an improvement when compared to existing methods.

The main issue with the presented data is the question of the representative nature of the samples taken from the loop seals. There is a clear deviation between the carbon based and oxygen based solid flux calculation (Fig. 6, IV), and the carbon based results do not show the expected trends (Fig. 7). Thus, it can be asserted that the sampling of the carbon is not representative, which makes the overall carbon based calculation invalid for the presented data. The oxygen based calculation does not suffer from this problem as it requires correction only for the carbon residing in the sample and is not dependent on the correct sampling of the transported carbon. Here, the remaining issue are regions without material transport inside the loop seal which can potentially influence the sample. However, this is mitigated by the N_2 flushing of the sample line. Both issues can be resolved with taking samples at a location where the samples would be representative, e.g. the down comer pipes below the cyclones.

5. Conclusions

A new method for the calculation of the solid circulation in dual fluidized bed reactor systems has been developed and tested in CLG experiments in the 1 MW_{th} range. It utilizes online measurement of gas flows and compositions of one reactor in combination with balance equations and compositions of solid samples.

- The method can be applied to hot reactor systems without breaking the loop and relies on measurement equipment already required for system control requiring only additional solid sample analysis. The sample point locations must ensure sample compositions representative for the circulated solids.
- The method does not impact reactor hydrodynamic or chemistry in any way.

- For species transported as part of the circulating material lattice structure the time required for steady-state operation is smaller than for species transported outside the lattice structure as separate particles. The actual time depends on reactor size and bed material inventory and lies in the time range required for the bed material inventory to be cycled through the system once.
- Species which are transported as part of the solid lattice should be preferred over species transported in separate particles as it reduces the likelihood of sampling errors.
- The solid circulation determined by the method fluctuates inside the range of the propagated uncertainty for steady-state operation.
- The uncertainty of the method reduces with increasing fraction of the transported and balanced species. The accuracy of solid flux measurement is – depending on the transported species – better than with other available methods. It is below 20 % for the presented experimental data with a species which comprises of about 0.6 wt. – % to 1.4 wt. – % of the solids flux.

CRediT authorship contribution statement

Falko Marx: Conceptualization, Methodology, Investigation, Software, Writing – original draft, Writing – review & editing, Visualization. **Paul Dieringer:** Investigation, Software, Writing – review & editing. **Jochen Ströhle:** Writing – review & editing, Project administration, Funding acquisition. **Bernd Epple:** Supervision, Funding acquisition.

Declaration of competing interest

The authors declare that they have no known competing financial interests or personal relationships that could have appeared to influence the work reported in this paper.

Data availability

Data will be made available on request.

Funding

This work has received funding of the European Union's Horizon 2020-Research and Innovation Framework Programme under grant agreement No. 817841 (Chemical Looping gasification foR sustainAble production of biofuels — CLARA). The content of this work reflects only the author's view, and the European Commission is not responsible for any use that may be made of the information it contains.

Appendix A. Detailed equations

A.1. General equations

$$0 = x_{i,in}\cdot\dot{m}_{S,in} - x_{i,out}\cdot\dot{m}_{S,out} + y_{i,in}\dot{m}_{gas,in} - y_{i,out}\dot{m}_{gas,out} \tag{A.1}$$

$$0 = \dot{m}_{S,in} - \dot{m}_{S,out} + \sum_{j\neq i} y_{j,in}\cdot\dot{m}_{Gas,in} - \sum_{j\neq i} y_{j,out}\cdot\dot{m}_{Gas,out} \tag{A.2}$$

$$\begin{aligned}\Delta\dot{m}_S &= -\dot{m}_{S,in} + \dot{m}_{S,out} \\ &= \sum_{j\neq i} y_{j,in}\cdot\dot{m}_{Gas,in} - \sum_{j\neq i} y_{j,out}\cdot\dot{m}_{Gas,out}\end{aligned} \tag{A.3}$$

$$\begin{aligned}0 = {} & x_{i,in}\cdot\dot{m}_{S,in} - x_{i,out}\left(\dot{m}_{S,in} + \sum_{j\neq i} y_{j,in}\cdot\dot{m}_{Gas,in} - \sum_{j\neq i} y_{j,out}\cdot\dot{m}_{Gas,out}\right) \\ & + y_{i,in}\dot{m}_{gas,in} - y_{i,out}\dot{m}_{gas,out} \\ = {} & \dot{m}_{S,in}(x_{i,in} - x_{i,out}) - x_{i,out}\left(\sum_{j\neq i} y_{j,in}\cdot\dot{m}_{Gas,in} - \sum_{j\neq i} y_{j,out}\cdot\dot{m}_{Gas,out}\right) \\ & + y_{i,in}\dot{m}_{gas,in} - y_{i,out}\dot{m}_{gas,out} \\ = {} & \dot{m}_{S,in}(x_{i,in} - x_{i,out}) \\ & + \dot{m}_{Gas,in}(y_{i,in} - \sum_{j\neq i} y_{j,in}\cdot x_{i,out}) \\ & - \dot{m}_{gas,out}(y_{i,out} - \sum_{j\neq i} y_{j,out}\cdot x_{i,out})\end{aligned} \tag{A.4}$$

$$\dot{m}_S = \frac{\dot{m}_{Gas,in}(y_{i,in} - \sum_{j\neq i} y_{j,in}\cdot x_{i,out}) - \dot{m}_{Gas,out}(y_{i,out} - \sum_{j\neq i} y_{j,out}\cdot x_{i,out})}{x_{i,out} - x_{i,in}} \tag{A.5}$$

A.1.1. x_O from scale and oven

$$x_{O,in} = \frac{m_{s,in}}{m_{s,in}} - 1 = 0 \tag{A.6}$$

$$x_{O,max} = \frac{m_{e,in}}{m_{s,in}} - 1 \tag{A.7}$$

$$x_{O,out} = \frac{m_{s,out}}{m^f_{s,out}} - 1 \tag{A.8}$$

$$m_{e,in} = (1 + x_{O,max})m_{s,in} \tag{A.9}$$

$$m_{e,out} = (1 + x_{O,max})m^f_{s,out} \tag{A.10}$$

$$m^f_{s,out} = \frac{m_{e,out}}{1 + x_{O,max}} \tag{A.11}$$

$$= \frac{m_{e,out}}{1 + \frac{m_{e,in}}{m_{s,in}} - 1} \tag{A.12}$$

$$= \frac{m_{e,out}}{\frac{m_{e,in}}{m_{s,in}}} \tag{A.13}$$

$$= m_{e,out}\cdot\frac{m_{s,in}}{m_{e,in}} \tag{A.14}$$

It follows:

$$x_{O,out} = \frac{m_{s,out}}{m_{e,out}\cdot\frac{m_{s,in}}{m_{e,in}}} - 1 \tag{A.15}$$

$$= \frac{m_{s,out}m_{e,in}}{m_{e,out}\cdot m_{s,in}} - 1 \tag{A.16}$$

Partial derivatives:

$$\frac{\partial x_{O,out}}{\partial m_{s,out}} = \frac{m_{e,in}}{m_{e,out}\cdot m_{s,in}} \tag{A.17}$$

$$\frac{\partial x_{O,out}}{\partial m_{e,out}} = -\frac{m_{s,out}m_{e,in}}{m^2_{e,out}\cdot m_{s,in}} \tag{A.18}$$

$$\frac{\partial x_{O,out}}{\partial m_{s,in}} = -\frac{m_{s,out}m_{e,in}}{m_{e,out}\cdot m^2_{s,in}} \tag{A.19}$$

$$\frac{\partial x_{O,out}}{\partial m_{e,in}} = \frac{m_{s,out}}{m_{e,out}\cdot m_{s,in}} \tag{A.20}$$

A.2. Derivatives for the calculation of the propagation of uncertainties

A.2.1. Derivatives for oxygen

$$\frac{\partial\dot{m}_{OC}}{\partial\dot{m}_{Gas,in}} = \frac{y_{O2,in} + \frac{W_{O_2}}{W_{CO_2}}y_{CO_2,in}}{x_{O,out} - x_{O,in}} \tag{A.21}$$

Table B.7
Results for the solid circulation including uncertainty from pilot testing. The rows with grey background are taken during reactor restart and shutdown.

Time	Label	Sample mass		$x_{c,in}$	$x_{c,out}$	$X_{S,out}$	$X_{S,in}$	Carbon			Oxygen			ΔT
		AR	FR					$\dot{m}_{OC}$	$\Delta\dot{m}_{OC}$	$\frac{\Delta\dot{m}_{OC}}{\dot{m}_{OC}}$	$\dot{m}_{OC}$	$\Delta\dot{m}_{OC}$	$\frac{\Delta\dot{m}_{OC}}{\dot{m}_{OC}}$	
		kg	kg	wt. – %	wt. – %			kg s^{-1}	kg s^{-1}		kg s^{-1}	kg s^{-1}		K
20.06. 22:00	CLA2-S-18	0.83	1.51	0,12	0,00	0,74	1,02	4,99	3,36	0,67	3,01	0,31	0,10	86
21.06. 09:54	CLA2-S-22	0.76	1.24	0,50	0,00	0,79	0,97	1,39	0,27	0,19	0,79	0,43	0,55	190
21.06. 12:11	CLA2-S-24	0.84	1.19	0,21	0,01	0,71	0,99	3,96	1,54	0,39	1,91	0,28	0,15	124
21.06. 14:38	CLA2-S-26	0.85	1.39	0,17	0,01	0,64	0,95	4,01	1,83	0,45	2,93	0,26	0,09	104
21.06. 17:27	CLA2-S-28	1.46	1.41	0,26	0,01	0,63	0,97	2,37	0,55	0,23	3,11	0,24	0,08	103
21.06. 20:16	CLA2-S-31	0.43	1.53	0,15	0,00	0,54	0,95	4,30	1,63	0,38	2,21	0,15	0,07	111
21.06. 22:30	CLA2-S-33	1.28	1.06	0,18	0,03	0,51	0,89	4,85	1,81	0,37	2,29	0,17	0,07	112
22.06. 00:30	CLA2-S-35	0.67	0.67	0,33	0,02	0,57	0,85	2,66	0,47	0,18	2,49	0,25	0,10	118
22.06. 01:58	CLA2-S-38	1.31	1.44	0,27	0,03	0,63	0,89	3,80	0,83	0,22	2,08	0,26	0,13	123
22.06. 04:30	CLA2-S-40	0.78	1.43	0,32	0,02	0,72	0,99	3,16	0,57	0,18	2,08	0,26	0,12	129
22.06. 06:00	CLA2-S-42	0.99	1.29	0,54	0,04	0,74	0,99	2,19	0,25	0,11	1,82	0,27	0,15	139
22.06. 10:52	CLA2-S-45	1.05	1.04	0,72	0,03	0,79	0,91	1,92	0,17	0,09	2,21	0,65	0,29	166
22.06. 13:08	CLA2-S-47	1.21	0.60	0,33	0,02	0,76	0,95	3,06	0,72	0,23	2,12	0,41	0,19	152
22.06. 14:52	CLA2-S-51	1.19	0.91	0,33	0,01	0,80	0,97	2,74	0,62	0,23	2,70	0,50	0,19	145
23.06. 00:15	CLA2-S-53	1.58	1.16	0,49	0,01	0,68	0,96	1,88	0,28	0,15	1,84	0,28	0,15	151
23.06. 02:15	CLA2-S-54	1.19	1.43	0,45	0,02	0,69	0,96	1,95	0,33	0,17	2,10	0,29	0,14	137
23.06. 05:15	CLA2-S-59	1.37	0.78	0,17	0,02	0,75	0,95	5,75	2,48	0,43	3,12	0,43	0,14	131
24.06. 21:25	CLA2-S-80	1.41	0.93	0,50	0,02	0,73	0,96	2,07	0,31	0,15	2,76	0,36	0,13	137
25.06. 21:45	CLA2-S-82	1.20	1.04	0,19	0,01	0,81	1,04	4,62	1,46	0,32	3,03	0,34	0,11	131
26.06. 14:20	CLA2-S-92	1.01	1.21	0,43	0,02	0,73	0,95	2,08	0,32	0,16	3,33	0,38	0,11	99
26.06. 16:24	CLA2-S-96	1.08	0.98	0,21	0,02	0,71	0,94	4,62	1,32	0,28	3,72	0,37	0,10	93
26.06. 19:10	CLA2-S-98	0.90	0.76	0,22	0,03	0,61	0,85	4,68	1,49	0,32	3,00	0,33	0,11	96
26.06. 20:51	CLA2-S-100	1.48	1.25	0,32	0,15	0,57	0,77	5,99	2,14	0,36	3,04	0,39	0,13	103
26.06. 23:50	CLA2-S-102	1.42	1.40	0,79	0,06	0,64	0,84	1,50	0,14	0,10	2,64	0,38	0,14	104
27.06. 02:07	CLA2-S-104	1.37	1.45	0,60	0,06	0,59	0,76	1,89	0,24	0,12	3,38	0,49	0,15	77
27.06. 04:45	CLA2-S-106	1.28	1.31	0,23	0,06	0,57	0,70	6,20	2,27	0,37	4,18	0,68	0,16	67
27.06. 06:14	CLA2-S-110	1.39	1.35	0,45	0,12	0,66	0,76	3,03	0,58	0,19	5,55	1,06	0,19	53
27.06. 08:31	CLA2-S-112	1.29	1.36	0,60	0,11	0,61	0,70	2,15	0,29	0,14	5,66	1,14	0,20	56
27.06. 10:02	CLA2-S-114	1.00	1.31	0,74	0,07	0,61	0,71	1,64	0,17	0,10	5,48	1,00	0,18	54
27.06. 12:08	CLA2-S-117	1.33	1.31	0,34	0,07	0,62	0,71	3,85	0,89	0,23	7,64	1,55	0,20	59
27.06. 14:20	CLA2-S-121	0.97	1.39	0,55	0,09	0,60	0,72	2,21	0,31	0,14	5,44	0,81	0,15	51
27.06. 22:50	CLA2-S-126	1.42	1.34	0,38	0,14	0,57	0,70	3,70	0,93	0,25	6,33	0,86	0,14	39
28.06. 02:30	CLA2-S-130	1.08	1.15	0,38	0,15	0,56	0,69	4,38	1,18	0,27	5,10	0,80	0,16	38
28.06. 05:37	CLA2-S-132	1.40	1.35	0,53	0,22	0,63	0,72	3,16	0,62	0,20	7,39	1,51	0,20	37
28.06. 07:51	CLA2-S-136	1.25	1.16	0,51	0,14	0,61	0,74	2,74	0,47	0,17	6,13	0,83	0,14	50
28.06. 10:14	CLA2-S-142	0.87	1.30	0,51	0,10	0,65	0,82	2,09	0,33	0,16	5,53	0,61	0,11	61
28.06. 18:26	CLA2-S-145	0.88	1.13	0,29	0,02	0,50	0,73	3,53	0,76	0,22	3,89	0,37	0,09	85
28.06. 21:46	CLA2-S-149	0.66	0.57	0,92	0,19	0,79	0,86	1,38	0,13	0,10	3,61	1,14	0,32	109

$$\frac{\partial \dot{m}_{OC}}{\partial \dot{m}_{Gas,out}} = \frac{-(y_{O2,out} + \frac{W_{O_2}}{W_{CO_2}} y_{CO_2,out})}{x_{O,out} - x_{O,in}} \tag{A.22}$$

$$\frac{\partial \dot{m}_{OC}}{\partial y_{CO_2,in}} = \frac{\dot{m}_{Gas,in} \frac{W_{O_2}}{W_{CO_2}}}{x_{O,out} - x_{O,in}} \tag{A.23}$$

$$\frac{\partial \dot{m}_{OC}}{\partial y_{CO_2,out}} = -\frac{\dot{m}_{Gas,out} \frac{W_{O_2}}{W_{CO_2}}}{x_{O,out} - x_{O,in}} \tag{A.24}$$

$$\frac{\partial \dot{m}_{OC}}{\partial y_{O_2,in}} = \frac{\dot{m}_{Gas,in}}{x_{O,out} - x_{O,in}} \tag{A.25}$$

$$\frac{\partial \dot{m}_{OC}}{\partial y_{O_2,out}} = -\frac{\dot{m}_{Gas,out}}{x_{O,out} - x_{O,in}} \tag{A.26}$$

$$\frac{\partial \dot{m}_{OC}}{\partial x_{O,in}} = \frac{\dot{m}_{Gas,in}(y_{O2,in} + \frac{W_{O_2}}{W_{CO_2}} y_{CO_2,in}) - \dot{m}_{Gas,out}(y_{O2,out} + \frac{W_{O_2}}{W_{CO_2}} y_{CO_2,out})}{(x_{O,out} - x_{O,in})^2} \tag{A.27}$$

$$\frac{\partial \dot{m}_{OC}}{\partial x_{O,out}} = -\frac{\dot{m}_{Gas,in}(y_{O2,in} + \frac{W_{O_2}}{W_{CO_2}} y_{CO_2,in}) - \dot{m}_{Gas,out}(y_{O2,out} + \frac{W_{O_2}}{W_{CO_2}} y_{CO_2,out})}{(x_{O,out} - x_{O,in})^2} \tag{A.28}$$

A.2.2. Derivatives for carbon

$$\frac{\partial \dot{m}_{OC}}{\partial \dot{m}_{Gas,in}} = \frac{y_{C,in} - y_{O,in} \cdot x_{C,out}}{x_{C,out} - x_{C,in}} \tag{A.29}$$

$$\frac{\partial \dot{m}_{OC}}{\partial \dot{m}_{Gas,out}} = \frac{y_{C,out} - y_{O,out} \cdot x_{C,out}}{x_{C,out} - x_{C,in}} \tag{A.30}$$

$$\frac{\partial \dot{m}_{OC}}{\partial y_{CO_2,in}} = \frac{\dot{m}_{Gas,in}(\frac{W_C}{W_{CO_2}} - \frac{W_{O_2}}{W_{CO_2}} x_{C,out})}{x_{C,out} - x_{C,in}} \tag{A.31}$$

$$\frac{\partial \dot{m}_{OC}}{\partial y_{CO_2,out}} = -\frac{\dot{m}_{Gas,out}(\frac{W_C}{W_{CO_2}} - \frac{W_{O_2}}{W_{CO_2}} x_{C,out})}{x_{C,out} - x_{C,in}} \tag{A.32}$$

$$\frac{\partial \dot{m}_{OC}}{\partial y_{O_2,in}} = -\frac{\dot{m}_{Gas,in} \cdot x_{C,out}}{x_{C,out} - x_{C,in}} \tag{A.33}$$

$$\frac{\partial \dot{m}_{OC}}{\partial y_{O_2,out}} = \frac{\dot{m}_{Gas,out} \cdot x_{C,out}}{x_{C,out} - x_{C,in}} \tag{A.34}$$

$$\frac{\partial \dot{m}_{OC}}{\partial x_{C,in}} = \frac{\dot{m}_{Gas,in}(\frac{W_C}{W_{CO_2}} y_{CO_2,in} - (y_{O2,in} + \frac{W_{O_2}}{W_{CO_2}} y_{CO_2,in}) \cdot x_{C,out}) - \dot{m}_{Gas,out}(\frac{W_C}{W_{CO_2}} y_{CO_2,out} - (y_{O2,out} + \frac{W_{O_2}}{W_{CO_2}} y_{CO_2,out}) \cdot x_{C,out})}{(x_{C,out} - x_{C,in})^2} \tag{A.35}$$

$$\frac{\partial \dot{m}_{OC}}{\partial x_{C,out}} = -\frac{\begin{array}{c}\dot{m}_{Gas,in}\left(\frac{W_C}{W_{CO_2}} y_{CO_2,in} - \right.\\ \left.(y_{O2,in} + \frac{W_{O_2}}{W_{CO_2}} y_{CO_2,in}) \cdot x_{C,in}\right) + \\ \dot{m}_{Gas,out}\left(\frac{W_C}{W_{CO_2}} y_{CO_2,out} - \right.\\ \left.(y_{O2,out} + \frac{W_{O_2}}{W_{CO_2}} y_{CO_2,out}) \cdot x_{C,in}\right)\end{array}}{(x_{C,out} - x_{C,in})^2} \quad \text{(A.36)}$$

Appendix B. Results from offline samples

See Table B.7.

References

[1] Larsson A, Gunnarsson I, Tengberg F. The GoBiGas project demonstration of the production of biomethane from biomass via gasification. 2018, http://dx.doi.org/10.13140/RG.2.2.27352.55043.

[2] Larsson A, Kuba M, Berdugo Vilches T, Seemann M, Hofbauer H, Thunman H. Steam gasification of biomass – typical gas quality and operational strategies derived from industrial-scale plants. Fuel Process Technol 2021;212:106609. http://dx.doi.org/10.1016/j.fuproc.2020.106609.

[3] Guo Q, Cheng Y, Liu Y, Jia W, Ryu H-J. Coal chemical looping gasification for syngas generation using an iron-based oxygen carrier. Ind Eng Chem Res 2014;53(1):78–86. http://dx.doi.org/10.1021/ie401568x.

[4] Samprón I, de Diego LF, García-Labiano F, Izquierdo MT, Abad A, Adánez J. Biomass chemical looping gasification of pine wood using a synthetic Fe2O3/Al2O3 oxygen carrier in a continuous unit. Bioresour Technol 2020;316:123908. http://dx.doi.org/10.1016/j.biortech.2020.123908.

[5] Huseyin S, Wei G-q, Li H-b, He F, Huang Z. Chemical-looping gasification of biomass in a 10 kWth interconnected fluidized bed reactor using Fe2O3/Al2O3 oxygen carrier. J Fuel Chem Technol 2014;42(8):922–31. http://dx.doi.org/10.1016/S1872-5813(14)60039-6.

[6] Wei G, He F, Huang Z, Zheng A, Zhao K, Li H. Continuous operation of a 10 kW_{th} chemical looping integrated fluidized bed reactor for gasifying biomass using an iron-based oxygen carrier. Energy Fuels 2015;29(1):233–41. http://dx.doi.org/10.1021/ef5021457.

[7] Ge H, Guo W, Shen L, Song T, Xiao J. Biomass gasification using chemical looping in a 25 kW th reactor with natural hematite as oxygen carrier. Chem Eng J 2016;286:174–83. http://dx.doi.org/10.1016/j.cej.2015.10.092.

[8] Ge H, Guo W, Shen L, Song T, Xiao J. Experimental investigation on biomass gasification using chemical looping in a batch reactor and a continuous dual reactor. Chem Eng J 2016;286:689–700. http://dx.doi.org/10.1016/j.cej.2015.11.008.

[9] Condori O, García-Labiano F, de Diego LF, Izquierdo MT, Abad A, Adánez J. Biomass chemical looping gasification for syngas production using ilmenite as oxygen carrier in a 1.5 kWth unit. Chem Eng J 2021;405:126679. http://dx.doi.org/10.1016/j.cej.2020.126679.

[10] Condori O, García-Labiano F, de Diego LF, Izquierdo MT, Abad A, Adánez J. Biomass chemical looping gasification for syngas production using LD slag as oxygen carrier in a 1.5 kWth unit. Fuel Process Technol 2021;222:106963. http://dx.doi.org/10.1016/j.fuproc.2021.106963.

[11] Dieringer P, Marx F, Alobaid F, Ströhle J, Epple B. Process control strategies in chemical looping gasification– a novel process for the production of biofuels allowing for net negative CO2 emissions. Appl Sci 2020;10(12):26. http://dx.doi.org/10.3390/app10124271.

[12] Samprón I, de Diego LF, García-Labiano F, Izquierdo MT. Optimization of synthesis gas production in the biomass chemical looping gasification process operating under auto-thermal conditions. Energy 2021;226:120317. http://dx.doi.org/10.1016/j.energy.2021.120317.

[13] Marx F, Dieringer P, Ströhle J, Epple B. Design of a 1 MWth pilot plant for chemical looping gasification of biogenic residues. Energies 2021;14(9):2581. http://dx.doi.org/10.3390/en14092581.

[14] Bhusarapu S, Fongarland P, Al-Dahhan M, Duduković M. Measurement of overall solids mass flux in a gas– solid circulating fluidized bed. Powder Technol 2004;148(2–3):158–71. http://dx.doi.org/10.1016/j.powtec.2004.09.007.

[15] Stollhof M, Penthor S, Mayer K, Hofbauer H. Estimation of the solid circulation rate in circulating fluidized bed systems. Powder Technol 2018;336:1–11. http://dx.doi.org/10.1016/j.powtec.2018.05.033.

[16] Fuchs J, Schmid J, Benedikt F, Mauerhofer A, Müller S, Hofbauer H. A general method for the determination of the entrainment in fluidized beds. Int J Multiphys 2018;12(4). http://dx.doi.org/10.21152/1750-9548.12.4.359.

[17] Liu X, Zhang M, Zhang S, Ding Y, Huang Z, Zhou T, et al. Measuring technologies for CFB solid circulation rate: A review and future perspectives. Energies 2022;15(2):417. http://dx.doi.org/10.3390/en15020417.

[18] Matsuda S. Measurement of solid circulation rate in a circulating fluidized bed. Powder Technol 2008;187(2):200–4. http://dx.doi.org/10.1016/j.powtec.2008.02.004.

[19] Medrano J, Nordio M, Manzolini G, van Sint Annaland M, Gallucci F. On the measurement of solids circulation rates in interconnected fluidized beds: Comparison of different experimental techniques. Powder Technol 2016;302:81–9. http://dx.doi.org/10.1016/j.powtec.2016.08.035.

[20] Ludlow JC, Monazam ER, Shadle LJ. Improvement of continuous solid circulation rate measurement in a cold flow circulating fluidized bed. Powder Technol 2008;182(3):379–87. http://dx.doi.org/10.1016/j.powtec.2007.06.031.

[21] Pang L, Shao Y, Geng C, Zhong W, Liu G, Liu L, et al. Measurement of solid mass flow rate by a non-intrusive microwave method. Powder Technol 2018;323:525–32. http://dx.doi.org/10.1016/j.powtec.2017.10.030.

[22] Guío-Pérez DC, Dietrich F, Ferreira Cala JN, Pröll T, Hofbauer H. Estimation of solids circulation rate through magnetic tracer tests. Powder Technol 2017;316:650–7. http://dx.doi.org/10.1016/j.powtec.2017.04.062.

[23] Rahman MH, Bi XT, Grace JR, Lim CJ. Measurement of solids circulation rate in a high-temperature dual fluidized bed pilot plant. Powder Technol 2017;316:658–69. http://dx.doi.org/10.1016/j.powtec.2017.01.073.

[24] Rahman MH, Bi XT, Grace JR, Lim CJ. Comparison of techniques for measuring CFB solids circulation rates at low and high temperatures. Powder Technol 2020;360:43–54. http://dx.doi.org/10.1016/j.powtec.2019.10.033.

[25] Rahman MH, Daniel L, Shah U, Bi X, Grace JR, Lim CJ. Estimation of solids circulation rate and char transfer rate from gasifier to combustor in a dual fluidized-bed pilot plant for biomass steam gasification. Particuology 2019;46:22–9. http://dx.doi.org/10.1016/j.partic.2019.03.004.

[26] Lu X, Li Y. Experimental study on an on-line measurement of high temperature circulating ash flux in a circulating fluidized bed boiler. J Therm Sci 2001;10(2):188–92. http://dx.doi.org/10.1007/s11630-001-0064-z.

[27] Linderholm C, Schmitz M, Lyngfelt A. Estimating the solids circulation rate in a 100-kW chemical looping combustor. Chem Eng Sci 2017;171:351–9. http://dx.doi.org/10.1016/j.ces.2017.05.025.

[28] Ohlemüller P, Busch J-P, Reitz M, Ströhle J, Epple B. Chemical-looping combustion of hard coal: Autothermal operation of a 1 MWth pilot plant. J Energy Res Technol 2016;138(4):042203. http://dx.doi.org/10.1115/1.4032357.

[29] Ohlemüller P, Ströhle J, Epple B. Chemical looping combustion of hard coal and torrefied biomass in a 1 MW th pilot plant. Int J Greenh Gas Control 2017;65:149–59. http://dx.doi.org/10.1016/j.ijggc.2017.08.013.

[30] Hilz J, Helbig M, Haaf M, Daikeler A, Ströhle J, Epple B. Long-term pilot testing of the carbonate looping process in 1 MWth scale. Fuel 2017;210:892–9. http://dx.doi.org/10.1016/j.fuel.2017.08.105.

[31] Haaf M, Peters J, Hilz J, Unger A, Ströhle J, Epple B. Combustion of solid recovered fuels within the calcium looping process – experimental demonstration at 1 MWth scale. Exp Therm Fluid Sci 2020;113:110023. http://dx.doi.org/10.1016/j.expthermflusci.2019.110023.

[32] Reitz M, Junk M, Ströhle J, Epple B. Design and operation of a 300 kW th indirectly heated carbonate looping pilot plant. Int J Greenh Gas Control 2016;54:272–81. http://dx.doi.org/10.1016/j.ijggc.2016.09.016.

[33] Hongrapipat J, Messner M, Henrich C, Koch M, Nenning L, Rauch R, et al. 1 MWel Prototype Dual Fluidised Bed Gasifier Fuelled with Renewable Energy Resources by Gussing Renewable Energy, Vol. 15.

[34] Larsson A, Israelsson M, Lind F, Seemann M, Thunman H. Using ilmenite to reduce the Tar yield in a dual fluidized bed gasification system. Energy Fuels 2014;28(4):2632–44. http://dx.doi.org/10.1021/ef500132p.

[35] Abad A, Adánez J, Cuadrat A, García-Labiano F, Gayán P, de Diego LF. Kinetics of redox reactions of ilmenite for chemical-looping combustion. Chem Eng Sci 2011;66(4):689–702. http://dx.doi.org/10.1016/j.ces.2010.11.010.

[36] Chen L. The direct solid–solid reaction between coal char and iron-based oxygen carrier and its contribution to solid-fueled chemical looping combustion. Appl Energy 2016;10. http://dx.doi.org/10.1016/j.apenergy.2016.09.085.

[37] Leion H, Mattisson T, Lyngfelt A. Solid fuels in chemical-looping combustion. Int J Greenh Gas Control 2008;2(2):180–93. http://dx.doi.org/10.1016/S1750-5836(07)00117-X.

[38] Song Q, Xiao R, Deng Z, Zhang H, Shen L, Xiao J, et al. Chemical-looping combustion of methane with CaSO4 oxygen carrier in a fixed bed reactor. Energy Convers Manage 2008;49(11):3178–87. http://dx.doi.org/10.1016/j.enconman.2008.05.020.

[39] Bareschino P, Solimene R, Chirone R, Salatino P. Gas and solid flow patterns in the loop-seal of a circulating fluidized bed. Powder Technol 2014;264:197–202. http://dx.doi.org/10.1016/j.powtec.2014.05.036.

3.4 Fourth Research Paper

Design and control concept of a 1 MW_{th} chemical looping gasifier allowing for efficient autothermal syngas production

Authors: Falko Marx, Paul Dieringer, Benjamin Michel, Jochen Ströhle, Bernd Epple
Journal: International Journal of Greenhouse Gas Control
Date: 2023-06-19
ISSN: 1750-5836
DOI: 10.1016/j.ijggc.2023.103929

International Journal of Greenhouse Gas Control 127 (2023) 103929

Contents lists available at ScienceDirect

International Journal of Greenhouse Gas Control

journal homepage: www.elsevier.com/locate/ijggc

Design and control concept of a 1 MW_{th} chemical looping gasifier allowing for efficient autothermal syngas production

Paul Dieringer *, Falko Marx, Benjamin Michel, Jochen Ströhle, Bernd Epple

Institute for Energy Systems and Technology, Technical University Darmstadt, Otto-Berndt-Str. 2, 64287 Darmstadt, Germany

ARTICLE INFO

Keywords:
Chemical looping
Biomass
Gasification
Process control
Pilot scale
Autothermal

ABSTRACT

Chemical looping gasification (CLG) is a novel gasification concept, allowing for the efficient production of a high calorific, N_2-free syngas with low tar content. Previous studies showed that the inherent process characteristics require a dedicated process control concept in order to allow for sufficient solid and thus heat transport between the two reactors (air and fuel reactor) of the gasification unit, while at the same time being able to accurately tailor the air-to-fuel equivalence ratio (λ), thus obtaining stable gasification conditions. To demonstrate its viability, a suitable control concept was implemented in the 1 MW_{th} modular pilot plant located at the Technical University Darmstadt. In this paper, results obtained during the first ever autothermal CLG operation, achieved in this unit using biomass pellets as the feedstock, are presented, highlighting important process fundamentals. It is demonstrated that the novel process control concept allows for an accurate control of λ in semi-industrial scale, while at the same time guaranteeing stable hydrodynamics and thus solid and heat transport between the air and fuel reactor, making it a suitable control concept for large-scale implementation. Moreover, it is demonstrated that the underlying phenomena of the CLG process lead to substantial system inertia, as the solid bed inventory of the gasifier acts as an oxygen storage during transient periods, evoked by changes in the air-to-fuel equivalence ratio.

1. Introduction

In light of the current challenges in terms of climate protection and energy transition, novel, sustainable and yet competitive processes and technologies in the energy, transport, and industry sector are urgently needed. Thus, innovative carbon-negative process chains for the production of 2nd generation biofuels are required (DIRECTIVE (EU) 2018). Here, one option under broad consideration is converting biogenic residues into a high-calorific syngas, before further treatment and fuel synthesis (Atsonios et al., 2020; Roshan Kumar et al., 2022).

Oxygen-blown gasifiers, allowing for the efficient production of a N_2-free syngas, thus facilitating its direct utilization in syntheses, have been widely researched, going back to the start of the last century (Higman and van der Burgt, 2008). With recent developments encouraging routes of valorizing residues (e.g. biomass, municipal waste, etc.) chemically, research interest in this field has been revived (Heinze et al., 2023; Langner et al., 2023). Apart from their maturity, the advantages of oxygen-blown gasifiers arise from the direct utilization of molecular oxygen in the gasification chamber, thus facilitating high reaction temperatures and excellent feedstock conversion. Therefore, cold gas efficiencies above 75% can be obtained, depending on the gasifier type and the utilized feedstock (Higman and van der Burgt, 2008).

A novel gasification technology, allowing for an efficient conversion of biomass residues into a high-calorific syngas, is the chemical looping gasification (CLG) process, illustrated in Fig. 1. Its major advantage is that the oxygen required for efficient feedstock conversion is supplied through the cyclic reduction and oxidation of an oxygen carrier (OC). Hence, CLG does not rely on a costly air separation unit, commonly required for oxygen-driven gasification processes. Moreover, despite air being used as the oxygen source in the gasification process, CLG allows for an efficient capturing of the CO_2 formed during the autothermal gasification step from the N_2-free product gas in the downstream syngas purification unit, thus allowing for net negative CO_2 emissions of the biomass-to-biofuel process chain (Nguyen et al., 2021; Huang et al., Oct. 2016; Huang et al., Jan. 2014; Ge et al., 2016a; Guo et al., 2014; Huang et al., Jul. 2013).

Initial advances in the CLG were mainly restricted to lab-scale investigations. Here, the CLG technology was investigated in batch (Huang et al., Jan. 2014; Huang et al., Jul. 2013; Xu et al., Nov. 2021) as well as continuous reactor setups (Huseyin et al., 2014; Acharya et al., 2009), operated as fixed bed (Yan et al., May 2020; Liu et al., Nov. 2019)

* Corresponding author.
E-mail address: paul.dieringer@est.tu-darmstadt.de (P. Dieringer).

https://doi.org/10.1016/j.ijggc.2023.103929
Received 19 January 2023; Received in revised form 27 April 2023; Accepted 8 June 2023
Available online 19 June 2023

Nomenclature

Latin Symbols

d	Diameter
l	length
LHV	Lower heating value
m_i	Mass of species i
$\dot{m}_i$	Mass Flow of species i
$\dot{n}_i$	Mole Flow of species i
P	Power
$\dot{Q}_{cool}$	Cooling Duty
RR	Recycling Ratio
R_{OC}	Oxygen transport capability
R_{Feed}	Oxygen requirement of feedstock
R_{C3H8}	Oxygen requirement of Propane
T	Temperature
u_0	Gas Velocity
$\dot{V}_{Rec.}$	Volume flow of recycled AR flue gas
$\dot{V}_{Air}$	Volume flow of fresh air
w_i	Mass fraction of species i
x_i	Mole fraction of species i
X_i	Conversion of species i

Greek Symbols

ΔX_s	Difference in oxidation degree of OC
ΔH_R	Reaction enthalpy
λ	Air-to-fuel equivalence ratio
η_{CGE}	Cold gas efficiency
ϕ_λ	Ratio of effective air-to-fuel equivalence ratios for FR and AR
τ_s	Solids residence time

Abbreviations/Acronyms

AR	Air Reactor
BP	Operating Period
CFB	Circulating Fluidized Bed Reactor
CGE	Cold Gas Efficiency
CLG	Chemical Looping Gasification
CLC	Chemical Looping Combustion
DFBG	Dual Fluidized Bed Gasification
FR	Fuel Reactor
LS	Loop Seal
MSR	Measurement and Control
OC	Oxygen Carrier
TP	Transient Period

Indices

AR	Air Reactor
C	Carbon
eff	Effective
gas	Gas
Feed	Feedstock
FR	Fuel Reactor
fine	Fine fraction
in	Inlet
O	Oxygen
OC	Oxygen Carrier
out	Outlet
ox	Oxidized
red	Reduced
RL	Refractory Lining
S	Solid
tot	Total
th	Thermal

or fluidized bed reactors (Huseyin et al., 2014; Condori et al., 2021a; Condori et al., 2021b), using oxygen carriers of different nature (Huang et al., Jan. 2014; Hildor et al., 2020; Moldenhauer et al., 2018; He et al., 2011; Zhao et al., 2015; Abdalazeez et al., 2022). Moreover, the suitability of various biomass-based feedstocks, such as rice husks (Ge et al., 2016a; Abdalazeez et al., 2022; Ge et al., 2016b), rice straw (Hu et al., Feb. 2019), sawdust (Xu et al., Nov. 2021; He et al., 2011), and wood pellets (Condori et al., 2021b; Hildor et al., 2020; Moldenhauer et al., 2018) has been established for CLG operation. In their review, Goel et al. (2022) present a comprehensive overview over those endeavors, highlighting the most important variables affecting the efficiency of the CLG system, such as FR temperature, gasification agent, or properties of the utilized OC. More recent advances, conducted in larger pilot plants, aim towards the large-scale implementation of the CLG technology (Ge et al., 2016a; Pissot et al., 2018; Condori et al., 2022), thus tackling fundamental questions with regard to process stability, operability, and efficiency.

One aspect that has been found to be crucial for up-scaling of the CLG

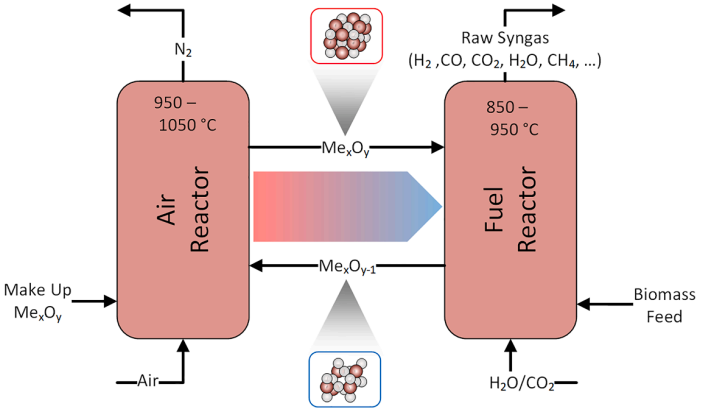

Fig. 1. Illustration of CLG process.

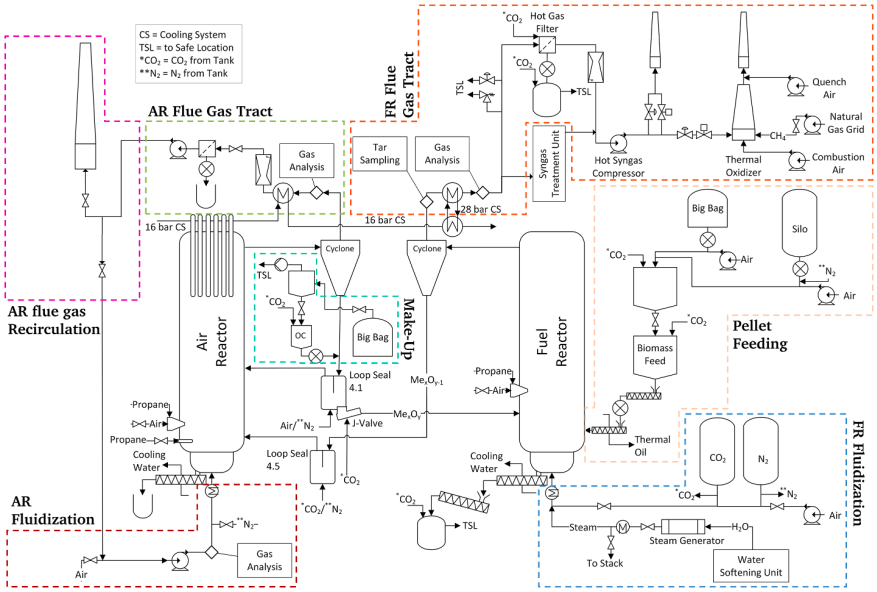

Fig. 2. Simplified process flow diagram of the 1 MW_{th} CLG pilot plant.

technology is related to the dual-purpose of the OC material, circulating between AR and FR (Dieringer et al., 2020; Samprón et al., 2021). As it does not only transport O_2 from the air reactor (AR) to the fuel reactor (FR), but is also responsible for the transport of sensible heat between the two reactors (Ohlemüller et al., 2016; Pröll et al., 2010), it allows for a N_2-free oxidation of the feedstock inside the FR and facilitates a stabilization of FR temperatures at the desired levels (i.e. >800 °C). In contrast to chemical looping combustion, partial oxidation of the feedstock is desired inside the FR in CLG (Huseyin et al., 2014; Ge et al., 2016b). This means that the oxygen availability in the FR has to be limited, while large heat fluxes to the FR are required, in order to maintain a stable fuel reactor temperature despite the pronounced occurrence of endothermic gasification reactions (Dieringer et al., 2020; Samprón et al., 2021). Therefore, novel process control strategies and plant designs, allowing for a de-coupling of oxygen and heat transport between the AR and FR are required in CLG (Dieringer et al., 2020; Samprón et al., 2021). In theory, a number of process control concepts are viable to achieve autothermal (i.e. without external heating) CLG operation. Yet, modeling approaches (Dieringer et al., 2020; Samprón et al., 2021) as well as initial test runs in small (Condori et al., 2021a,b) and medium-sized pilots (Condori et al., 2022) showed that restricting the air supply in the AR to reduce the overall air-to-fuel ratio to values below unity, hence obtaining gasification conditions, is the most promising approach. Therefore, the 1 MW_{th} pilot plant located at the Technical University Darmstadt, was adapted accordingly, to allow for autothermal CLG operation in an industrially relevant environment.

The aim of this study was to demonstrate that the production of a high-grade synthesis gas is feasible via autothermal CLG, using the adapted 1 MW_{th} pilot plant in combination with a tailored novel process control concept. The presented work comprises overarching results of the first-ever successful autothermal CLG operation, including a comprehensive set of live-data for the most important system variables, as well as characterization of OC samples collected throughout the continuous 14 days of operation. On the basis of these data-sets, a wholistic acting mechanism for the CLG technology is proposed, laying the ground-work for the systemic understanding of an industrially operated chemical looping gasifier. Moreover, the presented results show that using the suggested process control strategy allows for the production of a high-calorific syngas in semi-industrial scale, underlining the competitiveness of the CLG technology.

2. Experimental

2.1. 1 MW_{th} pilot plant layout

The layout of the 1 MW_{th} CLG pilot plant is described in detail elsewhere (Marx et al., 2021). Therefore, only the main features of the pilot, schematically shown in Fig. 2, are elaborated hereinafter.

The reactor system, consisting of an air reactor (0.59 m inner diameter, 8.66 m height), a fuel reactor (0.4 m inner diameter, 11.35 m height), and three coupling elements (two loop seals and a J-valve), is refractory lined to minimize heat losses, allowing for autothermal operation (i.e. without electrical heating). Both reactors are designed as circulating fluidized bed (CFB) reactors and are equipped with water-cooled ash sluicing screws for continuous or batch-wise material extraction from the bed. Moreover, each reactor can be additionally heated with propane, using a start-up burner or a bed lance. The AR has a design temperature of 1050 °C and can be fluidized with air or a mixture of air and recycled AR flue gas, which can be electrically pre-heated to temperatures up to 375 °C. For process control reasons, the inlet gas composition (O_2, CO_2) is measured for the AR (see Section 2.3.2) .[1] The fuel reactor has a design temperature of 970 °C and can be fluidized with air, steam, a mixture of steam and CO_2, or a mixture of air and CO_2. The fluidization media can be electrically pre-heated to temperatures up to 450 °C. Each reactor is equipped with a cyclone for gas solid separation and a loop seal to prevent bypassing of gasses. Global solid circulation between the two reactors is achieved with a J-valve, connecting the loop seal (LS) of the AR (LS4.1) with the fuel reactor. The circulating mass flow between both reactors can be adjusted by changing the fluidization flow of the J-Valve, which can be fluidized with nitrogen or CO_2. For the fuel reactor, all entrained material leaving the

[1] CO_2 is measured inside the AR primary air line as CO_2 formed inside the AR through the combustion of residual char coming from the FR can be recycled back to the primary air line when AR flue gas recirculation is initiated.

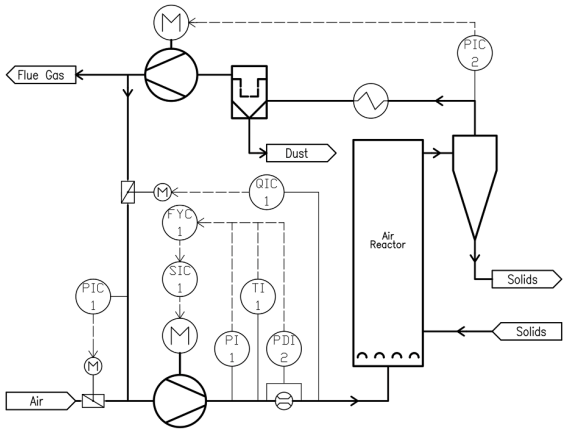

Fig. 3. Illustration of CLG control concept utilized in 1 MW_{th} pilot plant.

riser is directly transferred into the AR via LS4.5, which is fluidized with nitrogen or CO_2. On the other hand, the option of internal solid circulation via LS4.1, fluidized with nitrogen,[2] exists for the AR. This internal solid circulation stabilizes the hydrodynamics of the overall system. A solid fuel flow up to 250 kg/h corresponding to a thermal power of about 1.24 MW is introduced into the dense bed of the FR via an oil-cooled feeding screw. Fuel supply is either achieved from a fuel silo or via big bags through a weighted container equipped with a dosing screw, allowing for an exact control of the fuel mass flow. The fuel reactor off-gasses first pass a syngas cooler, where it is cooled to a temperature of approx. 350 °C. Subsequently, the gas composition (CO, CO_2, O_2, H_2, CH_4) is measured online. To allow for safe venting to the environment, the FR product gas is then transferred through a hot gas filter, operated at up to 250 °C, using a hot syngas compressor, before it enters a thermal oxidizer, required for full conversion of all hydrocarbon species to CO_2 and H_2O. After online gas sampling (CO, CO_2, O_2, SO_2, NO), the off-gasses from the AR are cooled in a heat exchanger, to a temperature <250 °C. Thereafter, the gas enters a fabric filter for dedusting. Downstream of the induced draft fan controlling the freeboard pressure of the AR (see PIC2 in Fig. 3), the AR flue gasses can be vented to the environment through a stack or can be partly recycled back to the AR airbox via the primary-air fan. In order to maintain constant reactor inventories throughout operation, the pilot is equipped with a pneumatically fed, make-up feeding system, allowing for the controlled introduction of up to 200 kg/h of the OC ilmenite into the standpipe of LS4.1.

2.2. Materials

2.2.1. OC bed material - ilmenite

Ilmenite from the Norwegian Company Titania AS, which was successfully deployed during previous chemical looping experiments in the 1 MW_{th} pilot (Ohlemüller et al., 2016; Ströhle et al., 2015; Ohlemüller et al., 2017), was used as OC for the CLG experiments presented in this study. For the fresh material, a bulk density of 2550 kg/m^3, a particle density of 4486 kg/m^3, and a mean particle diameter of 111 μm ($d_{p,10}$ = 31 μm, $d_{p,90}$ = 224 μm) was determined.

2.2.2. Feedstock

The feedstock used for pilot testing are industrial wood pellets conforming to the Norm ENPlus A1, purchased from Eckard GmbH, Germany.

[2] Fluidization with air is also possible for LS4.1, however this option is neglected due to safety reasons (risk of air bypassing to FR).

Table 1
Proximate and Ultimate analysis for industrial wood pellets.

Component	wt.-% (d.a.f.)	Component	wt.-% (a.r.)
C	50.8	C-fix	13.3
H	6	Volatiles	79.6
O	43.2	Ash	0.65
N	0.07	Moisture	6.5
S	0.008		
Cl	0.006		

The pellets exhibit a cylindrical shape (l ~10-25 mm, d ~6 mm), a bulk density of 650 kg/m^3, and a lower heating value of 17.96 MJ/kg. Proximate and Ultimate analysis for the pellets are given in Table 1.

2.3. Process control concept

2.3.1. Process control alternatives

Previous studies concluded that restricting the air supply in the AR, thus lowering the air-to-fuel equivalence ratio (λ) of the entire process below unity, is the most auspicious approach to obtain gasification conditions in chemical looping (Dieringer et al., 2020; Samprón et al., 2021). Yet, as the air supplied in the AR is not only responsible for providing the oxygen driving the chemical looping process, but is also crucial for obtaining sufficient solid circulation between the two reactors (Dieringer et al., 2020; Samprón et al., 2021), there are three conceivable options to achieve the desired gas velocity in the AR ($u_{0,AR}$) and the reduction in λ simultaneously:

(i) Designing the AR specifically for CLG operation (i.e. with a smaller inner diameter than for CLC operation) to reduce the amount of fluidization medium required.
(ii) Recycling AR flue gasses to the AR air box and mixing it with the inlet air.
(iii) Diluting the inlet air to the AR with an inert (e.g. N_2).

The last option signifies a straight-forward as well as easy to implement and validated (Condori et al., 2021a,b, 2022) option, however leads to significant operational costs due to the constant consumption of inerts. Hence, this option should be neglected for units of substantial thermal load (>50–100 kW_{th}). The second option leads to starkly reduced operational costs, when compared to (iii), yet comes with additional process complexity, requiring additional measurement and control (MSR) equipment for process control. Moreover, the recycled AR flue gas leads to increased compression demands for the AR primary-air fan and has to be brought to reactor temperatures, requiring additional heat. In contrast, the first approach allows for a direct process control in CLG without additional operational costs for inerts and pre-heating of recycled AR flue gas or equipment requirements, owing to its direct tailoring to the required process conditions. However, it is clear that this approach is only viable for greenfield plants, as variations in reactor dimensions are not easily attainable for existing units. Moreover, when using this approach, the plant layout does not allow for meaningful variations in λ (e.g. in case of significant changes in the composition of the supplied feedstock, requiring more or less heat supply in the gasifier), as λ and $u_{0,AR}$ are directly coupled. Therefore, the plant flexibility is reduced.

Based on this brief evaluation, it becomes obvious that only the second option, i.e. the extension of the existing 1 MW_{th} pilot plant with an AR flue gas recirculation line, signifies a viable option for its adaption for chemical looping gasification, allowing for meaningful parameter variations. On top of this, the suggested process control concept could

also be considered for a full-scale CLG setup, in which feedstock of varying quality, source, or nature is to be converted, necessitating operation at varying λ to fulfill the heat balance. The implementation of this concept is described in detail in the subsequent chapter.

2.3.2. Implementation of process control concept

For the independent control of two parameters, the AR gas velocity $u_{0,AR}$ and the air-to-fuel equivalence ratio λ, two separate control loops are necessary. The process control concept described below, relying on three independent control loops, is illustrated in Fig. 3.

Firstly, the gas velocity in the AR is controlled indirectly via the total inlet volume flow into the AR (FY1 from FYC1). The volume flow is measured with an aperture measurement, consisting of an orifice plate, a pressure measurement (PI1), a differential pressure measurement (PDI2), and a temperature measurement (TI1) inside the primary-air line of the AR. The calculated value for the inlet volume flow is then controlled through a speed controller (SIC1), controlling the rotary speed of the primary-air fan via a frequency converter. This control loop thus allows for an independent control of $u_{0,AR}$ via the total volume flow by the operator through either setting a fixed rotational speed for the primary-air fan or selecting the desired volume flow for the controller (FYC1). In order to control the oxygen input into the reactor and hence the air-to-fuel equivalence ratio λ of the CLG process, the primary-air line is equipped with an online oxygen measurement (QI1 from QIC1). To determine the oxygen input, the oxygen concentration (QI1 from QIC1) is multiplied with the volume flow entering the AR (FY1). With this knowledge, the oxygen input can then be controlled via a regulating flap in the AR flue gas recycle, which is opened automatically by a dedicated controller (QIC1) to increase the flue gas recycle, thus decreasing the air input and vice versa. Consequently, the operator can set a desired oxygen input and hence a fixed value for λ by either selecting the desired oxygen concentration inside the primary-air line or by manually positioning the regulating flap to a designated position. In theory, these two control loops are sufficient for the desired purpose. However, to further increase system stability, a third control loop was implemented. This control loop regulates the pressure upstream of the primary-air fan through a second gas flap located inside the air intake line. Here, the pressure controller (PIC1) opens the regulating flap to reduce the pressure and closes it to increase the pressure. By setting a fixed value for the pressure upstream of the primary-air fan, it is guaranteed that the primary-air fan runs at a constant rotational speed for a given volume flow even when the AR flue gas recirculation is adjusted to control the air-to-fuel equivalence ratio of the process.

2.4. Operating conditions

In March and April 2022, several periods of stable multi-hour CLG operation were obtained within a two-week test campaign, during which the 1 MW_{th} pilot unit was continuously operated 24 h/day. In total, the pilot was operated for ~100 h in chemical looping mode during this period. To allow for meaningful comparisons and illustrations of important trends, thirty Operating periods (BP) were selected for analysis, during each of which the most important boundary conditions, summarized in Table 4 in the appendix, were kept constant. All thirty Operating periods were split into 20-minutes sub-periods, yielding a total of 177 sub-periods for subsequent analysis, which also facilitates the investigation of potential changes occurring within the individual operating points. Moreover, three transient periods (denoted as TP-1, TP-2, and TP-3) with a duration of approx. 5–8 hours, leading up to stable CLG operation, are described in detail in this paper. These transient periods are characterized by a transient sub-period induced through a targeted adaption of the AR recycling ratio by the operator, entailing a characteristic switch towards gasification conditions. The boundary conditions for these periods are given in Table 5 in the appendix.

2.5. Evaluation parameters

To evaluate the merit of the novel CLG control concept, several evaluation parameters are introduced. Firstly, the air-to-fuel equivalence ratio, given by the ratio between the available oxygen for solid feedstock conversion and the oxygen required for full feedstock combustion, is used to quantify the oxygen input into the gasifier system. Here, the numerator constitutes the difference of the oxygen fed to the AR, $\dot{m}_{O,AR,in}$, and the amount of oxygen required for combustion of the additional propane fed to the AR via the propane lance:

$$\lambda = \frac{\dot{m}_{O,AR,in} - \dot{m}_{C3H8,AR}.R_{C3H8}}{\dot{m}_{Feed}.R_{Feed}} \tag{1}$$

In Eq. (1), R_{C3H8} (3.628 kg_O/kg) and R_{Feed} (1.306 kg_O/kg) signify the oxygen demand for full conversion of propane and the biomass feedstock, estimated from the elemental composition, respectively. According to this definition, (close to) full combustion of the feedstock is attained for air-to-fuel equivalence ratios larger than unity ($\lambda > 1$), while gasification processes require sub-stoichiometric oxygen feeding (i.e. $\lambda < 1$). However, it has to be noted that in chemical looping processes incomplete feedstock conversion is generally obtained for $\lambda \geq 1$ (Adánez et al., 2006; Pérez-Vega et al., 2016; Ohlemüller, 2019), as the oxidation of volatiles by the OC in the FR is limited by kinetics (Fossdal et al., May 2011; Liu et al., Oct. 2013) as well as gas/solid mixing.

As for some Operating periods, not all oxygen fed to the AR is consumed in it, the effective air-to-fuel equivalence ratio, considering the difference between the input and output of elemental oxygen for the AR ($\dot{m}_{O,AR,in}$, $\dot{m}_{O,AR,out}$), is a useful tool to evaluate how much oxygen is taken up by the OC inside the AR (Condori et al., 2022) :[3]

$$\lambda_{AR,eff} = \frac{\dot{m}_{O,AR,in} - \dot{m}_{O,AR,out}}{\dot{m}_{Feed}.R_{Feed}} \tag{2}$$

Similarly, the effective air-to-fuel equivalence ratio in the FR can be calculated considering the input and output of elemental oxygen for the FR, thereby constituting how much oxygen is released inside the FR by the OC (Condori et al., 2022):

$$\lambda_{FR,eff} = \frac{\dot{m}_{O,FR,out} - \dot{m}_{O,FR,in}}{\dot{m}_{Feed}.R_{Feed}} \tag{3}$$

Clearly, the system is in steady state if $\lambda_{AR,eff}$=$\lambda_{FR,eff}$, which means that the OC takes up and releases the same amount of oxygen in the AR and FR, respectively. Hence, the quotient of the effective air-to-fuel equivalence ratios of the AR and FR (ϕ_λ) can be utilized to evaluate the state of the CLG unit (Condori et al., 2022):

$$\phi_\lambda = \frac{\lambda_{FR,eff}}{\lambda_{AR,eff}} \begin{cases} < 1 & \text{Oxygen accumulation in OC} \\ = 1 & \text{System in steady state} \\ > 1 & \text{Oxygen depletion from OC} \end{cases} \tag{4}$$

As described in Section 2.3.2, λ is controlled through a recycling of AR flue gasses for AR fluidization. To quantify the extent of recirculation, the AR flue gas recycling ratio is introduced:

$$RR_{AR} = \frac{\dot{V}_{Rec.,AR}}{\dot{V}_{Rec.,AR} + \dot{V}_{Air,AR}} \tag{5}$$

Here RR_{AR}=0 signifies operation with pure air, while RR_{AR}=1 signifies operation with pure AR flue gas. The recirculation rate can easily be calculated by a mass balance around the primary-air line (more details, see derivation in Chapter A.1 in the appendix):

$$RR_{AR} = \frac{x_{O2,AR,in} - 21\ \text{vol.\%}}{x_{O2,AR,out} - 21\ \text{vol.\%}} = \frac{x_{CO2,AR,in}}{x_{CO2,AR,out}} \tag{6}$$

[3] In Eq. (1), (2) and (3), the oxygen inlet and outlet into the AR/FR are evaluated by using the respective volume flow measurements (venturi nozzles and orifice plates) and online gas analyzers (see Fig. 2).

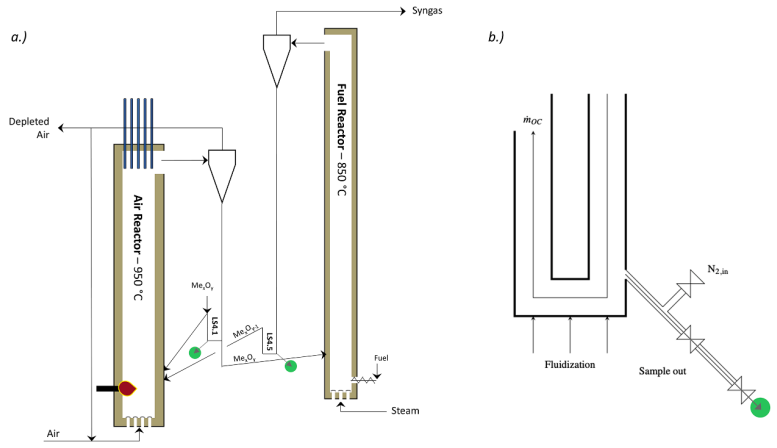

Fig. 4. a) Illustration of reactor system with indication of solid sampling points. b) Schematical detail view of solid sampling setup.

$$X_{C,AR} = \frac{\dot{m}_{gas,AR}\cdot\left(\frac{w_{CO,AR}}{M_{CO}} + \frac{w_{CO2,AR}}{M_{CO2}}\right)\cdot M_C - \dot{m}_{C3H8,AR}\cdot w_{C,C3H8,AR} - \frac{x_{CO2,AR,in}}{M_{CO2}}\cdot\left(\dot{m}_{Rec.,AR} + \dot{m}_{Air,AR}\right)\cdot M_C}{\dot{m}_{Feed}\cdot w_{C,Feed}} \quad (9)$$

In order to simplify the subsequent considerations, the cold gas efficiency (CGE), η_{CGE}, relating the energy content of the produced syngas at the FR outlet to the energy input through the solid feedstock (Higman and van der Burgt, 2008; De et al., 2018), is used to describe the efficiency of the gasification processes:

$$\eta_{CGE} = \frac{\dot{n}_{gas,FR,out}\cdot\left(x_{CH4,FR,out}\cdot LHV_{CH4} + x_{CO,FR,out}\cdot LHV_{CO,FR} + x_{H2,FR,out}\cdot LHV_{H2}\right)}{\dot{m}_{Feed}\cdot LHV_{Feed} + \dot{m}_{C3H8,AR}\cdot LHV_{C3H8} - \dot{Q}_{cool,AR}} \quad (7)$$

Here the propane input ($P_{th,C3H8} = \dot{m}_{C3H8,AR}\cdot LHV_{C3H8}$) and the cooling duty ($\dot{Q}_{cool,AR}$) of the AR cooling lances[4] are considered, to obtain a meaningful value.

Another important parameter for the CLG unit is the amount of carbon converted in the FR, which is given by:

$$X_{C,FR} = \frac{\dot{n}_{gas,FR,out}\cdot\left(x_{CH4,FR,out}\cdot\frac{M_C}{M_{CH4}} + x_{CO,FR,out}\cdot\frac{M_C}{M_{CO}} + x_{CO2,FR,out}\cdot\frac{M_C}{M_{CO2}}\right)\cdot M_C}{\dot{m}_{Feed}\cdot w_{C,Feed}} \quad (8)$$

Char travelling to the AR together with the circulating solid is converted to CO_2 there. In case of $\lambda \ll 1$, CO can also be formed in minor amounts inside the AR, so that the carbon conversion inside the AR is given by:

The total carbon conversion inside the CLG unit is the sum of the AR and FR char conversion and should be close to 1, as the only way for carbon to "escape" the unit is in particulate form towards the FR or AR filter.

$$X_{C,tot} = X_{C,FR} + X_{C,AR} \leq 1 \quad (10)$$

2.6. Solid sampling and analysis

A detailed elaboration of the sampling and analysis procedure of the OC samples is presented by Marx et al. (2023). To further expand analysis, this methodology is also applied in this study. Here, solid samples were taken from the standpipe of the two loop seals during CLG operation (see Fig. 4a), using a dedicated sampling setup illustrated in Fig. 4b. In order to ensure samples representing the current process state, the sampling tube was flushed with nitrogen to remove all material in the sampling tube and replace it with fresh material. The process was observed via infra-red thermometer and was deemed successful when temperatures 300 °C on the outside were reached, signifying that "fresh", hot material had entered the sampling line. The sample (300–700 g) was then discharged from the loop seal via ball valves into a sealed vessel where it was left for cool down for approx. two hours in order to prevent reaction with ambient air. Afterwards the sample was removed from the system.

For analysis of the carbon content, the samples were first classified into two particle fractions using a 400 µm sieve. The coarse fraction (containing the majority of the transported char) was not considered further, as due to the particle size of the raw material (see Chapter 2.2.1) it can be assumed that ilmenite particles are not present inside the coarse fraction. The fine fraction was processed in a commercially available elemental analysis system (Elementar vario MACRO cube in CHNS

[4] Generally, cooling in the AR is not desired during CLG operation. However, due to constructional reasons, the cooling lances of the AR in the 1 MW_{th} unit cannot be fully extracted from the reactor and hence lead to heat extraction during operation.

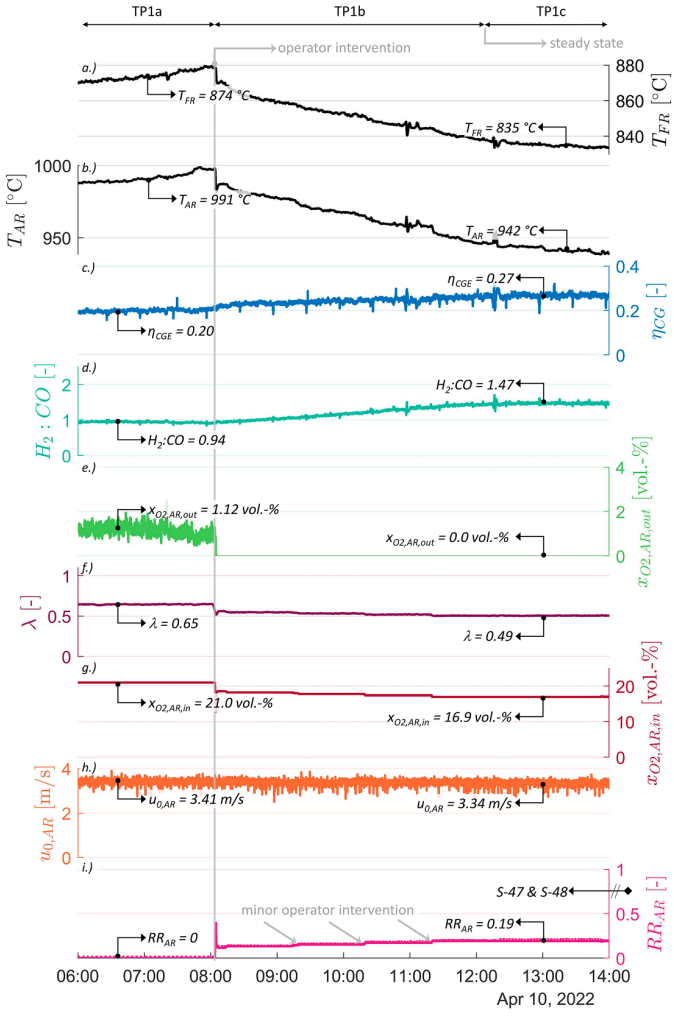

Fig. 5. Progression of important process and evaluation parameters over time for TP-1.
From top to bottom: a.) FR and b.) AR temperature, c.) cold gas efficiency (η_{CGE}), d.) H_2/CO-ratio in FR product gas, e.) oxygen concentration at AR outlet ($x_{O2,AR,out}$), f.) air-to-fuel equivalence ratio (λ), g.) oxygen concentration at AR inlet ($x_{O_2,AR,in}$), h.) AR gas velocity, and i.) AR flue gas recycling ratio (RR_{AR}), calculated from O_2 (-) and CO_2 (:) balance. Arrows with diamonds at the end signify the sampling time of a given solid sample.

setup). Each fraction was analyzed in triplicate with a sample mass of 50 mg, using a method providing oxygen according to the approximate carbon content and oxygen uptake. To determine the oxidation degree (X_s) of the samples, their weight change in an oxidizing atmosphere was subsequently determined by oxidizing a sample mass of approx. 5 g in a laboratory oven at 900 °C with the mass being determined before ($m_{LS,1}$) and after ($m_{LS,2}$) oxidation.

In chemical looping, the oxidation degree of the OC is generally given by Adanez et al. (2012); Larsson et al. (2014):

$$X_{s,i} = \frac{m_{OC,i} - m_{OC,red}}{R_{OC} \cdot m_{OC,ox}}. \tag{11}$$

Here, $m_{OC,red}$ and $m_{OC,ox}$ are the mass of an OC sample in a fully reduced and oxidized state respectively, while $m_{OC,i}$ is the mass of the OC sample in its current state. Using the mass of loop seal samples before and after oxidation and assuming that the latter signifies a fully oxidized OC sample (i.e. $m_{OC,ox} = m_{LS,2}$), one can thus calculate the oxidation degree:

$$\begin{aligned} X_{s,i} &= \frac{m_{LS,1} \cdot (1 - w_{C,LS,fine}) - m_{LS,2} \cdot (1 - R_{OC})}{R_{OC} \cdot m_{LS,2}} \\ &= 1 - \frac{m_{LS,2} - m_{LS,1} \cdot (1 - w_{C,LS,fine})}{R_{OC} \cdot m_{LS,2}} \end{aligned} \tag{12}$$

To arrive at Eq. (12), the following assumptions are used:

i The extent to which the OC sample can be reduced is given by the oxygen transport capacity (R_{OC}). For the utilized ilmenite, an oxygen transport capacity of 3.7 wt.-% was determined (Condori et al., 2021b). This value falls slightly below the theoretical oxygen transport capacity for the redox couple Fe_2TiO_5/$FeTiO_3$ (Adanez et al., 2012). With the given value of R_{OC} the samples' reduced mass can be calculated by:

$$m_{OC,red} = m_{OC,ox} \cdot (1 - R_{OC}) = m_{LS,2} \cdot (1 - R_{OC}) \tag{13}$$

ii Since the fresh loop seal sample contains small fraction of char, originating from the carbon slip occurring between AR and FR (Huseyin et al., 2014; Markström et al., 2013; Cuadrat et al., 2012), the carbon content of the LS samples has to be considered for the calculation of the oxidation degree. As the char can be assumed to be fully burned-off inside the laboratory oven, the "real" loop seal mass ($m_{OC,i}$), can be calculated by:

$$m_{OC,i} = m_{LS,1} - m_{c,fine} = m_{LS,1} \cdot (1 - w_{C,LS,fine}) \tag{14}$$

iii Due to the low content of ash for the raw feedstock (see Table 1), it can be assumed that the ash content inside the LS samples is negligible.

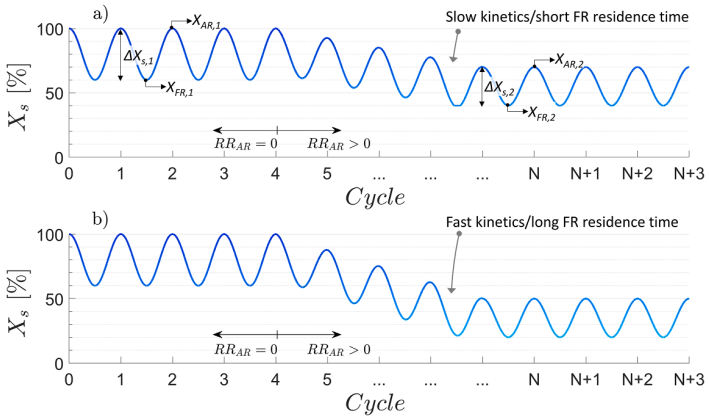

Fig. 6. Progression OC oxidation degree when increasing the air reactor recycling ratio (RR_{AR}). The reduction extent at the FR outlet is determined by FR reaction kinetics and the FR residence time. a) Minor decrease in oxidation degree at FR outlet ($X_{s,FR}$,), b) Significant decrease in oxidation degree at FR outlet. Adapted from Dieringer et al. (2020).

3. Results and discussion

During application of the novel process control concept in the 1 MW_{th} scale, it was observed that the CLG unit displays a characteristic transient system response to changes in the AR recycling ratio, giving meaningful insights into the mechanics of the CLG process. This behavior is explained on the basis of three different transient periods in Chapter 3.1. Subsequently, Chapter 3.2 illustrates how the new process control concept affects process efficiency in steady-state.

3.1. Transient system response to application of novel process control concept

3.1.1. System response of 1 MW_{th} CLG unit during transient periods

The progression of the most important process parameters for the first transient period under consideration (TP-1) is illustrated in Fig. 5. It includes three distinct sub-periods on April 10th, 2022. Between 6:00 and approx. 8:00 h, the pilot plant was operated in steady state without AR flue gas recirculation (TP-1a). Thereafter, operators started AR flue gas recirculation at approx. 8:00 h, initiating the transient sub-period of the process stretching until approx. 12:00 h (TP-1b). During this sub-period, minor adaptions with regard to the AR flue gas recycling were carried out by the operator to reach the destined operating period. Between 12:00 h and 14:00 h the process reached steady state and did not show any major variations in the operating and evaluation parameters (TP-1c).

When considering Fig. 5, the interventions by the operator are best visible in the AR recycling ratio (Fig. 5i). By repositioning the flue gas recirculation flap, the recirculation rate of the process was sharply increased from 0 to 0.15 at 8:00 h.[5] As a consequence, the inlet oxygen concentration to the AR decreased from 21 to 16.9 vol.-% (see Fig. 5g). Due to the process control concept, described in detail in Section 2.3.2, the gas velocity $u_{0,AR}$ was maintained at a constant value of 3.3–3.4 m/s (see Fig. 5h), leading to stable hydrodynamics for the CLG process throughout the entire transient period under consideration.[6] However, as the air-input into the system was reduced, while the thermal load of the gasifier was kept constant throughout the entire transient period, the air-to-fuel equivalence ratio dropped from a value of 0.65 to 0.49 (see Fig. 5f).

The first notable observation which can be made is that due to this decrease in λ, the oxygen concentration at the AR outlet immediately dropped to a value of 0 vol-% (see Fig. 5e), meaning that all oxygen is consumed inside the AR. This means that the inlet oxygen is fully required for the re-oxidation of the OC, the combustion of the propane input into the AR and the combustion of char coming from the FR, denoted as carbon slip (Huseyin et al., 2014; Markström et al., 2013; Cuadrat et al., 2012). As the oxygen concentration remains at 0 vol.-% after this change in recirculation rate, it can be postulated that the OC is not fully oxidized inside the AR, as the oxygen availability is reduced. Yet, the oxygen release inside the FR is not altered instantly (see below), as the boundary conditions in the FR are not altered directly. Consequently, it can be assumed that the oxidation degree of the OC (X_s), given by the Eq. (11), is periodically decreased during each cycle, as postulated in a previous study (Dieringer et al., 2020), until new steady-state conditions are found.

To cast further light on this behavior, the theoretical progression of the oxidation degree of the oxygen carrier is illustrated in Fig. 6. Clearly, not only the oxidation degree at the AR outlet, but also the change in oxidation degree between FR and AR (ΔX_S, see Eq. (15)) has to decrease for the new steady-state conditions (see Fig. 6, $\Delta X_{S,1} > \Delta X_{S,2}$), as the OC circulation rate between the FR and AR is kept constant, yet less oxygen is being transported from the AR to the FR, due to the decrease in air input (Samprón et al., 2021):

$$\Delta X_s = X_{s,AR} - X_{s,FR} = \frac{m_{OC,AR} - m_{OC,FR}}{R_{OC} \cdot m_{OC,ox}} \quad (15)$$

Depending on the interplay of the kinetics of the different occurring reactions and the OC residence time in the FR, determining to which extent the OC is reduced in the FR (Liu et al., Oct. 2013), the oxidation degree at the outlet of the AR and FR can either decrease slightly (see Fig. 6a) or sharply (see Fig. 6b) until steady state conditions are attained.[7]

The above elucidations on the ensuing shift in the oxidation degree of the OC are supported, when considering the progression of the H_2/CO ratio (see Fig. 5d), and the cold gas efficiency (see Fig. 5c), over time. Clearly, the hydrogen to carbon monoxide ratio in the FR product gas increases continuously after the increase in the AR recycling ratio during sub-period TP-1b. This can be explained by the fact, that due to its more favorable reaction kinetics when compared to CO, hydrogen is preferentially oxidized on the oxygen carrier (Abad et al., 2011). As less oxygen is available from the OC with decreasing $X_{s,AR}$, oxidation of syngas

[5] Minor operator adaptions at later stages lead to an increase of this value to 0.19 over the considered period.

[6] Apart from $u_{0,AR}$=const., this requires a constant reactor inventory, a constant gas velocity in the FR ($u_{0,FR}$) and constant volume flows for both loop seals and the J-Valve, which was the case here.

[7] For long residence times and high FR temperatures values close to zero can also be obtained for $X_{S,FR}$ (Condori et al., Feb. 2021).

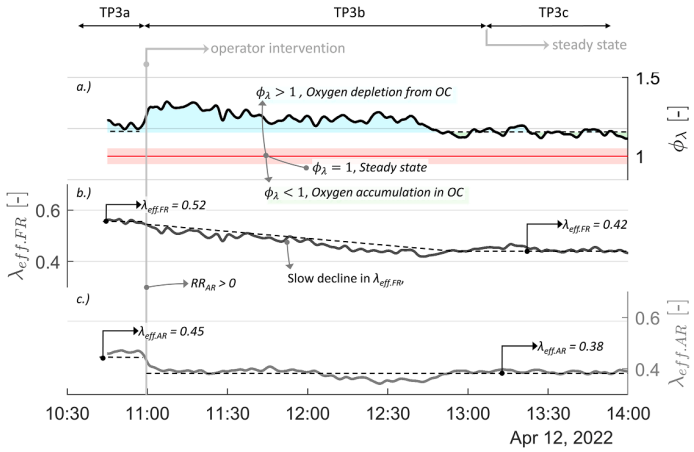

Fig. 7. Progression of effective air-to-fuel equivalence ratio of FR (b) and AR (c) and their ratio (a) over time for TP-3. The red shaded area in (c) denotes steady state conditions with ϕ_λ=1 ± 0.05.

Table 2
Oxidation degree (X_S) in% for OC samples collected from LS4.1 and LS4.5 during the transient periods TP-1, TP-2, and TP-3. Sampling times for each sample are indicated in Fig. 5 (TP-1), Fig. 17 (TP-2), and Fig. 18 (TP-3) and are listed in Table 3 in the Appendix.

Period	TP-1		TP-2		TP-3	
Loop Seal	LS4.1	LS4.5	LS4.1	LS4.5	LS4.1	LS4.5
Sub-Period	TP-1a		TP-2b		–	
Sample-#	S-42	S-43	S-60	S-59	–	–
X_S **[%]**	94.6 ± 0.1	74.7 ± 0.5	81.2 ± 0.3	60.9 ± 0.2	–	–
ΔX_S **[%]**	19.9 ± 0.3		20.4 ± 0.2		–	
Sub-Period	–		TP-2c		TP-3c	
Sample-#	–	–	S-61	S-62	S-66	S-65
X_S **[%]**	–	–	81.8 ± 0.1	65.8 ± 0.4	83.7 ± 1.1	64.4 ± 0.6
ΔX_S **[%]**	–		16.0 ± 0.3		19.3 ± 0.8	

species on the oxygen carrier occurs less pronouncedly and as hydrogen was previously oxidized to greater extents, the H_2/CO ratio increases from 0.94 to 1.47.[8] Following the same logic, the cold gas efficiency of the process steadily increases from a value of 0.20 to 0.27, as less oxygen is released by the OC inside the FR and hence more chemical energy is maintained in the FR product gasses. Yet, in contrast to the other variables previously discussed, the change in H_2/CO-ratio and the cold gas efficiency does not occur instantly, but over a duration of approx. four hours. Firstly, this system inertia can be explained by the fact that each OC particle has to gradually reach new steady-state conditions (e.g. getting reduced from $X_{s,FR,1}$ to $X_{s,FR,2}$). Secondly, it can be explained by the fact that in order to reach steady-state conditions, the entire reactor inventory, (800–1000 kg), has to be reduced to lower oxidation degrees until equilibrium is reached. Thus, this chemical inertia of the system has to be considered, when adapting process variables affecting the air-to-fuel equivalence ratio of the process.

When considering the reactor temperatures measured during the transient period TP-1 (see Fig. 5a & Fig. 5b), it becomes visible, that all reactor temperatures decrease as soon as the AR flue gas recirculation is switched on, with average AR temperatures dropping from 991 to 942 °C, while FR temperatures decrease from 874 to 835 °C over the duration of the transient period. This can be explained by the fact, that less oxidizing reactions occur and hence reaction exothermicity decreases. Similar to the H_2/CO ratio and the cold gas efficiency, reactor temperatures require approx. four hours to reach stable values. Again, this can be explained by the fact that as the oxygen release from the OC inside the FR is diminished during sub-period TP-1b, the total reaction exothermicity decreases. Consequently, the heat release from the CLG unit decreases and system temperatures drop along with the decrease in oxygen transport from the AR to the FR. Moreover, this finding suggests that the transient behavior of the reactor system might in part also be related to the refractory lining of the reactor system, slowly reacting to the changes occurring inside the reactor and hence cushioning a rapid drop in reactor temperatures. As reactor temperatures are also dependent on the temperature of the refractory lining, with the temperature gradient between gas phase and refractory wall determining the heat flux to the surroundings, this means that there exists a feedback loop between the reactor temperature, determined by the chemical reactions occurring inside the reactor system, and the refractory lining temperature. Therefore, larger CLG units, for which the surface-to-volume ratio is much smaller than for the 1 MW_{th} unit, might show a more rapid system response than what has been observed here, depending on which effect is the more dominant (i.e. the slow reduction of the OC or the thermal inertia of the refractory lining). Another important finding that can be derived from the temperature profiles shown in Fig. 5a and Fig. 5b is that the temperature difference between both reactors stays constant during the entire transient period, starting at a value of 117 K and ending at a 107 K. This again shows that throughout the entire period, solid circulation was maintained constant, underlining the effectivity of the novel process control concept.

A similar behavior was observed for all parameters and variables highlighted above for the other two transient periods under consideration (TP-2 & TP-3), meaning that the observed behavior occurs in a comparable fashion, when the AR flue gas recirculation is initiated (see Chapter A.2 in the appendix). This means that although slight differences in terms of the transient switch-over times or the extent to which the evaluation parameters change are visible, the governing phenomena

[8] Another reason for this could be the decrease in FR temperature, going in hand with the increase in RR_{AR}, which leads to shift in the WGS equilibrium and a decrease in char conversion.

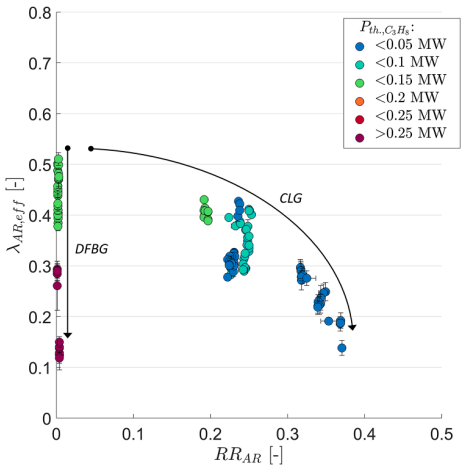

Fig. 8. Effective air-to-fuel equivalence ratio in the AR as a function of the flue gas recycling ratio in the AR for different thermal loads of propane firing for all operating periods given in Table 4.

for the observed behavior are the same.

3.1.2. Oxygen balancing during transient periods

As mentioned before, it is postulated that by reducing the oxygen input into the AR through initiating AR flue gas recycling, the extent to which the OC is oxidized inside the AR reduces with each cycle (see Fig. 6). If this is the case, it should also be visible in the oxygen balance of the CLG system, as the oxygen carrier should be depleted of oxygen during the transient period (i.e. ϕ_λ>1, see Eq. (4)). Fig. 7 shows that the expected behavior was observed during the transient periods, showing the effective air-to-fuel equivalence ratios as well as their quotient for the period TP-3. Fig. 7c shows that as soon as the recycling ratio is started by the operator at 11:00 on 12th April 2022, initiating the transient sub-period TP-3b, the effective air-to-fuel equivalence ratio in the AR immediately drops from a value of 0.45 to a value of 0.38. This indicates that less oxygen is taken up by the OC inside the AR instantly, due to the limitation in oxygen availability. On the other hand, the effective air-to-fuel equivalence ratio inside the FR declines slowly over the entire duration of TP-3b (see Fig. 7b). For one, this shows that the OC releases less and less oxygen inside the FR until a new steady-state is obtained, indicating that its oxygen release inside the FR is slowly restricted and the control concept yields the desired results. When considering the transient response, Fig. 7b suggests that the lowered oxygen release inside the FR results from gradual changes taking place within the OC throughout the entire transient period. Again, this points to the fact that for each cycle the OC gets more reduced and hence its oxygen release kinetics decelerate inside the FR (Abad et al., 2011; Ohlemüller et al., 2018), leading to lower oxygen release rates. The ensuing oxygen depletion of the OC is visually highlighted in blue shading in Fig. 7a, showing that ϕ_λ increases to an elevated level throughout the entire transient sub-period TP-3b, indicating that oxygen is "consumed" by the occurring chemical reactions within the transient period, before it drops to its initial value as soon as steady state conditions are reached in sub-period TP-3c.[9] Consequently, it can be summarized that the OC inventory of the CLG unit serves as an oxygen storage, slowly releasing oxygen until a new steady state is reached, thereby playing an important role in the transient system response.

3.1.3. Behavior of the oxygen carrier inventory during transient periods

To further cast light onto the system's behavior during the transient periods, analyses of solid samples at the AR and FR outlet can be considered, in order to enhance process understanding. One important question is which oxidation degree is reached at the FR and AR outlet in steady state. Moreover, it remains open whether each particle requires multiple cycles to reach this steady state, or if the length of the transient period is primarily dominated by the size of the reactor inventory (i.e. individual particles reach steady state conditions within < 1–2 cycles, yet multiple hours are required for a unit of the considered size until all particles have been cycled through the system). To cast light onto this, the oxidation degree of samples taken from both loop seals at different stages of the transient period TP-1, TP-2, and TP-3 are listed in Table 2. As expected, the higher oxidation degrees (X_S) are obtained for LS4.1 prior to the onset of AR flue gas recirculation (e.g. TP-1a: S-42: X_s =94.6 ± 0.1% vs. TP-3c S-66: X_s =83.7 ± 1.1) which can again be explained by the fact that while close to full oxidation of the OC is achieved in the AR when sufficient amounts of oxygen are supplied (i.e. RR_{AR}=0), only partial oxidation of the OC is attained in an oxygen deficient AR atmosphere. Consequently, as illustrated in Fig. 6, AR flue gas recirculation leads to a general drop in X_s for the entire CLG system (i.e. for AR & FR). While this observation supports the general mechanics of the process control concept, it does not directly explain how its application leads to a higher CLG process efficiency (i.e. higher CGEs). As stated before, cold gas efficiencies correlate with the amount of oxygen released inside the FR, leading to more or less complete feedstock conversion. The oxygen released in the FR is the one transported to it via the OC from the AR given by:

$$\dot{m}_{O,AR\rightarrow FR} = \dot{m}_{OC} \cdot R_{OC} \cdot \Delta X_s \ . \tag{16}$$

Hence, for a constant global solid circulation ($\dot{m}_{OC}$), which can be assumed here as the hydrodynamic boundary conditions were not altered within each transient period, the change in the oxidation degree between AR and FR (ΔX_s) should decrease when RR_{AR} is increased. Again, this is corroborated by the data listed in Table 2 (e.g. TP-2b: S-59/60: ΔX_s =20.4 ± 0.2%) vs. TP-2c S-61/62: ΔX_s =16.0 ± 0.3%). The observed decrease in ΔX_s thus means due to its incomplete oxidation in the AR, the OC is less "keen" to release oxygen inside the FR, leading to a lower overall oxygen transport to the FR and hence higher cold gas efficiencies. This observation is also supported by kinetic studies performed with ilmenite, showing that OC reaction kinetics generally decrease with decreasing oxidation degree (Abad et al., 2011; Ohlemüller et al., 2018). In summary, the mechanics of the suggested process control concept can thus also be verified on the basis of solid samples collected from both loop seals during operation. Here, it can be observed that while the restriction of oxygen supply in the AR leads to a direct drop in X_s, this drop then leads to a subsequent decrease in ΔX_s and hence oxygen transport due to kinetic reasons. Moreover, it can be seen that all values obtained for oxidation degrees of the solid samples from LS4.5 listed in Table 2 are larger than 50%. Therefore, it can be postulated that the oxygen release inside the FR is restricted kinetically, preventing a full reduction (X_s=0%, i.e. bulk of particle in $FeTiO_3$ phase) of the OC inside the FR. In a 1.5 kWth unit, exhibiting a dissimilar layout to the 1 MW_{th} unit (i.e. FR in bubbling regime), allowing for distinctly larger solid residence times inside the FR, oxidation degrees 0%<$X_{s,FR}$<20% were determined for λ<0.3 at temperatures between 820 and 940 °C (Condori et al., 2021b). This shows that in case of more favorable kinetics (higher FR temperatures) (Abad et al., 2011; Ohlemüller et al., 2018) and longer residence times (Liu et al., Oct. 2013), the OC is reduced to lower oxidation degrees inside the FR. Yet, even at these conditions, full reduction is not attained due to kinetic reasons. In case

[9] As visible from Eq. (4) oxygen depletion occurs for ϕ_λ>1. However, in Fig. 7c the baseline for oxygen depletion is set at a value of 1.15 for which ϕ_λ stagnates for the steady-state conditions TP-3a and TP-3c. Although mass and component (C, H, O) balances could be closed with an accuracy of ±5 % for all operating points under consideration, it is believed that this upwards skew in ϕ_λ in Fig. 7c by 15 % in the data can be accredited to measurement inaccuracy (e.g. venturi/aperture flow measurements, moisture measurement).

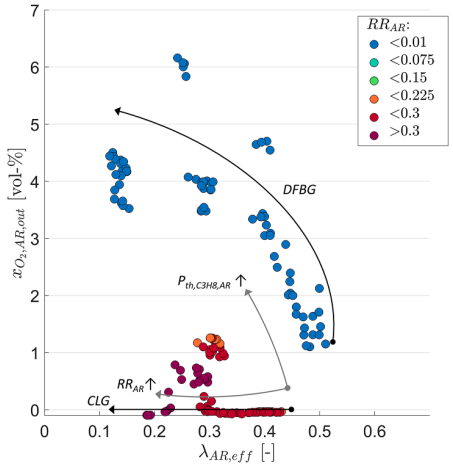

Fig. 9. Outlet AR O_2 concentration as a function of the effective air-to-fuel equivalence ratio in the AR as a function of the flue gas recycling ratio in the AR for different oxygen concentrations at AR outlet for all operating periods given in Table 4. Gray arrows denote the progression of $x_{O2,AR,out}$ with increasing RR_{AR} (CLG) and $P_{th,C3H8,AR}$ (DFBG), respectively.

this kinetic barrier is overcome (e.g. through higher FR temperatures) and the oxygen release inside the FR is restricted due to thermodynamic reasons (i.e. $X_{s,FR}$=0), the time required to reach steady state conditions after changes in RR_{AR} would decrease, as steady state conditions are reached inside the FR as soon as $X_{s,FR}$=0 is attained. Nonetheless, the system would still require a certain stabilization time for the entire OC inventory to reach its fully reduced state.

3.2. Steady-state system response to application of novel process control concept

While the investigation of the transient system response of the CLG unit to changes in the air supply provides insights into the underlying phenomena, comparisons of steady-state operating periods with different boundary conditions allow for a holistic analysis of the merit the process control concept to optimize CLG process efficiency. During the 60 h of steady-state chemical looping operation investigated within this work, the process control concept was successfully applied for a total duration of ~35 h. Results of these endeavors are summarized in Fig. 8, showing the dependency of the AR recycling ratio and the effective air-to-fuel equivalence ratio in the AR. Here, two regions can clearly be observed. On the y-axis of Fig. 8, 78 operating sub-periods, for which flue gas recirculation in the AR were switched off, are visible. For the remaining 99 operating sub-periods, AR recycling ratios larger than zero were employed. Before AR flue gas recirculation was initiated (RR_{AR}=0), the pilot was operated with propane firing at different thermal loads in the AR for given operating periods. While propane injection was used to counter the high relative heat losses of the 1 MW_{th} pilot (10–15% of thermal input) for selected operating periods, (gaseous) fuel injection is commonly applied in DFBG applications as a mean of temperature control in both reactors (Ripfel-Nitsche et al., 2007; Bolhar--Nordenkampf et al., 2002; Bolhàr-Nordenkampf et al., 2003), meaning that the deeper investigation of this measure on CLG efficiency provides further important insights.

3.2.1. Effect of process control concept on oxygen transport from AR to FR

Evaluation of all 177 operating sub-periods showed that for the given plant layout two options to control the oxygen transport to the FR exist. For the sub-periods, located on the y-axis of Fig. 8 (i.e. RR_{AR}=0), a clear dependency between $\lambda_{AR,eff}$ and the propane input is visible. This indicates that in the case of significant propane injection in the AR, oxygen uptake by the OC is impaired leading to lower values of $\lambda_{AR,eff}$. Since oxygen concentrations larger than 1 vol.-% were measured at the outlet of the AR for all operating periods with RR_{AR}=0 (see Fig. 9), the drop in the effective air-to-fuel equivalence ratio in the AR cannot be associated to thermodynamic constraints (i.e. enough oxygen for full-reoxidation of the OC was available inside the AR for all operating periods with RR_{AR}=0). This suggests that the injection of propane into the dense bed of the AR impairs the oxygen uptake of the OC kinetically (e.g. by leading to a reducing atmosphere in the dense bed, where gas-solid contacting is high), which is also supported by the fact that for RR_{AR}=0, the outlet AR O_2 concentration increases with decreasing $\lambda_{AR,eff}$. Regardless of the mechanism, this means that through propane injection, the OC behaves more and more as an "inert" inside the FR, as the OC enters the FR in a more reduced state, thus impairing reaction kinetics inside the FR. Ultimately, the control concept enforced by propane injection can thus be seen as a form of dual-fluidized bed

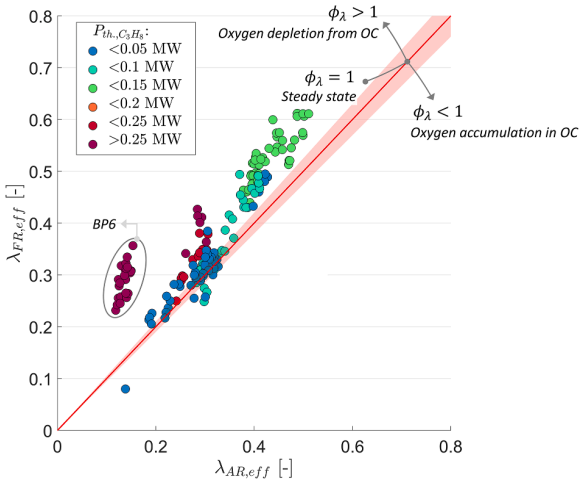

Fig. 10. Effective air-to-fuel equivalence ratio in FR as a function of air-to-fuel equivalence ratio in AR for varying propane loads for all operating periods given in Table 4. The red shaded area indicates a deviation of 5% from the angle bisector.

Table 3
Oxidation degree (Xs) in% for all OC samples collected from LS4.1 and LS4.5 during operation.

Sample-#	Location	X_S [%]	ΔX_S [%]	Sampling Time
CLA1-S-10	LS4.1	104.4 ± 1.2	–	15:38 02.04.2022
CLA1-S-13	LS4.1	15.2 ± 0.6	–	05:30 03.04.2022
CLA1-S-42	LS4.1	94.6 ± 0.1	19.9 ± 0.3	03:30 10.04.2022
CLA1-S-43	LS4.5	74.7 ± 0.5		
CLA1-S-49	LS4.1	86.7 ± 0.0	–	15:30 10.04.2022
CLA1-S-59	LS4.5	60.9 ± 0.2	20.4 ± 0.2	21:30 11.04.2022
CLA1-S-60	LS4.1	81.2 ± 0.3		
CLA1-S-61	LS4.1	81.8 ± 0.1	16.0 ± 0.3	03:20 12.04.2022
CLA1-S-62	LS4.5	65.8 ± 0.4		
CLA1-S-65	LS4.5	64.4 ± 0.6	19.3 ± 0.8	14:30 12.04.2022
CLA1-S-66	LS4.1	83.7 ± 1.1		
CLA1-S-69	LS4.5	75.4 ± 0.9	14.9 ± 0.8	17:05 13.04.2022
CLA1-S-70	LS4.1	90.3 ± 0.8		
CLA1-S-73	LS4.5	73.8 ± 0.9	17.3 ± 0.4	20:30 13.04.2022
CLA1-S-74	LS4.1	91.1 ± 0.0		
CLA1-S-75	LS4.1	93.5 ± 0.1	14.8 ± 0.1	20:30 13.04.2022
CLA1-S-76	LS4.5	78.7 ± 0.1		
CLA1-S-78	LS4.1	90.5 ± 0.2	13.7 ± 0.4	11:15 14.04.2022
CLA1-S-79	LS4.5	76.8 ± 0.7		
CLA1-S-84	LS4.5	77.1 ± 0.5	13.1 ± 0.4	11:15 14.04.2022
CLA1-S-85	LS4.1	90.2 ± 0.4		
CLA1-S-86	LS4.5	76.7 ± 0.1	10.3 ± 0.2	18:10 14.04.2022
CLA1-S-87	LS4.1	87.0 ± 0.2		

gasification (DFBG), for which fuel introduction in the AR is used to drive up AR temperatures and thus obtain a driving force for the chemical reactions in the FR and an inert bed material is used to transport the reaction heat between the two reactors (Ripfel-Nitsche et al., 2007; Bolhar-Nordenkampf et al., 2002; Bolhàr-Nordenkampf et al., 2003).

On the other hand, the desired effect on $\lambda_{AR,eff}$ is obtained by using the suggested process control concept, manipulating the AR recycling ratio at low propane input. For the given operating periods this translates into a drop of $\lambda_{AR,eff}$. from ~0.5 to ~0.2 as the AR recycling ratio is increased from 0 to 0.38. As elucidated in detail in Chapter 3.1, this can be explained by the fact that the oxygen uptake by the OC in the AR is diminished as the oxygen availability in the AR decreases. This lack in oxygen availability in the AR for $RR_{AR}>0$ is also seen in Fig. 9, as outlet O_2 concentrations <2 vol-% (generally <1 vol-%) were measured for the AR, when the AR flue gas recirculation was switched-on ($RR_{AR}>0.1$).

Efficient CLG operation is only obtained if the decrease in $\lambda_{AR,eff}$ with increasing RR_{AR}, also translates into a drop in the effective air-to-fuel equivalence ratio inside the FR. This is the case as $\lambda_{FR,eff}$ primarily governs the CLG process efficiency, by determining how much oxygen is released inside the FR, leading to a given degree of feedstock oxidation. To determine the correlation between the two effective air-to-fuel equivalence ratios, $\lambda_{FR,eff}$ and $\lambda_{AR,eff}$ are shown in Fig. 10 for all 177 operating sub-periods under investigation. It becomes clear that in case of low amounts of propane firing, all values fall onto or close to the angle bisector, signifying ϕ_λ=1.[10] Thus, the CLG unit is in steady state for those operating conditions, and oxygen release in the FR is equal to the oxygen uptake in the AR, meaning that given sufficient stabilization times (see Chapter 3.1), a decrease in $\lambda_{AR,eff}$. also translates into an equivalent decrease in $\lambda_{FR,eff}$. However, as soon as propane loads exceed 150 kW, a clear upwards deviation from the angle bisector is visible, signifying that more oxygen is released in the FR than is taken up in the AR. This again underlines the previous hypothesis (see above), that in case of strong propane firing, oxygen uptake in the AR might be the rate-limiting step. This means when operating the CLG unit for long times with propane firing, the entire OC inventory slowly becomes more and more reduced until a new steady state is reached.[11] A finding supporting this hypothesis is that a solid sample taken from LS4.1 towards the end of BP6 (highlighted in Fig. 10) showed a strong degree of reduction (S-13: $X_{s,AR}$= 15.2%, see Table 3 in the Appendix), when its oxidation degree was determined. Therefore, co-firing of propane or any other feedstock in the AR has to be considered undesired for CLG operation as it prevents meaningful oxygen transport from the AR to the FR. On the other hand, when striving for DFBG operation (i.e. no/limited oxygen transport) it yields the option to obtain a strongly reduced OC entering the FR, releasing low amounts of oxygen and potentially catalyzing certain chemical reactions (e.g. tar or methane reforming) (Zhou et al., 2022; Min et al., 2011). However, this approach is not considered further here, as efficient CLG operation, signified by meaningful oxygen transport between AR and FR, is targeted.

3.2.2. Acting mechanism of novel process control concept

Further insights into the underlying phenomena of the novel process control concept can be obtained when considering the oxidation degree of solid samples collected during different operating periods. As elaborated in Chapter 3.1, the pursued measure to obtain a more deeply reduced OC entering the FR is the restriction of air supply in the AR.

[10] As explained above (see Chapter 3.1.2), measurement inaccuracy leads to minor deviations from ϕ_λ=1 for some operating points, although mass and component (C, H, O) balances could be closed with an accuracy of ±5 % for all operating points.

[11] Within the entire duration of BP6 (>7 h), steady-state conditions were not reached, meaning that the OC was further reduced throughout the entire duration.

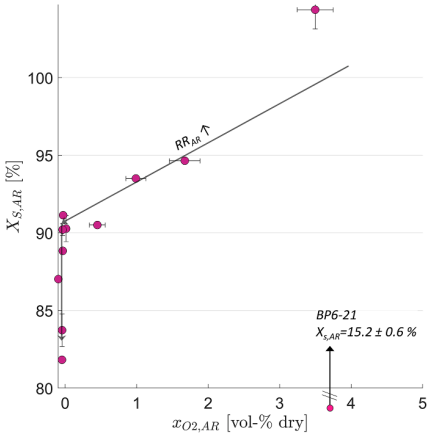

Fig. 11. Oxidation degree of samples collected from LS4.1 as a function of the oxygen content at the AR outlet (for sampling times for the respective samples please refer to Table 3). Gray arrows denote the progression of $X_{s,AR}$ as RR_{AR} is increased.

Fig. 11, showing the dependency of the oxidation degree of samples collected from LS4.1 with the oxygen content at the AR outlet, displays a clear correlation between the two parameters. In case of oxygen excess ($x_{O2,AR}$>3 vol-%), full oxidation of the OC is achieved in the AR (for low amounts of propane firing). Yet, with decreasing oxygen content at the AR outlet, $X_{s,AR}$ drops to a value of approx. 90% at $x_{O2,AR}$=0 vol-%, indicating that OC oxidation kinetics play a crucial role inside the AR at low oxygen concentrations. When further decreasing the oxygen input at $x_{O2,AR}$=0 vol-% through increasing RR_{AR}, the oxidation degree of the OC further decreases, as its oxidation is hindered through thermodynamic constraints. Consequently, the application of flue gas recirculation for the AR is an efficient measure to prevent full OC oxidation in the AR. As mentioned before, another approach to achieve this is the injection of significant amounts of propane into the AR, as practiced during BP6. Fig. 15 shows that as an effect of continuous propane-induced oxygen depletion of the OC during BP6 (see also Fig. 10), the OC sample collected from LS4.1 towards the end of BP6 exhibited a close to fully reduced state. Therefore, the solid sample corroborates the previous hypothesis that propane injection hinders oxygen uptake inside the AR. Moreover, it can be postulated that the OC was further reduced with each redox cycle, as more oxygen was released inside the FR than taken up inside the AR during BP6 (see Fig. 10), requiring a given time until the entire OC inventory was reduced to $X_{s,AR}$< 20%. This would also explain why the 21 sub-periods of BP6 fall onto a line rather than an individual point in Fig. 10 and Fig. 15 (see Chapter 3.2.3) as the OC was continuously reduced further throughout the entire length of BP6 (>7 h). This finding makes another strong point for using the suggested process control strategy, relying on AR flue gas recirculation, to control the degree of oxidation of the OC at the AR outlet, as opposed to propane injection - while rapid and tailored adjustments of the system are attainable for the former, extensive stabilization times are necessary for the latter.

Ultimately, the decrease in $X_{s,AR}$ obtained for either approach only yields the desired result (i.e. an increase in the CGE), if oxygen release in the FR is reduced. As explained before, this means that the change in oxidation degree between AR and FR and thus the effective air-to-fuel equivalence ratio have to be reduced for a given solid circulation rate (see Eq. (16)). It is known that as $X_{s,AR}$ is reduced (e.g. through oxygen restriction in the AR), the propensity of the OC to release oxygen inside the FR is reduced (Abad et al., 2011; Ohlemüller et al., 2018). The ensuing slower reaction kinetics, thus ultimately lead to an increase in the CGE, as the feedstock is oxidized to lesser extents inside the FR. This

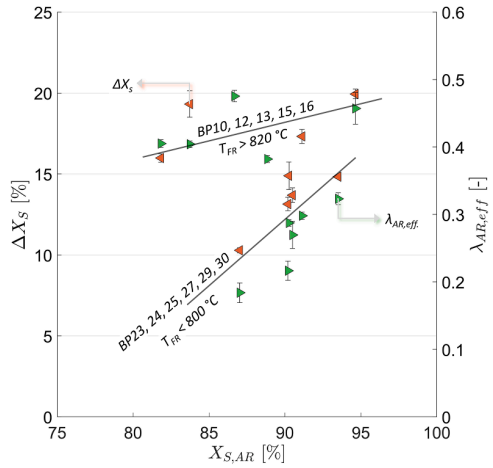

Fig. 12. Change in oxidation degree between AR and FR determined for samples collected from LS4.1 & LS4.5 and efficient AR air-to-fuel equivalence ratio as a function of AR oxidation degree (for sampling times for the respective solid samples refer to Table 3).

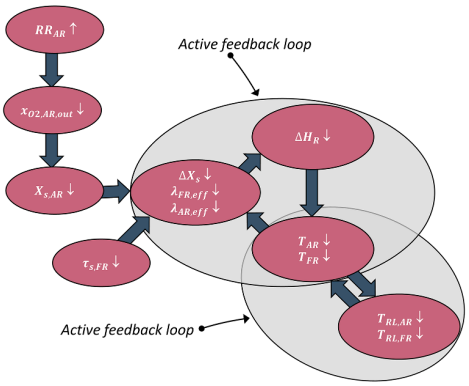

Fig. 13. Schematic illustration of the suggested mechanism of action of the CLG process control concept - Effect of an increase in the AR recycling ratio (RR_{AR} ↑) on important process variables.

correlation is illustrated in Fig. 12, showing a distinct impact of $X_{s,AR}$ on ΔX_s and $\lambda_{AR,eff}$. However, it becomes visible, that the oxidation degree at the AR outlet is not the only variable affecting the oxygen release inside the FR. For BP10, 12, 13, 15, and 16 for which FR temperatures fell into the range of 820–890 °C, significantly higher values were obtained for ΔX_s and $\lambda_{AR,eff}$ for a given value of $X_{s,AR}$ than for BP23, 24, 25, 27, 29, and 30, for which FR temperatures were below 800 °C. This can be related to the fact, that apart from X_s, the FR temperature is another crucial parameter affecting OC reaction kinetics (Abad et al., 2011; Ohlemüller et al., 2018). Consequently, one has to consider this active feedback loop between $X_{s,AR}$, ΔX_s, and T_{FR}, when attempting to explain the behavior of the CLG unit during the transient switch-over periods.

To further understand this, the entire mechanism of action proposed for the CLG process control concept, which is illustrated in Fig. 13, has to be considered. As explained above, the oxygen release inside the FR is kinetically limited for the 1 MW_{th} unit, and is thus dependent on the oxidation degree of the OC entering the FR ($X_{s,AR}$), FR temperatures, and the solids residence time inside the FR ($\tau_{s,FR}$). Subsequent to the increase in RR_{AR}, entailing a decrease in the oxygen content in the AR, $X_{s,AR}$ decreases. This parameter being one factor impacting OC kinetics, thus

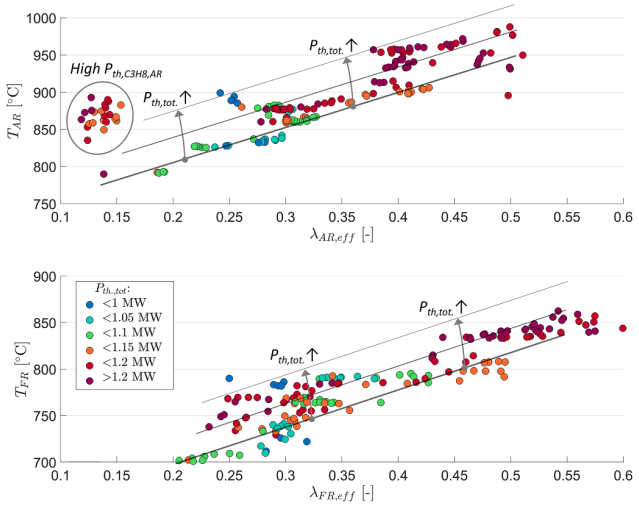

Fig. 14. AR (top) and FR (bottom) reactor temperatures as a function of the effective air-to-fuel equivalence ratio for different thermal loads for all operating periods given in Table 4. Gray markup to guide the eye: Straight lines mark the effect of λ_{eff} on reactor temperatures, whereas arrows mark the effect of increasing total thermal loads.

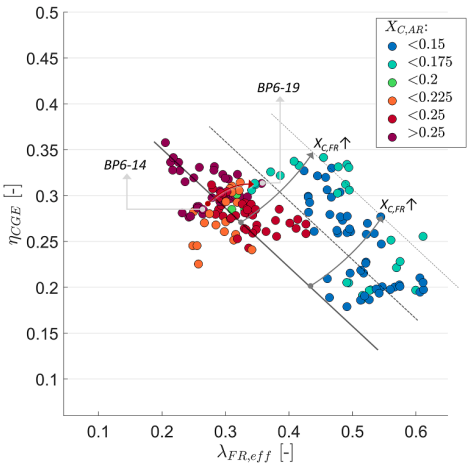

Fig. 15. Cold gas efficiency as a function of the effective air-to-fuel equivalence ratio in the FR for varying AR carbon conversions for all operating periods given in Table 4. Gray markup to guide the eye: Straight lines mark the effect of $\lambda_{FR,eff}$ on the cold gas efficiency, whereas arrows mark the effect of increasing $X_{C,FR}$ (=decreasing $X_{C,AR}$).

leads to a drop in the oxygen release in the FR (i.e. ΔX_s, $\lambda_{FR,eff}$ and $\lambda_{AR,eff}$ decrease[12]). Due to this, the enthalpy of reaction (i.e. ΔH) of the entire system decreases, as exothermic oxidation reactions occur to lesser extents inside the FR and AR. As a result of this, reactor temperatures decrease (see Fig. 5 in Chapter 3.1.1 and Fig. 14 in Chapter 3.2.3), which again leads to slower OC reaction kinetics and thus a decrease in oxygen release inside the FR. The time required for this active feedback loop between OC reaction kinetics, reactor enthalpies, and reactor temperatures to stabilize, can be named as another factor playing into the

[12] Fig. 12 and Fig. 19 (see appendix) show a close correlation between ΔX_s and $\lambda_{AR,eff}$, demonstrating that the decrease in oxygen release in the FR and uptake in the AR ($\lambda_{FR,eff}$ and $\lambda_{AR,eff}$), which can be derived from the FR and AR product gas composition, is also clearly visible in the solids composition (ΔX_s).

transient behavior of the CLG unit after changes of RR_{AR}. Clearly, the duration required for this feedback loop to stabilize depends on several factors, such as the size of the reactor inventory (i.e. total OC mass), the interplay of gas-phase and refractory temperatures (T_{RL}) ,[13] as well as the extent to which the oxygen availability inside the AR is reduced, explaining why the duration required to reach steady state varied for TP-1, TP-2, and TP-3 (2–4 h).

On the one hand, the inclusion of data collected from the solid samples thus corroborate all fundamental hypotheses derived from online data, such as the fact that changes in the oxidation degree of the OC, induced through reduced oxygen availability in the AR, are responsible for the increased CGE of the CLG unit. On the other hand, the combined analysis of online and offline data collected for different steady state CLG operating periods allowed for deeper insights into the mechanisms occurring inside the CLG unit, further promoting the understanding of the novel gasification technology.

3.2.3. Effect of novel process control concept on CLG process efficiency

After presenting the acting mechanism of the novel process control concept, the question is how it affects the overall efficiency of the process. When evaluating CLG efficiency in the 1 MW_{th} scale, it has to be kept in mind that in contrast to other units, a free variation of individual parameters is not possible, due to the entanglement of hydrodynamics, product and educt compositions, reaction kinetics, temperatures, etc. One important example for this is given in Fig. 14. Here, it becomes obvious that in chemical looping mode the effective air-to-fuel equivalence ratios primarily determine reactor temperatures.[14] This can be related to the fact that depending on the oxygen release (FR) and uptake (AR), the exothermicity of the chemical reactions vary, leading to changes in reactor temperatures, which was already observed in Chapter 3.1. As it is known that changes in FR temperatures affect the CLG efficiency (Condori et al., 2021a,b, 2022), this means that altering $\lambda_{FR,eff}$ impacts CLG efficiency directly (i.e. through reduced oxygen release) as well as indirectly (i.e. via decreasing FR temperatures). Another effect visible in Fig. 14 is that higher reactor temperatures are generally attainable for given air-to-fuel equivalence ratios by increasing the total thermal input. Again this observation can be explained by considering the heat balance of the system, as for higher thermal loads, the relative impact of heat losses from the reactor walls as well as the cooling effect of the cooling lances decreases and hence higher reactor temperatures can be sustained.

These observations ultimately underline an inherent trade-off also faced in full-scale units: Although higher reactor temperatures are generally preferable (esp. for reaction kinetics), they also mean that higher air-to-fuel equivalence ratios are required, lowering key performance indicators such as the cold gas efficiency of the process. Therefore, there exists a “sweet spot” for which reactor temperatures are sufficiently high to drive the underlying chemical reactions, yet air-to-fuel equivalence ratios are low enough to obtain meaningful CGEs (see below). However, when extrapolating these results to a full-scale gasifier, the following peculiarities of the 1 MW_{th} pilot have to be factored-in:

i Because of the high surface-to-volume ratio of the pilot plant, heat losses amount to approx. 10–15% of the thermal input, reducing the amount of energy available for the chemical reactions.

ii Due to the setup of the reactor system, the cooling lances in the AR cannot be fully removed from the pilot plant and hence continuously extract heat from the reactor system. For the given operating periods, heat extraction via those cooling lances amounts to 7–11% of the thermal input, further reducing the energy available for chemical reactions.[15]

iii Due to i. and ii., reactor temperatures in the 1 MW_{th} unit are lower than in an industrial setup for a given set of boundary conditions. Hence, reaction kinetics are slower, leading to lower feedstock conversions inside the FR and ultimately to lower overall efficiencies.

iv The calculation of the cold gas efficiency (see Eq. (7)) neglects all hydrocarbons except for methane (i.e. C $\geq$ 2). This means the energy contained in these species in not represented in the cold gas efficiency.

Therefore, when operating an industry-scale chemical looping gasifier autothermally and when considering the full heating value of the FR product gas, process simulations show that cold gas efficiencies well above 60% can be expected at FR temperatures above 850 °C and air-to-fuel equivalence ratios around 0.3 (Dieringer et al., 2020; Samprón et al., 2021). Due to the peculiarities of the 1 MW_{th} unit, values for the CGE obtained here fall short of this value. Nonetheless, the analysis of the impact of important process variables on the cold gas efficiency in the 1 MW_{th} unit yields unique insights, regardless of the absolute value obtained, due to the industry-like setup of the CLG system.

Previous studies found that for externally heated CLG units, the most important variable affecting the CGE is the efficient FR air-to-fuel equivalence ratio (Condori et al., 2021a; Condori et al., 2022). The dependency for those two parameters obtained for the 1 MW_{th} pilot plant is shown in Fig. 15. As expected, the cold gas efficiency increases with decreasing $\lambda_{FR,eff}$. as less oxygen is released in the FR, leading to an increase in the heating value of the FR product gasses, supporting the findings made in Chapter 3.1. For the operating periods under investigation, the cold gas efficiency increases from 20% to above 35% when decreasing $\lambda_{FR,eff}$ from 0.4 to 0.2 by using AR flue gas recirculation.

A second trend visible in Fig. 15 is that η_{CGE} increases with decreasing carbon conversion in the AR. This means that as the feedstock is converted to a greater degree inside the FR ($X_{C,AR}\downarrow$ & $X_{C,FR}\uparrow$, see Eq. (10)), more gas or gas with a higher heating value is obtained from the FR. Strategies to increase char conversion inside the FR are for example increased FR temperatures [(Cetin et al., 2005; Barrio and Hustad, 2001; Barrio et al., 2001; Keller et al., 2011; DIRECTIVE (EU) 1997; Ollero et al., 2003)], an increase in residence times of all solids in the FR (e.g. higher reactor inventories or alternative FR layout) (Condori et al., 2022; Pérez-Vega et al., 2016), or an exclusive increase in char residence times in the FR, e.g. via intermediate char separation and reintroduction in a so-called carbon stripper (Pérez-Vega et al., 2016; Abad et al., 2013; Abad et al., 2015). Yet, for a given reactor layout, optimizing char conversion inside the FR without jeopardizing the cold gas efficiency is not easily done, due to the system’s entanglement. One example for this being that higher FR char conversions were generally obtained at higher FR temperatures. However, as shown in Fig. 14, these are obtained for higher values of $\lambda_{FR,eff}$, for which lower CGEs are obtained (see Fig. 15), thus signifying an additional trade-off, which needs to be optimized to increase process efficiency. Another interesting trend visible in Fig. 15, which was observed towards the end of BP-6, where large amounts of propane were fired (see Fig. 10), is that the cold gas efficiency increases slightly as the effective air-to-fuel equivalence ratio increases between BP6–14 and BP6–19. To this point, it is unclear why

[13] As elaborated in Chapter 3.1, the interplay between reactor gas phase temperatures and refractory lining temperatures decelerates rapid temperature drops/increases, esp. for reactors with a high surface-to-volume ratio.

[14] In an autothermal setup reactor temperatures are dependent on the entire set of boundary conditions (see also Fig. 13). Apart from the efficient air-to-fuel equivalence ratio and the thermal load highlighted in Fig. 14, this includes solid circulation, the amount of gas used for fluidization, and heat losses, amongst others (Dieringer et al., Jun. 2020).

[15] This circumstance is accounted for in the calculation of the CGE, yet clearly still impacts reactor temperatures.

this behavior was observed. Yet, this again indicates that at very low OC oxidation degrees,[16] the OC could catalyze endothermic gas phase reactions (e.g. tar/methane reforming), thereby increasing the energy content of the FR product gas. The catalytic effect of reduced ilmenite on different reactions has also been observed in literature (Zhou et al., 2022; Min et al., 2011). Hence, the results presented in Fig. 15 suggest that lower air-to-fuel equivalence ratios in the FR could enhance cold gas efficiencies of the CLG process not only by lowering the oxygen release in the FR, but also by catalyzing endothermic gas-phase reactions, favoring the formation of syngas species, through the presence of a more reduced OC inside the FR at lower values of $\lambda_{FR,eff}$. This hypothesis needs to be confirmed by further studies, e.g. measurements of higher hydrocarbons.

4. Conclusions

One crucial aspect in up-scaling the CLG technology is the demonstration of a viable process control concept, allowing for autothermal operation. In the course of this work, it has been shown that the suggested process control concept, utilizing AR flue gas recirculation to restrict the air supply in the AR, allows for an independent control of reactor hydrodynamics and the air-to-fuel equivalence ratio of the CLG process, forming the basis for efficient CLG operation. Based on experimental results gathered in 1 MW_{th} scale, the following conclusions can be made:

- The presented CLG concept satisfies all relevant criteria, i.e. facilitating the production of a high-calorific raw synthesis gas through guaranteeing sufficiently high temperatures in the FR, without jeopardizing the chemical energy contained in the feedstock.
- The selected route of implementation, i.e. flue gas recycling for the AR, showed promising results during the 1 MW_{th} test campaigns, as the oxygen input was controlled accurately, without disturbing reactor hydrodynamics on thus, solid and heat transport between the reactors.
- Other process-wise implementation options, such as diluting the inlet air for the AR with an inert (e.g. N_2) or tailoring AR dimensions, briefly described in this paper, should show similar results and can be employed, depending on their suitability for the given plant layout. Hence, the general control concept of reducing the air-to-fuel equivalence ratio (λ) is suitable for large-scale (>100 MW_{th}) CLG units.
- Experimental data shows, that changes in λ propagate slowly into the system. This considerable inertia of the system is caused by the fact that the OC inventory of the gasifier effectively acts as an oxygen storage, releasing surplus oxygen during the transient adjustment process. Moreover, the interplay of reactor temperatures, OC reaction kinetics and reaction enthalpies is deemed to play a crucial role in the system's transient response. For the 1 MW_{th} unit, switch-over times of up to 4 h were observed when reducing λ through initiating flue gas recycling inside the AR. Consequently, this system inertia has to be considered, when operating CLG units of substantial size.
- Qualitative and quantitative comparisons between different transient switch-over periods showed that the observed behavior occurs consistently regardless of the exact boundary conditions, indicating that the observed transient behavior is a key aspect in operation of large-scale CLG units.
- Through analysis of solid OC samples extracted from both loop seals during operation, the postulated progression of the oxidation degree of the OC during the transient switch-over periods was verified. With the inclusion of this data set, a detailed mechanism of action of the CLG process control concept was formulated.

In summary, the results presented in this paper provide a comprehensive understanding of the CLG technology and its governing phenomena and thus can be considered to be a crucial building block in advancing it towards market maturity. To further extend process understanding and to be able to further refine the process control concept, it is foreseen to apply it to concept to reach lower λ (0.35–0.45) at thermal loads up to 1.5 MW_{th}, to increase the cold gas efficiency in semi-industrial scale, further underlining the competitiveness of the CLG technology.

Author contribution

Paul Dieringer: Conceptualization, Methodology, Investigation, Data Curation, Writing – Original Draft, Visualization. **Falko Marx:** Writing – Review & Editing, Methodology, Investigation, Data Curation. **Benjamin Michel:** Investigation. **Jochen Ströhle:** Writing – Review & Editing, Supervision, Project Administration, Funding Acquisition. **Bernd Epple:** Resources, Funding Acquisition.

All authors have read and agreed to the published version of the manuscript.

Funding

This work has received funding of the European Union's Horizon 2020-Research and Innovation Framework Programme under grant agreement No. 817841 (Chemical Looping gasification foR sustainAble production of biofuels-CLARA).

The content of this work reflects only the author's view, and the European Commission is not responsible for any use that may be made of the information it contains.

The funders had no role in the design of the study; in the collection, analyses, or interpretation of data; in the writing of the manuscript, or in the decision to publish the results.

Declaration of Competing Interest

The authors declare that they have no known competing financial interests or personal relationships that could have appeared to influence the work reported in this paper.

Data availability

Data will be made available on request.

Acknowledgements

The authors would like to thank Aichernig Engineering GmbH, Austria fortheir support in the design and safety analysis of the 1 MW_{th} CLG unit.

[16] As stated in Chapter 3.2.2, low values for X_S were found to be present toward the end of BP-6, associated to the prolonged duration of oxygen depletion during BP-6, see Fig. 10 & Fig. 11.

Annex 1. Additional Information

A.1. Derivation of calculation for AR recycling ratio (RR_{AR})

The calculation of RR_{AR} is achieved by calculating a component balance (C or O) around the primary-air line (system boundaries, see Fig. 16).

As the only unit operation taking place inside these system boundaries is the mixing of the recycled AR flue gas and fresh air, the total mass and thus volume flow stays constant:

$$\dot{V}_{in,AR} = \dot{V}_{Rec.,AR} + \dot{V}_{Air,AR} \tag{17}$$

i) Oxygen Balance

The oxygen balance around the primary-air line thus can be formulated as:

$$\dot{V}_{in,AR} \cdot x_{O2,AR,in} = \dot{V}_{Rec.,AR} \cdot x_{O2,AR,out} + \dot{V}_{Air,AR} \cdot 21\ \text{vol.\%} \tag{18}$$

With consideration of Eq. (17), Eq. (18) can be formulated as:

$$\dot{V}_{in,AR} \cdot x_{O2,AR,in} = \left(\dot{V}_{in,AR} - \dot{V}_{Air,AR}\right) \cdot x_{O2,AR,out} + \dot{V}_{Air,AR} \cdot 21\ \text{vol.\%} \tag{19}$$

Reordering of Eq. (19) yields:

$$\dot{V}_{Air,AR} = \dot{V}_{in,AR} \cdot \frac{x_{O2,AR,in} - x_{O2,AR,out}}{21\ \text{vol.\%} - x_{O2,AR,out}} \tag{20}$$

Combination of Eq. (5), Eq. (17), and Eq. (18) thus results in:

$$RR_{AR} = \frac{\dot{V}_{Rec.,AR}}{\dot{V}_{Rec.,AR} + \dot{V}_{Air,AR}} = \frac{\dot{V}_{in,AR} - \dot{V}_{in,AR} \cdot \frac{x_{O2,AR,in} - x_{O2,AR,out}}{21\ \text{vol.\%} - x_{O2,AR,out}}}{\dot{V}_{in,AR}} = \frac{x_{O2,AR,in} - 21\ \text{vol.\%}}{x_{O2,AR,out} - 21\ \text{vol.\%}} \tag{21}$$

If the desired CLG operation is achieved, the outlet O_2 concentration for the AR drops to 0 vol-%, and Eq. (21), simplifies to:

$$RR_{AR} = \frac{x_{O2,AR,in} - 21\ \text{vol.\%}}{-21\ \text{vol.\%}} \tag{22}$$

ii) Carbon Balance

For the carbon balance, it is assumed that the CO_2 content of ambient air can be neglected:

$$\dot{V}_{in,AR} \cdot x_{CO2,AR,in} = \dot{V}_{Rec.,AR} \cdot x_{CO2,AR,out} \tag{23}$$

Combination of Eq. (5), and Eq. (23) thus results in:

$$RR_{AR} = \frac{x_{CO2,AR,in}}{x_{CO2,AR,out}} \tag{24}$$

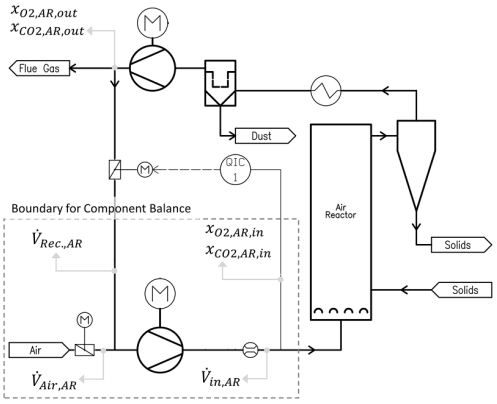

Fig. 16. Illustration of CLG control concept utilized in 1 MW_{th} pilot plant with system boundary (dashed line) and all variables (grey arrows) used for derivation of AR recycling.

A.2. Progression of Evaluation Parameters during TP-2 & TP-3

Fig. 17 and Fig. 18 show the progression of the most important evaluation parameters for the transient periods TP-2 and TP-3, respectively. It is visible that for all three transient periods similar observations can be made. These are presented in detail in Chapter 3.1.

A.3. Oxidation degree of OC samples collected during 1 MW_{th} operation

Table 3 shows a summary of the oxidation degrees (X_S) of all loop seal samples collected during CLG operation, with the corresponding sampling location and time. The change in oxidation degree between AR and FR (ΔX_S) for those solid samples is visualized as a function of the efficient AR air-to-fuel equivalence ratio in Fig. 19.

A.4. Boundary conditions of operating periods under consideration

The boundary conditions for each steady-state operating point under consideration are listed in Table 4, while boundary conditions for the transient periods are given in Table 5.

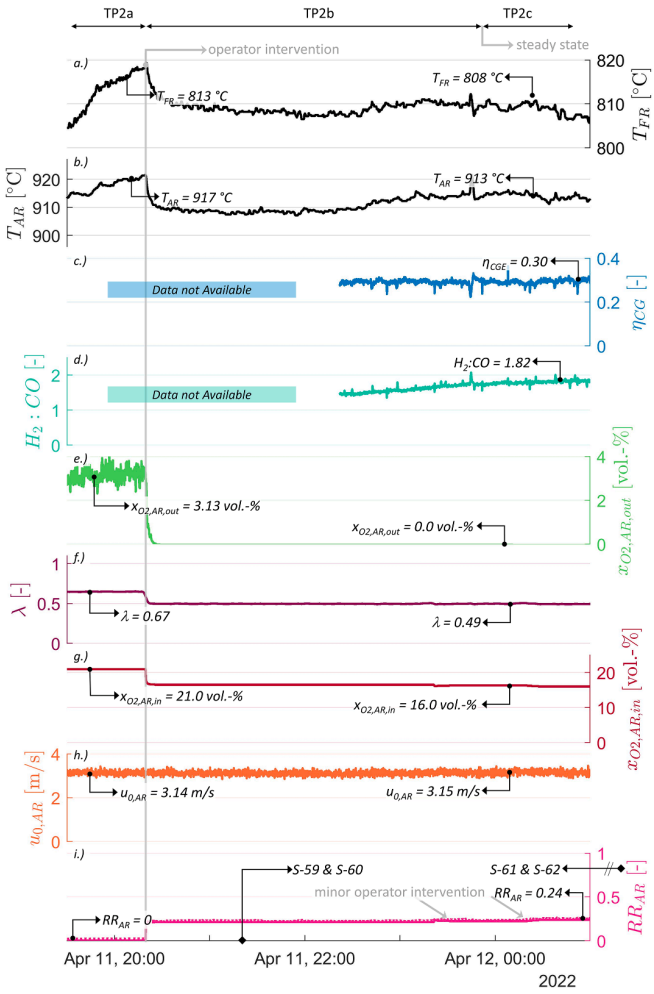

Fig. 17. Progression of important process and evaluation parameters over time for TP-2.
From top to bottom: a.) FR and b.) AR temperature, c.) cold gas efficiency (η_{CGE}), d.) H_2/CO-ratio in FR product gas, e.) oxygen concentration at AR outlet ($x_{O2,AR,out}$), f.) air-to-fuel equivalence ratio (λ), g.) oxygen concentration at AR inlet ($x_{O2,AR,in}$), h.) AR gas velocity, and i.) AR flue gas recycling ratio (RR_{AR}), calculated from O_2 (-) and CO_2 (:) balance. Arrows with diamonds at the end signify the sampling time of a given solid sample.

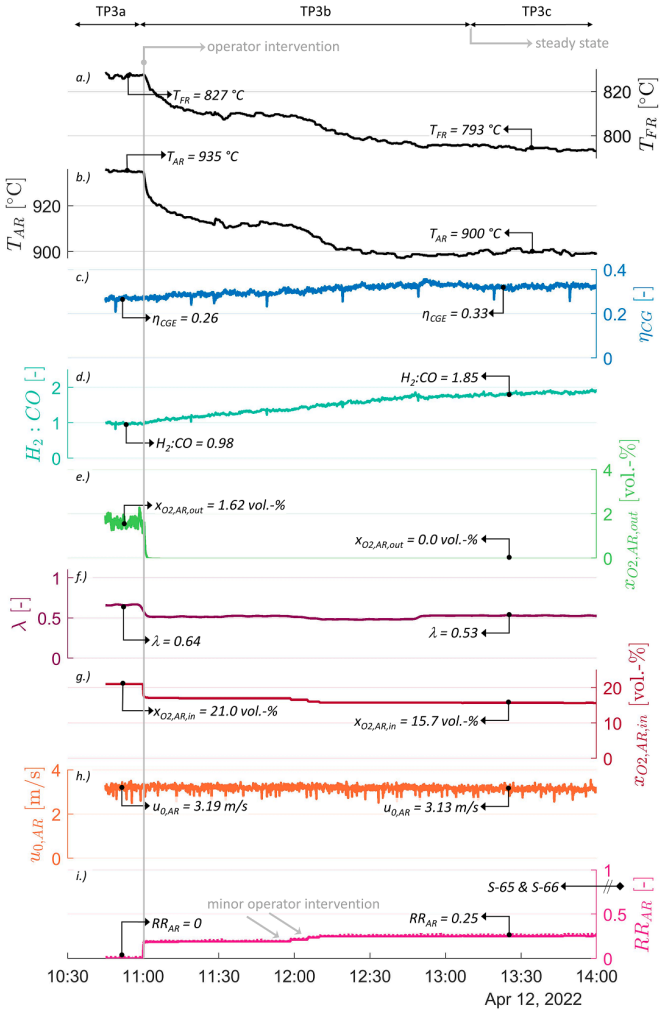

Fig. 18. Progression of important process and evaluation parameters over time for TP-3.
From top to bottom: a.) FR and b.) AR temperature, c.) cold gas efficiency (η_{CGE}), d.) H_2/CO-ratio in FR product gas, e.) oxygen concentration at AR outlet ($x_{O2,AR,out}$), f.) air-to-fuel equivalence ratio (λ), g.) oxygen concentration at AR inlet ($x_{O_2,AR,in}$), h.) AR gas velocity, and i.) AR flue gas recycling ratio (RR_{AR}), calculated from O_2 (-) and CO_2 (:) balance. Arrows with diamonds at the end signify the sampling time of a given solid sample.

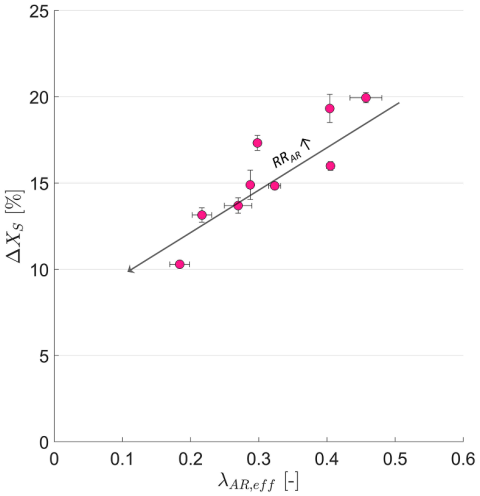

Fig. 19. Correlation between the measured efficient AR air-to-fuel equivalence ratio and the oxidation degree between AR and FR determined for samples collected from LS4.1 & LS4.5.

Table 4
Operating conditions for steady-state operating periods under investigation. BPX (steady-state operating period).

Variable	Description	BP1	BP2	BP3	BP4	BP5	BP6	BP7	Unit
$m_{Feedstock}$	Mass flow of biomass pellets to FR	156.1	167.5	163.4	175.4	190.3	191.5	223.2	kg/h
$m_{Make-Up}$	Mass flow of OC to LS4.1	34.7	88.4	68.2	56.6	0.0	41.9	0.0	kg/h
T_{AR}	AR max. temperature	898.6	885.2	879.3	884.8	843.6	877.2	958.6	°C
T_{FR}	FR max. temperature	812.2	820.9	821.7	821.9	756.7	772.9	858.9	°C
Δp_{AR}	AR pressure drop (inventory)	21.5	32.9	44.4	39.5	29.0	32.8	41.7	mbar
$p_{AR,Cyclone}$	Pressure downstream of AR cyclone	−3.1	−3.1	−3.1	−3.1	−3.1	−3.1	−1.0	mbar
Δp_{FR}	FR pressure drop (inventory)	37.5	45.9	49.5	50.3	65.1	65.8	70.6	mbar
$p_{FR,Cyclone}$	Pressure downstream of FR cyclone	5.5	5.4	5.5	5.6	5.1	5.2	7.4	mbar
$\dot{m}_{FM,FR}$	Mass flow of FR fluidization (H_2O)	304.8	306.0	301.6	297.2	249.8	253.7	237.7	kg/h
$\dot{m}_{FM,AR}$	Mass flow of AR fluidization*	953.7	952.3	952.1	953.9	932.5	921.7	1004.8	kg/h
$\dot{m}_{C3H8,AR}$	Mass flow of propane entering AR	16.6	18.3	19.4	19.4	19.4	19.4	8.6	kg/h
$\dot{m}_{FM,LS4.1}$	Vol. flow of LS4.1 fluidization	19.2 (N_2)	19.3 (N_2)	19.2 (N_2)	19.4 (N_2)	20.5 (N_2)	22 (N_2)	16 (N_2)	Nm^3/h
$\dot{m}_{FM,LS4.5}$	Vol. flow of LS4.5 fluidization	26.7 (N_2)	29.2 (N_2)	29.9 (N_2)	30.8 (N_2)	30.4 (N_2)	31 (N_2)	20.6 (CO_2)	Nm^3/h
$\dot{m}_{FM,J-Valve}$	Vol. flow of J-Valve fluidization	13.4 (N_2)	15.7 (N_2)	16.8 (N_2)	16.9 (N_2)	18.3 (N_2)	18.1 (CO_2)	18.4 (N_2)	Nm^3/h
RR_{AR}	AR flue gas recycling ratio	0.00	0.00	0.00	0.00	0.00	0.00	0.00	–

Variable	Description	BP8	BP9	BP10	BP11	BP12	BP13	BP14	BP15	Unit
$m_{Feedstock}$	Mass flow of biomass pellets to FR	222.8	223.6	226.4	220.8	231.8	226.4	235.0	229.1	kg/h
$m_{Make-Up}$	Mass flow of OC to LS4.1	0.0	33.2	35.3	24.9	46.1	53.8	0.0	50.9	kg/h
T_{AR}	AR max. temperature	957.9	963.1	974.5	992.6	943.3	948.0	919.8	911.6	°C
T_{FR}	FR max. temperature	858.7	869.0	892.3	908.7	864.6	881.4	839.5	833.6	°C
Δp_{AR}	AR pressure drop (inventory)	37.8	45.0	52.0	48.7	47.3	39.8	55.4	53.7	mbar
$p_{AR,Cyclone}$	Pressure downstream of AR cyclone	−1.0	−1.0	−1.0	−1.0	−1.1	−1.1	−0.9	−0.9	mbar
Δp_{FR}	FR pressure drop (inventory)	69.6	61.4	68.0	66.4	70.6	69.3	75.9	73.4	mbar
$p_{FR,Cyclone}$	Pressure downstream of FR cyclone	7.8	7.2	7.6	5.8	6.8	7.2	5.1	5.2	mbar
$\dot{m}_{FM,FR}$	Mass flow of FR fluidization (H_2O)	239.1	232.1	227.0	229.9	230.9	235.7	216.8	217.9	kg/h
$\dot{m}_{FM,AR}$	Mass flow of AR fluidization*	1005.7	965.6	965.6	966.2	970.2	1000.6	969.4	971.0	kg/h
$\dot{m}_{C3H8,AR}$	Mass flow of propane entering AR	8.6	10.1	10.1	10.1	10.1	10.1	6.8	3.6	kg/h
$\dot{m}_{FM,LS4.1}$	Vol. flow of LS4.1 fluidization	15.9 (N_2)	15.7 (N_2)	15.1 (N_2)	14.9 (N_2)	15.6 (N_2)	15.2 (N_2)	15.7 (N_2)	15.6 (N_2)	Nm^3/h
$\dot{m}_{FM,LS4.5}$	Vol. flow of LS4.5 fluidization	19.6 (CO_2)	18.8 (CO_2)	19.5 (CO_2)	19.1 (CO_2)	19.3 (CO_2)	16.5 (CO_2)	14.9 (CO_2)	15.3 (CO_2)	Nm^3/h
$\dot{m}_{FM,J-Valve}$	Vol. flow of J-Valve fluidization	20.9 (CO_2)	21.8 (CO_2)	22 (CO_2)	22 (CO_2)	22.9 (CO_2)	23.7 (CO_2)	19.5 (CO_2)	18.9 (CO_2)	Nm^3/h
RR_{AR}	AR flue gas recycling ratio	0.00	0.00	0.00	0.00	0.19	0.00	0.23	0.24	–

Variable	Description	BP16	BP17	BP18	BP19	BP20	BP21	BP22	BP23	Unit
$m_{Feedstock}$	Mass flow of biomass pellets to FR	221.3	223.7	221.5	228.9	228.9	230.2	226.6	232.5	kg/h
$m_{Make-Up}$	Mass flow of OC to LS4.1	0.0	1.7	0.0	0.0	23.2	91.8	0.0	13.0	kg/h
T_{AR}	AR max. temperature	906.2	904.0	903.3	902.2	893.8	884.4	883.7	882.1	°C
T_{FR}	FR max. temperature	821.7	821.3	816.0	814.2	808.8	806.6	800.5	792.9	°C
Δp_{AR}	AR pressure drop (inventory)	44.0	42.3	47.2	45.2	47.6	56.5	64.4	63.8	mbar
$p_{AR,Cyclone}$	Pressure downstream of AR cyclone	−1.1	−1.1	−1.1	−1.1	−1.1	−1.1	−1.2	−1.2	mbar
Δp_{FR}	FR pressure drop (inventory)	90.0	91.0	77.8	74.7	74.2	73.5	65.2	63.5	mbar
$p_{FR,Cyclone}$	Pressure downstream of FR cyclone	7.4	6.9	7.0	8.1	6.4	7.3	7.2	7.1	mbar
$\dot{m}_{FM,FR}$	Mass flow of FR fluidization (H_2O)	186.5	183.7	164.7	181.8	183.8	193.8	195.8	197.3	kg/h
$\dot{m}_{FM,AR}$	Mass flow of AR fluidization*	972.8	968.2	928.2	929.3	928.2	969.3	933.1	927.2	kg/h
$\dot{m}_{C3H8,AR}$	Mass flow of propane entering AR	5.4	5.4	5.4	5.4	5.4	7.2	5.4	5.4	kg/h
$\dot{m}_{FM,LS4.1}$	Vol. flow of LS4.1 fluidization	15 (N_2)	15 (N_2)	15.2 (N_2)	15.3 (N_2)	15.2 (N_2)	16 (N_2)	16 (N_2)	16.1 (N_2)	Nm^3/h
$\dot{m}_{FM,LS4.5}$	Vol. flow of LS4.5 fluidization	14.9 (CO_2)	14.8 (CO_2)	15.7 (CO_2)	15.5 (CO_2)	15.8 (CO_2)	20.3 (N_2)	20.6 (N_2)	20.5 (N_2)	Nm^3/h
$\dot{m}_{FM,J-Valve}$	Vol. flow of J-Valve fluidization	11.8 (CO_2)	11.6 (CO_2)	11.6 (CO_2)	11.6 (CO_2)	12.4 (CO_2)	14.7 (CO_2)	13.3 (CO_2)	12.5 (CO_2)	Nm^3/h
RR_{AR}	AR flue gas recycling ratio	0.25	0.25	0.25	0.25	0.25	0.24	0.24	0.24	–

Variable	Description	BP24	BP25	BP26	BP27	BP28	BP29	BP30	Unit
$m_{Feedstock}$	Mass flow of biomass pellets to FR	229.8	228.9	213.7	209.5	209.6	221.9	238.8	kg/h
$m_{Make-Up}$	Mass flow of OC to LS4.1	0.0	10.6	20.9	0.0	0.0	0.0	5.5	kg/h
T_{AR}	AR max. temperature	882.5	868.6	844.0	840.7	834.0	833.0	797.3	°C
T_{FR}	FR max. temperature	794.4	788.9	757.7	746.0	730.3	725.4	722.8	°C
Δp_{AR}	AR pressure drop (inventory)	64.5	64.0	63.4	56.0	50.8	49.0	74.3	mbar
$p_{AR,Cyclone}$	Pressure downstream of AR cyclone	−1.1	−1.0	−1.0	−1.0	−1.0	−1.0	−0.8	mbar
Δp_{FR}	FR pressure drop (inventory)	65.5	76.8	106.7	124.7	134.3	135.6	65.0	mbar
$p_{FR,Cyclone}$	Pressure downstream of FR cyclone	7.6	7.2	7.4	7.1	7.0	7.1	7.0	mbar
$\dot{m}_{FM,FR}$	Mass flow of FR fluidization (H_2O)	196.4	200.6	200.9	203.0	203.2	204.3	251.1	kg/h
$\dot{m}_{FM,AR}$	Mass flow of AR fluidization*	927.2	944.7	952.1	953.5	956.5	957.3	960.4	kg/h
$\dot{m}_{C3H8,AR}$	Mass flow of propane entering AR	5.4	0.9	0.9	0.9	0.9	0.9	0.9	kg/h
$\dot{m}_{FM,LS4.1}$	Vol. flow of LS4.1 fluidization	16.1 (N_2)	16.5 (N_2)	16.7 (N_2)	16.7 (N_2)	16.8 (N_2)	16.9 (N_2)	17.7 (N_2)	Nm^3/h
$\dot{m}_{FM,LS4.5}$	Vol. flow of LS4.5 fluidization	20.1 (N_2)	18.9 (N_2)	16.1 (CO_2)	16.3 (CO_2)	16.1 (CO_2)	16.4 (CO_2)	16.8 (CO_2)	Nm^3/h
$\dot{m}_{FM,J-Valve}$	Vol. flow of J-Valve fluidization	12.5 (CO_2)	18.4 (CO_2)	19.4 (CO_2)	19.8 (CO_2)	20.1 (CO_2)	20.9 (CO_2)	21.8 (CO_2)	Nm^3/h
RR_{AR}	AR flue gas recycling ratio	0.23	0.23	0.32	0.32	0.35	0.34	0.37	–

* AR fluidization medium: pure air or mixture of air & AR recycled flue gas.

Table 5
Operating conditions for the transient operating periods under investigation. TP-X (Transient Period).

Variable	Description	TP-1	TP-2	TP-3	Unit
$m_{Feedstock}$	Mass flow of biomass pellets to FR	227.6	234.9	223.3	kg/h
$m_{Make-Up}$	Mass flow of OC to LS4.1	44.4	37.4	10.8	kg/h
T_{AR}	AR max. temperature	973.1	918.5	914.1	°C
T_{FR}	FR max. temperature	889.9	842.2	835.2	°C
Δp_{AR}	AR pressure drop (inventory)	48.6	56.1	46.8	mbar
$p_{AR,Cyclone}$	Pressure downstream of AR cyclone	−1.0	−1.0	−1.1	mbar
Δp_{FR}	FR pressure drop (inventory)	68.0	70.3	87.6	mbar
$p_{FR,Cyclone}$	Pressure downstream of FR cyclone	7.2	5.2	7.1	mbar
$\dot{m}_{FM,FR}$	Mass flow of FR fluidization (H_2O)	239.5	239.7	217.1	kg/h
$\dot{m}_{FM,AR}$	Mass flow of AR fluidization*	968.4	950.3	971.3	kg/h
$\dot{m}_{C3H8,AR}$	Mass flow of propane entering AR	10.1	6.8	7.7	kg/h
$\dot{m}_{FM,LS4.1}$	Vol. flow of LS4.1 fluidization	15.2 (N_2)	15.4 (N_2)	14.8 (N_2)	Nm^3/h
$\dot{m}_{FM,LS4.5}$	Vol. flow of LS4.5 fluidization	22.4 (CO_2)	14.8 (CO_2)	16.5 (CO_2)	Nm^3/h
$\dot{m}_{FM,J-Valve}$	Vol. flow of J-Valve fluidization	19.6 (CO_2)	19.8 (CO_2)	15.6 (CO_2)	Nm^3/h

* AR fluidization medium: pure air or mixture of air & recycled AR flue gas.

References

Abad, A., Adánez, J., Cuadrat, A., García-Labiano, F., Gayán, P., d.e Diego, L.F., Feb. 2011. Kinetics of redox reactions of ilmenite for chemical-looping combustion. Chem. Eng. Sci. 66 (4), 689–702. https://doi.org/10.1016/j.ces.2010.11.010.

Abad, A., Adánez, J., d.e Diego, L.F., Gayán, P., García-Labiano, F., Lyngfelt, A., Nov. 2013. Fuel reactor model validation: assessment of the key parameters affecting the chemical-looping combustion of coal. Int. J. Greenhouse Gas Control 19, 541–551. https://doi.org/10.1016/j.ijggc.2013.10.020.

Abad, A., Adánez, J., Gayán, P., d.e Diego, L.F., García-Labiano, F., Sprachmann, G., Nov. 2015. Conceptual design of a 100 MWth CLC unit for solid fuel combustion. Appl. Energy 157, 462–474. https://doi.org/10.1016/j.apenergy.2015.04.043.

Abdalazeez, A., Tianle, L., Cao, Y., Wang, W., Abuelgasim, S., Liu, C., Dec. 2022. Syngas production from chemical looping gasification of rice husk-derived biochar using BaFe2O4 as an oxygen carrier. J. Energy Inst. 105, 376–387. https://doi.org/10.1016/j.joei.2022.10.009.

Acharya, B., Dutta, A., Basu, P., Oct. 2009. Chemical-looping gasification of biomass for hydrogen-enriched gas production with in-process carbon dioxide capture. Energy Fuels 23 (10), 5077–5083. https://doi.org/10.1021/ef9003889.

Adanez, J., Abad, A., Garcia-Labiano, F., Gayan, P., d.e Diego, L.F., Apr. 2012. Progress in chemical-looping combustion and reforming technologies. Prog. Energy Combust. Sci. 38 (2), 215–282. https://doi.org/10.1016/j.pecs.2011.09.001.

Adánez, J., Gayán, P., Celaya, J., d.e Diego, L.F., García-Labiano, F., Abad, A., Aug. 2006. Chemical looping combustion in a 10kW $_{th}$ prototype using a CuO/Al $_2$ O $_3$ oxygen carrier: effect of operating conditions on methane combustion. Ind. Eng. Chem. Res. 45 (17), 6075–6080. https://doi.org/10.1021/ie060364l.

Atsonios, K., Nesiadis, A., Detsios, N., Koutita, K., Nikolopoulos, N., Grammelis, P., Jan. 2020. Review on dynamic process modeling of gasification based biorefineries and bio-based heat & power plants. Fuel Process. Technol. 197, 106188 https://doi.org/10.1016/j.fuproc.2019.106188.

Barrio, M., Gbel, B., Rimes, H., Henriksen, U., H.ustad, J.E., S.rensen, L.H., 2001. Steam gasification of wood char and the effect of hydrogen inhibition on the chemical kinetics. In: Bridgwater, A.V. (Ed.), Progress in Thermochemical Biomass Conversion. Blackwell Science Ltd, Oxford, UK, pp. 32–46. https://doi.org/10.1002/9780470694954.ch2.

Barrio, M., H.ustad, J.E., 2001. CO2 gasification of birch char and the effect of CO inhibition on the calculation of chemical kinetics. In: Bridgwater, A.V. (Ed.), Progress in Thermochemical Biomass Conversion. Blackwell Science Ltd, Oxford, UK, pp. 47–60. https://doi.org/10.1002/9780470694954.ch3.

Bolhar-Nordenkampf, M., et al., 2002. Scale-up of a 100kWth pilot FICFB-gasifier to a 8 MWth FICFB-gasifier demonstration plant in Güssing (Austria). presented at the. In: Proc. 1st International Ukrainian Conference on Biomass For Energy. Kyiv, Ukraine.

Bolhàr-Nordenkampf, M., Rauch, R., Bosch, K., Aichernig, C., 2003. Biomass CHP plant Güssing – using gasification for power generation. In: Proceeding of the 2nd Regional Conference on Energy Technology Towards a Clean Environment, p. 7.

Cetin, E., Moghtaderi, B., Gupta, R., W.all, T.F., Apr. 2005. Biomass gasification kinetics: influences of pressure and char structure. Combust. Sci. Technol. 177 (4), 765–791. https://doi.org/10.1080/00102200590917266.

Condori, O., García-Labiano, F., d.e Diego, L.F., I.zquierdo, M.T., Abad, A., Adánez, J., 2022. Syngas production via Biomass Chemical Looping Gasification (BCLG) in a 50 kWth unit using ilmenite as oxygen carrier. In: Proceedings of the Fluidized Bed Conversion Conference 2022, p. 10.

Condori, O., García-Labiano, F., d.e Diego, L.F., I.zquierdo, M.T., Abad, A., Adánez, J., 2021b. Biomass chemical looping gasification for syngas production using ilmenite as oxygen carrier in a 1.5 kWth unit. Chem. Eng. J. 405, 126679 https://doi.org/10.1016/j.cej.2020.126679.

Condori, O., García-Labiano, F., d.e Diego, L.F., I.zquierdo, M.T., Abad, A., Adánez, J., 2021a. Biomass chemical looping gasification for syngas production using LD Slag as oxygen carrier in a 1.5 kWth unit. Fuel Process. Technol. 222, 106963 https://doi.org/10.1016/j.fuproc.2021.106963.

Cuadrat, A., Abad, A., García-Labiano, F., Gayán, P., d.e Diego, L.F., Adánez, J., Jan. 2012. Effect of operating conditions in Chemical-Looping Combustion of coal in a 500Wth unit. Int. J. Greenhouse Gas Control 6, 153–163. https://doi.org/10.1016/j.ijggc.2011.10.013.

De, S., A.garwal, A.K., M.oholkar, V.S., Thallada, B., 2018. Coal and Biomass Gasification: Recent Advances and Future Challenges.

Dieringer, P., Marx, F., Alobaid, F., Ströhle, J., Epple, B., Jun. 2020. Process control strategies in chemical looping gasification—a novel process for the production of biofuels allowing for net negative CO2 emissions. Appl. Sci. 10 (12), 4271. https://doi.org/10.3390/app10124271.

"DIRECTIVE (EU) 2018/2001 OF THE EUROPEAN PARLIAMENT AND OF THE COUNCIL - of 11 December 2018 - on the promotion of the use of energy from renewable sources," p. 128.

Fossdal, A., et al., May 2011. Study of inexpensive oxygen carriers for chemical looping combustion. Int. J. Greenhouse Gas Control 5 (3), 483–488. https://doi.org/10.1016/j.ijggc.2010.08.001.

Ge, H., Guo, W., Shen, L., Song, T., Xiao, J., 2016a. Biomass gasification using chemical looping in a 25kW th reactor with natural hematite as oxygen carrier. Chem. Eng. J. 286, 174–183. https://doi.org/10.1016/j.cej.2015.10.092.

Ge, H., Guo, W., Shen, L., Song, T., Xiao, J., 2016b. Experimental investigation on biomass gasification using chemical looping in a batch reactor and a continuous dual reactor. Chem. Eng. J. 286, 689–700. https://doi.org/10.1016/j.cej.2015.11.008.

Goel, A., M.oghaddam, E.M., Liu, W., He, C., Konttinen, J., Sep. 2022. Biomass chemical looping gasification for high-quality syngas: a critical review and technological outlooks. Energy Convers. Manage. 268, 116020 https://doi.org/10.1016/j.enconman.2022.116020.

Guo, Q., Cheng, Y., Liu, Y., Jia, W., Ryu, H.-J., Jan. 2014. Coal chemical looping gasification for syngas generation using an iron-based oxygen carrier. Ind. Eng. Chem. Res. 53 (1), 78–86. https://doi.org/10.1021/ie401568x.

Hansen, L.K. (Ed.), 1997. Steam Gasification of Wheat Straw, Barley straw, Willow and Giganteus. Risø National Laboratory, Roskilde in Risø-R, no. 944.

He, F., Huang, Z., Li, H., Zhao, Z., Mar. 2011. Biomass direct chemical looping conversion in a fluidized bed reactor with natural hematite as an oxygen carrier. In: 2011 Asia-Pacific Power and Energy Engineering Conference. IEEE, Wuhan, China, pp. 1–7. https://doi.org/10.1109/APPEEC.2011.5748486.

Heinze, C., May, J., Langner, E., Ströhle, J., Epple, B., Feb. 2023. High Temperature Winkler gasification of Rhenish lignite in an optimized 500 kWth pilot plant. Fuel 333, 126289. https://doi.org/10.1016/j.fuel.2022.126289.

Higman, C., van der Burgt, M., 2008. Gasification, 2nd ed. Gulf Professional Pub./ Elsevier Science, Amsterdam ; Boston.

Hildor, F., Leion, H., L.inderholm, C.J., Mattisson, T., Dec. 2020. Steel converter slag as an oxygen carrier for chemical-looping gasification. Fuel Process. Technol. 210, 106576 https://doi.org/10.1016/j.fuproc.2020.106576.

Hu, J., et al., Feb. 2019. Using chemical looping gasification with Fe2O3/Al2O3 oxygen carrier to produce syngas (H2+CO) from rice straw. Int. J. Hydrogen Energy 44 (6), 3382–3386. https://doi.org/10.1016/j.ijhydene.2018.06.147.

Huang, Z., et al., Jan. 2014. Biomass char direct chemical looping gasification using NiO-modified iron ore as an oxygen carrier. Energy Fuels 28 (1), 183–191. https://doi.org/10.1021/ef401528k.

Huang, Z., et al., Jul. 2013. Synthesis gas production through biomass direct chemical looping conversion with natural hematite as an oxygen carrier. Bioresour. Technol. 140, 138–145. https://doi.org/10.1016/j.biortech.2013.04.055.

Huang, Z., et al., Oct. 2016. Chemical looping gasification of biomass char using iron ore as an oxygen carrier. Int. J. Hydrogen Energy 41 (40), 17871–17883. https://doi.org/10.1016/j.ijhydene.2016.07.089.

Huseyin, S., Wei, G., Li, H., He, F., Huang, Z., Aug. 2014. Chemical-looping gasification of biomass in a 10 kWth interconnected fluidized bed reactor using Fe2O3/Al2O3 oxygen carrier. J. Fuel Chem. Technol. 42 (8), 922–931. https://doi.org/10.1016/S1872-5813(14)60039-6.

Keller, M., Leion, H., Mattisson, T., Lyngfelt, A., Mar. 2011. Gasification inhibition in chemical-looping combustion with solid fuels. Combust. Flame 158 (3), 393–400. https://doi.org/10.1016/j.combustflame.2010.09.009.

Langner, E., Kaltenmorgen, J., Heinze, C., Ströhle, J., Epple, B., Jul. 2023. Fluidized bed gasification of solid recovered fuels in a 500 kWth pilot plant. Fuel 344, 127901. https://doi.org/10.1016/j.fuel.2023.127901.

Larsson, A., Israelsson, M., Lind, F., Seemann, M., Thunman, H., Apr. 2014. Using Ilmenite to reduce the tar yield in a dual fluidized bed gasification system. Energy Fuels 28 (4), 2632–2644. https://doi.org/10.1021/ef500132p.

Liu, F., et al., Oct. 2013. Investigation of a Canadian Ilmenite as an oxygen carrier for chemical looping combustion. Energy Fuels 27 (10), 5987–5995. https://doi.org/10.1021/ef401513p.

Liu, Q., et al., Nov. 2019. High H2/CO ratio syngas production from chemical looping co-gasification of biomass and polyethylene with CaO/Fe2O3 oxygen carrier. Energy Convers. Manage. 199, 111951 https://doi.org/10.1016/j.enconman.2019.111951.

Markström, P., Linderholm, C., Lyngfelt, A., Jul. 2013. Chemical-looping combustion of solid fuels – design and operation of a 100kW unit with bituminous coal. Int. J. Greenhouse Gas Control 15, 150–162. https://doi.org/10.1016/j.ijggc.2013.01.048.

Marx, F., Dieringer, P., Ströhle, J., Epple, B., Apr. 2021. Design of a 1 MWth pilot plant for chemical looping gasification of biogenic residues. Energies 14 (9), 2581. https://doi.org/10.3390/en14092581.

Marx, F., Dieringer, P., Ströhle, J., Epple, B., Jun. 2023. Solid flux measurement in dual fluidized bed processes based on solid samples. Fuel 341, 127589. https://doi.org/10.1016/j.fuel.2023.127589.

Min, Z., Asadullah, M., Yimsiri, P., Zhang, S., Wu, H., Li, C.-Z., 2011. Catalytic reforming of tar during gasification. Part I. Steam reforming of biomass tar using ilmenite as a catalyst. Fuel 90 (5), 1847–1854. https://doi.org/10.1016/j.fuel.2010.12.039.

Moldenhauer, P., Linderholm, C., Rydén, M., et al., 2018. Experimental investigation of chemical-looping combustion and chemical-looping gasification of biomass-based fuels using steel converter slag as oxygen carrier. In: Proceedings of the International Conference on Negative CO2 Emissions, p. 18.

N.guyen, N.M., Alobaid, F., Dieringer, P., Epple, B., Jul. 2021. Biomass-based chemical looping gasification: overview and recent developments. Appl. Sci. 11 (15), 7069. https://doi.org/10.3390/app11157069.

O.hlemüller, P.G., 2019. *Untersuchung Von Chemical-Looping-Combustion im Megawatt-Maßstab*, 1. Auflage. Cuvillier Verlag, Göttingen.

Ohlemüller, P., Alobaid, F., Abad, A., Adanez, J., Ströhle, J., Epple, B., Jun. 2018. Development and validation of a 1D process model with autothermal operation of a 1 MW th chemical looping pilot plant. Int. J. Greenhouse Gas Control 73, 29–41. https://doi.org/10.1016/j.ijggc.2018.03.013.

Ohlemüller, P., Busch, J.-P., Reitz, M., Ströhle, J., Epple, B., Jul. 2016. Chemical-looping combustion of hard coal: autothermal operation of a 1 MWth pilot plant. J. Energy Resour. Technol. 138 (4), 042203 https://doi.org/10.1115/1.4032357.

Ohlemüller, P., Ströhle, J., Epple, B., Oct. 2017. Chemical looping combustion of hard coal and torrefied biomass in a 1 MW th pilot plant. Int. J. Greenhouse Gas Control 65, 149–159. https://doi.org/10.1016/j.ijggc.2017.08.013.

Ollero, P., Serrera, A., Arjona, R., Alcantarilla, S., 2003. The CO2 gasification kinetics of olive residue. Biomass Bioenergy 11.

Pérez-Vega, R., Abad, A., García-Labiano, F., Gayán, P., d.e Diego, L.F., Adánez, J., Jul. 2016. Coal combustion in a 50kWth chemical looping combustion unit: seeking operating conditions to maximize CO2 capture and combustion efficiency. Int. J. Greenhouse Gas Control 50, 80–92. https://doi.org/10.1016/j.ijggc.2016.04.006.

Pissot, S., V.ilches, T.B., Maric, J., Seemann, M., May 2018. Chemical looping gasification in a 2-4 MWth dual fluidized bed gasifier. In: Proceedings of the 23rd International Conference on Fluidized Bed Conversion. Seoul, South Korea, p. 10.

Pröll, T., Bolhàr-Nordenkampf, J., Kolbitsch, P., Hofbauer, H., Jun. 2010. Syngas and a separate nitrogen/argon stream via chemical looping reforming – a 140kW pilot plant study. Fuel 89 (6), 1249–1256. https://doi.org/10.1016/j.fuel.2009.09.033.

Ripfel-Nitsche, K., Hofbauer, H., Rauch, R., Goritschnig, M., 2007. BTL – biomass to liquid (Fischer Tropsch process at the biomass gasifier in Güssing). In: Proceedings of the 15th European Biomass Conference & Exhibition, p. 4.

Roshan Kumar, T., Mattisson, T., Rydén, M., Stenberg, V., 2022. Process analysis of chemical looping gasification of biomass for Fischer–Tropsch crude production with net-negative CO $_2$ emissions: part 1. Energy Fuels. https://doi.org/10.1021/acs.energyfuels.2c00819 p. acs.energyfuels.2c00819, Jun.

Samprón, I., d.e Diego, L.F., García-Labiano, F., I.zquierdo, M.T., Jul. 2021. Optimization of synthesis gas production in the biomass chemical looping gasification process operating under auto-thermal conditions. Energy 226, 120317. https://doi.org/10.1016/j.energy.2021.120317.

Ströhle, J., Orth, M., Epple, B., Nov. 2015. Chemical looping combustion of hard coal in a 1 MW th pilot plant using ilmenite as oxygen carrier. Appl. Energy 157, 288–294. https://doi.org/10.1016/j.apenergy.2015.06.035.

Xu, F., et al., Nov. 2021. Direct chemical looping gasification of pine sawdust using Fe2O3-rich sludge ash as an oxygen carrier: thermal conversion characteristics, product distributions, and gasification performances. Fuel 304, 121499. https://doi.org/10.1016/j.fuel.2021.121499.

Yan, J., et al., May 2020. Hydrogen-rich syngas production with tar elimination via biomass chemical looping gasification (BCLG) using BaFe2O4/Al2O3 as oxygen carrier. Chem. Eng. J. 387, 124107 https://doi.org/10.1016/j.cej.2020.124107.

Zhao, H., Guo, L., Zou, X., Nov. 2015. Chemical-looping auto-thermal reforming of biomass using Cu-based oxygen carrier. Appl. Energy 157, 408–415. https://doi.org/10.1016/j.apenergy.2015.04.093.

Zhou, Z., Li, L., Liu, X., Zhou, Z., Sun, Z., Duan, L., 2022. Accelerated syngas generation from chemical looping CH4 reforming by using reduced ilmenite ore as catalyst. Fuel Process. Technol. 232, 107270 https://doi.org/10.1016/j.fuproc.2022.107270.

3.5 Fifth Research Paper

Process Efficiency and Syngas Quality from Autothermal Operation of a 1 MW_{th} Chemical Looping Gasifier with Biogenic Residues

Authors: Falko Marx, Paul Dieringer, Jochen Ströhle, Bernd Epple
Journal: Applications in Energy and Combustion Science
Date: 2023-10-31
ISSN: 2666-352X
DOI: 10.1016/j.jaecs.2023.100217

Applications in Energy and Combustion Science 16 (2023) 100217

Contents lists available at ScienceDirect

Applications in Energy and Combustion Science

journal homepage: www.elsevier.com/locate/jaecs

Process efficiency and syngas quality from autothermal operation of a 1 MW_{th} chemical looping gasifier with biogenic residues☆

Falko Marx *, Paul Dieringer, Jochen Ströhle, Bernd Epple

Institute for Energy Systems & Technology, Technische Universität Darmstadt, Otto-Bernd-Str. 2, Darmstadt, 64287, Germany

ARTICLE INFO

Keywords:
Chemical looping
Biomass
Wood
Foresting residue
Ilmenite
Dual fluidized bed
Syngas
Gasification
Biomass tar
Tar protocol
Pilot plant
Experimental data

ABSTRACT

Chemical looping gasification is a novel dual fluidized bed technology for the conversion of solid feedstock to a nitrogen-free syngas without the need of pure oxygen. While multiple electrically heated lab-scale experiments have been performed, data on gas quality including tars formed during operation have not been reported yet for autothermal process operation. In this study we present autothermal operation of a chemical looping gasifier with a thermal input in the 1 MW_{th} range, utilizing two circulating fluidized bed reactors with foresting residue and industrial wood pellets as feedstock and Norwegian ilmenite as bed material. A cold gas efficiency of around 50 % was achieved in the non optimized pilot plant, indicating that higher values can be reached in a commercial unit when minimizing heat losses. The carbon conversion was around 90 %, and this value is expected to increase to almost 100 % when raising the temperature, residence time, and cyclone efficiency in a commercial unit. The syngas has a very high quality with methane concentrations in the range of 7 vol. – % to 10 vol. – % and gravimetric tar content below 1 g/Nm^3 measured via tar protocol.

1. Introduction

In light of the current climate change, new and renewable sources for hydro-carbons are required. Especially applications where electrification is not an option, such as the maritime transport and aviation sector, and also the production of base chemicals require a constant source of carbon. One such source is biomass, preferably biogenic residues, which can be utilized by gasification. Here oxygen assisted gasification technologies, which produce a nitrogen free syngas, are advantageous as they supply oxygen for heat generation towards the gasifier and no post-gasification separation of N_2 is required. However, for autothermal operation of the gasification process, oxygen needs to be supplied to be able to convert a fraction of the feedstock for the purpose of heat generation, as required by the process. Usually this is done in the form of molecular oxygen provided by an air separation unit (ASU) (e.g. [1]). However, the ASU adds a costly and energy intensive step to the gasification process reducing the efficiency.

One technology avoiding an ASU is dual fluidized bed gasification (DFBG). Endeavours to scale-up the DFBG technology, which supplies only heat and gasification medium but no oxygen to the gasifier, have generated operating experience for approx. 20 yr of demo-plant scale operation [2,3], producing syngas from biomass with a high amount of tars [2]. However, no large scale (> 20 MW_{th}), commercial DFBG plant is known to the authors, indicating that there are still some technical issues to be resolved. An alternative route is the CLG process which has lately seen increased research activity with multiple review papers being published [4–6]. It combines the idea of supplying heat to the gasifier — like DFBG — with the provision of oxygen by a metal oxide lattice in the circulating bed material, promising to enhance the performance of the DFBG technology.

The CLG process is depicted in Fig. 1 and deploys two reactors, the air reactor (AR) where the metal oxide called OC is oxidized, and the fuel reactor (FR) where the feedstock is converted and the OC is reduced. Both reactors are usually fluidized bed reactors, enabling efficient transport of the solid OC material between the reactors and providing high heating rates and good gas–solid contact for the heterogeneous reactions. Compared to the similar DFBG process, CLG has the advantage of increased char conversion inside the FR, which shifts the generated CO_2 to the FR output. Therefore, almost all produced CO_2 is part of the FR product stream where a CO_2 removal step is already necessary for most use-cases of the produced syngas, allowing for net

☆ This work has received funding of the European Union's Horizon 2020-Research and Innovation Framework Programme under grant agreement No. 817841 (Chemical Looping gasification foR sustainAble production of biofuels — CLARA). The content of this work reflects only the author's view, and the European Commission is not responsible for any use that may be made of the information it contains.

* Corresponding author.
E-mail address: falko.marx@est.tu-darmstadt.de (F. Marx).

https://doi.org/10.1016/j.jaecs.2023.100217
Received 1 August 2023; Received in revised form 9 October 2023; Accepted 25 October 2023

Abbreviations

AR	Air reactor
ASU	Air separation unit
CFB	Circulating fluidized bed
CLC	Chemical looping combustion
CLG	Chemical looping gasification
d.b.	Dry base
DFBG	Dual fluidized bed gasification
FI	Flow indicator
FR	Fuel reactor
GA	Gas analysis
GSB	Gas sample bag
IWP	Industrial wood pellets
KPI	Key performance indicator
LS	Loop seal
OC	Oxygen carrier
OCAC	Oxygen carrier aided combustion
PA	Proximate analysis
PFR	Pine forest residue
PSD	Particle size distribution
SP	Sample point
TAR	Tar measurement
TI	Temperature indicator
UA	Ultimate analysis

Symbols

LHV	Lower heating value (MJ kg^{-1}, MJ mol^{-1})
M	Molar mass, atomic mass (g mol^{-1})
P_{th}	Thermal load (W)
R_{OC}	Oxygen transport capacity
T	Temperature (K, °C)
X_C	Carbon conversion
X_{SG}	Syngas content
Y_{SG}	Syngas yield (N m^3/kg)
ΔH	Reaction enthalpy (J mol^{-1})
$\dot{Q}$	Heat flux (W)
$\dot{m}$	Mass flow (kg s^{-1})
$\dot{n}$	Molar flow (mol s^{-1})
η_{CG}	Cold gas efficiency
λ	Air to fuel equivalence ratio
c_p	Specific heat (J kg^{-1} K^{-1})
w	Mass fraction in solid phase
x	Mole fraction

Subscripts

AR	Air reactor
FM	Fluidization medium Stock
FR	Fuel reactor
FS	Feed stock
OC	Oxygen carrier
O	Oxygen
eff	Effective
in	Stream entering reactor
out	Stream leaving reactor
ox	Oxidized
red	Reduced

negative process chains. Furthermore, the introduction of an active bed material, the OC, adds the possibility of reduced tar generation due to catalytic effects [7–10].

Related research topics range from the experimental investigation of different feedstocks like biogenic residues [11–13] and coal [14] over various bed materials consisting of synthetic oxygen carriers [15], natural minerals [16,17], and waste materials [11]. Moreover, basic de-fluidization phenomena, which can potentially hinder commercial application, resulting from interaction of OC and feedstock ash were studied [18–20], finding no so called "show stoppers". Additionally to these lab scale investigations, there is activity related to scale-up, with a recent publication on autothermal pilot plant experiments [21] investigating process control concepts relevant for commercial application. Furthermore, simulations are used to optimize process control under autothermal conditions [22,23] and to predict process performance for commercial scale units [24].

So far, no detailed report on generated syngas including higher hydro-carbons from autothermal operation of CLG has been published. However, for large-scale application accurate knowledge of so called tars as well as all permanent gases are vital, as they might restrict use cases or require further processing equipment either for removal or conversion. Furthermore, in contrast to small scale units with external electrical heating, the free variation of process parameters like steam to biomass ratio, air to fuel equivalence ratio, and thermal input to bed inventory is not possible in autothermal operation and the interdependence and restrictions limit the operation range. In this paper we report on syngas compositions, carbon conversion, cold gas efficiencies, and other operation variables obtained from various biogenic feedstocks in the 1 MW_{th} modular pilot plant located at Technische Universität Darmstadt in Germany.

2. Experiment

Fig. 2 shows a simplified flow sheet of the 1 MW_{th} pilot plant used for the experiments. A detailed description is available elsewhere [25]. It depicts the two circulating fluidized bed (CFB) reactors, the cyclones for gas–solid separation, the loop seals and the J-valve for solids transport, as well as the corresponding streams entering and leaving the reactor system. The AR features a height of 8.66 m and an inner diameter of 0.59 m and the FR a height of 11.35 m and an inner diameter of 0.4 m. Measurement sites for the major process streams are indicated, while all other streams entering the reactors are equipped with controlling and measurement devices. The composition of the FR output stream is continuously measured via gas analysis equipment (see Table 1) for the species O_2, CO_2, CO, CH_4, H_2, and H_2O, while the AR output stream is analysed for the components O_2, CO_2, and CO. Additionally the FR output is equipped for tar sampling according to tar protocol/CEN TS 15 439 and for the collection of gas sample bags to obtain data for higher hydro-carbons. The AR fluidization stream is measured for O_2 and CO_2 to determine the oxygen input to the reactor system. Moreover, the AR is equipped with a flue gas recirculation to enable the control of the air to fuel equivalence ratio λ of the process without impacting the hydrodynamics of the AR, as described in [22] and demonstrated by Dieringer et al. [21]. The AR fluidization medium can be electrically heated up to 360 °C and the steam for FR fluidization up to 465 °C.

All OC material discharged from the FR is transported to the AR via a loop seal, while the solids transport from the AR to the FR is controlled via a J-valve. The amount of OC discharged from the AR exceeding the transport between the reactors is returned towards the AR via the loop seal. Both loop seals have sampling ports where solid samples can be obtained and cooled before exposure to the atmosphere to preserve the process oxidation state. From the oxidation state of the solid loop seal samples and the oxygen balance of the AR, the solid circulation is calculated [26]. Both reactors are equipped with an ash sluicing screw to remove bed material and agglomerates, which was used only for the collection of sample material as no agglomeration or meaningful OC deactivation was observed.

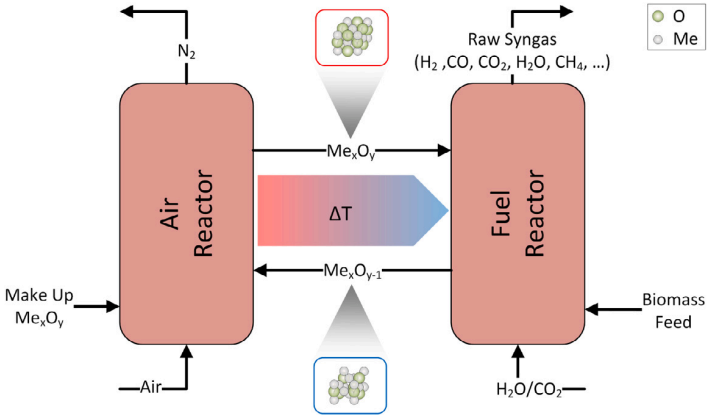

Fig. 1. Schematic of the CLG process showing the cyclic reduction and oxidation of an OC material which is oxidized in the air reactor (AR) and reduced in the fuel reactor (FR).

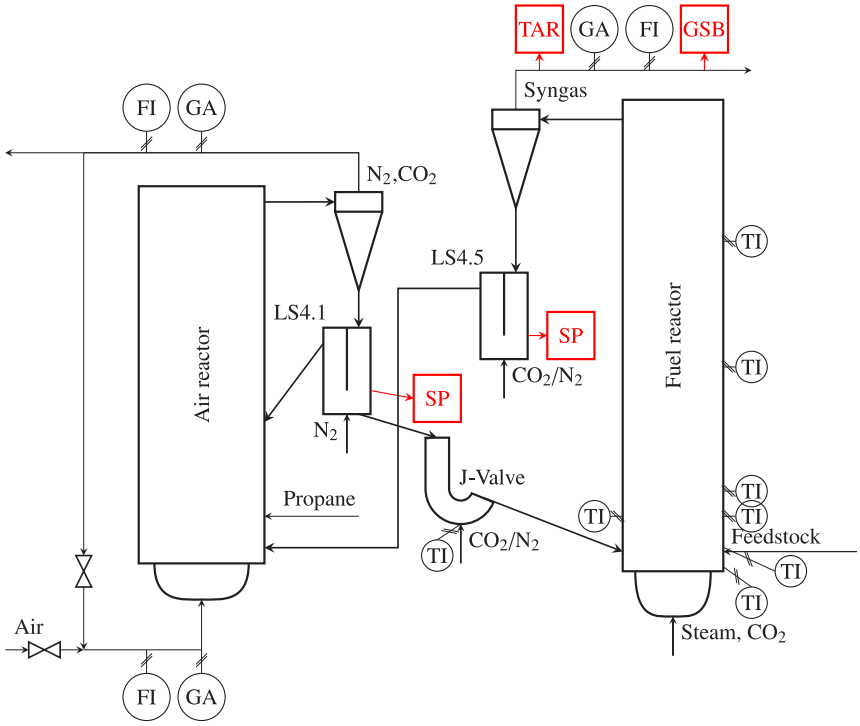

Fig. 2. Schematic of the chemical looping gasification process indicating relevant measurement sites, and sample position. FI: flow indicator, TI: temperature indicator, GA: gas analysis, SP: sample point, GSB: gas sample bag, TAR: tar measurement according to CEN TS 15439.

The option to feed propane to the AR exists to artificially increase system temperature in case of low thermal load P_{th} but was only used for a short time. The produced syngas is cooled and routed to a gas treatment plant for cleaning and sour gas removal to obtain a cleaned syngas useable for the synthesis of liquid hydro-carbons.

2.1. Materials

The feedstocks used for CLG pilot testing are industrial wood pellets (IWP) and pine forest residue (PFR) in pellet form. The industrial wood pellets (IWP) are commercially available wood pellets adhering to the norm EN plus A1. The pine forest residue (PFR) was obtained from foresting operations in Sweden and pelleted by AB Torkapparater. The PFR includes a high amount of bark and pine needles as can be seen in Fig. 3. The properties of the feedstocks are listed in Table 2.

As OC material the natural mineral Norwegian ilmenite was used. Although, thermo-gravimetric analysis show lower reactivity of ilmenite compared to other OC (e.g. nickel based [9,10]) it is still considered a primary option [27] for chemical looping. This is the case, as OC reactivity is not the major concern in CLG where oxygen release by the OC inside the FR has to be actively limited [21–23]. Moreover, it is non-toxic, inexpensive, and commercially availability in the required quantity. In addition operation experience exists for chemical looping combustion (CLC) [28,29]. During experiments, two different Particle size distributions (PSDs), as depicted in Fig. 4, were used. The fine particle fraction has approx. 20% of fines (smaller 50 μm) which cannot be efficiently separated by the existing FR cyclone as shown in previous experiments [28,29] leading to increased make-up rates cooling down the reactor system. In contrast, the coarse material exhibits only 20% of particle smaller 200 μm, leading to lower entrainment from the reactors and thus lower solid circulation [26]. A perfectly matched PSD is

Table 1
Listing of gas analysis equipment for all reactors.

Reactor	Equipment	Measurement principle	Component	Range	Error	Unit
FR	Magnos 206	Paramagnetic	O_2	0 to 25	0.9	vol. – %
	Caldos 27	Thermal conductivity	H_2	0 to 40	1.8	vol. – %
	Uras 26	NDIR	CO_2	0 to 100	3.0	vol. – %
	Uras 26	NDIR	CO	0 to 40	1.2	vol. – %
	Uras 26	NDIR	CH_4	0 to 20	0.6	vol. – %
	Hygrophil H4320	Psychrometric	H_2O	2 to 100	0.3	vol. – %
AR outlet	Magnos 206	Paramagnetic	O_2	0 to 25	0.9	vol. – %
	Uras 26	NDIR	CO_2	0 to 30	0.9	vol. – %
	Uras 26	NDIR	CO	0 to 5	0.15	vol. – %
	Hygrophil H4320	Psychrometric	H_2O	2 to 100	0.3	vol. – %
AR inlet	Magnos 206	Paramagnetic	O_2	0 to 25	0.9	vol. – %
	Uras 26	NDIR	CO_2	0 to 100	3.0	vol. – %

Fig. 3. Raw pine forest residue (PFR) material.

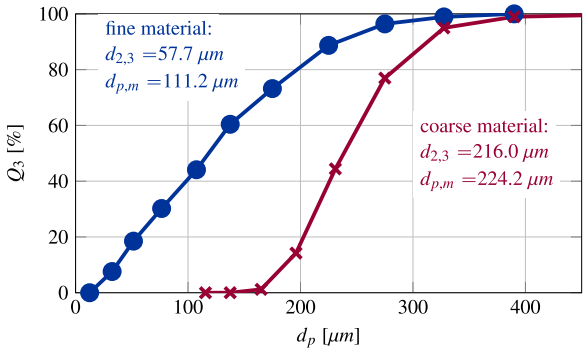

Fig. 4. Particle size distribution of the ilmenite used as oxygen carrier material during experiments.

Table 2
Proximate and ultimate analysis of feedstock used during experiments. LHV: lower heating value, PA: proximate analysis, UA: ultimate analysis, d.b.: dry base, IWP: industrial wood pellets, PFR: pine forest residue.

	Component	IWP	PFR
PA [wt. – %]	Moisture	8.3	4.4
	Ash (dry base (d.b.))	0.3	2.3
	Volatiles (d.b.)	84.6	80.3
	Fixed carbon (d.b.)	15.1	17.4
UA [wt. – %]	C (d.b.)	50.7	51.1
	H (d.b.)	6.1	6.1
	N (d.b.)	0.33	0.44
	O (d.b.)	42.5	40.1
	S (d.b.)	0.008	0.025
	Cl (d.b.)	0.008	0.010
LHV [MJ kg^{-1}]		17.2	18.30

not commercially available and sieving proofed to be economically infeasibly for the pilot tests. The oxygen carrying capacity for the ilmenite was determined to be $R_{OC} = 3.7\%$.

2.2. Operation and balance points

The data was obtained during two test campaigns consisting of more than 14 d of 24 h d^{-1} operation each. The balance points consist of stable operation without operator intervention for approx. 1 h, before a full set of samples — consisting of tar sample, gas sample bag, and loop seal OC material sample — was taken. Gas sample bags are analysed for permanent gases O_2, CO_2, CO, CH_4, N_2, and C_2 to C_3 species. As these balance points feature a full set of samples, they are selected for further in-depth analysis.[1]

A calculated mean reactor temperature $\overline{T}$ is used during analysis calculated as the mean of all temperature measurements inside the reactor.

$$\overline{T} = \frac{\sum_{i=1}^{N} T_i}{N} \tag{1}$$

Although the temperature inside the reactor spans a range of over 100 K and $\overline{T}$ is therefore subject to change with temperature measurement location, it is a useful value for the investigation of the temperature dependency of various parameters. The temperature inside the reactor is a result of feed stock input, OC circulation and amount of fluidization medium supplied to the reactors [22,26]. The main influencing parameter is the solid circulation which can be influenced through adjustments of the J-valve and the system hydrodynamics [21].

For the calculation of the key performance indicators (KPIs), the output gas streams are corrected for the amount of CO_2 input coming from fluidization media i.e. recirculated flue gas in case of the AR and CO_2-fluidization in case of the FR. The loop seal fluidization was switched to N_2 and back to CO_2 for all coupling elements individually to assess the individual impact on each reactor. The input streams were than added during calculation accordingly.

Additional data outside of these balance points is averaged for 20 min and reported here in addition to the balance points to give an indication of further system behaviour. However, transient states —

[1] As this was the first time the plant was operated, the focus was on determining the operation range of the process and plant and not on the optimization of individual operation points. As such, the data set represents a range of possible operation points which are not optimized for cold gas efficiency, carbon conversion, tar generation, or syngas composition.

which are likely to produce large deviations from stable operation because of various system inertias, as have been reported before [21,26] — are included as well.

2.3. Evaluation parameters

The process performance is evaluated using the following parameters:

Cold Gas Efficiency η_{CG}

$$\eta_{CG} = \frac{\dot{n}_{FR,out}(x_{CH_4} \cdot LHV_{CH_4} + x_{CO} \cdot LHV_{CO} + x_{H_2} \cdot LHV_{H_2})}{\dot{m}_{FS} \cdot LHV_{FS}} \quad (2)$$

with x_i being the mole fraction of species i, LHV the lower heating value, and $\dot{n}_{FR,out}$ and $\dot{m}_{FS}$ being the product gas output and the feedstock input, respectively.

Air to Fuel Equivalence Ratio λ[2]

$$\lambda = \frac{\dot{m}_{O,AR}}{\dot{m}_{FS} \cdot R_{FS}} \quad (3)$$

with the mass streams $\dot{m}$ and the oxygen requirements for full oxidation R_{FS}. For CLG a slightly modified term for the efficient air to fuel equivalence ratio inside the FR is sometimes more appropriate [21]:

$$\lambda_{FR,eff} = \frac{\dot{m}_{O,FR,out} - \dot{m}_{O,FR,in}}{\dot{m}_{FS} \cdot R_{FS}} \quad (4)$$

The range of $\lambda_{FR,eff}$ in stable operation is between the lower limit of no oxygen release from the bed material $\lambda_{FR,eff} = 0$ like in DFBG, to the upper limit of the oxygen input of the process $\lambda_{FR,eff} = \lambda$.

The **Carbon Conversion** X_C is the fraction of feedstock carbon converted into gaseous species:

$$X_{C,FR} = \frac{\dot{n}_{gas,FR} \cdot (x_{CH_4} + x_{CO} + x_{CO_2}) \cdot M_C - \dot{m}_{CO_2,fluidization} \cdot \frac{M_C}{M_{CO2}}}{\dot{m}_{FS} \cdot w_{C,FS}} \quad (5)$$

with the AR carbon conversion being calculated from CO_2 only:

$$X_{C,AR} = \frac{\dot{n}_{gas,AR} \cdot x_{CO_2} \cdot M_C - \dot{m}_{CO_2,fluidization} \cdot \frac{M_C}{M_{CO2}}}{\dot{m}_{FS} \cdot w_{C,FS}} \quad (6)$$

where M denotes the molar mass of the species i and $w_{C,FS}$ the carbon fraction inside the feedstock. Additionally, the **syngas fraction** in the dry product gas is defined as:

$$X_{SG} = \frac{x_{CO} + x_{H_2}}{x_{CH_4} + x_{CO} + x_{H_2} + x_{CO_2} + x_{N_2}} \quad (7)$$

and the syngas yield as:

$$Y_{SG} = \frac{\dot{n}_{gas,FR}(x_{CO} + x_{H_2})}{\dot{m}_{FS}} \quad (8)$$

The **oxidation degree** of the OC material is defined as:

$$X_S = \frac{m_{OC} - m_{OC,red}}{R_{OC} \cdot m_{OC,ox}} \quad (9)$$

In this definition, R_{OC} is the oxygen transport capacity of the OC material, X_S is the oxidation degree of the OC, $m_{OC,red}$ and $m_{OC,ox}$ are the mass of the fully reduced and oxidized state respectively, while the mass of the OC leaving the reactor is m_{OC}.

The sensible **heat transport** $\dot{Q}$ between the reactors can be calculated to:

$$\dot{Q} = \dot{m}_{OC} \cdot c_p \cdot \Delta T \quad (10)$$

with c_p, the heat capacity of the OC and ΔT, the temperature difference of OC particles at AR and FR output. This neglects heat losses and can therefore be seen as the lower boundary for the sensible heat transported between the reactors. The solid flux between the reactors required for the calculation of the sensible heat transported from AR to FR with the OC material according to Eq. (10) is determined via solid samples and an oxygen balance around the AR [26]. It is assumed, that the heat capacity for ilmenite calculated according to [30] is valid for both oxidation states. The temperature measurements used for calculation are located inside the J-valve and at the top of the FR.

[2] In the case of propane co-firing in the AR, λ is corrected by the mass of propane $\dot{m}_{C_3H_8}$ and the corresponding oxygen demand $R_{C_3H_8}$ ($R_{C_3H_8}$ = 3.628 kg kg^{-1}).

3. Results

The main operation variables for the balance points are given in Table 3. For the first four balance points IWP was used as feedstock, while for the last four balance points PFR was used. For the last point no tar measurement is available.

The temperature profiles in the FR, which are influencing pyrolysis and gasification reactions, are visualized in Fig. 5 with the additional information on fuel input height and OC input height. It can be seen that the reactor is at a constant temperature along almost the full height with only the lower region being much cooler. This is caused by the fluidization medium, which can only be preheated to 465 °C, and the fuel input. From the height were the hot OC from the AR is introduced into the FR upwards, the temperature is at an almost constant level. OC circulation is in the range of 1.8 kg s^{-1} to 5.7 kg s^{-1} leading to a feed stock related circulation of 1.2 kg s^{-1} MW^{-1} to 4.3 kg s^{-1} MW^{-1}.

3.1. Syngas production and composition

The dry composition of FR of gases is plotted over FR temperature (a), and $\lambda_{FR,eff}$ (b) in Fig. 6. The high CO_2 concentration is caused by some amount of instrument purge gas inside the FR off gas, loop seal (LS) fluidization medium and by the high energy requirement for the heating of the process streams to reactor temperature. This energy is supplied by Reactions R10 and R9 (details on important reactions are given in Appendix), converting syngas species into CO_2 and H_2O, visible by the increase of the CO_2 content with increasing temperature. The amount of CO_2 coming from purge gases and LS fluidization can be estimated by the difference in CO_2 content of the marked region in Fig. 6 a, where all CO_2 entering the pilot plant was switched to N_2. The difference is 5 vol. – % to 15 vol. – % in the pilot plant and is expected to be much smaller in large-scale commercial application. This clear trend of increasing CO_2 can also be seen with $\lambda_{FR,eff}$, where higher $\lambda_{FR,eff}$ means higher conversion of syngas species, leading to higher heat release and thus higher system temperatures [21].

For the syngas species CO and H_2, the opposite trend is visible, low temperatures and $\lambda_{FR,eff}$ correspond with higher volume fraction. In contrast, the methane content shows no change with either temperature or $\lambda_{FR,eff}$, being stable at about 7 vol. – % to 11 vol. – %. This is the same behaviour and range as measured by Condori et al. for a thermal input of 1.5 kW where no dependence of CH_4 to either temperature or λ was observed [17]. Moreover, the range is typical for biomass gasification technologies with steam as gasification agent [2,3,31,32].

The syngas yield per biomass feedstock in Fig. 7 shows the same trends, as the individual species of CO and H_2, as it is calculated from these species. With increasing temperature and $\lambda_{FR,eff}$ decreases the production of syngas species. The range is with 0.15 N m^3/kg to 0.45 N m^3/kg lower as for externally heated units (0.34 N m^3/kg to 0.89 N m^3/kg) [13,17].

The content of syngas species reported here are lower when compared to data reported in literature with corresponding higher amounts of CO_2. This is not only caused by the reasons stated above (syngas conversion because of autothermal operation, syngas conversion to reach higher temperature, high amount of purges and fluidization for coupling elements) but also by the fact that the values for syngas species reported in literature are normally on a N_2-free basis (e.g. [11,13,17,33–35]) while coupling elements are usually fluidized with nitrogen.

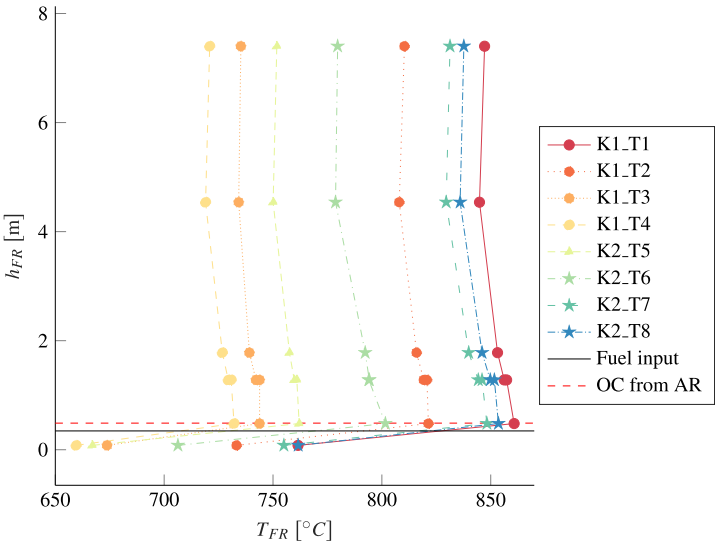

Fig. 5. Temperature profiles in the fuel reactor during balance points. Feedstocks: •— IWP/fine ilmenite, ▶— PFR/coarse ilmenite, ★— PFR/fine ilmenite.

Table 3
Variables of the operating periods used for the investigation in this work.

Description	Variable	Unit	Balancepoint							
			BP_T1	BP_T2	BP_T3	BP_T4	BP_T5	BP_T6	BP_T7	BP_T8
Feedstock	–		IWP	IWP	IWP	IWP	PFR	PFR	PFR	PFR
Bed material PSD	–		Fine	Fine	Fine	Fine	Coarse	Fine	Fine	Fine
Thermal input	P_{th}	MW	1.10	1.10	1.10	1.10	1.51	1.56	1.78	1.82
Mass flow of biomass pellets to FR	$\dot{m}_{FS}$	kg h^{-1}	230.80	230.80	230.80	230.80	297.30	307.80	350.10	357.20
Mass flow of FR fluidization (H_2O)	$\dot{m}_{FM,FR}$	kg h^{-1}	264.83	213.98	233.02	261.89	299.44	329.68	253.72	230.50
Mass flow of AR fluidization	$\dot{m}_{FM,AR}$	kg h^{-1}	969.73	972.42	953.47	959.08	1045.20	1100.25	1115.15	1117.41
Mass flow of propane entering AR	$\dot{m}_{C_3H_8,AR}$	kg h^{-1}	10.04	5.38	0	0	0	0	0	0
Mass flow for LS4.1 fluidization (N_2)	$\dot{m}_{FM,4.1,N_2}$	kg h^{-1}	15.62	15.00	16.77	17.40	14.66	16.00	14.18	13.86
CO_2 flow for LS4.5 fluidization	$\dot{m}_{FM,4.5,CO_2}$	kg h^{-1}	19.63	14.66	16.66	16.95	0	13.45	13.13	9.11
N_2 flow for LS4.5 fluidization	$\dot{m}_{FM,4.5,N_2}$	kg h^{-1}	0	0	0	0	15.09	0	0	0
Flow for J-Valve fluidization (CO_2)	$\dot{m}_{FM,J-Valve}$	kg h^{-1}	22.98	11.65	20.21	21.83	18.11	17.86	8.71	8.58
FR pressure drop	$\Delta_{p,FR}$	mbar	70.68	92.11	125.72	78.79	89.32	61.77	95.25	86.16
Air to fuel equivalence ratio	λ		0.50	0.52	0.49	0.46	0.39	0.38	0.39	0.40
FR efficient air to fuel equivalence ratio	$\lambda_{FR,eff}$		0.35	0.35	0.14	0.13	0.08	0.18	0.15	0.17
Cold gas efficiency	η_{CG}		0.28	0.31	0.27	0.30	0.34	0.38	0.33	0.40
Carbon conversion	$X_{C,FR}$		0.75	0.77	0.59	0.57	0.55	0.66	0.65	0.69
	$X_{C,AR}$		0.11	0.14	0.23	0.28	0.30	0.25	0.18	0.21
Syngas fraction	X_{SG}		0.18	0.22	0.27	0.31	0.40	0.37	0.33	0.39
Syngas yield	Y_{SG}	N m^3 kg^{-1}	0.17	0.20	0.21	0.25	0.32	0.34	0.27	0.35
Steam to biomass ratio	S/B	kg kg^{-1}	1.15	0.93	1.01	1.13	1.01	1.07	0.72	0.65
Mean reactor temperature	$\overline{T_{AR}}$	°C	933.4	897.6	832.2	808.9	928.2	865.9	915.6	946.3
	$\overline{T_{FR}}$	°C	840.1	804.1	730.3	716.9	744.2	778.1	827.8	833.7
Oxidation degree	$X_{S,AR}$	%	89.1	82.7	90.7	87.2	99.4	73.6	83.8	75.9
	$X_{S,FR}$	%	61.4	65.0	77.5	76.9	76.9	65.0	68.5	55.6
OC transport between reactors	$\dot{m}_{OC}$	kg s^{-1}	2.7	4.2	4.2	4.7	1.8	5.7	5.6	3.8
Heat transport between reactors	$\dot{Q}$	kW	147.3	270.1	308.8	300.3	263.7	414.9	400.9	363.4
FR syngas flow	$\dot{V}_{FR,SG}$	N m^3 h^{-1}	616.6	529.4	506.5	551.2	618.1	696.3	584.1	599.3
Gas composition	x_{H_2O}	vol. – %	63.7	59.3	61.4	64.3	61.5	59.7	52.2	47.4
	x_{CO}	vol. – % dry	6.7	7.1	9.7	12.6	15.9	13.2	13.1	15.9
	x_{CO_2}	vol. – % dry	69.7	65.4	62.3	58.0	51.1	55.1	59.6	50.4
	x_{O_2}	vol. – % dry	0.2	0	0.2	0.3	0.0	0.1	0.2	0.1
	x_{H_2}	vol. – % dry	10.4	13.8	15.5	16.9	23.6	24.3	20.8	23.7
	x_{CH_4}	vol. – % dry	8.3	9.2	7.2	7.2	9.1	9.0	10.1	10.7
Gravimetric tar	$m_{tar,grav}$	g N^{-1} m^{-3} dry	0.505	0.124	0.876	2.397	5.156	1.127	1.092	
AR inlet	$x_{CO_2,AR,in}$	vol. – % dry	2.0	2.6	4.2	5.3	4.0	4.7	2.6	2.8
	$x_{O_2,AR,in}$	vol. – % dry	16.9	15.8	14.5	13.8	14.5	14.0	16.0	16.0
AR outlet	$x_{H_2O,AR,out}$	vol. – %	2.7	1.6	0.0	0.0	0.0	0.0	0.0	0.0
	$x_{CO,AR,out}$	ppm dry	2985	1857	262	1370	0	1033	1789	394
	$x_{CO_2,AR,out}$	vol. – % dry	9.7	9.8	12.6	15.0	12.7	14.1	10.6	11.6
	$x_{O_2,AR,out}$	vol. – % dry	0.0	0.0	0.0	0.0	0.2	0.0	0.0	0.0
	$\dot{m}_{AR,out}$	kg h^{-1}	976	949	994	1017	1138	1188	1161	1159

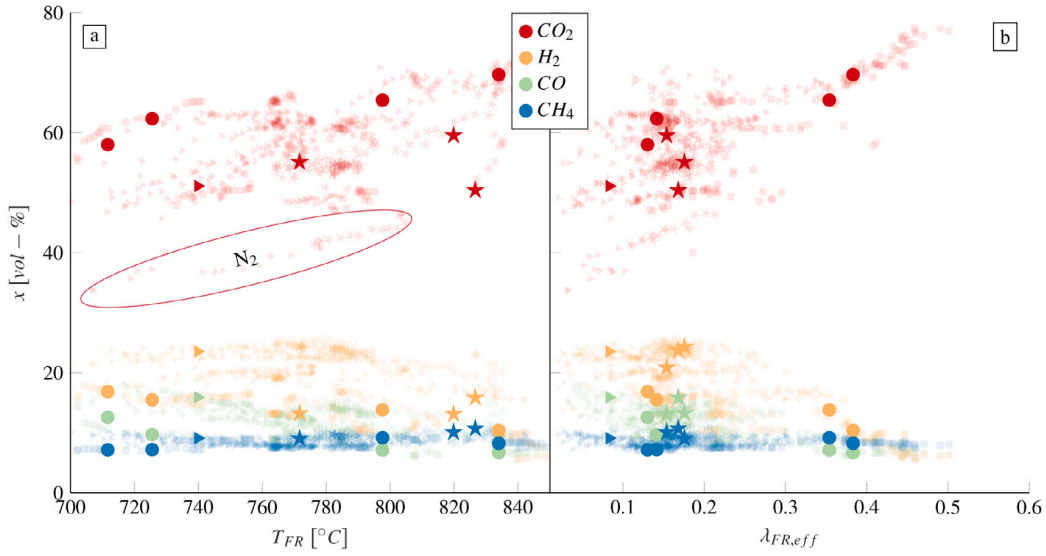

Fig. 6. Dry gas composition. Feedstocks: •— IWP/fine ilmenite, ▶— PFR/coarse ilmenite, ★— PFR/fine ilmenite.

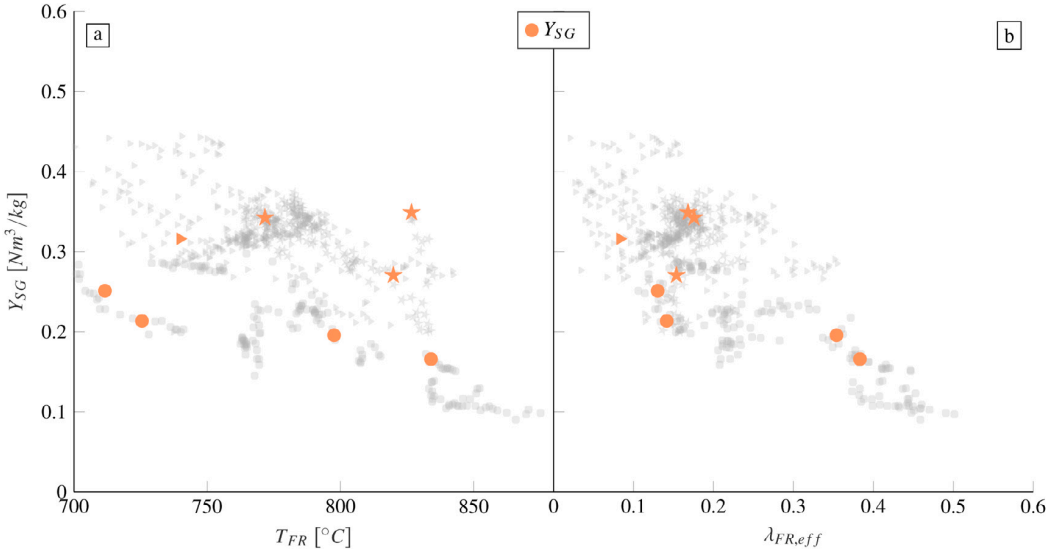

Fig. 7. Syngas yield per feedstock mass. •— IWP/fine ilmenite, ▶— PFR/coarse ilmenite, ★— PFR/fine ilmenite.

Thus, the amount of syngas species is artificiality boosted compared to the ones reported here, where actual process data is reported.[3] Therefore, the syngas yield is a more appropriate indicator, as it is independent of the gas species used for fluidization and purging and directly influenced by the feed and performance. The reported values are a bit lower than for externally heated units for the reasons already stated: autothermal operation with comparatively high relative heat losses which are counteracted via higher conversion of the feedstock.

[3] N_2 can be considered as an inert and therefore it is reasonable to report N_2-free syngas compositions. However, the situation is different for CO_2. As the CO_2 content has an influence on reaction kinetics correcting for the amount of purge gas and fluidization medium would severely reduce the value of the reported data. The main reason to use CO_2 as purge gas and fluidization medium for the coupling elements is to not dilute the syngas with an inert, as it is later cleaned in a gas cleaning pilot plant and subsequently used for liquid fuel synthesis experiments.

3.2. Cold gas efficiency and carbon conversion

The cold gas efficiency η_{CG} and the total (AR and FR combined) carbon conversion X_C of the CLG pilot tests are depicted in Fig. 8 a and b.

The cold gas efficiency is only calculated from online gas analysis as they are the species of interest for further valorization of the product gas stream. As such, higher hydrocarbons (see Section 3.3), which contain an appreciable amount of energy are not included in the calculation. Moreover, the scale of the experiment and the autothermal operation require a significant amount of energy which has to be generated by the conversion of syngas species, resulting in the visible low cold gas efficiencies. In Fig. 8 b two trends C to D and E to F (⟶) for η_{CG} for all operation periods can be observed. They both show the same behaviour at slightly different levels of η_{CG}: with increasing $\lambda_{FR,eff}$ η_{CG} increases, levels off at approx. $\lambda_{FR,eff} = 0.3$, and decreasing again. The initial increase of η_{CG} with $\lambda_{FR,eff}$ is a result of the temperature increase, which in turn leads to higher fraction of fixed

carbon being converted inside the FR. By further increasing $\lambda_{FR,eff}$ the higher conversion of syngas species becomes more important ant η_{CG} decreases again. The difference in η_{CG} is caused by the much higher feedstock input for PFR on line C to D compared to IWP on line E to F (see also Table 3). As heat losses are mainly defined by the constant reactor surface an increase in thermal load decreases the relative heat losses and therefore η_{CG} is increased for PFR.

In comparison to literature data on experimentally obtained cold gas efficiency, the values are well below the reported values for very small units (e.g. 1.5 kW [11,17]) and at the lower end of the range reported for small units (20 kW to 50 kW [13]). The range including all operating points (grey markers) indicate that the cold gas efficiency is in the range of other similar sized autothermal gasification plants [32]. Therefore it can be supposed, that η_{CG} will be higher for a large-scale commercial unit than for the pilot plant. In fact, 80% are reported for simulation of a 200 kW unit [24].

It is visible that the carbon conversion exceeds unity for some operating periods which is theoretically impossible for stable operation. However, this is not a problem as long as the average carbon conversion is below unity as during transient operation a carbon inventory can be build up inside the FR or be reduced and converted into gaseous species. In fact, the initial build up of carbon inventory can be seen in Fig. 8 following the path from A to B (→). At point A the system was transferred from oxygen carrier aided combustion (OCAC) to chemical looping by switching the FR fluidization from air to steam. The initial drop of carbon conversion can be explained by the slower conversion of the feedstock carbon into detectable gases by steam when compared to air. Therefore, the carbon conversion drops and increases again until a stable carbon inventory inside the FR is reached.

For the balance points where stable operation was targeted, the carbon conversion is always below unity indicating that some amount of unconverted carbon is lost. This loss can happen either through the bottom ash removal or more likely as fines through the FR cyclone. Here the dust passing the cyclone contains about 8 wt. – % to 40 wt. – % of carbon depending on operation condition. The split of the carbon conversion between the reactors is depicted in Fig. 9 a and b and shows a clear trend with FR temperature. The higher the FR temperature, the higher the carbon conversion inside the FR and the lower the carbon conversion inside the AR. Extrapolating the trends observed, the carbon conversion inside the AR — a result of unwanted carbon slip — is expected to reach negligible levels at around 950 °C. For the stable balance points, there is a clear distinction between the utilized feedstocks in the observed carbon slip. The IWP show a higher amount of carbon being converted inside the FR and a lower amount inside the AR when compared to the PFR. This behaviour can be explained by the feedstocks composition (Table 2), where PFR has a higher amount of fixed carbon which needs to be converted either in the FR by gasification through reactions R2 and R1 (see Appendix), or the AR by reaction R14(see Appendix). As the gasification is kinetically limited, the amount of char inside the feedstock influences the observed carbon slip. For bigger units, i.e. demonstration and commercial scale, an even lower carbon slip is expected, due to a larger reactor size [36]. The higher residence time in larger units allows for more conversion of fixed carbon resulting in lower carbon slip for the same FR temperatures. Therefore, lower CO_2-emissions from the AR are expected in demonstration and commercial plants.

The observed range of $\lambda_{FR,eff}$ is from nearly zero (DFBG-like conditions) to approx. 0.55 and is always below λ. This can be explained by the observed conversion of carbon inside the AR. As some oxygen is used for reaction R14 (see Appendix) not all O_2 is available for the re-oxidation of the OC material through R13(see Appendix). Consequently the oxygen release inside the FR $\lambda_{FR,eff}$ must be lower than λ if carbon slip is present in a system. Moreover, this explains the observed linear dependency between $\lambda_{FR,eff}$ and $X_{C,AR}$ in Fig. 9 and additionally the fact that higher $\lambda_{FR,eff}$ can correlate with higher η_{CG} in some regions. When more carbon is converted inside the FR and less in the AR, more syngas can be produced, thus enhancing the cold gas efficiency.

3.3. Production of higher hydrocarbons

The gas analysis equipment in the pilot plant (Table 1) cannot detect species with more than one carbon atom. However, it is known, that a significant amount of feedstock energy is converted into the fraction of hydrocarbons C_2H_4, C_2H_6, C_3H_6, and C_3H_8 during biomass gasification [3,11,17,31]. The production of higher hydrocarbons is analysed for the balance points via gas sample bags and gas chromatography. The production of C_2-species is by far the most dominant not captured by the online gas analysis with a total production of approx. 3 vol. – % and is strongly correlating with the production of CH_4 as depicted in Fig. 10. Moreover, the quantitative value is also in the same range as is reported in literature for C_2-species generated by CLG [13,17,34] and at the lower end of the range reported for DFBG [2]. It can therefore be concluded, that CLG produces syngas with a C_2 and C_3 content slightly lower than DFBG due to the switch to an active bed material.

The production of gravimetric tar as sampled by tar protocol/CEN TS 15439 is visualized in Fig. 11 with additional literature data for steam/O_2 and DFBG as reference. The gravimetric tars give an indication of the generation of species which may cause problems during down-stream utilization of the produced syngas. It is visible, that the amount of gravimetric tars reduces with increasing temperature. There is also a clear difference in the level generated by the different feedstocks, with the PFR pellets producing a higher amount of gravimetric tars than the IWP. However, it is clear from the trend-lines that the gravimetric tars reduce to very low levels for higher operating temperatures. Moreover, the amount of gravimetric tar is below the range reported for steam/oxygen gasification [32] by a factor of 7 to 10 for the same gasification reactor temperature. But even higher tar loads are observed for steam oxygen gasification [31].[4] DFBG exhibits gravimetric tars in the same range at slightly higher temperatures [37], but values in the same range as measured in the CLG pilot plant are reported for DFBG demonstration plants [38].

The difference between the feedstocks is likely caused by the addition of bark and pine needle in the PFR which is reported to generate a higher amount of tars when compared to wood pellets [3]. The feedstock moisture [38] and the amount of steam available during initial pyrolysis is also reported to have an influence on the generation of gravimetric tars [11,38,39] where lower steam supply or feedstock moisture lead to increased tar formation. This is consistent with the data in Fig. 11, where PFR has lower moisture and produces more gravimetric tars. Considering the higher feedstock moisture and higher gasification temperature reported for DFBG [38] when compared to the data reported here, and the gravimetric tar being in the same region for temperatures from 770 °C upwards, it can be expected that gravimetric tar production is lower for CLG than for DFBG, once again showing the benefit of the active bed material.

The tar species measured via gas chromatography are visualized in Fig. 12 for the balance points. More species were measured but are either not detected or in very low quantities and are therefore not depicted here. There is an appreciable amount of Benzene and Toluene in the produced syngas with some Styrene, Phenol, Benzofuran, and Dibenzofuran. The amount of gas chromatography measured tars is higher than in smaller units with ilmenite [17] by a factor of about 2 to 3. Explanations for this difference include the electrical heating of the smaller units, resulting in a more uniform temperature distribution inside the FR exceeding the temperatures reported here. The autothermal pilot plant has overall lower temperature and a less

[4] it is not perfectly clear what species are included in “Heavy Tar”. As such the gravimetric tar is probably lower and some gas chromatography tars with high dew points are included as well.

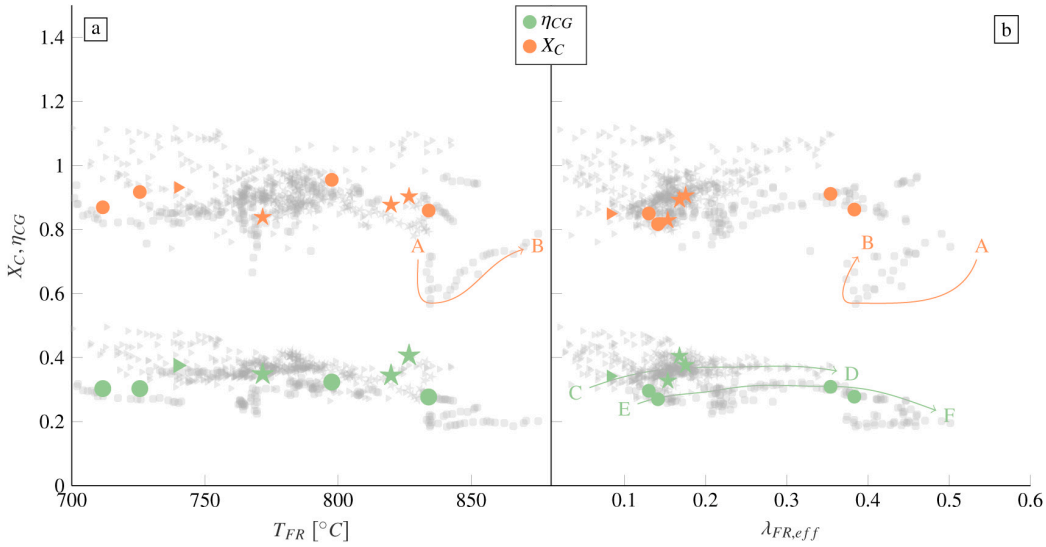

Fig. 8. Cold gas efficiency and carbon conversion. Feedstocks: ●— IWP/fine ilmenite, ▶— PFR/coarse ilmenite, ★— PFR/fine ilmenite.

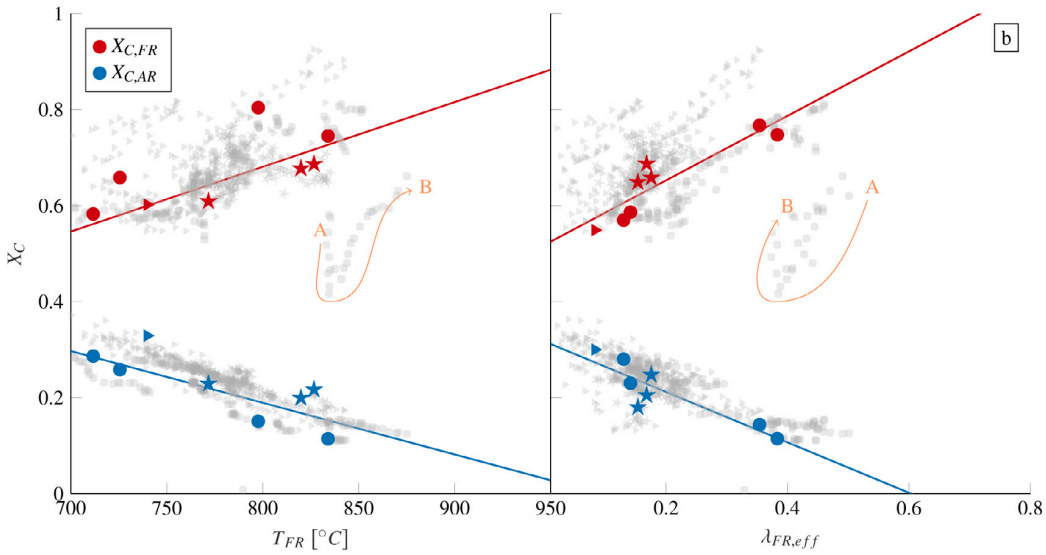

Fig. 9. Carbon Conversion. Feedstocks: ●— IWP/fine ilmenite, ▶— PFR/coarse ilmenite, ★— PFR/fine ilmenite.

uniform temperature profile with much lower temperature at the point of fuel feeding, leading to lower temperatures for initial pyrolysis and char gasification. High temperature is known to be beneficial for low tar production leading to the observed difference. Additionally, the steam content might play a role in tar production [11] but the steam to biomass ratio cannot be freely varied during operation of the autothermal pilot plant due to hydrodynamic constraints [25,40] and are higher $0.65\,kg\,kg^{-1}$ to $1.15\,kg\,kg^{-1}$ than reported for smaller units $0.05\,kg\,kg^{-1}$ to $0.9\,kg\,kg^{-1}$ (1.5 kW) [17].

Furthermore, the distribution of tars is different than the one reported by Condori et al. [17] for experiments with wood and ilmenite in a 1.5 kW unit, which features high relative amount of Naphthalene and low Benzene. It is more similar to the distribution for ilmenite and wheat straw in a 20 kW unit [13], with high relative amount of Benzene and Toluene. The difference is most likely caused by the lower reactor temperature, especially at the feedstock entry point as lower temperatures favour the production of benzenes over naphthalenes in biomass gasification [41, p. 4f]. However, there might be additional effects of scale influencing tar generation as the smallest of the units compared here generates a different profile of tars.

Compared to similar sized gasification plants using steam/oxygen gasification [32], higher amounts of Benzene are observed for CLG but lower amounts of Toluene, Phenol, and Indene. However, the total amount of gas chromatography tars is roughly the same. For DFBG plants, the reported gas chromatograph tars reach much higher levels even though gasifier temperatures are higher [2], showing another improvement with the active bed material.

Possibilities in further reducing the amount of tars are the increase of the temperature, the selection of an OC material which results in lower tar production e.g. steel converter slag (LD-slag) [12], or the increase of FR inventory and thus bed pressure drop [38]. The first option is the obvious one, but has the trade-off of lower η_{CG}. The second would require the replacement of the bed material and can therefore not be assessed with the available data, while for the third the data set is to small to show clear trends. Moreover, it is unclear whether effects of bed inventory on tar generation observed by [38] are an effect of

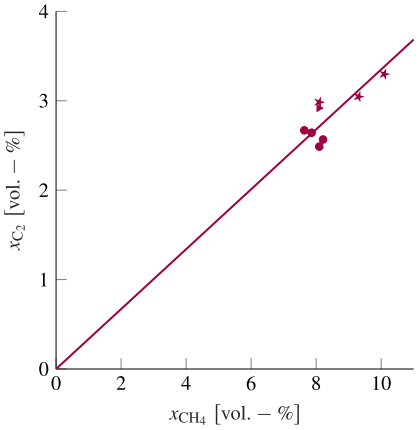

Fig. 10. C_2-production. Feedstocks: •— IWP/fine ilmenite, ▶— PFR/coarse ilmenite, ★— PFR/fine ilmenite.

the bed or of feeding location in relation to the bed, which is known to make a difference [37,42]. Nonetheless, the presence of bed material above the feedstock entry point seems to play an important role in tar reduction. When the feedstock is introduced in the lower bed region, the tars generated from initial pyrolysis have a higher residence time in the dense zone of the bed and therefore a higher likelihood of being converted by the bed material.

4. Discussion

Combining the results obtained from the pilot tests of the 1 MW_{th} pilot plant allows to establish various optimization routes and strategies for further development. However, as with all gasification technologies, there exists a trade-off between high carbon conversion and syngas quality (i.e. low tar content) one side and high cold gas efficiency on the other. The carbon conversion and syngas quality require high temperature, as was shown in Sections 3.2 and 3.3, while the cold gas efficiency is necessarily reduced when operating at higher temperature, as the heat has to be generated from feedstock conversion. However, it was observed that higher temperatures can lead to an increase of the cold gas efficiency, in cases where the benefit from the reduction of the carbon slip from FR towards FR was higher than the required feedstock conversion for the temperature increase.

Effects of the scale of the experiment, where relative heat losses of the reactor system are in the range of 12% to 19% [29,43] for the Balance points, are clearly the low cold gas efficiency and the comparatively low temperature. While optimum FR temperature regarding carbon conversion and gas yield is in the range of 850 °C to 900 °C for the CLG process with Fe based OC [6,34,35,44], this temperature could not be reached during the experiments. However, attaining higher FR temperatures will not pose an issue in commercial CLG units, as relative heat losses are significantly reduced due to the better surface-to-volume ratio. Furthermore, the modular pilot plant has fluidization medium preheating up to 360 °C at the AR and 465 °C at the FR, and the final heating to process temperature occurs inside the reactors. The required energy for the heat up of all process streams to reactor temperature is 18% to 28%. However, higher preheating temperatures are realistically obtainable, especially for the AR, reducing the cooling effect of the fluidization on the reactor temperature and increasing cold gas efficiency [23]. Increasing the fluidization medium temperature at the FR will also increase the temperature of the initial pyrolysis, therefore reducing the tar production. Moreover, char conversion inside the FR will be enhanced with the increase of the bed temperature, resulting in lower carbon slip towards the AR and thus increased syngas production inside the FR. It can be supposed that the extrapolated FR temperature for very low carbon slip, as indicated in Fig. 9, is actually lower. This will also reduce the difference between λ and $\lambda_{FR,eff}$ as less oxygen is consumed for the conversion of carbon inside the AR. Considering these effects, the heat losses, and the energy requirement for fluidization medium heating, which is combined about 30% to 50%, the 80% cold gas efficiency obtained from simulation for a 200 MW unit [24] seems plausible.

Further optimization regarding the syngas quality are obtainable for green field plants by optimizing the feedstock input location in regards to the bed height and the FR fluidization medium temperature. The longer the residence time of the pyrolysis gases inside the bed, the higher the likelihood of conversion with the OC material. However, placing the feedstock input right at the bottom results in temperatures during initial pyrolysis close to the fluidization medium temperature. The increase of the reactor inventory as much as possible without negatively impacting reactor hydrodynamic is therefore the first option, and can also be varied during operation. The complete replacement of bed inventory with a different OC material to enhance tar conversion is also possible during operation as long as a suitable PSD can be obtained. Here, changes are possible during operation, but require more time than the variation of the reactor inventory. Moreover, selection of bed material should be done to balance multiple requirements [25,45] and not just one parameter.

The presented data exhibits lower temperatures (700 °C to 850 °C) than would be ideal for the process (850 °C to 900 °C) which results in estimations and extrapolations to process temperature, which are not ideal. Moreover, some extrapolations are inevitable, as the modular pilot plant, the size of the experiment, and the autothermal operation lead to comparatively low efficiencies. However, the data gives valuable insight in the operation range and interdependence of process parameters, important trends identified and discussed are still valid. Although quantitative values differ from optimal process range, the results from autothermal pilot testing indicate the technical feasibility and the range of expectable KPIs of industrial scale CLG.

5. Conclusion

Based on the presented results from experimental autothermal operation of CLG in the 1 MW_{th} scale where more than 100 t of biomass have been converted in over 400 h of CLG operation, the following conclusions can be made:

- The possibility of syngas production using autothermal CLG was demonstrated. Although temperatures were about 100 °C below the range for optimal process performance, caused by the scale and autothermal operation.
- The analysis of the syngas generated from biogenic feedstocks showed that CLG produces a high calorific syngas which can be further processed. The amount of CH_4 generated is with 7 vol. – % to 10 vol. – % in the same range as with other biomass gasification technologies.
- The obtained cold gas efficiencies of up to 50% is in the same range as reported for similar sized pilot plants for other gasification technologies. It is expected that the cold gas efficiency reaches up to 80% for commercial CLG units, due to lower relative heat losses and heat integration.
- The observed carbon slip is dependent on the amount of fixed carbon of the feedstock and the FR temperature.
- The amount of higher hydrocarbons is lower than for other gasification technologies. Gravimetric tar productions below 1 g/N m^3 make CLG a prime candidate for the syngas production where low tar loads are required. Optimization of reactor temperature and inventory will reduce the amount of tars even further.

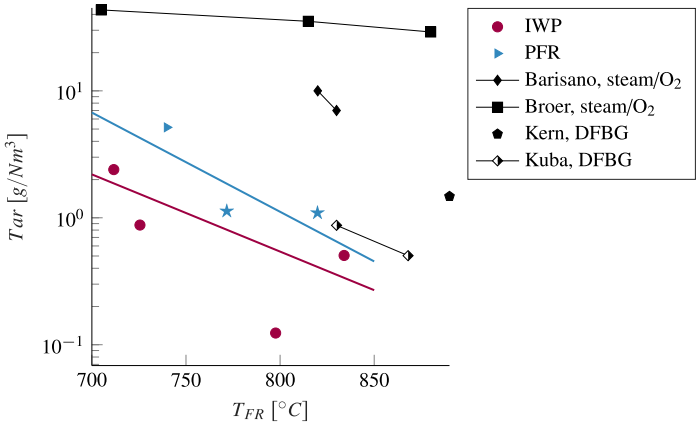

Fig. 11. Gravimetric tar on a dry gas basis. Feedstocks: •— IWP/fine ilmenite, ▶— PFR/coarse ilmenite, ★— PFR/fine ilmenite, Barsiano et al. [32], Broer et al. ("Heavy Tars") [31], Kern et al. [37], Kuba et al. [38].

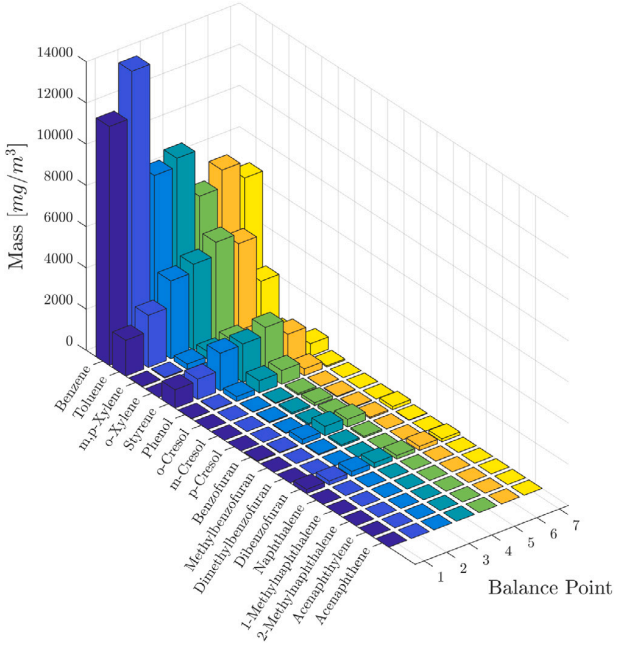

Fig. 12. Tars as measured by gas chromatography for the Balance points.

- The utilization of the active OC as bed material is advantageous compared to inert bed material with higher conversion of C_2 and C_3 species as well as pyrolysis tars.
- Although no optimization of operation was performed, the results are comparable or even better than for other gasification technologies. It is expected, that optimization for either of the KPI will lead to a superior process performance of CLG.

Therefore, CLG can be considered as an option for the sourcing of carbon from biomass for either chemical production or synthetic fuels. Nonetheless, more research is required for optimization of individual KPI. The effects of reactor inventory and feedstock entry location on carbon conversion and tar production need to be quantified to be able to optimize reactor design. Experiments with different OC material could show improvements for individual KPI, especially a lower tar production.

CRediT authorship contribution statement

Falko Marx: Conceptualization, Investigation, Data curation, Software, Writing – original draft, Writing – review & editing, Visualization. **Paul Dieringer:** Investigation, Data curation, Software, Writing – review & editing. **Jochen Ströhle:** Writing – review & editing, Project administration, Funding acquisition. **Bernd Epple:** Supervision, Funding acquisition.

Declaration of competing interest

The authors declare that they have no known competing financial interests or personal relationships that could have appeared to influence the work reported in this paper.

Data availability

Data will be made available on request.

Funding

This work has received funding of the European Union's Horizon 2020-Research and Innovation Framework Programme under grant agreement No. 817841 (Chemical Looping gasification foR sustainAble production of biofuels — CLARA). The content of this work reflects only the author's view, and the European Commission is not responsible for any use that may be made of the information it contains.

Appendix. Important reactions for the chemical looping gasification process

In order to adequately understand the phenomena described in this study, some underlying fundamental reactions have to be considered. The feedstock conversion process, from solid to syngas, starts with an initial pyrolysis and afterwards the following heterogeneous gas–solid reactions occur during CLG, converting the fixed carbon to the gas phase:

$$C + CO_2 \longleftrightarrow 2\,CO \qquad \Delta H = 172.4\,kJ\,mol^{-1} \qquad \text{Boudouard reaction} \qquad [R1]$$

$$C + H_2O \longleftrightarrow CO + H_2 \qquad \Delta H = 131.3\,kJ\,mol^{-1} \qquad \text{char reforming} \qquad [R2]$$

$$C + 2\,H_2 \longleftrightarrow CH_4 \qquad \Delta H = -74.8\,kJ\,mol^{-1} \qquad \text{methanation} \qquad [R3]$$

The homogeneous gas phase reactions between pyrolysis gases, converted fixed carbon, and the gasification agent steam are:

$$CO + H_2O \longleftrightarrow CO_2 + H_2 \qquad \Delta H = -41.1\,kJ\,mol^{-1} \qquad \text{water gas shift} \qquad [R4]$$

$$CH_4 + H_2O \longleftrightarrow CO + 3\,H_2 \qquad \Delta H = 206.1\,kJ\,mol^{-1} \qquad \text{steam methane reforming} \qquad [R5]$$

$$CH_4 + 2\,H_2O \longleftrightarrow CO_2 + 4\,H_2 \qquad \Delta H = 165\,kJ\,mol^{-1} \qquad \text{steam methane reforming} \qquad [R6]$$

with reaction R6 being the combination of the two reactions R5 and R4. As only R3 and R4 are exothermic it becomes clear that the gasification process inside the FR is endothermic. Moreover, the reaction enthalpies of R5 and R6 show that CH_4 decreases with increasing temperature. The heat required for the FR reactions to occur is provided as sensible heat by the OC material to the gasification process and the following heterogeneous gas–OC reactions occurring inside the FR:

$$Me_x O_y + CH_4 \longrightarrow Me_x O_{y-1} + 2\,H_2 + CO \qquad [R7]$$

$$4\,Me_x O_y + CH_4 \longrightarrow 4\,Me_x O_{y-1} + 2\,H_2O + CO_2 \qquad [R8]$$

$$Me_x O_y + CO \longrightarrow Me_x O_{y-1} + CO_2 \qquad [R9]$$

$$Me_x O_y + H_2 \longrightarrow Me_x O_{y-1} + H_2O \qquad [R10]$$

$$m\,Me_x O_y + C_m H_n \longrightarrow m\,Me_x O_{y-1} + mCO + n/2\,H_2O \qquad [R11]$$

$$2\,Me_x O_y + C \longrightarrow 2\,Me_x O_{y-1} + CO_2 \qquad [R12]$$

The solid–solid reaction R12 between char and OC is less relevant than the gas–OC reactions R7 to R10 as it is slower [46,47] except for very high reaction temperatures [48].

The sensible heat provided to the FR by the solid OC material is generated by the following exothermic reactions inside the AR:

$$2\,Me_x O_{y-1} + O_2 \longrightarrow 2\,Me_x O_y \qquad \text{OC (re)oxidation} \qquad [R13]$$

$$C + O_2 \longrightarrow CO_2 \qquad \Delta H = -393.5\,kJ\,mol^{-1} \qquad \text{carbon oxidation} \qquad [R14]$$

The reaction enthalpy of the heterogeneous gas–solid oxidation reaction is dependent on the used OC. For ilmenite it is actually a combination of the reactions $O_2 + Fe_2TiO_5 \longrightarrow FeTiO_3$ and $O_2 + Fe_2O_3 \longrightarrow Fe_3O_4$, with reaction enthalpies being $\Delta H = -454.4\,kJ\,mol^{-1}$ and $\Delta H = -472\,kJ\,mol^{-1}$ respectively [27]. Thus, the OC transports sensible heat and oxygen from the AR to the FR and chemical energy from the FR to the AR. R14 is caused by the undesired carbon slip from FR to AR and is favoured above reaction R13. However, in practical operation of CLG, some amount of the carbon slip is not converted inside the AR and transported back towards the FR [26].

References

[1] Langner E, Kaltenmorgen J, Heinze C, Ströhle J, Epple B. Fluidized bed gasification of solid recovered fuels in a 500 kWth pilot plant. Fuel 2023;344:127901. http://dx.doi.org/10.1016/j.fuel.2023.127901.

[2] Larsson A, Kuba M, Berdugo Vilches T, Seemann M, Hofbauer H, Thunman H. Steam gasification of biomass – typical gas quality and operational strategies derived from industrial-scale plants. Fuel Process Technol 2021;212:106609. http://dx.doi.org/10.1016/j.fuproc.2020.106609.

[3] Larsson A, Gunnarsson I, Tengberg F. The GoBiGas project demonstration of the production of biomethane from biomass via gasification. 2018, http://dx.doi.org/10.13140/RG.2.2.27352.55043.

[4] Nguyen NM, Alobaid F, Dieringer P, Epple B. Biomass-based chemical looping gasification: Overview and recent developments. Appl Sci 2021;11(15):7069. http://dx.doi.org/10.3390/app11157069.

[5] Di Giuliano A, Capone S, Anatone M, Gallucci K. Chemical looping combustion and gasification: A review and a focus on European research projects. Ind Eng Chem Res 2022;61(39):14403–32. http://dx.doi.org/10.1021/acs.iecr.2c02677.

[6] Goel A, Moghaddam EM, Liu W, He C, Konttinen J. Biomass chemical looping gasification for high-quality syngas: A critical review and technological outlooks. Energy Convers Manage 2022;268:116020. http://dx.doi.org/10.1016/j.enconman.2022.116020.

[7] Larsson A, Israelsson M, Lind F, Seemann M, Thunman H. Using ilmenite to reduce the tar yield in a dual fluidized bed gasification system. Energy Fuels 2014;28(4):2632–44. http://dx.doi.org/10.1021/ef500132p.

[8] Virginie M, Adánez J, Courson C, de Diego L, García-Labiano F, Niznansky D, Kiennemann A, Gayán P, Abad A. Effect of Fe– olivine on the tar content during biomass gasification in a dual fluidized bed. Appl Catal B 2012;121–122:214–22. http://dx.doi.org/10.1016/j.apcatb.2012.04.005.

[9] Mendiara T, Johansen JM, Utrilla R, Geraldo P, Jensen AD, Glarborg P. Evaluation of different oxygen carriers for biomass tar reforming (i): Carbon deposition in experiments with toluene. Fuel 2011;90(3):1049–60. http://dx.doi.org/10.1016/j.fuel.2010.11.028.

[10] Mendiara T, Johansen JM, Utrilla R, Jensen AD, Glarborg P. Evaluation of different oxygen carriers for biomass tar reforming (II): Carbon deposition in experiments with methane and other gases. Fuel 2011;90(4):1370–82. http://dx.doi.org/10.1016/j.fuel.2010.12.034.

[11] Condori O, García-Labiano F, de Diego LF, Izquierdo MT, Abad A, Adánez J. Biomass chemical looping gasification for syngas production using LD slag as oxygen carrier in a 1.5 kWth unit. Fuel Process Technol 2021;222:106963. http://dx.doi.org/10.1016/j.fuproc.2021.106963.

[12] Hildor F, Soleimanisalim AH, Seemann M, Mattisson T, Leion H. Tar characteristics generated from a 10 kWth chemical-looping biomass gasifier using steel converter slag as an oxygen carrier. Fuel 2023;331:125770. http://dx.doi.org/10.1016/j.fuel.2022.125770.

[13] Condori O, Abad A, Izquierdo MT, de Diego LF, García-Labiano F, Adánez J. Assessment of the chemical looping gasification of wheat straw pellets at the 20 kWth scale. Fuel 2023;344:128059. http://dx.doi.org/10.1016/j.fuel.2023.128059.

[14] Guo Q, Cheng Y, Liu Y, Jia W, Ryu H-J. Coal chemical looping gasification for syngas generation using an iron-based oxygen carrier. Ind Eng Chem Res 2014;53(1):78–86. http://dx.doi.org/10.1021/ie401568x.

[15] Samprón I, de Diego LF, García-Labiano F, Izquierdo MT, Abad A, Adánez J. Biomass chemical looping gasification of pine wood using a synthetic Fe2O3/Al2o3 oxygen carrier in a continuous unit. Bioresour Technol 2020;316:123908. http://dx.doi.org/10.1016/j.biortech.2020.123908.

[16] Hedayati A, Soleimanisalim AH, Linderholm CJ, Mattisson T, Lyngfelt A. Experimental evaluation of manganese ores for chemical looping conversion of synthetic biomass volatiles in a 300 w reactor system. J Environ Chem Eng 2021;9(2):105112. http://dx.doi.org/10.1016/j.jece.2021.105112.

[17] Condori O, García-Labiano F, de Diego LF, Izquierdo MT, Abad A, Adánez J. Biomass chemical looping gasification for syngas production using ilmenite as oxygen carrier in a 1.5 kWth unit. Chem Eng J 2021;405:126679. http://dx.doi.org/10.1016/j.cej.2020.126679.

[18] Di Giuliano A, Funcia I, Pérez-Vega R, Gil J, Gallucci K. Novel application of pretreatment and diagnostic method using dynamic pressure fluctuations to resolve and detect issues related to biogenic residue ash in chemical looping gasification. Processes 2020;8(9):1137. http://dx.doi.org/10.3390/pr8091137.

[19] Di Giuliano A, Lucantonio S, Gallucci K. Devolatilization of residual biomasses for chemical looping gasification in fluidized beds made up of oxygen-carriers. Energies 2021;14(2):311. http://dx.doi.org/10.3390/en14020311.

[20] Purnomo V, Yilmaz D, Leion H, Mattisson T. Study of defluidization of iron- and manganese-based oxygen carriers under highly reducing conditions in a lab-scale fluidized-bed batch reactor. Fuel Process Technol 2021;219:106874. http://dx.doi.org/10.1016/j.fuproc.2021.106874.

[21] Dieringer P, Marx F, Michel B, Ströhle J, Epple B. Design and control concept of a 1 MWth chemical looping gasifier allowing for efficient autothermal syngas production. Int J Greenh Gas Control 2023;127:103929. http://dx.doi.org/10.1016/j.ijggc.2023.103929.

[22] Dieringer P, Marx F, Alobaid F, Ströhle J, Epple B. Process control strategies in chemical looping gasification—A novel process for the production of biofuels allowing for net negative CO2 emissions. Appl Sci 2020;10(12):26. http://dx.doi.org/10.3390/app10124271.

[23] Samprón I, de Diego LF, García-Labiano F, Izquierdo MT. Optimization of synthesis gas production in the biomass chemical looping gasification process operating under auto-thermal conditions. Energy 2021;226:120317. http://dx.doi.org/10.1016/j.energy.2021.120317.

[24] Detsios N, Atsonios K, Grammelis P, Dieringer P, Ströhle J, Nikkanen V, Orfanoudakis N. A comparative analysis and assessment of dual fluidized bed and chemical looping gasification: Design considerations for commercial use and applicability in BTL schemes. In: Proceedings of the 31st European biomass conference and exhibition 5-8 june 2023. 2023, p. 6. http://dx.doi.org/10.5071/31STEUBCE2023-4AO.5.2.

[25] Marx F, Dieringer P, Ströhle J, Epple B. Design of a 1 MWth pilot plant for chemical looping gasification of biogenic residues. Energies 2021;14(9):2581. http://dx.doi.org/10.3390/en14092581.

[26] Marx F, Dieringer P, Ströhle J, Epple B. Solid flux measurement in dual fluidized bed processes based on solid samples. Fuel 2023;341:127589. http://dx.doi.org/10.1016/j.fuel.2023.127589.

[27] Bartocci P, Abad A, Flores AC, de las Obras Loscertales M. Ilmenite: A promising oxygen carrier for the scale-up of chemical looping. Fuel 2023;337:126644. http://dx.doi.org/10.1016/j.fuel.2022.126644.
[28] Ohlemüller P, Busch J-P, Reitz M, Ströhle J, Epple B. Chemical-looping combustion of hard coal: Autothermal operation of a 1 MWth pilot plant. J Energy Resour Technol 2016;138(4):042203. http://dx.doi.org/10.1115/1.4032357.
[29] Ohlemüller P, Ströhle J, Epple B. Chemical looping combustion of hard coal and torrefied biomass in a 1 MW th pilot plant. Int J Greenh Gas Control 2017;65:149–59. http://dx.doi.org/10.1016/j.ijggc.2017.08.013.
[30] Anovitz LM, Treiman AH, Essene EJ, Hemingway BS, Westrum EF, Wall VJ, Burriel R, Bohlen SR. The heat-capacity of ilmenite and phase equilibria in the system fe-t-o. Geochim Cosmochim Acta 1985;49(10):2027–40. http://dx.doi.org/10.1016/0016-7037(85)90061-4.
[31] Broer KM, Woolcock PJ, Johnston PA, Brown RC. Steam/oxygen gasification system for the production of clean syngas from switchgrass. Fuel 2015;140:282–92. http://dx.doi.org/10.1016/j.fuel.2014.09.078.
[32] Barisano D, Canneto G, Nanna F, Alvino E, Pinto G, Villone A, Carnevale M, Valerio V, Battafarano A, Braccio G. Steam/oxygen biomass gasification at pilot scale in an internally circulating bubbling fluidized bed reactor. Fuel Process Technol 2016;141:74–81. http://dx.doi.org/10.1016/j.fuproc.2015.06.008.
[33] Wei Y, Cheng L, Leckner B, Wu E, Li L, Zhang Q. Design of an industrial chemical looping gasification system. Fuel 2022;330:125541. http://dx.doi.org/10.1016/j.fuel.2022.125541.
[34] Ge H, Guo W, Shen L, Song T, Xiao J. Biomass gasification using chemical looping in a 25 kw th reactor with natural hematite as oxygen carrier. Chem Eng J 2016;286:174–83. http://dx.doi.org/10.1016/j.cej.2015.10.092.
[35] Ge H, Guo W, Shen L, Song T, Xiao J. Experimental investigation on biomass gasification using chemical looping in a batch reactor and a continuous dual reactor. Chem Eng J 2016;286:689–700. http://dx.doi.org/10.1016/j.cej.2015.11.008.
[36] Lyngfelt A, Leckner B. A 1000 MWth boiler for chemical-looping combustion of solid fuels – discussion of design and costs. Appl Energy 2015;157:475–87. http://dx.doi.org/10.1016/j.apenergy.2015.04.057.
[37] Kern S, Pfeifer C, Hofbauer H. Gasification of wood in a dual fluidized bed gasifier: Influence of fuel feeding on process performance. Chem Eng Sci 2013;90:284–98. http://dx.doi.org/10.1016/j.ces.2012.12.044.
[38] Kuba M, Hofbauer H. Experimental parametric study on product gas and tar composition in dual fluid bed gasification of woody biomass. Biomass Bioenergy 2018;115:35–44. http://dx.doi.org/10.1016/j.biombioe.2018.04.007.
[39] Condori O, De Diego LF, Garcia-Labiano F, Izquierdo MT, Abad A, Adánez J. Syngas production in a 1.5 kW_{th} biomass chemical looping gasification unit using Fe and Mn ores as the oxygen carrier. Energy Fuels 2021;35(21):17182–96. http://dx.doi.org/10.1021/acs.energyfuels.1c01878.
[40] Dieringer P, Marx F, Ströhle J, Epple B. System hydrodynamics of a 1 MWth dual circulating fluidized bed chemical looping gasifier. Energies 2023. http://dx.doi.org/10.3390/en16155630.
[41] Milne TA, Evans RJ, Abatzaglou N. Biomass Gasifier Tars: Their Nature, Formation, and Conversion. Tech. Rep. NREL/TP-570-25357, 1998, p. 3726. http://dx.doi.org/10.2172/3726, ON: DE00003726.
[42] Gómez-Barea A, Ollero P, Leckner B. Optimization of char and tar conversion in fluidized bed biomass gasifiers. Fuel 2013;103:42–52. http://dx.doi.org/10.1016/j.fuel.2011.04.042.
[43] Ströhle J, Orth M, Epple B. Chemical looping combustion of hard coal in a 1 MWth pilot plant using ilmenite as oxygen carrier. Appl Energy 2015;157:288–94. http://dx.doi.org/10.1016/j.apenergy.2015.06.035.
[44] Huseyin S, q. Wei G, b. Li H, He F, Huang Z. Chemical-looping gasification of biomass in a 10 kWth interconnected fluidized bed reactor using fe2o3/Al2o3 oxygen carrier. J Fuel Chem Technol 2014;42(8):922–31. http://dx.doi.org/10.1016/S1872-5813(14)60039-6.
[45] Adanez J, Abad A, Garcia-Labiano F, Gayan P, de Diego LF. Progress in chemical-looping combustion and reforming technologies. Prog Energy Combust Sci 2012;38(2):215–82. http://dx.doi.org/10.1016/j.pecs.2011.09.001.
[46] Brown TA, Dennis JS, Scott SA, Davidson JF, Hayhurst AN. Gasification and chemical-looping combustion of a lignite char in a fluidized bed of iron oxide. Energy Fuels 2010;24(5):3034–48. http://dx.doi.org/10.1021/ef100068m.
[47] Leion H, Mattisson T, Lyngfelt A. The use of petroleum coke as fuel in chemical-looping combustion. Fuel 2007;86(12–13):1947–58. http://dx.doi.org/10.1016/j.fuel.2006.11.037.
[48] Chen L. The direct solid–solid reaction between coal char and iron-based oxygen carrier and its contribution to solid-fueled chemical looping combustion. Appl Energy 2016;10. http://dx.doi.org/10.1016/j.apenergy.2016.09.085.